THE BIOLOGY AND EXPRESSION OF HUNTINGTIN-INTERACTING PROTEIN 14

by

Fiona Bridget Julia Young

B. Sc. (Hon), McGill University, 2005

A THESIS SUBMITTED IN PARTIAL FULFILLMENT OF
THE REQUIREMENTS FOR THE DEGREE OF

COMBINED DOCTOR OF MEDICINE AND DOCTOR OF PHILOSOPHY

in

THE FACULTY OF GRADUATE STUDIES

(Medical Genetics)

THE UNIVERSITY OF BRITISH COLUMBIA
(Vancouver)

August, 2011

© Fiona Bridget Julia Young, 2011

ABSTRACT

Huntingtin Interacting Protein 14 (HIP14) is a palmitoyl acyl transferase (PAT) that was first identified due to altered interaction with mutant huntingtin, the protein responsible for Huntington Disease. HIP14 palmitoylates a specific set of neuronal substrates critical at the synapse, and downregulation of HIP14 by siRNA *in vitro* results in increased cell death in neurons. Recent findings have revealed that mice lacking murine *Hip14* (*Hip14-/-*) demonstrate a Huntington-Disease-like phenotype. In the current study, we have generated and characterized human *HIP14* BAC transgenic mice. We generated humanized *HIP14* transgenic mice by crossing the *HIP14* BAC mouse to the *Hip14-/-* model. Rescue of the *Hip14-/-* phenotype indicates that the defects seen in *Hip14-/-* mice are in fact due to loss of HIP14. In addition, our findings indicate human HIP14 can compensate for the loss of the murine ortholog, and that very low levels of HIP14 are sufficient to rescue the *Hip14-/-* phenotype. Finally, we assess patterns of HIP14 expression in early development. Our findings further our understanding of HIP14 *in vivo,* and point to several potential avenues for future studies.

PREFACE

For data presented in chapter 3, neuropathological assessments in stereology and neurochemistry were done by Sonia Franciosi and Amanda Spreeuw. Weining Zhang assisted with rotarod testing as well as Swimming T-maze testing. All mRNA and protein expression, most behavioural testing, all data analysis, and remaining assessments were done by the author.

Chapter 4 is adapted from a manuscript in preparation. I was responsible for experimental design, mRNA and protein expression analysis, most behaviour testing, and all data analysis. Stereology and neurochemistry assessments were done by Sonia Franciosi and Amanda Spreeuw. Weining Zhang performed rotarod testing. Shaun Sanders and Kun Huang provided invaluable assistance in palmitoylation assays.

The Western Blot analysis of HIP14 expression described in chapter 5 will be included in a future publication. Assessment of fertility and testicular phenotype will be submitted for publication as part of a brief report.

I was responsible for the written contents of this study, with the following exceptions:

The description of the *Hip14-/-* mice (section 1.3) was adapted from the following study: Singaraja, R.R., et al., *Replication of features of Huntington Disease in mice lacking HIP14*, Hum. Mol. Genet., Jul 20. [Epub ahead of print].

Section 1.4 is a summary of unpublished work by Liza Sutton, which will follow publication of the study described in section 1.3.

The Animal Care certificates relevant to this study are:
1. A07-0106 Animal Model of Huntington's Disease
2. A07-0262 BREEDING: Animal Model of HD

TABLE OF CONTENTS

LIST OF TABLES

LIST OF FIGURES

LIST OF ABBREVIATIONS

2BP	2-bromopalmitate
Aa	amino acid
AAV	adeno-associated virus
ABA	Allan Brain Atlas
ABE	acyl biotin exchange
ABE/IP	acyl biotin exchange with immunoprecipitation
AD	Alzheimer's disease
Akr1p	ankyrin repeat containing protein 1
AMPA	α-amino-3-hydroxy-5-methyl-4-isoxazolepropionic acid
AMPAR	α-amino-3-hydroxy-5-methylisoxazole-4-propionic acid type glutamate receptors
ANK	ankyrin repeat
ANOVA	analysis of variance
APH1	anterior pharynx-defective 1
APP	amyloid precursor protein
APT	acyl-protein thioesterase
APTL1	acyl protein thioesterase like 1
ASO	Antisense Oligonucleotides
BAC	bacterial artificial chromosome
BACE	beta-secretase 1
Biotin BMCC	1-biotinamido-4-[4´-(maleimidomethyl)cyclohexanecarboxamido]butane
BMP	bone morphogenetic protein
bp	base pair
BSA	bovine serum albumin
BrdU	bromodeoxyuridine
C214	cysteine 214 (of the HTT protein)
CAG	cytosine, adenine, and guanine)
CAGGS	containing the chicken beta-actin promoter and cytomegalovirus enhancer, beta-actin intron and bovine globin poly-adenylation signal
Cdc42	cell division control protein 42
cDNA	complementary DNA
CHORI	Children's Hospital Oakland Research Institute
CMMT	Centre for Molecular Medicine and Therapeutics
CFTR	cystic fibrosis transmembrane conductance regulator
CLN1	Ceroid Lipofuscinosis Neuronal 1
CNS	central nervous system
CRD	cysteine rich domain
CSP	cysteine string protein
CSS-palm	clustering and scoring strategy palmitoylation prediction software
D1	dopamine receptor D1

D2	dopamine receptor D2
DAB	diaminobenzidine
DARPP-32	dopamine- and cAMP-regulated phosphoprotein, 32 kDa
DHHC	aspartate-histidine-histidine-cysteine
D. melanogaster	*Drosophila melanogaster* (fruit fly)
DNA	deoxyribonucleic acid
D. rerio	*Danio rerio* (zebrafish)
dNTP	deoxyribonucleotide triphosphate
E	embryonic day
EDTA	ethylenediaminetetraacetic acid
EGTA	ethylene glycol tetraacetic acid
EM	electron microscope
eNOS	endothelial nitric oxide synthase
EPM	elevated plus maze
ENU	N-ethyl-N-nitrosourea
ER	endoplasmic reticulum
ES	embryonic stem
EtBr	ethidium bromide
FSH	follicle stimulating hormone
FVB/N	Inbred strain of mouse (Friend Virus B)
GABA	gamma-aminobutyric acid
GAP-43	growth associated protein 43
GAD65	glutamic acid decarboxylase 65
GAPDH	glyceraldehyde 3-phosphate dehydrogenase
GENSAT	Gene Expression Nervous System Atlas
GluR1	glutamate receptor 1 (*GRIA1*)
GluR2	glutamate receptor 2 (*GRIA2*)
GNF	Genomics Institute of the Novartis Research Foundation
GODZ	Golgi-specific DHHC zinc finger protein
GTPase	enzyme that binds and hydrolyzes guanosine triphosphate (GTP)
GXD	MGI-Mouse Gene Expression Database
H&E	hematoxylin and eosin stain
HAM	hydroxylamine
Hap1	huntingtin associated protein 1
HD	Huntington disease
Hdh	murine HD ortholog
HIP	huntingtin interacting protein
HIP14	huntingtin interacting protein - human gene (alternately known as *ZDHHC17* or *DHHC17*)
Hip14	huntingtin interacting protein - mouse gene ((alternately known as *Zdhhc17* or *dhhc17*)
HIP14	huntingtin interacting protein - human or mouse protein
Hip14L	huntingtin interacting protein-like - mouse gene
HIP14L	huntingtin interacting protein-like - mouse protein
HPLC	High-performance liquid chromatography

H. sapiens	*Homo sapiens* (Human)
HTT	huntingtin
ICR	imprinting control region
INCL	infantile neuronal ceroid lipofuscinoses
in vitro	experiments performed in cultured cells
in vivo	experiments performed in/from tissue
IOD	integrated optical density
IP	immunoprecipitation
ITI	inter-trial interval
kDa	kilo-dalton
LB	Luria broth
Lck	lymphocyte-specific protein tyrosine kinase
LGE	lateral ganglionic eminence
LH	leutinizing hormone
LTP	long-term potentiation
MBOAT	membrane-bound-O-acyltransferase
miRNA	microRNA
mRNA	messenger ribonucleic acid
MSN	medium spiny neuron
M. musculus	*Mus musculus* (house mouse)
mHTT	mutant huntingtin
MRI	magnetic resonance imaging
mRNA	messenger ribonucleic acid
NCL	Neuronal Ceroid Lipofuscinoses
NEM	N-ethylmaleimide
NGS	normal goat serum
NINDS	National Institute of Neurological Disorders and Stroke
NMDA	N-methyl-D-aspartate
NMDA	N-methyl-D-aspartate receptor
NO	nitric oxide
NOD/SCID	nonobese diabetes/severe combined immunodeficiency (inbred mouse strain)
NR2B	N-methyl D-aspartate receptor subtype 2B
NR2E1	nuclear receptor subfamily 2 group E member 1
NRSF	neuron restrictive silencing factor
nt	nucleotide
OSBPL8	oxysterol binding protein-like 8
P	postnatal day
PAT	palmitoyl acyltransferase
Poly-Q	poly-glutamine
PBS	phosphate buffered saline
PCR	polymerase chain reaction
PEN2	presenilin enhancer 2
PKA	protein kinase A
PM	plasma membrane
PMSF	phenylmethanesulfonylfluoride

PPI	pre-pulse inhibition
PPT1	palmitoyl protein thioesterase 1
PS1	presenilin 1
PS2	presenilin 2
PSD	post-synaptic density
PSD-95	postsynaptic density protein 95
PTM	post-translational modification
PVDF	polyvinylidene fluoride
qPCR	quantitative polymerase chain reaction
qrtPCR	quantitative real time polymerase chain reaction
Ras	RAt Sarcoma
REAM	reduced expression associated with metastasis
RPM	revolutions per minute
S2 cells	*Drosophila* Schneider 2 cells
S. cerevisiae	*Saccharomyces cerevisiae* (budding yeast)
SDS	sodium dodecyl sulfate
SDS-PAGE	sodium dodecyl sulfate polyacrylamide gel electrophoresis;
SEM	standard error of the mean
siRNA	small interfering RNA
SNAP25	synaptosomal-associated protein 25
SNARE	soluble NSF (N-ethylmaleimide-sensitive factor) attachment receptor
SNP	single nucleotide polymorphism
Sog	short gastrulation
SYBR	a dye that binds to nucleic acid (Synergy Brands, Inc)
Syt1	synaptotagmin 1
TE	buffer containing tris and EDTA
TEEN	buffer containing Tris, EDTA, EGTA, and NaCl
TGF-beta	transforming growth factor beta
TPPP	tubulin polymerization-promoting protein
TSR	transcription start region
UCSC	University of California Santa Cruz
UTR	untranslated region
WT	wildtype
XLMR	X-linked mental retardation
YAC	yeast artificial chromosome
YAC128	yeast artificial chromosome mouse model of HD containing 128 CAG repeats in the human HD gene
Yck2p	yeast casein kinase 2p
ZDHHC17	official name for the human HIP14 gene (alternately known as DHHC17)
Zdhhc17	official name for the mouse HIP14 gene (alternately known as DHHC17)

ACKNOWLEDGEMENTS

There are many people I would like to thank for their support. I would like to thank my supervisor, Dr. Michael Hayden, for taking me on in his lab and persevering through this journey with me. An immense thank you to my supervisory committee: Dr. Lynn Raymond for her guidance and support in this capacity and also in supporting myself and other MD/PhD students; Dr. Blair Leavitt for his invaluable mentorship and patient support; Dr. Liz Conibear for her guidance and support, as well as the late Dr. Alaa El-Husseini who I had the pleasure of working with for only a very brief time. Thank you also to Dr. Wyeth Wasserman and Dr. Elodie Portales-Casamar for their bioinformatics expertise assisting in selection of the BAC construct. Thank you to Dr. Beth Simpson for her expert advice and ideas. Finally, a huge thank you to Dr. Wayne Vogl for his collaboration and enthusiasm.

I am immensely grateful to Simon Warby for his mentorship, friendship, and advocacy- you made an immense difference in my experience here. Thanks also to Roshni Singaraja for her mentorship, support, patience, and friendship, as well as for patiently reviewing a very early version of this thesis and many, many versions of my manuscript. You are both inspiring and wonderful friends.

Thanks also go to Rona Graham, Jeff Carroll, Mahmoud Pouladi, and Stefanie Butland for their expert guidance and mentorship. I am fortunate and grateful to be working with so many brilliant and gifted colleagues, particularly: Shaun Sanders, Kun Huang, Liza Sutton, Amber Southwell, Bibiana Wong, Valeria Uribe, and Safia Ladha. Nagat Bissada, Mark Wang, Tess Algara, and Qingwen Xia all work hard every day to keep the lab's animal facility running smoothly and their support is invaluable. Thank you to the brilliant technicians who have supported my projects: Natalie Tam, Betty Nguyen, and Chris Kay-all brilliant rising stars with very bright days ahead. Thanks also go to Crystal Doty, whose

advice and technical expertise were hugely valuable to me. Thank you to (Deb) Yu Deng for expertise in preparing the BAC construct and in qrtPCR expertise.

I am very grateful for the help of Jen Witmer; without her skilled hand at microinjection and her enthusiastic willingness to help out, this project would have never gotten off the ground. Sonia Franciosi and Amanda Spreeuw deserve ample recognition, for their hard work and expertise on the neuropathological assessments in this study, as well as to Weining Zhang for his support in the behaviour suite. The administrative staff of the Hayden lab ensure its smooth running-we would be lost without you: Dawn Ng, Seetha Kumaran, Tammy Wilson, Mahsa Amirabbasi, and Michael Hockertz among many others. Thank you also to Five Seventeen for his help and expertise in Adobe Illustrator. It has been a pleasure and privilege to work with the fantastic team that makes up the Hayden lab; they are all incredible and talented friends and colleagues.

I send a nod to my two brilliant and talented sisters, Eleanor and Gillian Young, who both amaze and inspire me. Thanks go to my wonderful and loving dad, Richard Young, who has never failed to support me in whatever I choose to do, and also to my mother, Jeannine Simon, an incredible woman and doctor, for whom I have a huge amount of love, admiration and respect. I am hugely thankful to both my parents for providing me with all the opportunities in life that they have.

To all my friends in Montreal and Toronto, particularly: Dylann McLean, Phil Reiter, Tiffany Nicholson, Kim Kotar, Sarah Puskas and Sarah Tabah, Rachelle Wilson, and many countless others who go unnamed but who helped me to get here today-your friendship and support is truly invaluable. I am also grateful for the amazing friends I have encountered here in Vancouver, particularly Andrew Gray, Claire Heslop, and Kate Potter, among many others. Finally, to Topher Stephenson; I might never have finished this work without your friendship and support.

1. INTRODUCTION

1.1. Protein palmitoylation

1.1.1. General overview

The term palmitoylation is generally used to describe the post-translational addition of the16-carbon fatty acid palmitate to a cysteine residue via a thioester bond (Conibear and Davis, 2010, Fukata Yuko and Fukata, 2010, Linder and Deschenes, 2007, Salaun *et al.*, 2010). S-acylation, a broader term which includes palmitoylation, describes the addition of any number of fatty acids in a similar manner, though palmitic acid is the most common; therefore S-acylation is often referred to as palmitoylation (Zeidman *et al.*, 2009). Less commonly, acylation may occur at an N-terminal cysteine (N-acylation) and is linked via an amide, as opposed to thioester bond. When involving the fatty acid palmitate, this latter process is known as N-palmitoylation (Nadolski and Linder, 2007). Other common lipid modifications of proteins include protein prenylation, wherein a farnesyl or geranyl-geranyl moiety is added post-translationally to a C-terminal cysteine via a stable thioether bond (Zhang Fang L and Casey, 1996), and myristoylation, which involves the co-translational addition of myristic acid to a glycine residue via a stable amide bond (Johnson *et al.*, 1994). Notably, the relatively rare process of N-palmitoylation, by the nature of its different chemistry, is not reversible and is not involved in dynamic regulation of proteins. Similarly, protein prenylation and myristoylation are not reversible protein modifications. The term “palmitoylation” in the remainder of this thesis refers specifically to the addition of palmitic acid to a cysteine residue via a thioester bond.

A diverse array of protein substrates are now known to undergo palmitoylation. A major group of palmitoylated proteins are transmembrane proteins (Charollais and Van Der Goot, 2009, Fukata Yuko and Fukata, 2010). The large number of substrates includes signaling proteins (Smotrys and Linder, 2004) such as H- and N-Ras (Hancock *et al.*, 1989), ion channel components such as GluR1 and

GluR2 (Hayashi T *et al.*, 2005), scaffold proteins such as PSD-95 (Topinka and Bredt, 1998), membrane-associated proteins involved in vesicle trafficking such as the SNARE proteins (Kang Rujun *et al.*, 2008), as well as secreted (Chang and Magee, 2009) and viral proteins (Veit *et al.*, 1996).

Palmitoylation plays a key role in several cellular processes, including tethering signaling proteins to membranes, protein trafficking, protein stability, protein-protein interactions, membrane association, and segregation of substrates to particular protein subdomains (Conibear and Davis, 2010, Fukata Yuko and Fukata, 2010, Huang and El-Husseini, 2005, Linder and Deschenes, 2007, Salaun, 2010, Zeidman, 2009).

Palmitoylation increases the lipophilic nature of a protein, in turn facilitating its association with various membranes throughout the cell, and targeting its subcellular distribution of the substrate. For example, upon palmitoylation, cytoplasmic proteins become membrane associated (Conibear and Davis, 2010, Salaun, 2010). For many proteins, mono-lipidation (involving palmitate or other lipid modifications) results in a weak, relatively unstable membrane association. The addition of a second lipid group to the substrate in the form of palmitate strengthens and stabilizes the membrane association, resulting in a longer membrane association, often with functional implications. This stable membrane association may be alternatively achieved via the presence of multiple palmitoylation sites (Conibear and Davis, 2010, Salaun, 2010).

In many cases, protein palmitoylation of membrane-associated proteins leads to their segregation into membrane microdomains (Conibear and Davis, 2010, Salaun, 2010). Lipid raft domains are islands of altered lipid composition that exist within a membrane, and are residence to a distinct population of peripheral and integral membrane proteins (Brown, 2006). Upon palmitoylation, many proteins are sorted into lipid rafts, placing the substrate in proximity to other proteins and serving a key role in cell signaling.

Finally, protein palmitoylation may alter the hydrophobicity of a particular domain by inducing a tilt within a membrane bilayer, resulting in a conformational change and potentially enabling or inhibiting particular protein interactions (Conibear and Davis, 2010).

A critical role for palmitoylation in the central nervous system, particularly its role in synaptic plasticity, has been borne out by a number of studies over the last decade (El-Husseini Alaa El-Din and Bredt, 2002, Fukata Yuko and Fukata, 2010, Huang and El-Husseini, 2005). Palmitoylation reversibly regulates the assembly and compartmentalization of many neuronal proteins at specific subcellular domains such as the presynaptic terminal and postsynaptic sites (El-Husseini Alaa El-Din and Bredt, 2002, Fukata Yuko and Fukata, 2010, Huang and El-Husseini, 2005, Prescott *et al.*, 2009). This process influences the assembly of protein complexes at the synapse that modulate synaptic transmission and neuronal function. For example, palmitoylation regulates the postsynaptic targeting of postsynaptic density-95 (PSD-95), a molecule involved in excitatory synapse development and plasticity (Craven *et al.*, 1999, Ehrlich, 2004, El-Husseini Alaa El-Din and Bredt, 2002, Kim and Sheng, 2004, Schnell *et al.*, 2002, Stein *et al.*, 2003). At presynaptic nerve terminals, palmitoylation modulates trafficking and assembly of proteins that regulate neurotransmitter release such as the GABA synthesizing enzyme GAD65 and synaptotagmin I (Kanaani *et al.*, 2002, Kanaani *et al.*, 2004, Kang Rujun *et al.*, 2004). Other studies suggest an important role for protein palmitoylation in the control of other aspects of neuronal development such as neurite outgrowth, axon pathfinding, and filopodia and spine development (Arstikaitis *et al.*, 2008, Gauthier-Campbell *et al.*, 2004, Kato *et al.*, 2000, Kutzleb *et al.*, 1998, Laux *et al.*, 2000, Strittmatter *et al.*, 1995, Ueno, 2000).

Finally, in the developing and adult CNS, palmitoylation regulates signal transduction by modulating adhesion molecules, neurotransmitter receptors and ion channels implicated in establishing neuronal connectivity, excitability and

synaptic plasticity (Bizzozero, 1997, Dunphy and Linder, 1998, Hess *et al.*, 2002). Alterations in neuronal excitability and plasticity underlie many neuropsychiatric disorders (Citri and Malenka, 2008, Humeau *et al.*, 2009, Kreitzer and Malenka, 2008, Lee and Silva, 2009). The labile nature of the thioester bond lends to the reversibility of protein palmitoylation, and is an important feature that distinguishes this process from other forms of protein lipidation (Baekkeskov and Kanaani, 2009, Conibear and Davis, 2010, Salaun, 2010, Zeidman, 2009). This unique aspect of palmitoylation is the mechanism by which dynamic control of protein localization and function occurs in the CNS and elsewhere. Indeed, many proteins are seen to undergo dynamic cycles of palmitoylation/depalmitoylation, having important functional implications (Conibear and Davis, 2010).

A well-studied example of this dynamic cycling and its critical importance for synaptic plasticity is observed with PSD-95, a scaffold protein for AMPARs and NMDARs at the post-synapse (Ehrlich, 2004, El-Husseini Alaa E *et al.*, 2000a, El-Husseini Alaa El-Din *et al.*, 2000b, El-Husseini Alaa El-Din *et al.*, 2002). Palmitoylation of PSD-95 is required for its membrane scaffolding function (El-Husseini Alaa E, 2000a). The dual palmitoylation at the PSD-95 N-terminus undergoes constitutive turnover (El-Husseini Alaa E, 2000a, El-Husseini Alaa El-Din, 2002), which is enhanced by synaptic activity. Strong neuronal excitation accelerates the depalmitoylation of PSD-95, reducing the amount of PSD-95 at the post-synapse resulting in a reduction in synaptic strength (El-Husseini Alaa El-Din, 2002), which in turn may influence learning and memory (El-Husseini Alaa El-Din and Bredt, 2002, El-Husseini Alaa El-Din, 2002, Hayashi T, 2005, Osten P *et al.*, 2000). In contrast, it has more recently been shown that lowering of synaptic activity increases PSD-95 palmitoylation and localization to the PM (Noritake *et al.*, 2009).

Other examples of dynamic regulation of neuronal proteins are abundant (Kang Rujun, 2008, Roth A. *et al.*, 2006). For example, binding of ligand to the β-adrenoreceptor markedly accelerates the depalmitoylation of the associated Gαs

subunit, which dampens G-protein signaling (Qanbar and Bouvier, 2003). Reversible palmitoylation regulates the cycling of Ras family GTPases to different membrane compartments, providing an important mechanism for controlling the signaling of many neurotrophic factors (Baker Tara L. *et al.*, 2000, Rocks Oliver *et al.*, 2005, Rocks Oliver *et al.*, 2006).

Notably, reversible palmitoylation has only been demonstrated for a small proportion of palmitoylated proteins thus far (Conibear and Davis, 2010), suggesting that this means of regulation does not apply to all palmitoylated proteins. The half-life of palmitate on proteins can vary widely, ranging from minutes to days, and this has important functional implications (Planey and Zacharias, 2009). For example, aberrant turnover is often seen in states of pathology; this is seen in an oncogenic form of H-Ras, which binds GTP with greater affinity than wildtype Ras. While steady-state palmitoylation remains unchanged, oncogenic H-Ras has a shorter palmitate half-life (thus increased signaling) than wildtype H-Ras (Baker Tara L. *et al.*, 2003).

Differential regulation via palmitoylation at different sites in the same substrate has been described in two ionotropic glutamate receptors (Hayashi T, 2005, Hayashi Takashi *et al.*, 2009). All AMPAR subunits are palmitoylated on two domains: their second transmembrane domain and in the C-terminal region. Palmitoylation in the first juxtamembrane region leads to Golgi accumulation of the receptor and reduced surface expression, whereas palmitoylation in the C-terminus reduces AMPAR interaction with the 4.1N protein and regulates AMPAR internalization (Hayashi T, 2005). NMDA receptor subunits, which play a critical role in synaptic plasticity and excitotoxicity in disease processes (Fan and Raymond, 2007), display two distinct C-terminal clusters of palmitoylation (Hayashi Takashi, 2009). Palmitoylation in the first cluster enhances Src-kinase-mediated tyrosine phosphorylation, leading to increased stability of surface NMDAR expression. Palmitoylation of these sites also plays an important role in regulation of constitutive internalization of NMDARSs in developing neurons. In

contrast, palmitoylation of the second cluster by distinct enzymes reduces NMDAR surface expression and increases localization to the Golgi. Given these examples, it is likely that differential palmitoylation-mediated regulation occurs for other substrates.

Alternative splicing has also been shown to play an important role in affecting protein palmitoylation status and function. For example, Cdc42, a small GTPase that directs neuronal morphogenesis, is normally prenylated. Brain-specific alternative splicing serves as a "switch" to yield a variant that becomes instead palmitoylated. While both isoforms are expressed in developing neurons, the palmitoylated isoform is required for the extension of dendritic filopodia, which later develop into dendritic spines (Kang Rujun, 2008).

The dynamic "on/off" nature of protein palmitoylation leads to its frequent comparison to another dynamic PTM, protein phosphorylation. In the latter, kinases and phosphatases regulate the addition and removal of phosphate groups from proteins; the opposing actions of enzymes that add and remove palmitate can rapidly modulate membrane targeting in response to extracellular cues. The enzymes that catalyse these reactions are further described below.

These various findings underline the fact that palmitoylation levels are tightly controlled *in vivo*, and that aberrant regulation of this process can affect a wide range of key proteins that influence an array of physiological processes, both in the brain and in the periphery.

1.1.2. Enzymes that modify palmitoylation

The first descriptions of protein palmitoylation (Schmidt *et al.*, 1979) and the first studies identifying the enzymes that catalyze the process (Lobo *et al.*, 2002, Roth Amy F. *et al.*, 2002) were separated by decades of repeated attempts at isolating and characterizing these enzymes (Greaves *et al.*, 2009, Mitchell *et al.*, 2006). During this intervening time, the existence of such enzymes remained

controversial (Dietrich and Ungermann, 2004). Spontaneous, autocatalytic palmitoylation had been observed to occur for some proteins *in vitro*, when incubated with acyl-CoA (e.g. SNAP-25) (Veit, 2000). However, this was not a universal process. Some proteins failed to undergo autoacylation under the same conditions, and not all reactions were observed to occur at physiological pH and acyl CoA concentrations (Zeidman, 2009). Almost a decade after the identification of the first enzymes that catalyze palmitoylation, the process is now believed to be enzymatically driven for the majority of proteins (Zeidman, 2009).

1.1.2.1. Palmitoyl-Acyl Transferases

In 2002, two landmark papers reported on the discovery of the enzymes that catalyze the addition of palmitate to proteins (Palmitoyl-Acyl Transferases, or PATs) in yeast. Erf2p and Erf4p together were identified to have *in vitro* PAT activity toward Ras2p (Lobo, 2002) and very soon after, Akr1p was identified as a PAT for Yck2p (Roth Amy F., 2002). Simultaneously, HIP14 was reported as the mammalian ortholog of Akr1p (Singaraja *et al.*, 2002), to be later identified as the first mammalian PAT (Huang *et al.*, 2004). The fact that these PATs all contained a highly conserved core DHHC (Asp-His-His-Cys) motif (Putilina *et al.*, 1999) suggested that other members of the DHHC protein family may also be PATs. A series of papers describing mammalian DHHC PAT orthologs soon followed (Fukata M *et al.*, 2004, Huang, 2004), as well as further characterization of the DHHC PATs in yeast (Roth A., 2006).

The DHHC PATs are multipass transmembrane proteins with four to six predicted transmembrane domains (TMDs), in contrast to prenyl- and myristoyl-transfereases, which are cytoplasmic (Conibear and Davis, 2010). The signature DHHC cysteine-rich domain is similar to the C_2H_2 zinc finger motif and consists of ~50-amino acids and resides on the cytoplasmic face of the membrane (Conibear and Davis, 2010, Greaves and Chamberlain, 2011, Mitchell, 2006, Putilina, 1999, Roth Amy F., 2002). The DHHC protein family is identified throughout evolutionary stages, found *in Saccharomyces cerevisiae, Arabidopsis thaliana,*

Drosophila melanogaster, Caenorhabditis elegans, Mus musculus, and Homo sapiens among others (Roth Amy F., 2002). Seven proteins are found in yeast, and 23 in mammals, all demonstrating distinct substrate specificities (Fukata M, 2004).

The DHHC domain in particular is highly conserved, and is essential for catalytic function both *in vitro* and *in vivo* (Mitchell, 2006). Although variants of the DHHC domain do occur (e.g. DHYC in yeast Akr1p), this domain is critical to PAT function, as mutation of this domain to AAYC or DHYA abolishes palmitoylation activity in Akr1p (Roth Amy F., 2002). PATs undergo autopalmitoylation on the active site cysteine in this motif; this is thought to serve as a transient acyl-enzyme intermediate prior to transfer of palmitate to the substrate. In accordance with this mechanism, mutation of this active site cysteine abolishes palmitoylation of both the enzyme and substrate. In addition, the enzymatic reaction requires membrane localization of the PAT (Mitchell, 2006).

DHHC PATs can be found largely on Golgi, ER, and endosomes but also on the PM (Ohno *et al.*, 2006). Their localization within the cell appears to be an important determinant of substrate specificity (Planey and Zacharias, 2009). However, determining the localization of DHHC PATs had yielded inconsistent findings, even within the same laboratory (Planey and Zacharias, 2009). The results appear to be affected by the stage of cell cycle, cell health and type, and the location of the epitope tag on the protein (Planey and Zacharias, 2009).

Because palmitoylation occurs in a wide range of soluble and transmembrane proteins, identifying a consensus sequence for protein palmitoylation has been challenging. This lack of consensus sequence is a trend seen in S-acylated substrates in general; however, some patterns have emerged (El-Husseini Alaa El-Din and Bredt, 2002). The distance between the target cysteine and the transmembrane domain, as well as the cysteine's predicted proximity to the membrane surface are found to be crucial for palmitoylation in integral membrane

proteins (Ten Brinke *et al.*, 2002). Transmembrane proteins (e.g. Synaptotagmin) are often palmitoylated at cysteines near the final transmembrane domain (El-Husseini Alaa El-Din and Bredt, 2002). Four to five residues surrounding the palmitoylated cysteine appears to be required in cytosolic proteins that are exclusively palmitoylated (e.g. PSD-95) (El-Husseini Alaa E, 2000a, El-Husseini Alaa El-Din and Bredt, 2002). Many palmitoylated cysteines are flanked by neighboring basic amino acids, a possible means to facilitate membrane association by binding of the acidic head groups of phospholipids.

In proteins that undergo both palmitoylation and another fatty acid modification, their additions are sequential (El-Husseini Alaa El-Din and Bredt, 2002). In this case, myristoylation or isoprenylation occur first; the weak membrane association brings the substrate in proximity with membrane-bound DHHC PATs for subsequent palmitoylation, which stabilizes the membrane association (El-Husseini Alaa El-Din and Bredt, 2002, Salaun, 2010, Shahinian and Silvius, 2003). Frequent examples include N-terminal dual palmitoylation and myristoylation, and C-terminal dual palmitoylation (El-Husseini Alaa El-Din and Bredt, 2002, Smotrys and Linder, 2004).

Effective palmitoylation appears to require close proximity of the palmitoylation site to the membrane, achieved when a target cysteine is either close to or inside a TMD, adjacent to other lipid modifications, or surrounded by basic or hydrophobic amino acids. All of these features would presumably bring the substrate in close proximity to the DHHC PAT, facilitating transfer of palmitate to the target cysteine (El-Husseini Alaa El-Din and Bredt, 2002, Salaun, 2010). The diverse number of features influencing palmitoylation suggests that three-dimensional structure, as opposed to sequence, may influence palmitoylation (Bijlmakers and Marsh, 2002).

Some of the DHHC PATs appear to display an affinity for particular types of substrate, such as a particular family of proteins, for proteins with cytoplasmic

cysteines adjacent to a TMD, or for heterolipidated proteins (Roth A., 2006). Akr1, the yeast ortholog of HIP14, appears to preferentially palmitoylate exclusively N- or C-terminally palmitoylated hydrophilic proteins (Roth A., 2006). The palmitoylation of some substrates appears remarkably dependent on a particular DHHC PAT (Roth A., 2006), whereas other proteins can clearly undergo palmitoylation by multiple PATs (Fukata M, 2004, Huang *et al.*, 2009, Salaun, 2010). Thus, DHHC PATs appear to demonstrate both specific and overlapping substrate specificities, and a particular substrate may be palmitoylated by one or many PATs. Whether all of these PAT-substrate pairings occur *in vivo* is unclear; deletion of a particular major PAT may drive palmitoylation by another PAT that would not occur under physiological circumstances (Salaun, 2010).

Despite the lack of a consensus sequence for palmitoylation, *in silico* prediction software has been developed. CSS-Palm is the most recent software available, and generates prediction of palmitoylation sites with a large training data set of known palmitoylated proteins using a cluster and scoring strategy (CSS) (Ren *et al.*, 2008). The authors declare the caveat that the software may not accurately predict certain types of palmitoylated substrates. As with all *in silico* prediction software, predicted sites should be experimentally verified (Kun Huang, personal communication).

Recent work has reported that while depalmitoylation appears to occur throughout the cell, palmitoylation only occurs on the Golgi. Rapid depalmitoylation allows mislocalized proteins to be redirected to the Golgi, thereby serving as a means of directional sorting of peripheral membrane proteins (Rocks Oliver *et al.*, 2010).

While the DHHC protein family catalyzes addition of palmitate to intracellular proteins, other PATs exist. A small subset of the membrane-bound-O-acyltransferase (MBOAT) family catalyzes the acylation of secreted proteins and

peptide substrates (Zeidman, 2009). A description of these proteins and their substrates is beyond the scope of this thesis but is reviewed elsewhere (Chang and Magee, 2009). The term PAT, therefore, refers to a member of the DHHC PAT family.

1.1.2.2. Acyl-Protein Thioesterases

Despite the impressive progress made in the discovery of the enzymes that catalyze palmitoylation enzymes over the past decade, progress in uncovering the enzymes that catalyze depalmitoylation has been limited. While palmitoylation is thought to be an enzymatic process for most proteins, autoacylation can occur. In contrast, removal of palmitate from proteins appears to be an enzymatic process, and is particularly important in proteins where palmitoylation appears dynamically regulated. In those substrates that are capable of undergoing autoacylation, the enzymatic removal of palmitate serves as a critical means of regulation (Zeidman, 2009).

To date, only two acyl protein thioesterases (APTs) have been identified to catalyze depalmitoylation: Acyl-protein thioesterase 1 (APT1) and Protein-Palmitoyl Thioesterase 1 (PPT1). APT1 is the only known cytoplasmic depalmitoylating enzyme (Hirano *et al.*, 2009, Lehtovirta *et al.*, 2001). It is expressed in a wide range of tissues (Toyoda *et al.*, 1999), and has been shown to depalmitoylate a growing list of proteins *in vitro*, including the Gα signaling molecules (Qanbar and Bouvier, 2003), Ras (Duncan and Gilman, 2002) and endothelial nitric oxide synthase (eNOS) (Yeh *et al.*, 1999), and cell-based experiments in yeast deficient in Apt1p have confirmed APT1 as a thioesterase (Yeh, 1999).

As described above, no defined consensus sequence for palmitoylation in PAT substrates exists (Smotrys and Linder, 2004), Similarly, there does not appear to be a defined recognition sequence for sites of APT1 depalmitoylation; the list of

APT1 substrates contains proteins that are structurally diverse and contain different combinations of lipid modifications (Zeidman, 2009). Nonetheless, there are examples of proteins for which APT1 does not catalyze deacylation (Yeh, 1999), and the efficiency of deacylation may be highly variable (Duncan and Gilman, 2002). Depalmitoylation activity is observed throughout the cell, and this has been suggested as a mechanism by which mislocalized proteins may be redirected within the cell (Rocks Oliver, 2010). While APT1 has no predicted transmembrane domains (Zeidman, 2009), a recent report suggests that APT1 itself may be palmitoylated, which may be a means to enable APT1 to interact with its membrane-associated targets (Yang W *et al.*, 2010).

A recent series of findings provides strong evidence suggesting an important role for APT1 *in vivo*. mRNA encoding APT1 was found to be downregulated by miRNA-138, mediating control of hippocampal dentritic spine morphogenesis (Siegel *et al.*, 2009). More recently, an inhibitor of APT1 was generated, palmostatin-B, which the authors used to interrupt the cycle of Ras acylation and demonstrate *in vivo* that APT1 mediates the release of H/N-Ras from the PM (Dekker *et al.*, 2010).

The crystal structure of APT1 reveals that it is a member of the alpha/beta hydrolase enzyme family and contains a “classic catalytic triad made up of Ser-114, His-203, and Asp-169” (Devedjiev *et al.*, 2000), and the high degree of conservation down to lower organisms implies a critical role for this enzyme (Zeidman, 2009).

A number of proteins, including many neuronal proteins, have been shown to be dynamically regulated by palmitoylation (Conibear and Davis, 2010, Salaun, 2010). APT1 is known to play an important role in synaptic function and spine morphogenesis, as knockdown of APT1 has been shown to suppress spine

enlargement (Siegel, 2009). Key neuronal proteins, such as HTT and PSD-95, have demonstrated rapid palmitate turnover rates; as such, APT1 remains a prime candidate in understanding the regulation of dynamic palmitoylation in these proteins. If APT1 is shown to play a significant role in the regulation of these proteins, the recent discovery of APT1 inhibitors will prove of great interest in the search for therapeutic approaches in HD and other diseases arising form aberrant palmitoylation (Dekker, 2010).

The second known APT is PPT1, a lysosomal thioesterase that cleaves fatty acids (usually palmitate) from cysteine residues (Camp and Hofmann, 1993), originally identified for its ability to depalmitoylate ^{3}H-palmitate labeled H-Ras (Camp and Hofmann, 1993). The lysosomal localization of PPT1 makes it unlikely to serve as a thioesterase for cytoplasmic proteins (Verkruyse and Hofmann, 1996). However, PPT1 has also been reported to localize to synaptosomes and synaptic vesicles in neurons (Heinonen *et al.*, 2000, Lehtovirta, 2001), and has also been shown to depalmitoylate a number of neuronal peptides (Cho Seongeun *et al.*, 2000) supporting a role for PPT1 in the CNS.

The normal function of PPT1 appears to be the removal of acyl chains from proteins undergoing degradation in the lysosome, and not in their removal as part of dynamic regulation going on in the cell. Mutations in PPT1 in humans results in a form of Batten disease known as Infantile Neuronal Ceroid Lipofuscinosis (INCL) (Vesa *et al.*, 1995), which features an accumulation of lysosomal autofluorescent deposits (Mitchison Hannah and Mole, 2001). PPT1 is now thought to serve a protective role against apoptosis, and INCL results from mutations that impair this function. This is further described in section 1.2.3.5 below. Despite its well-established role in human disease, the lysosomal localization of PPT1 makes it unlikely to serve as a cytoplasmic thioesterase.

The search for potential APTs continues. Two homologs of APT1 in mammals are potential thioesterase candidates. APT2 (lysophospholipase II), a homolog of APT1 with 64% identity, has been cloned (Toyoda, 1999), but the evidence that it serves as a thioesterase is still lacking and a yeast ortholog of APT2 does not appear to exist (Zeidman, 2009). Another identified homolog of APT1, lysophospholipase-like 1 (APTL1), which shares 31% identity with APT1 and contains the catalytic triad, is a thioesterase candidate but thus far has not been demonstrated to catalyze thioesterase activity (Gregory *et al.*, 2006). Finally, other members of the alpha/beta hydrolase family may emerge as potential depamitoylating enzymes.

1.1.2.3. Other influences on protein palmitoylation

In addition to the enzymatic regulation, there is mounting evidence that protein palmitoylation is also influenced by other post-translational modifications (Salaun, 2010). For example, many instances of co-regulation by palmitoylation and phosphorylation exist (Dorfleutner and Ruf, 2003, Hawtin *et al.*, 2001, Ponimaskin *et al.*, 2005, Soskic *et al.*, 1999). Phosphorylation may prevent palmitoylation of an adjacent cysteine, where the presence of the negatively charged phosphate group hinders membrane interaction with negatively-charged phospholipid heads (Salaun, 2010). Similarly, phosphorylation at a particular site within a protein may alter the rate of depalmitoylation of a nearby cysteine through altering access to thioesterases (Salaun, 2010).

On the other hand, palmitoylation of a substrate, leading to membrane association, may prevent protein kinases from accessing adjacent phosphorylation sites. For example, the PKA phosphorylation site of the C-terminal tail of a BK potassium channel variant known as STREK is known to mediate inhibition of the channel (Tian *et al.*, 2010). Palmitoylation of cysteines adjacent to the PKA site regulates PM binding of the C-terminal tail (Tian *et al.*, 2008). This palmitoylation-dependent PM association is disturbed upon PKA activation or phosphomimetic mutation at the PKA site; this was not observed

when the palmitoylated cysteines were mutated, suggesting that the phospho-regulation is mediated by palmitoylation changes (Salaun, 2010).

Protein nitrosylation can also influence palmitoylation. NO synthase enzymes (NOS) can generate nitric oxide from l-arginine and can directly modify cysteine residue via S-nitrosylation (Stamler *et al.*, 1992). Nitrosylation may alter palmitoylation either via competition for target cysteines or by direct displacement of palmitoyl moieties on palmitoylated cysteines (Salaun, 2010).

1.1.3. Palmitoylation and relevance to human disease

In recent years, it has become clear that the enzymes that regulate protein palmitoylation play a critical role in several biological processes, and when this is disturbed, can lead to disease. To date, seven PAT genes have been reported to be associated with human disease (Planey and Zacharias, 2009). In addition, other PAT genes have been associated with disease phenotypes in animal models (e.g. DHHC5, DHHC13 and DHHC21) (Li Y *et al.*, 2010, Mill *et al.*, 2009, Saleem *et al.*, 2010). Association with cancer and neurological disease appear to be major themes (Planey and Zacharias, 2009).

While PPT1 does not appear to play a major role in dynamic palmitoylation cycling, mutations in PPT1 lead to a well-described neurodegenerative phenotype in infants (Vesa, 1995). The possibility that APT1 is also implicated in disease processes can be inferred by its role as a thioesterase for key proteins involved in human cancers, such as H- and N-Ras (Duncan and Gilman, 2002). As research in the field of protein palmitoylation expands, the years to come will likely reveal further disease associations.

1.1.3.1. PATs implicated in cancers

Three DHHC PATs have been implicated in human cases of cancer. Lower expression of REAM (reduced expression associated with metastasis) on chromosome 8p21.3-22 was found to be associated with increased metastatic

potential, and lies within a region of chromosome 8 that is frequently deleted in colorectal and hepatocellular carcinoma (Oyama *et al.*, 2000). REAM was recently identified as DHHC2. Subsequent studies identified a substrate of DHHC2 that was frequently involved in bladder cancer (Zhang J *et al.*, 2008).

DHHC9 has been associated with a certain subtype of colorectal cancer tumours, showing high expression of transcript and protein in microsatellite-stable (as opposed to microsatellite instable) tumours (Mansilla *et al.*, 2007). Furthermore, gain of a region of chromosome 5 containing DHHC11 (5p15.33) is highly linked to disease progression and to advanced stage and high grade bladder cancer. Because this region also contains another gene, tubulin polymerization-promoting protein (TPPP), this function may be attributable in part to the presence of TPPP in the region of interest (Yamamoto *et al.*, 2007). Finally, while not associated with cases of cancer in humans, HIP14 (*ZDHHC17*) has been associated with oncogenic properties in cell culture and with tumour formation in mice (Ducker *et al.*, 2004). This and other roles for HIP14 is discussed further below in section 1.2.4.

1.1.3.2. PATs implicated in mental retardation

DHHC15 has been reported as a strong candidate for nonsyndromic X-linked mental retardation (XLMR). In the reported case of a 29 year old woman with severe nonsyndromic mental retardation, a balanced reciprocal translocation between chromosomes X and 15, very close to the DHHC15 gene, resulted in an absence of DHHC15 transcripts (Mansouri *et al.*, 2005).

Mutations in DHHC9, also in chromosome X, were found in 4 of 250 families with XLMR, though this finding was not validated in an assessment of DHHC9 enzyme expression nor functional assay. In three of these families, mental retardation was associated with a Marfanoid habitus (i.e. a body habitus resembling that of individuals with Marfan Syndrome, but falling short of the diagnostic criteria) (Raymond *et al.*, 2007).

1.1.3.3. PATs implicated in psychiatric illnesses

Microdeletions in chromosome 22q11 have been widely described and occur in 1/6000 births (Botto *et al.*, 2003). The phenotype is variable but can include neurodevelopmental delay, cognitive deficits, behavioural abnormalities, congenital heart defects, thymic hypoplasia, hypocalcemia, velopharyngeal defects, and facial dysmorphisms. Presence of certain subsets of these features can be grouped into characteristic syndromes recognized in the clinical literature (Drew *et al.*, 2010). A large proportion of these individuals will display neurodevelopmental and neuropsychiatric symptoms, and it is estimated that 25% will go on to develop schizophrenia in young adulthood (Karayiorgou and Gogos, 2004). In 2002, an association was reported between the *ZDHHC8* gene located in the 22q11 chromosomal region and schizophrenia. Significant association with three SNPs in DHHC8 was reported in US and South African populations (Liu *et al.*, 2002). Subsequently, one of these SNPs (rs175174) was reported to be significantly associated with schizophrenia in American and South African patients, particularly in female patients (Liu, 2002). This SNP was found to influence alternative splicing of *DHHC8*, resulting in retention of intron 4 and potentially reduced translation of DHHC8 or a dominant negative effect on the remaining allele. The same authors generated a *Dhhc8* knockout mouse and found similar sexual dimorphism; female mice demonstrated significant deficits in PPI and abnormalities in fear-related measures of spontaneous activity, features that were almost absent in male mice. The changes in behaviour were thought to arise at least in part from DHHC8 influence on glutamatergic transmission, as female *DHHC8*-null mice appeared less sensitive to a NMDA-receptor blocker (Mukai *et al.*, 2004). A follow-up study by the same group demonstrated that *DHHC8*-null mice have decreased density of dendritic spines, and expression of DHHC8 in these neurons rescued this phenotype to near-wildtype levels (Mukai *et al.*, 2008), confirming that the effects observed resulted from reduced levels of DHHC8.

In addition to schizophrenia, the region of chromosome 22 bearing *DHHC8* (22q11) has been significantly linked to bipolar disorder (Kelsoe *et al.*, 2001), but an association between DHHC8 and bipolar disease was not found (Otani *et al.*, 2005). Despite another study confirming an association between schizophrenia and DHHC8 in the Han Chinese population (Chen Wu-Yan *et al.*, 2004), several subsequent studies failed to identify this association in a number of different populations (Demily *et al.*, 2007, Glaser *et al.*, 2005, Glaser *et al.*, 2006, Otani, 2005, Saito *et al.*, 2005, Xu *et al.*, 2010). However, one group recently identified *ZDHHC8* polymorphisms associated with abnormalities in smooth eye movements, a common feature in schizophrenia (Shin *et al.*, 2010).

The inconsistent finding of an association may be partially attributed to the fact that studies were carried out in populations with different ethnic origins; it is possible that the association may be attributed to a closely linked genetic locus, and not DHHC8 itself. Nonetheless, the deficits seen in mice lacking DHHC8 would seem to support its role in neuropsychiatric deficits (Mukai, 2004), and highlighting that this association merits further study.

1.1.3.4. PATs implicated in neurodegenerative disease

A small number of studies have explored the role of palmitoylation in Alzheimer disease (AD) pathogenesis (Meckler *et al.*, 2010, Mizumaru *et al.*, 2009, Sidera *et al.*, 2005, Vetrivel *et al.*, 2009). Many of the proteins implicated in AD are palmitoylated, however the role of palmitoylation of these substrates in the pathogenesis of AD is less clear.

One study suggested a role for altered palmitoylation in the processing of proteins related to AD. β-secretase (BACE) cleaves amyloid precursor protein (APP) at cholesterol rafts. The authors noted that previous studies suggest that formation of Aβ (the toxic cleavage product of APP) was associated with a membrane bound, but not shed form of BACE and decreased BACE

palmitoylation leads to its displacement from membrane rafts, thus favouring the shed form. This study suggested that loss of BACE palmitoylation may be protective (Sidera, 2005).

However, contrasting findings were reported in a subsequent study (Vetrivel, 2009). Mutation of the four cysteine residues in BACE1 was sufficient to displace BACE1 from lipid rafts, and palmitoylation did not contribute to the subcellular localization of BACE1 nor of its protein stability (Vetrivel, 2009). Surprisingly, this altered localization of BACE1 does not appear to affect BACE1 processing of APP or Aβ secretion. In contrast to earlier studies, these findings suggested that palmitoylation of BACE1 and its localization to raft microdomains is not necessary for BACE1 cleavage of APP. This group suggested that the seemingly contradictory findings of the two studies may arise due to methodological differences (Vetrivel, 2009). The earlier study by Sidera *et al*. used cholesterol depletion to explore disruption of BACE1 localization to lipid raft microdomains. However, the multiple effects of cholesterol depletion on Golgi morphology, vesicular trafficking and membrane bulk fluidity complicate the interpretation of findings and their effect on cholesterol levels, APP trafficking, and BACE1 processing and how they influence one another (Abad-Rodriguez *et al.*, 2004).

γ-secretase acts in conjunction with β-secretase to generate the toxic APP cleavage product Aβ. γ-secretase consists of four subunits, presenilins (PS1 or PS2), PEN2, APH1, and nicastrin; the latter two are palmitoylated, and lack of palmitoylation destabilizes these substrates but does not alter γ-secretase processing of APP (Cheng *et al.*, 2009). Transgenic mice coexpressing palmitoylation-deficient APH1aL and nicastrin do not demonstrate impaired enzyme activity toward endogenous presenilin 1 and PEN2, and localization of γ-secretase subunits did not appear to be altered. When crossed to mice coexpressing variants of APP and presenilin 1 associated with familial AD, remarkable stabilization of transgenic presenilin 1 was observed in the brains of double transgenic mice. Mice expressing palmitoylation-deficient γ-secretase

subunits actually showed a reduction in amyloid deposits and insoluble Aβ40-42, as compared to mice overexpressing wt subunits, suggesting that γ-secretase palmitoylation can modulate amyloid deposits in AD brain (Meckler, 2010).

Another study showed that DHHC12 regulates APP trafficking and metabolism in multiple ways(Mizumaru, 2009). DHHC12 strongly inhibited APP metabolism and Aβ generation by retaining APP in the Golgi . However, this does not appear to be mediated by palmitoylation of APP itself, as APP lacks cytoplasmic cysteines normally associated with palmitoylation. Therefore, the authors concluded that APP is retained in the Golgi through means other than palmitoylation of APP. The authors identified a role for DHHC12 in regulating gamma-secretase activity, independent from its role in APP trafficking (Mizumaru, 2009). Possibly, this Golgi retention may occur through palmitoylation of another protein involved in this process. These studies in proteins related to AD together reiterate the complex but prominent role that palmitoylation serves in disease-related proteins, and in particular in relation to substrates involved in AD pathogenesis.

Finally, the importance of palmitoylation in neurodegenerative disease as it relates to HD is highlighted throughout this chapter but deserves brief mention here. HTT is palmitoylated at cysteine 214 by HIP14. The CAG-expanded form of HTT responsible for HD interacts less robustly with HIP14 (Singaraja, 2002), and is less robustly palmitoylated (Huang, 2004). Loss of palmitoylation is associated with increased cell death and inclusion formation, whereas HIP14 overexpression decreases inclusions (Yanai *et al.*, 2006). Most notably, mice lacking HIP14 recapitulate many phenotypes of HD mice, suggesting a possible role for HIP14 and palmitoylation in Huntington Disease pathogenesis (Singaraja *et al.* manuscript in preparation).

1.1.3.5. PPT1 and Batten Disease

In addition to the many DHHC-PAT disease associations, mutations in enzymes regulating palmitate removal can also result in disease. As described in section

1.1.2.2 above, mutations in the CLN1 gene on chromosome 1p32, coding for PPT1, results in INCL (Vesa, 1995). The neuronal ceroid lipofuscinoses are a group of genetically distinct diseases featuring an accumulation of lipofuscin (a granular autofluorescent lipopigment) and resulting in progressive blindness and neurodegeneration. INCL is a very early-onset form of NCL, featuring an infantile-onset neurodegeneration and loss of cortical neurons (Mitchison Hannah M *et al.*, 1998). After the crystal structure of PPT1 was identified, a correlation was observed between the severity of the INCL phenotype and the effect of the mutation on the catalytic site (Bellizzi III *et al.*, 2000).

The molecular mechanism of PPT1 deficiency appears to be activation of an apoptosis pathway in response to the accumulation of S-acylated proteins in the ER, as PPT1 knockout mice demonstrate an abnormal ER morphology and an accumulation of the palmitoylation substrate GAP-43 in the ER (Zhang Zhongjian *et al.*, 2005). Evidence that PPT1 may help protect against apoptosis stems from the observation of fewer neuroblastoma cells overexpressing PPT1 undergoing apoptosis after a chemotherapy treatment that caused apoptosis in control cells (Cho Seongeun and Dawson, 2000), and the observation that inhibition of PPT1 in the same neuroblastoma cells, either via PPT1 antisense or a PPT1 inhibitor, resulted in enhanced apoptosis (Cho Seongeun, 2000).

A PPT1 homolog, PPT2, is also a lysosomal thioesterase (Soyombo and Hofmann, 1997). While mutations in PPT2 in mice results in an NCL phenotype with slower onset and milder phenotype (Gupta *et al.*, 2001), the lack of substrate specificity toward palmitoylated proteins (Soyombo and Hofmann, 1997) together with a smaller lipid binding groove predicted by crystal structure (Calero, 2003) make it unlikely that PPT2 serves as a thioesterase for proteins undergoing degradation (Zeidman, 2009).

1.1.3.6. PAT involvement in dermatological and related abnormalities

Mutations in two DHHC PATs have been associated with skin and hair abnormalities, among other features. A single amino acid deletion in DHHC21 is responsible for the phenotype observed in a hair loss mutant mouse, depilated (dep). *dep* mice demonstrate variable hair loss and a greasy coat where thinner and shorter hairs remain. DHHC21 expression in the skin was restricted to particular hair lineages, noting that onset of expression correlated with appearance of abnormal morphology of hair follicles. Loss of DHHC21 resulted in hyperplasia of the interfollicular epidermis and sebaceous glands, as well as delayed differentiation of the hair shaft. The authors reported a member of the Src tyrosine protein kinases required for keratinocyte differentiation, Fyn, as a palmitoylation substrate of DHHC21. The DHHC21 mutation results in loss of palmitoylation activity and Fyn mislocalization (Mill, 2009).

DHHC13 mutant mice were identified in an N-ethyl-N-nitrosurea ENU mutagenesis screen. The mutation in DHHC13 was identified as a nonsense mutation in exon 12 of the *Zdhhc13* gene (c.1273A>T) resulting in a truncated protein (R425X). The resulting phenotype included a failure to thrive and impaired survival. Severe osteoporosis was observed, as well as skin and hair abnormalities such as alopecia. In addition, progressive amyloid deposition was found in the entire dermis as well as most other organs examined (Saleem, 2010). In addition, the authors obtained commercially available gene trap ES cells for *Zdhhc13*, and briefly report that a phenotype similar to ENU-mutagenesis-generated mice was observed (Saleem, 2010). Interestingly, our lab has also generated mice from the same gene trap vector (ES cell line AC0492) with significantly different findings, which we currently attribute to differences in mouse strain, which is widely known to significantly influence phenotype (Doetschman, 2009). Briefly, our Zdhhc13 mutant, generated on the FVB/N background to N5, demonstrates clear coat abnormalities and hair loss around the eye, a phenotype that resolved with antibiotic treatment. Failure to thrive or

survival deficits are not apparent; the mice are currently undergoing a more comprehensive assessment of neuropathology and behaviour (unpublished data).

1.1.3.7. Other phenotypes resulting from loss of PAT function

A mouse homozygous for a hypomorphic allele of DHHC5, generated using gene-trap-carrying ES cells, was recently described (Li Y, 2010). Enriched in the post-synaptic density, DHHC5 co-precipitates with PSD-95 and is expressed in the CA3 and dentate gyrus of the hippocampus. In homozygous mutant mice, a 50% reduction in expected births is observed. Moreover, surviving mice demonstrate reduced contextual fear conditioning, suggesting defective hippocampal-dependent learning. These results suggest a previously unexplored role for DHHC5 in learning and memory.

Disease class	Disease	Enzyme	References
Cancer	Hepatocellular carcinoma	DHHC 2	Oyama *et al.* 2000
	Colorectal cancer		
	Bladder cancer	DHHC 2	Zhang *et al.* 2008
	Colorectal cencer	DHHC 9	Mansilla *et al.* 2007
	Bladder cancer	DHHC 11	Yamamoto *et al.* 2007
	Oncogenic properties *in vitro*	DHHC 17	Ducker *et al.* 2004
X-linked mental retardation	XLMR with Marfanoid habitus	DHHC9	Raymond *et al.* 2007
	XLMR (nonsyndromic)	DHHC 15	Mansouri *et al.* 2005
Psychiatric disease	Schizophrenia	DHHC8	Liu *et al.* 2002, Mukai *et al.* 2004, Mukai *et al.* 2008, Shin *et al.* 2010
	Smooth eye movement abnormalities		
Neurodegenerative disease	Alzheimer Disease	DHHC 12	Mizumaru *et al.* 2009
	Huntington Disease	DHHC 17 (HIP14)	Singaraja *et al.* 2002, Huang *et al.* 2004, Yanai *et al.* 2006
Dermatological pathology	Hair loss & skin abnormalities	DHHC 21	Mill *et al.* 2009
	Hair & skin abnormalities, impaired survival, osteoporosis, amyloidosis	DHHC 13 (HIP14L)	Saleem *et al.* 2010, Liza Sutton (unpublished data)
Learning & memory	Impaired cognition, impaired survival	DHHC 5	Yi *et al.* 2010
Batten Disease	Infantile Neuronal Cereoid Lipofuscinosis (INCL)	PPT1	Vesa *et al.* 1995

Table 1.1 - PAT and APT involvement in disease processes. Table adapted from Fukata *et al.* 2010

1.2. Huntingtin Interacting Protein 14

1.2.1. General background

1.2.1.1. Huntington Disease

Huntington Disease (HD) is an autosomal dominant neurodegenerative disease that presents with cognitive, motor, and psychiatric signs and symptoms (Roos, 2010, Sturrock and Leavitt, 2010). Striatal volume loss and loss of medium spiny neurons (MSNs) of the striatum are key features of the disease (Vonsattel and Difiglia, 1998). HD results from an expansion of the CAG repeat in the HD gene of greater than 35, which results in a polyglutamine (poly-Q) expansion in the protein huntingtin (HTT) near the N-terminus of the protein (Huntington Disease Collaborative Research Group, 1993). The prevalence of HD in white populations is 5-7 per 100 000 individuals, with lower prevalence in some Asian and African populations (Walker, 2007).

1.2.1.2. Huntingtin and the search for huntingtin interacting proteins

HTT is a multi-domain protein whose function is unclear (Cattaneo *et al.*, 2005). The wildtype protein plays an important role in embryonic development (Dragatsis I *et al.*, 1998, Duyao *et al.*, 1995, Nasir *et al.*, 1995, Zeitlin *et al.*, 1995), transcription (Sugars and Rubinsztein, 2003), and protein trafficking (Caviston and Holzbaur, 2009), among others. HTT is now known to undergo many post-translational modifications, including palmitoylation (Huang, 2004), phosphorylation (Warby *et al.*, 2005), acetylation (Jeong *et al.*, 2009), and proteolysis (Gafni *et al.*, 2004, Graham *et al.*, 2006, Lunkes *et al.*, 2002, Wellington *et al.*, 1998). Despite the diverse roles reported for HTT in the cell, the exact function of the protein remains unclear (Cattaneo, 2005). HTT is ubiquitously expressed throughout both the periphery and within the CNS. Because HTT expression does not correlate with the pattern of cell loss observed in HD, the reason for selective pathology in these tissues is unclear. One

possible explanation could be particular interacting proteins within these tissues (for example a protein with selective expression within affected tissues) (Nasir, 1995).

The list of proteins that interact with HTT is vast (Harjes and Wanker, 2003); thus, several years ago, in an attempt to better delineate the pathways involved in HD pathogenesis, yeast-2-hybrid screens were designed to identify proteins whose interaction with HTT is altered in the presence of the CAG triplet repeat expansion known to cause HD (Faber *et al.*, 1998). HIP14 was first identified as part of these experiments (Faber, 1998, Kalchman *et al.*, 1996).

1.2.1.3. Identification of HIP14

HIP14 was first identified as part of a yeast-two-hybrid screen for HTT interactors (Faber, 1998, Kalchman, 1996). HIP14 was selected for further study, as its interaction with HTT was found to be inversely correlated with CAG length, suggesting a potentially important role in HD pathogenesis (Singaraja, 2002). Moreover, HIP14 was shown to be enriched in the brain and to be expressed in MSNs, the affected cell population in HD.

HIP14 protein displays sequence similarity to Akr1p, an essential protein for endocytosis in *S. cerevisiae*. Expression of human HIP14 was sufficient to rescue temperature-sensitive lethality and restore defects in endocytosis in yeast cells lacking Akr1p. These findings suggested a role for HIP14 in intracellular trafficking (Singaraja, 2002). The *D. melanogaster* ortholog of HIP14, CG6017 was identified as a gene controlling synaptogenesis and embryonic motor axon guidance prior to the first formal descriptions of HIP14 in mammals (Kraut *et al.*, 2001).

Two mRNA transcripts of the *HIP14* gene of 9 and 6Kb were reported, the latter with predominant expression in the brain (Singaraja, 2002). Human *HIP14* mRNA is expressed most highly in the brain, with highest-to-lowest expression ranging

from cerebellum, cortex, occipital lobe, frontal lobe, medulla, putamen, temporal lobe, and finally lowest expression in the spinal cord. In peripheral tissues, after brain, *HIP14* is expressed most highly in heart, followed by pancreas, kidney, skeletal muscle, lung, and liver. Notably, appreciable expression is seen in the placenta (Singaraja, 2002). A subsequent study reported on *HIP14* mRNA expression in humans: highest levels were found in kidney, testis, thymus, brain and placenta. Moderate levels were detected in heart, liver, and lung, with relatively low levels in skeletal muscle, small intestine, and leukocytes. The authors concluded that *HIP14* expression is ubiquitous (Ohno, 2006).

HIP14 protein is expressed in all brain regions, with highest expression in the cortex, caudate, temporal lobe, cerebellum, and occipital lobe, with weaker expression in the putamen and lowest expression in the spinal cord (Singaraja, 2002). Peripherally, expression is seen in testis, pancreas, heart and kidney, with no detectable expression in the lung (Singaraja, 2002). Interestingly, while HIP14 is expressed in the liver in mice, it does not appear to be expressed in human liver (Singaraja, 2002).

In the striatum, HIP14 partially co-localizes with HTT. Within the cell, HIP14 localizes to Golgi and vesicles of the cytoplasm (Singaraja, 2002). In a *D. melanogaster* study, the HIP14 ortholog dHIP14 was reported at the presynapse and found to play a critical role in presynaptic function (Ohyama *et al.*, 2007). In a second study on dHIP14 mutants, dHIP14 was reported to co-localize with presynaptic markers; Golgi colocalization was observed only in non-neuronal cells. However, further assessment in HIP14-GFP transfected cultured mammalian neurons reveals colocalization with both cellular structures (Stowers and Isacoff, 2007). The original description of HIP14 localization to the Golgi assessed localization of the endogenous protein by EM imaging (Singaraja, 2002), and subsequent studies have substantiated this finding (Huang, 2009, Ohno, 2006). The cumulative findings reveal that HIP14 localizes to Golgi, as well as to presynaptic and cytoplasmic vesicles.

The official name for the *HIP14* gene in humans is *ZDHHC17*. Alternate names include DHHC17, HIP3, HYPH, HSPC294 , and KIAA0946 (NCBI Gene ID 23390). In mice, the official gene name is *Zdhhc17;* alternatives include *Hip14, dhhc17*, and less commonly BB187739, KIAA0946, A230053P19Rik, or D130071N24Rik (NCBI Gene ID: 320150).

A search of databases revealed a human EST clone for a gene homologous to HIP14 on chromosome 11, encoding a protein with 48% identity and 57% similarity to HIP14 (Singaraja, 2002). This protein was designated *HIP14-related protein* (*HIP14L*). The official gene name for *HIP14L* is *ZDHHC13,* alternately called DHHC13 or HIP14-RP.

HIP14 and HIP14L are highly similar members of a family of 23 DHHC-domain containing putative PATs (Greaves and Chamberlain, 2011, Mitchell, 2006). Notably, HIP14 and HIP14L are the only DHHC PATs to contain ankyrin domains, which are tandemly repeated 33aa sequences that are known to mediate protein-protein interactions and thought to play a role in substrate recognition (Li Junan *et al.*, 2006).

For the remainder of this thesis, the genes *ZDHHC17 and Zdhhc17* are referred to as *HIP14* (human) and *Hip14* (mouse). Similarly, the genes *ZDHHC13 and Zdhhc13* are referred to as *HIP14L* (human) and *Hip14L* (mouse).

1.2.2. HIP14 is a palmitoyl-acyl transferase

HIP14 was formally characterized as a PAT by the labs of the late Alaa El-Husseini and Michael Hayden (Huang, 2004). HIP14 was reported to enhance palmitoylation-dependent trafficking of several proteins in neurons, and siRNA interference with HIP14 endogenous expression in neurons reduced the clustering of PSD-95 and GAD65 (Huang, 2004). This study was the first of many to explore the role of HIP14 as a PAT and its importance normal biology as well as its potential role in human disease.

1.2.2.1. Protein substrates for palmitoylation by HIP14

The first palmitoylation substrates of HIP14 were reported as part of its initial characterization as a PAT. The neuronal proteins PSD-95, SNAP-25, GAD65, synaptotagmin 1, and HTT were all shown to be palmitoylated by HIP14, whereas paralemmin and synaptotagmin VII were shown to not be palmitoylation substrates of HIP14 (Huang, 2004). The same year, another report identified Lck as an additional HIP14 substrate, finding that HIP14 displayed no PAT activity toward PSD-95, GAP-43, and G-alpha (Fukata M, 2004). Despite these contradictory findings, subsequent reports clearly demonstrate that HIP14 can serve as a PAT for PSD-95 (Huang, 2004, Huang, 2009). It is possible that this may not be the case in all assay conditions.

Two papers published in close succession reported on the effects of disruption of the HIP14 ortholog, dHIP14, in *D. melanogaster* (Ohyama, 2007, Stowers and Isacoff, 2007). dHIP14 mutants were identified as part of genetic screens; mutation in dHIP14 was found to result in loss of CSP palmitoylation and mislocalization, consistent with reports in mammalian cells (Greaves *et al.*, 2008).

Interestingly, both groups reported a presynaptic localization, either on synaptic vesicles (Stowers and Isacoff, 2007) or presynaptic plasma membrane (Ohyama, 2007), conflicting with earlier reports of Golgi localization (Singaraja, 2002). One possibility for the discrepancy with earlier studies is species differences. Notably, these later studies did not assay palmitoylation through direct biochemical experiments but rather by examining changes in protein localization; in this regard, the finding that PSD-95 and Syt1 localization were unchanged in dHIP14 mutants is difficult to interpret (Ohyama, 2007). More recently, dHIP14 has been described as a PAT for the BMP antagonist Sog (Short Gastrulation). dHIP14 binds to and palmitoylates Sog, stabilizing its membrane association and promoting its secretion in S2 cells (Kang Kyung-Hwa and Bier, 2010).

In 2006, a more detailed characterization of HIP14 palmitoylation of HTT was described. Briefly, downregulation of HIP14 in mouse neurons expressing wildtype and mutant HTT increased inclusion formation, while overexpression of HIP14 reduced inclusion formation (Yanai, 2006). In addition, cysteine 214 (C214) was identified as the major site of palmitoylation in HTT. When this site is mutated such that palmitoylation cannot occur, altered trafficking of HTT and an exacerbation of many *in vitro* features typical of HD, such as enhanced inclusions and increased toxicity are observed.

In addition to evidence in support of HIP14 substrates, a number of studies have reported on substrates that are not palmitoylated by HIP14. These include Paralemmin and Synaptotagmin VII (Huang, 2004), the γ-2 subunit of $GABA_A$ (Fang *et al.*, 2006), and GAP-43, Gα, and PSD-95 (Fukata M, 2004). Notably, while a number of DHHC PATs have been reported for PSD-95, there exists some debate as to whether these include HIP14. The apparent discrepancies in findings between studies may arise in the different experimental methodology used; HIP14 has been shown to act as a PAT for PSD-95, though this may not be true in all physiological contexts.

Interestingly, as further substrates for HIP14 have been identified, it appears that many are palmitoylated on internal cysteine-rich domains (Greaves and Chamberlain, 2011). This observation may be kept in mind in the search for further HIP14 substrates.

Reported palmitoylation substrates of HIP14	
Substrate	**Reference**
Cysteine String Protein (CSP)	Greaves J. *et al.* 2008
GAD65	Huang K. *et al.* 2004 and 2009
GluR1	Huang K. *et al*. 2009
GluR2	Huang K. *et al.* 2009
Huntingtin (HTT)	Yanai *et al.* 2006 and Huang K. *et al* 2009
Lymphocyte-specific protein tyrosine kinase (Lck)	Fukata M. *et al.* 2004
PSD-95	Huang K. *et al.* 2004 and 2009, Singaraja *et al.* 2011
SNAP-23	Greaves J. *et al.* 2010
SNAP-25	Greaves J. *et al.* 2010, Fukata *et al.* 2005 (isoform b), Huang *et al. 2009,* Singaraja *et al.* 2011
STREX	Tian L. *et al.* 2010
Synaptotagmin I	Kang R. *et al.* 2004
Short Gastrulation (Sog)-Drosophila	Kang K.H. *et al.* 2010

Table 1.2– Palmitoylation substrates of HIP14. A summary of palmitoylation substrates of HIP14. Table adapted from Greaves J *et al. 2010*.

1.2.2.2. HIP14 is a major PAT for HTT

As described above, HTT was identified as a substrate for HIP14 in 2004. Subsequently, Yanai et al. identified the major site of palmitoylation of HTT as cysteine 214. Mutation of this site to serine, rendering it palmitoylation-resistant, resulted in increased inclusion formation and increased neuronal toxicity. siRNA-mediated downregulation in neurons similarly results in increased inclusion formation. In contrast, overexpression of HIP14 significantly reduced inclusion formation. Finally, HTT palmitoylation was found to be reduced in brain of a YAC128 mouse model of HD. All of these findings combined suggested a protective role for HTT palmitoylation and for HIP14. Thus, enhancement of HIP14 function through overexpression was seen as a potential avenue to pursue in the search for therapeutic pathways to treat HD (Yanai, 2006). Most recently, HIP14L has been identified to be another major PAT for HTT (Huang, 2009).

1.2.2.3. HTT as a cofactor for HIP14

A unique role for HTT in the function of HIP14 as a PAT has recently been identified (Huang *et al.*, 2011). In addition to its palmitoylation at C214, wt HTT appears to modulate the palmitoylation of HIP14 itself. Palmitoylation of HIP14 was reduced in the brains of mice expressing one half the endogenous levels of wt HTT, and was further reduced in mouse cortical neurons in which HTT expression was knocked down via antisense oligonucleotides by 95%. Palmitoylation of HIP14 substrates was enhanced in the presence of wt, but not mutant, HTT *in vitro*. Palmitoylation still occurred in the absence of co-transfection with HTT, but was far less robust. *In vivo*, reduced expression of endogenous wt HTT resulted in reduced palmitoylation of HIP14 substrates in a dose-dependent manner.

Thus, wildtype HTT, but not mutant HTT, appears to modulate the palmitoylation of HIP14 itself and its enzymatic activity. In addition to serving as a palmitoylation substrate of HIP14, HTT may mediate this function as an allosteric activator of HIP14, influencing its three-dimensional structure and facilitating access to substrates. Alternatively, HTT serve as a scaffolding protein in binding HIP14 substrates and bringing them in close proximity with HIP14 to facilitate palmitoylation. Finally, HTT may facilitate trafficking of vesicles containing HIP14 to sites where HIP14 is active (Huang, 2011).

1.2.3. Structure of HIP14

An examination of gene structure may lead to insights into its function, both through similarity to other genes and identification of gene or protein motifs that may inform function. A description of the current knowledge on *HIP14* genomic and protein structure is described in the following sections.

1.2.3.1. Genomic structure of HIP14

A comparison of general features of human and mouse *HIP14* is shown in table 1.1 below. A comparison of human and mouse mRNA reveals 87% identity. The

overall structure of the two genes is similar. In both species, *HIP14* resides 5' to a neighboring gene CSRP2.

Previous reports described a major 6kb transcript for *HIP14* and an additional minor transcript at 9kb (Singaraja, 2002). There is no clear experimental evidence to support alternative isoforms of HIP14 at this time, although a comprehensive study in this area would be highly valuable.

	RefSeq Gene Record	Assembly	Chromosomal location	UCSC Genome Browser Location	Genomic size	Number of exons	mRNA size
Human	ZDHHC17	Feb. 2009 (GRCh37/hg19)	12 (12q21.2) + strand	chr12: 77157854-77247474	89,621 (bp)	17	4,771bp (NM_015336.2)
Mouse	Zdhhc17	July. 2007 (NCBI37/mm9)	10 (10qD1) - strand	chr10: 110378836-110447122	68,287 (bp)	17	4,563bp (NM172554.2)

Table 1.3 – Genomic comparison of human and mouse HIP14. The information summarized is obtained from the UCSC Genome Browser.

1.2.3.2. Protein structure of HIP14

HIP14 is a multipass transmembrane protein, containing 7 ankyrin repeats (Gao *et al.*, 2009) followed by 6 predicted transmembrane domains. The signature active site, the DHHC domain, is located between the 4th and 5th transmembrane domain. Both the ankyrin domains and the DHHC domain are predicted to reside on the cytoplasmic face of the membrane, allowing protein recognition (via ankyrin domains) and enzyme function (mediated via the DHHC domain) to occur on the same side of the membrane (Gao, 2009). Notably, the signature DHHC domain occurs as DHYC in yeast Akr1p (Roth Amy F., 2002) Both HIP14 and the related HIP14L appear to bind substrates via their ankyrin repeats during palmitoylation; this interaction is unimpaired by mutation of the catalytic DHHC domain (Huang, 2011).

The HIP14 protein is a 632aa (622 aa in mouse) protein highly conserved throughout evolution. Human and mouse HIP14 proteins are 98% identical. Their main difference lies in an extra 10 amino acids on the N-terminus of the human protein. *D. melanogaster*, dHIP14 (CG6017) shares 44% identity and 59% similarity with the human protein (Andrews, 2006), whereas Akr1p in yeast shares 24% identity and 40% similarity (Kao *et al.*, 1996). A sequence alignment highlighting the high level of sequence conservation across species as well as important functional regions within HIP14 is shown in Figure 1.1.

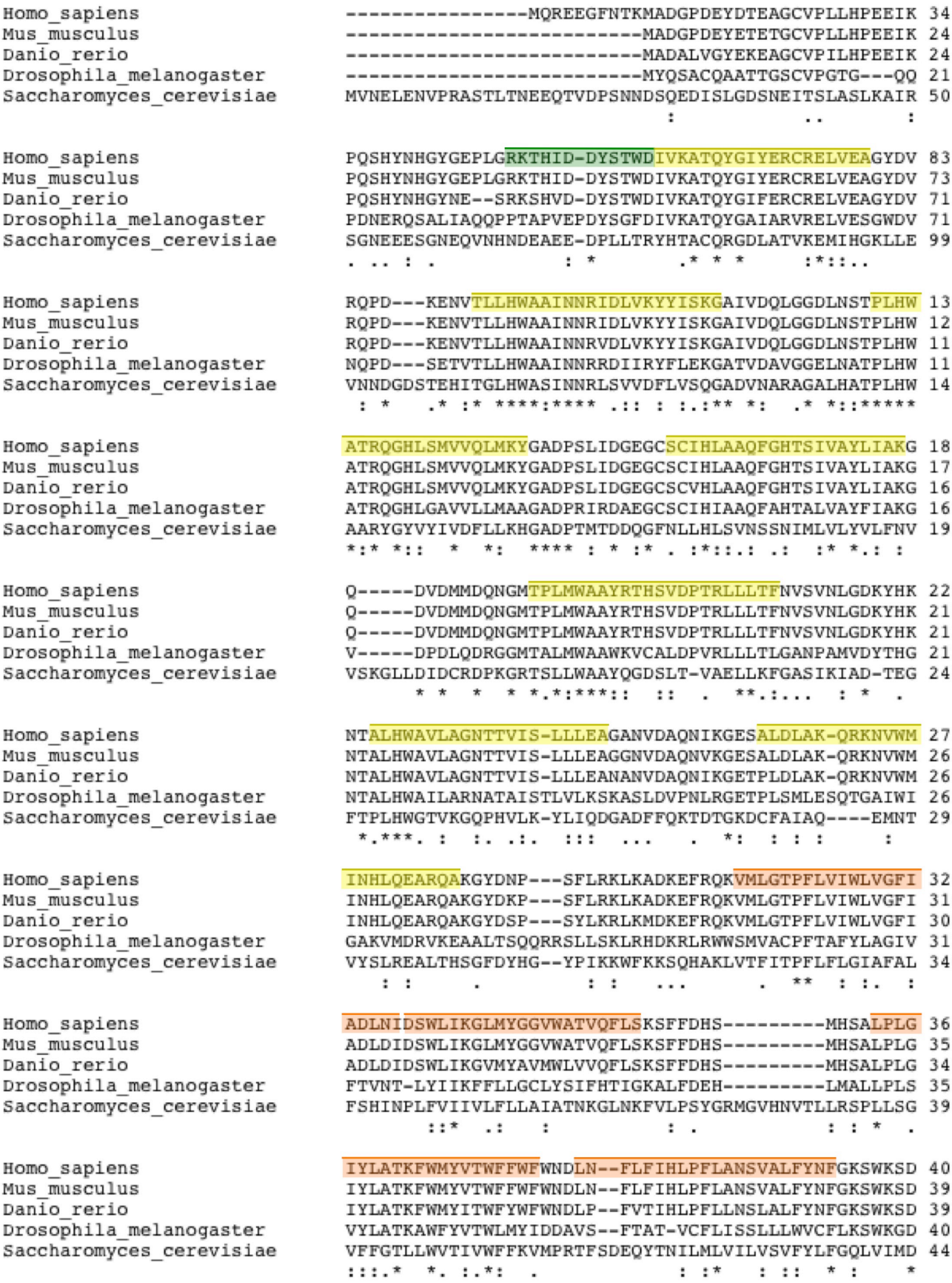
Homo_sapiens ----------MQREEGFNTKMADGPDEYDTEAGCVPLLHPEEIK 34
Mus_musculus ----------MADGPDEYETETGCVPLLHPEEIK 24
Danio_rerio ----------MADALVGYEKEAGCVPILHPEEIK 24
Drosophila_melanogaster ----------MYQSACQAATTGSCVPGTG---QQ 21
Saccharomyces_cerevisiae MVNELENVPRASTLTNEEQTVDPSNNDSQEDISLGDSNEITSLASLKAIR 50
Homo_sapiens PQSHYNHGYGEPLGRKTHID-DYSTWDIVKATQYGIYERCRELVEAGYDV 83
Mus_musculus PQSHYNHGYGEPLGRKTHID-DYSTWDIVKATQYGIYERCRELVEAGYDV 73
Danio_rerio PQSHYNHGYNE--SRKSHVD-DYSTWDIVKATQYGIFERCRELVEAGYDV 71
Drosophila_melanogaster PDNERQSALIAQQPPTAPVEPDYSGFDIVKATQYGAIARVRELVESGWDV 71
Saccharomyces_cerevisiae SGNEEESGNEQVNHNDEAEE-DPLLTRYHTACQRGDLATVKEMIHGKLLE 99
Homo_sapiens RQPD---KENVTLLHWAAINNRIDLVKYYISKGAIVDQLGGDLNSTPLHW 130
Mus_musculus RQPD---KENVTLLHWAAINNRIDLVKYYISKGAIVDQLGGDLNSTPLHW 120
Danio_rerio RQPD---KENVTLLHWAAINNRVDLVKYYISKGAIVDQLGGDLNSTPLHW 118
Drosophila_melanogaster NQPD---SETVTLLHWAAINNRRDIIRYFLEKGATVDAVGGELNATPLHW 118
Saccharomyces_cerevisiae VNNDGDSTEHITGLHWASINNRLSVVDFLVSQGADVNARAGALHATPLHW 149
Homo_sapiens ATRQGHLSMVVQLMKYGADPSLIDGEGCSCIHLAAQFGHTSIVAYLIAKG 180
Mus_musculus ATRQGHLSMVVQLMKYGADPSLIDGEGCSCIHLAAQFGHTSIVAYLIAKG 170
Danio_rerio ATRQGHLSMVVQLMKYGADPSLIDGEGCSCVHLAAQFGHTSIVAYLIAKG 168
Drosophila_melanogaster ATRQGHLGAVVLLMAAGADPRIRDAEGCSCIHIAAQFAHTALVAYFIAKG 168
Saccharomyces_cerevisiae AARYGYVYIVDFLLKHGADPTMTDDQGFNLLHLSVNSSNIMLVLYVLFNV 199
Homo_sapiens Q-----DVDMMDQNGMTPLMWAAYRTHSVDPTRLLLTFNVSVNLGDKYHK 225
Mus_musculus Q-----DVDMMDQNGMTPLMWAAYRTHSVDPTRLLLTFNVSVNLGDKYHK 215
Danio_rerio Q-----DVDMMDQNGMTPLMWAAYRTHSVDPTRLLLTFNVSVNLGDKYHK 213
Drosophila_melanogaster V-----DPDLQDRGGMTALMWAAWKVCALDPVRLLLTLGANPAMVDYTHG 213
Saccharomyces_cerevisiae VSKGLLDIDCRDPKGRTSLLWAAYQGDSLT-VAELLKFGASIKIAD-TEG 247
Homo_sapiens NTALHWAVLAGNTTVIS-LLLEAGANVDAQNIKGESALDLAK-QRKNVWM 273
Mus_musculus NTALHWAVLAGNTTVIS-LLLEAGGNVDAQNVKGESALDLAK-QRKNVWM 263
Danio_rerio NTALHWAVLAGNTTVIS-LLLEANANVDAQNIKGETPLDLAK-QRKNVWM 261
Drosophila_melanogaster NTALHWAILARNATAISTLVLKSKASLDVPNLRGETPLSMLESQTGAIWI 263
Saccharomyces_cerevisiae FTPLHWGTVKGQPHVLK-YLIQDGADFFQKTDTGKDCFAIAQ----EMNT 292
Homo_sapiens INHLQEARQAKGYDNP---SFLRKLKADKEFRQKVMLGTPFLVIWLVGFI 320
Mus_musculus INHLQEARQAKGYDKP---SFLRKLKADKEFRQKVMLGTPFLVIWLVGFI 310
Danio_rerio INHLQEARQAKGYDSP---SYLKRLKMDKEFRQKVMLGTPFLVIWLVGFI 308
Drosophila_melanogaster GAKVMDRVKEAALTSQQRRSLLSKLRHDKRLRWWSMVACPFTAFYLAGIV 313
Saccharomyces_cerevisiae VYSLREALTHSGFDYHG--YPIKKWFKKSQHAKLVTFITPFLFLGIAFAL 340
Homo_sapiens ADLNIDSWLIKGLMYGGVWATVQFLSKSFFDHS---------MHSALPLG 361
Mus_musculus ADLDIDSWLIKGLMYGGVWATVQFLSKSFFDHS---------MHSALPLG 351
Danio_rerio ADLDIDSWLIKGVMYAVMWLVVQFLSKSFFDHS---------MHSALPLG 349
Drosophila_melanogaster FTVNT-LYIIKFFLLGCLYSIFHTIGKALFDEH---------LMALLPLS 353
Saccharomyces_cerevisiae FSHINPLFVIIVLFLLAIATNKGLNKFVLPSYGRMGVHNVTLLRSPLLSG 390
Homo_sapiens IYLATKFWMYVTWFFWFWNDLN--FLFIHLPFLANSVALFYNFGKSWKSD 409
Mus_musculus IYLATKFWMYVTWFFWFWNDLN--FLFIHLPFLANSVALFYNFGKSWKSD 399
Danio_rerio IYLATKFWMYITWFYWFWNDLP--FVTIHLPFLLNSLALFYNFGKSWKSD 397
Drosophila_melanogaster VYLATKAWFYVTWLMYIDDAVS--FTAT-VCFLISSLLLWVCFLKSWKGD 400
Saccharomyces_cerevisiae VFFGTLLWVTIVWFFKVMPRTFSDEQYTNILMLVILVSVFYLFGQLVIMD 440

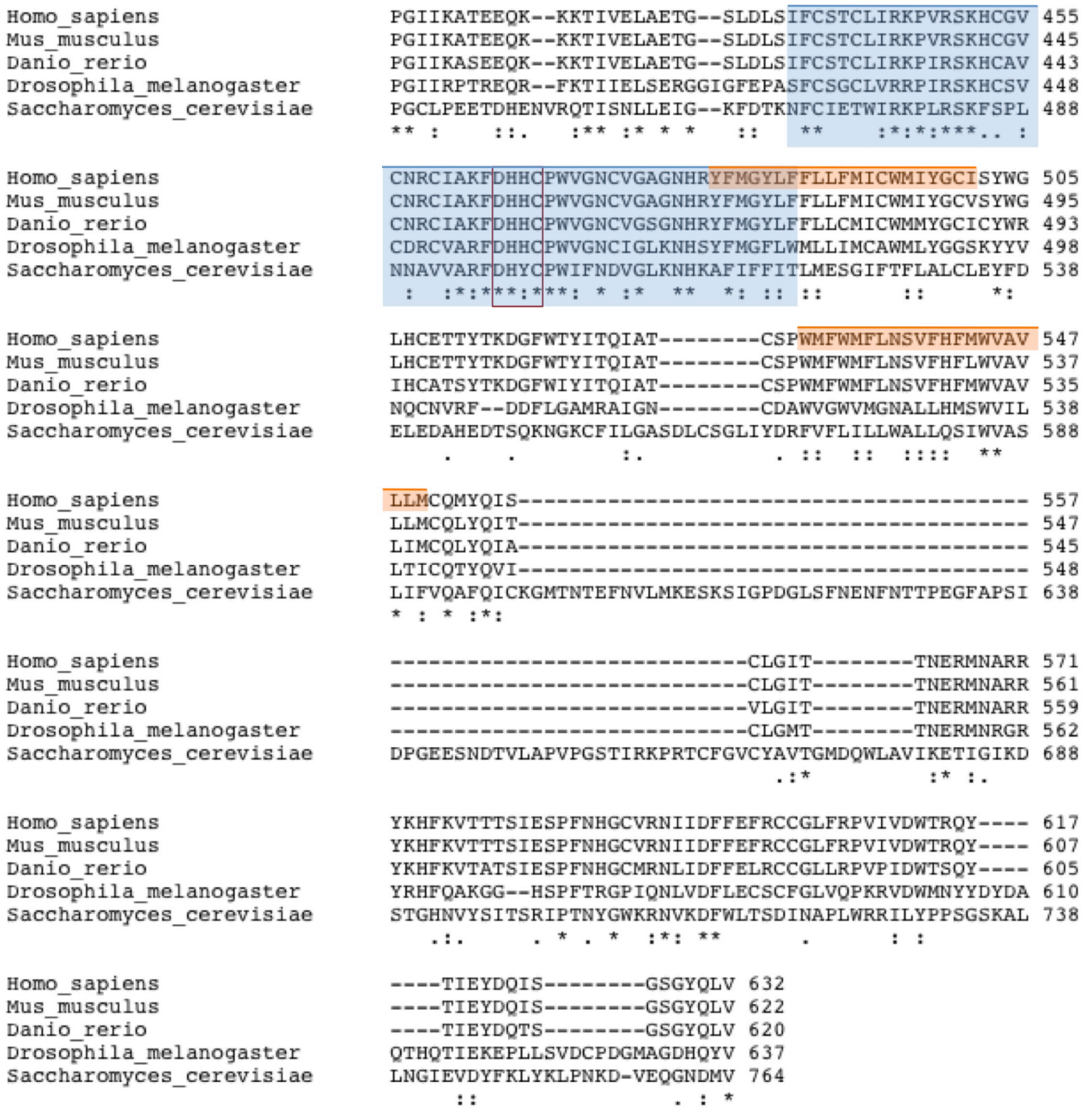

Figure 1.1 - HIP14 protein sequence alignment in multiple species. Alignment of human HIP14 and HIP14 orthologs in *Mus musculus* (mouse), *Danio rerio* (zebrafish), *Drosophila melanogaster* (fruit fly), and *Saccharomyces cerevisiae* (yeast). The conserved DHHC motif is shown in a red box; the full cysteine-rich DHHC domain is shaded in light blue. Predicted transmembrane domains are shaded in orange according to Uniprot (http://www.uniprot.org/uniprot/Q8IUH5). Predicted Ankyrin repeats are shaded in orange according to Gao *et al.* 2009. * indicates that the residues or nucleotides in that column are identical in all sequences in the alignment. : indicates that conserved substitutions have been observed, and . indicates that semi-conserved substitutions are observed. The PEP1 epitope of the HIP14 antibody used for western blot analysis in this thesis is also shown shaded in green.

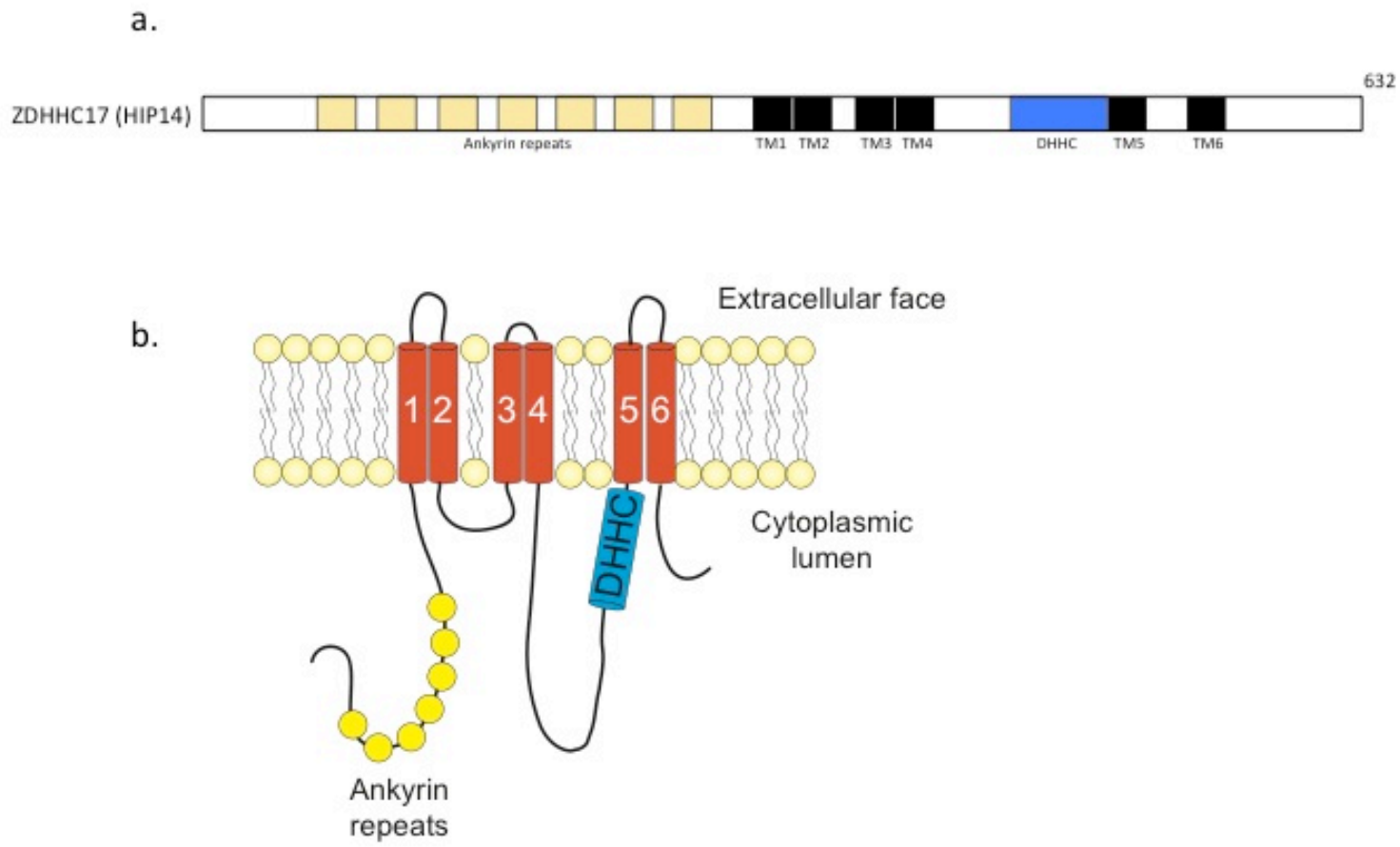

Figure 1.2 - Schematic of the HIP14 protein. a. A linear schematic illustrates the seven ankyrin repeats (yellow boxes), transmembrane domains (black boxes), and conserved DHHC domain (blue box). **b.** A schematic of HIP14 membrane topology. The ankyrin repeats and DHHC domain lie on the cytoplasmic face, where palmitoylation of substrates occurs.

1.2.4. Other roles for HIP14

HIP14 is well characterized to function as a palmitoyl-acyl transferase, but following its initial characterization, other novel roles for HIP14 have been reported.

1.2.4.1. HIP14 as a potential oncogene

Soon after its initial characterization, HIP14 was reported to have oncogenic properties (Ducker, 2004). The authors reported that HIP14 demonstrated a preference for a farnesyl-dependent palmitoylation motif found in H- and N-Ras, correlating high palmitoylation activity with high expression of HIP14 and inhibition of this phenomenon with siRNA knockdown of HIP14. Mutation of the active site cysteine appeared to abolish palmitoylation activity, as assessed by HPLC. The authors reported anchorage-independent growth and increase in colony formation in HIP14-transfected 3t3-3 cells *in vitro*. In addition, the authors injected HIP14-transfected cells subcutaneously into NOD/SCID mice and observed tumour formation. HIP14 siRNA injection into these tumours markedly slowed the growth of tumours compared to control-injected mice. Western blot analysis revealed higher HIP14 expression in untreated tumours compared with the cells used for injection, suggesting upregulation of HIP14 in the tumour environment. These findings are interesting in light of reports of other DHHC PAT involvement in cancers described above (Section 1.1.3.1), suggesting that a common theme may be emerging. Nonetheless, further reports of ZDHHC17 involvement in cancer have not since emerged.

1.2.4.2. HIP14 as a potential magnesium transporter

Most recently, HIP14 (and the related HIP14L) has been proposed to act as a Mg^{2+} transporter (Goytain *et al.*, 2008). The authors reported increased HIP14 mRNA and protein expression in cells grown with low Mg^{2+}. HIP14 and HIP14L expressed in Xenopus oocytes facilitated Mg^{2+} uptake, and growth of transfected cells in low magnesium medium appeared to increase HIP14-GFP and HIP14L-

GFP localization to Golgi complex and post-Golgi vesicles. Treatment with 2-Bromopamitate (2BP) or deletion of the HIP14 catalytic DHHC domain resulted in reduced Mg^{2+} transport. The authors did not directly assess HIP14 palmitoylation, but the results were supportive of a role for HIP14 and HIP14L in Mg^{2+} transport. Whether mediated directly or via critical palmitoylation of another protein that may mediate this transport is unclear. The same group has since reported on another PAT, DHHC3 (GODZ), which they propose mediates Ca^{2+}transport (Hines *et al.*, 2010). While controversial, these findings bring attention to alternate potential roles for DHHC PATs and suggest that these findings may warrant further investigation.

1.2.4.3. HIP14 in the TGFβ pathway

A yeast two hybrid screen identified the short gastrulation (Sog) protein in *D. melanogaster* as a possible interactor of dHIP14 (Giot *et al.*, 2003). Because Sog is a component of the TGFβ signaling pathway, investigators at Simon Fraser University assessed what role dHIP14, which they named “Pinguid”, might play in this signaling, with a focus on wing development.

dHIP14 was overexpressed under a series of Gal4 drivers in the wing at different stages and in different wing components. In all cases, pathological changes were observed in wing vein patterning and in one case reduced survival was accompanied the very severe wing phenotype. The patched-Gal4 fly, which presented the mildest wing phenotype, was selected and crossed to other TGFβ signaling mutants to identify whether any of the latter could suppress or enhance the phenotype. Their findings suggested that dHIP14 may enhance TGFβ activity, and that this may be mediated via the Baboon-dSmad2 signalling pathway. Ectopic expression of dHIP14 in the wing revealed genetic interactions with *short gastrulation (Sog), crossveinles-2, baboon,* and the *ecdysone receptor* (Andrews, 2006). A subsequent study reported dHIP14 as a PAT for Sog, promoting stability in membrane association and secretion of Sog in S2 cells (Kang Kyung-Hwa and Bier, 2010). Interestingly, these investigators also

overexpressed Sog, dHIP14, or both in the wing, which resulted in similar findings.

1.2.4.4. Summary

In summary, while the role of HIP14 as a PAT is well-established (Huang, 2004, Huang, 2009, Yanai, 2006), the various studies summarized here have implicated the protein in a number of other processes. The significance of these findings, particularly *in vivo,* remains to be confirmed through further investigation and replication.

1.3. The *Hip14-/-* mouse

The accumulating *in vitro* evidence indicated an important role for HIP14 in neuronal protein trafficking and in measures related to HD. Both siRNA downregulation of HIP14 and mutation of the major site of palmitoylation in HTT resulted in an increase in cell death and inclusion formation, the *in vitro* correlates of HD pathogenesis. In contrast, overexpression of HIP14 *in vitro* appeared to have the opposite effect. (Yanai, 2006). Thus, *in vitro* evidence suggested a protective role for HIP14 in the pathogenesis of HD.

This prompted our laboratory to better understand the effects of manipulating levels of HIP14 *in vivo* by the creation of a mouse lacking HIP14. If HIP14 is important in the pathogenesis of HD, the phenotype of mice lacking HIP14 may be predicted to recapitulate some of those seen in mouse models of HD. Recapitulation of certain features may suggest a critical role for HIP14 in these processes, whereas features that are not reproduced may suggest processes in which HIP14 does not play a critical role.

The entire contents of the section that follows (section 1.3) describing the *Hip14-/-* mice is a summary of work by Singaraja *et al.* (Singaraja *et al.*, 2011). Because a large proportion of work described in this thesis is a follow-up study to the

original description of these mice, a thorough description of the original characterization was necessary for the understanding of the current study.

1.3.1. Generation of the *Hip14-/-* mouse

Mouse E14 embryonic stem (ES) cells harboring a gene trap insertion in intron 5 of mouse *Hip14* were purchased from Bay Genomics (RRJ233, California, USA). Primers specific for the gene and targeting vector were designed, and the correct targeting of *Hip14* was confirmed by sequencing of PCR products. Chimeras were back-crossed on the FVB/N strain to at least N6 (97%). Characterization of the mice was undertaken on the background of FVB/N, so as to enable easy future cross to other mouse models of interest that also exist on this background in our laboratory, for example the YAC128 mouse model of HD (Van Raamsdonk *et al.*, 2007b). *Hip14*-/- mice were born in the expected Mendelian ratios. Mice appeared slightly smaller than their littermates, but were otherwise grossly normal. Assessment of body weight revealed it to be significantly reduced as early as 3 months. Western blot analysis of HIP14 confirmed the absence of HIP14 expression (Singaraja, 2011).

1.3.2. Neuropathological characterization of the *Hip14-/-* mouse

Whole brain MRI assessment of *Hip14*-/- mice revealed a predominantly striatal volume reduction, in addition to significant reduction in cerebral cortex volume.
More detailed subsequent analysis comparing 64 brain regions also revealed reductions in hippocampus and cerebellum volume (Roshni Singaraja, data not shown).

In light of the MRI findings, neuropathological assessments were performed with emphasis on investigation of striatal pathology. Stereological assessment of *Hip14-/-* mice revealed neuropathological deficits beginning *in utero*. Brain weight was significantly reduced in *Hip14-/-* mice as early as 1 month of age and throughout life. In addition, *Hip14-/-* mice showed significant (~17%) decreases in both striatal volume and neuronal counts as early as embryonic day E17.5 when assessed by stereology. This 17% loss in striatal volume and neuronal

counts remained at 17% up to 12 months of age. Assessment of embryonic lateral ganglionic eminence (LGE), which gives rise to the striatum, revealed that striatal pathology appears between E14.5 and E17.5. To determine whether this may be due to a lack of striatal generation and development, cell proliferation was quantified using BrdU, an agent which incorporates into the DNA of dividing cells. However, no difference in the number of proliferating striatal cells was observed at E12.5 or E14.5. In order to then determine whether increased striatal cell death may explain the loss of striatal volume at E17.5, the number of cells undergoing cell death was quantified using TUNEL, an agent that intercalates into nicked DNA. A significant increase in the number of TUNEL positive, dying cells was observed at E14.5, but not at E12.5. Thus, the absence of *Hip14* appears to result in an increase in cell death in the striatum (Singaraja, 2011).

The formation of specific excitatory (glutamate-mediated) and inhibitory (GABA-mediated) synapses is critical for normal brain physiology. PSD-95, a postsynaptic scaffolding protein that is palmitoylated by HIP14, plays a critical role in synaptogenesis, especially in excitatory synapses, where it regulates the clustering of AMPA and NMDA receptors (El-Husseini Alaa El-Din, 2000b, Noritake, 2009). Since the *Hip14*-/- mice showed predominantly striatal neuropathology, an assessment of synaptic stability, structure, and numbers was performed using electron microscopy. Quantification of number of synapses per neuron revealed a significant reduction in striatal synapses per neuron. This decrease was found to be due to a specific loss of excitatory contacts, while number of inhibitory synapses remained unchanged. Morphological assessment of synapses revealed no differences in the numbers of reserve pool or docked vesicles, or the area of pre and postsynaptic compartments (Singaraja, 2011).

Striatal pathology was further assessed for neurochemical changes. The majority of striatal neurons are GABAergic, characterized by high DARPP32 expression (Deng *et al.*, 2004). Two populations of MSNs, including D2/met-Enkephalin and D1/substance P expressing cells are present (Deng, 2004). Assessment of

Hip14-/- striatum revealed significant decreases in both DARPP32 and enkephalin intensity, while substance P content was normal (Singaraja, 2011). In HD patients, DARPP-32 and enkephalin are both significantly reduced even in patients with mild pathology, while substance P is reduced only later with advanced disease (Deng, 2004). At 1 year, the same changes of reduced enkephalin and substance P were observed in YAC128 mice, while levels of Substance P remained unchanged (data not shown), once again demonstrating a recapitulation of the phenotype observed in *Hip14*-/- mice (Singaraja, 2011).

Striatal pathology is a prominent feature in both HD patients (Vonsattel and Difiglia, 1998) and in the YAC128 mouse model of HD (Slow Elizabeth J *et al.*, 2003). However, the striatal volume defect appeared as early as E17.5 in *Hip14*-/- mice and did not worsen, in contrast to HD patients and YAC128 mice, in which striatal volume loss appears at 9 months of age and is progressive (Slow Elizabeth J, 2003). The finding that striatal volume loss arises due to increased striatal cell death in the *Hip14*-/- mice is also a prominent feature of HD, where striatal cell death underlies the volume loss (Vonsattel and Difiglia, 1998). Similarly, the number of total and excitatory synapses is significantly reduced in YAC128 mice.

1.3.3. Behavioural characterization of the *Hip14-/-* mouse

Given the HD-like neuropathological features observed in *Hip14*-/- mice, behavioural assessments were performed using the same paradigm used to assess the YAC128 mouse model of HD. Behavioural testing in *Hip14*-/- mice revealed impairments as early as 3 months (Singaraja, 2011). Mice displayed deficits in motor coordination and balance, as indicated by a shorter latency to fall in both accelerating and fixed speed rotorod. In addition, *Hip14-/-* mice displayed decreased swim speed. Assessment of dark-phase spontaneous activity revealed hyperactivity, as mice displayed significantly increased stereotypic, horizontal and vertical movements. Assessment of sensorimotor gating, which is partially controlled through the cortico-striatal circuit (Graybiel, 2000) revealed significant deficits in pre-pulse inhibition (PPI) in *Hip14*-/- mice at 12 months

(Singaraja, 2011). Notably, motor coordination deficits are prominent in both HD patients (Hayden, 1981) and in YAC128 mice (Van Raamsdonk *et al.*, 2005b), and YAC128 mice present with early hyperactivity in dark phase testing (Slow Elizabeth J, 2003). Similarly, impairments in sensorimotor gating is a feature seen in both HD patients (Swerdlow *et al.*, 1995) and YAC128 mice (Van Raamsdonk, 2005b). Taken together, these data indicate that *Hip14*-/- mice display HD-like behavioural deficits (Singaraja, 2011).

1.3.4. Palmitoylation of HIP14 and HIP14 substrates in the *Hip14*-/- mouse

Features of HD in *Hip14*-/- mice could result from reduced or eliminated palmitoylation of key neuronal HIP14 substrates. Given the previous observation that polyglutamine expanded HTT displays reduced palmitoylation and mis-localization (Yanai, 2006), HTT palmitoylation was assessed. Surprisingly, HTT palmitoylation was not altered in *Hip14*-/- mice (Singaraja, 2011). While HIP14 palmitoylates HTT *in vitro*, and its overexpression results in enhanced HTT palmitoylation, the loss of HIP14 activity in *Hip14*-/- mice may be compensated by other PATs that also are able to palmitoylate HTT, such as the highly-related family member of HIP14, HIP14L (ZDHHC13). Overlaps in PAT-substrate specificity have been previously documented (Fukata M, 2004, Roth A., 2006). Indeed, the HIP14 paralog HIP14L robustly palmitoylates HTT *in vitro* (Huang, 2009, Huang, 2011), while having no discernible activity towards a second HIP14 substrate, PSD-95 (Singaraja R. *et al.,* manuscript in preparation). Thus, HIP14L may compensate for the loss of HIP14-mediated palmitoylation of HTT, but not of all HIP14 substrates. Palmitoylation of two known HIP14 substrates, SNAP-25 and PSD-95, was assessed in *Hip14-/-* brains, and was found to be decreased in the absence of HIP14 (Singaraja, 2011).

To explore the possibility that HIP14 function might be impaired in HD, HIP14 expression levels were assessed in YAC128 striatum and found to be unaltered, confirming that HD pathology is not a result of reduced HIP14 expression. Like all PATs, HIP14 itself is palmitoylated (Huang, 2004), and this auto-palmitoylation is

a conserved feature that is correlated with PAT activity (Fukata M, 2004, Huang, 2004). The palmitoylation of HIP14 itself was found to be reduced in brains of the YAC128 mouse model of HD, suggesting that HIP14 activity is reduced in the presence of mutant HTT. HIP14 isolated from YAC128 brains demonstrated significantly reduced palmitoyltransferase activity toward SNAP-25, indicating that HIP14 is dysfunctional in the presence of mutant HTT (Singaraja, 2011).

1.4. The HIP14 paralog DHHC13 (HIP14-Like): emerging understanding and similarities to HIP14

The entire contents of section 1.4, unless cited as part of published studies, is unpublished data by Liza Sutton. A summary of the *Hip14L*-/- mouse lends critical insights into the current study.

As described above, emerging data reveals many similarities between HIP14 and its paralog DHHC13 (HIP14L). Comparing the HIP14 and HIP14L protein sequence reveals 48% identity and 57% similarity in humans (Singaraja, 2002) and 46% identity and 63% similarity in mice (Liza Sutton, unpublished data). Both HIP14 and HIP14L are the only two DHHC PATs containing ankyrin repeats (Singaraja, 2002). A recent report assessing palmitoyl-transferase activity of all 23 DHHC PATs toward HTT revealed only HIP14 and HIP14L to be major HTT PATs (Huang 2009). More recent data have revealed that like HIP14 and HTT, the interaction between HIP14L and HTT is inversely correlated to HTT poly-Q expansion size (Liza Sutton, unpublished data).

As was summarized in section 1.1.3.6, a recent study described the phenotype of DHHC13 mutant mice generated in an ENU mutagenesis screen (Saleem, 2010). A point mutation in exon 12 of DHHC13 resulted in a severe phenotype including failure to thrive, impaired survival, skin and hair abnormalities, osteoporosis, and generalized amyloid deposition (Saleem, 2010). The authors also very briefly report on mice generated from the *Zdhhc13* gene trap ES cell line AC0492 on a mixed 129/B6 genetic background; the authors report that these mice exhibit

“similar phenotypes” to the ENU-mutagenesis generated DHHC13 mutant, but apart from histological abnormalities found in the skin, data is not shown.

The same *Zdhhc13* gene trap ES cell line was used to generate *Zdhhc13-/-* mice on an FVB/N background in our laboratory; the resultant mouse phenotype differs significantly from that reported by Saleem *et al.* This is likely partially attributable to differences in mouse strain, which is widely known to significantly influence phenotype (Doetschman, 2009).

Zdhhc13 null mice on the FVB/N strain are born in the expected Mendelian ratios and survival up to 12 months is not impaired. Compared to the severe hypotrichosis reported in *Zdhhc13* R425X mutants by Saleem *et al.*, milder but nonetheless obvious skin and hair changes are observed as mild hypotrichosis of the coat with a greasy appearance and periocular alopecia. Assessment of mRNA expression in wildtype mouse brain reveals highest levels in cerebellum and lowest in striatum. Neuropathological assessments reveal decreases in brain weight, cerebellum weight, striatal volume and counts, and cortical volume at 6 months. Preliminary behavioural assessments reveal hypoactivity, in contrast to hyperactivity in *Hip14-/-* mice. While HTT is the only known palmitoylation substrate of HIP14L *in vitro*, palmitoylation of SNAP-25 is decreased in *Hip14L-/-* brains. Further assessments are ongoing (Liza Sutton, manuscript in preparation).

Most notably, mice lacking both *Hip14* and *Hip14L* are embryonic lethal between E8.5 and E10.5, revealing an overlapping critical function in development (Shaun Sanders and Liza Sutton, unpublished data). From these preliminary findings it is clear that HIP14 and HIP14L share many features, and the similarity of null mice lacking for either gene suggests a potential critical role for both in the pathogenesis of HD.

1.5. Thesis objectives and hypothesis

The phenotype observed in *Hip14-/-* mice suggested a critical and protective role for HIP14 both in normal biology and as a key player in the pathogenesis of HD. Therefore, in this thesis we sought to further understand HIP14 biology by the overexpression of HIP14 in a mouse model.

The primary objectives of this thesis were initially to **1.)** Generate and characterize a mouse model of HIP14 overexpression, **2.)** To assess the functional integrity of the *HIP14* transgene and to **3.)** Assess whether HIP14 overexpression can delay or ameliorate the phenotype of a mouse model of HD.

Through initial characterization of the mice generated in **1.)** above, it became clear that the level of HIP14 overexpression obtained would not be sufficient to properly assess the third objective. Therefore, the goals of this thesis were modified to provide a more general understanding of HIP14 biology. Thus, the objectives were modified to the following:

1. Generate and characterize a mouse model of HIP14 overexpression

The HD-like phenotype in mice lacking *Hip14* suggested that HIP14 may play a critical role in HD. We therefore sought to further explore HIP14 overexpression *in vivo*. Can HIP14 be sufficiently overexpressed *in vivo*? Are there phenotypic consequences associated with HIP14 overexpression?

2. To assess the functional integrity of the human *HIP14* transgene

The human *HIP14* BAC transgenic mouse was created with an ultimate goal to be crossed to the YAC128 mouse model of HD, in order to determine if overexpression of HIP14 would ameliorate the YAC128 HD phenotype. Because the latter carry a human HD gene, and because we sought to understand HIP14 in a human disease context, we selected a human *HIP14* BAC transgene. In addition, a BAC transgenic approach allows the inclusion of endogenous regulatory regions of *HIP14*. Other questions we sought to address were: Does

the human protein function in the context of murine cellular machinery? Does the transgene result in a functional protein? Can BAC-derived human HIP14 compensate for the loss of murine *Hip14 in vivo*?

3. Further assessment of HIP14 biology in normal mice and consequences of loss of *Hip14*.

Our understanding of HIP14 biology is still limited. While earlier *in vitro* studies and the preliminary characterization of the *Hip14*-/- mouse have greatly enhanced our understanding of HIP14, many questions remain. Loss of *Hip14* in mice manifests phenotypically very early in development. What is the pattern of HIP14 expression in normal mice throughout development, specifically in the brain? Loss of *Hip14* results in an HD-like phenotype. Are other features of HD, for example testicular atrophy, recapitulated in the *Hip14*-/- mouse? What other organ systems might be affected by loss of *Hip14*?

2. MATERIALS AND METHODS

2.1. Mice

HIP14 BAC transgenic mice were generated on the FVB/N strain as described below. *Hip14-/-* mice were generated using mouse E14 embryonic stem (ES) cells harboring a gene trap insertion in intron 5 of mouse *Hip14*, purchased from Bay Genomics (RRJ233, California, USA). Chimeras were back-crossed on the FVB/N strain to at least N6 (97%), and maintained on the FVB/N strain thereafter. *HIP14* BAC+/-; *Hip14+/+* mice were bred to *Hip14+/-* mice to generate *HIP14* BAC+/-; *Hip14+/-* breeders, which were then intercrossed.

Pups of appropriate genotypes were selected from the resultant progeny to ensure subject mice were littermates. Mice housing and experiments were conducted in accordance protocols approved by the University of British Columbia Committee on Animal Care.

2.1.1. Generation of *HIP14* transgenic mice

2.1.1.1. Selection of a HIP14 BAC

We selected a human Bacterial Artificial Chromosome (BAC) containing the entire *HIP14* gene (RP11-463M12), as well as ~84kb of upstream regulatory sequence, ~6kb downstream sequence, excluding other intact genes or clearly defined promoter sequences (Figure 3.1a). The BAC was obtained from the Children's Hospital Oakland Research Institute (CHORI). The RP11 human BAC library was generated from a male, and details on the generation of the RP11 human BAC library are found elsewhere (Osoegawa *et al.*, 2001). The rationale for selection of the BAC used are discussed in further detail in chapter 3.1.1.

2.1.1.2. Purification of HIP14 BAC DNA

The BAC clone was received from CHORI as a LB agar stab culture and stored immediately at 4°C, where it was kept no longer than 1 week.

BAC DNA was prepared according to a standard protocol adapted from the Rockefeller University NINDS GENSAT BAC Transgenic project (http://www.gensat.org/GensatProtocols.pdf). The agar stab culture was streaked onto LB-agar plates, grown overnight, and a series of single colonies were selected. A fresh BAC 5ml starter culture was grown from a single colony for 8 hours, and was used to inoculate 4x 500ml cultures overnight. All LB or LB-agar contained 12.5ug/ml Chloramphenicol and all incubations were done at 37°C. An aliquot was used to generate glycerol stocks for long-term storage of clones at -80°C.

Cultures were pelleted and a standard alkaline lysis was performed, followed by CsCl overnight ultracentrifugation. The stronger lower band, representing supercoiled BAC DNA, was isolated and the BAC was handled with extreme caution in all subsequent steps to avoid mechanical damage. Extensive butanol extraction removed EtBr and DNA was ethanol precipitated in TE. The sample was then dialyzed against microinjection buffer for 4 hours.

Pulse-field gel electrophoresis analysis of uncut and linearized BAC DNA confirmed the correct size (190,052bp) and DNA purity (Figure 3.1c). In addition, a series of restriction enzyme digest analyses confirmed the expected BAC fingerprint (Figure 3.1b). The locations of BAC-ends were sequence-verified using standard T7 and SP6 primers:
T7 promoter 5'-GTAATACGACTCACTATAGGG-3'
T7 terminator 5'-GCTAGTTATTGCTCAGCGG-3'
SP6 5'-TACGATTTAGGTGACACTATAG-3'

2.1.1.3. Microinjection of HIP14 BAC DNA

An approximate range of BAC DNA concentration for use in microinjection is recommended as 0.5-4ng/ul (optimal of 1ng/gul), while higher concentrations above 6ng/ul are often toxic to the embryo (Marshall *et al.*, 2004). The BAC DNA

was provided to an in-house transgenic pronuclear microinjection service at a concentration of 10ng/ul in low-EDTA microinjection buffer (10mM Tris pH7.5, 0.1mM EDTA, 100mM NaCl). At the time of injection, DNA was diluted to a concentration of 1-2ng/ul. BAC DNA was injected into FVB/N pronuclei and transferred to psuedopregnant ICR females. Microinjections successfully resulting in founder mice were derived from injections at 2ng/ul in the absence of polyamines.

2.1.2. Collection of mouse tissue

For western blots and qrtPCR results described in chapters 3 and 4: Mice were sacrificed by CO_2. The whole brain was removed immediately and microdissected on ice. Fresh tissue was immediately snap-frozen in liquid nitrogen, and stored at -80°C.

For western blots and qrtPCR results described in chapter 5: All embryonic and P0 tissue (E9.5 whole embryo, subsequent ages as whole brain or brain subregion) was collected and immediately frozen on dry ice. Subsequent ages were either snap-frozen as described above or collected in RNAlater and stored at -80°C.

2.2. Molecular biology

2.2.1. PCR genotyping

2.2.1.1. DNA isolation from tail clip

A small tail clip was collected from pups upon weaning and stored at -20°C. DNA was isolated from tail clips using a standard quick-lyse protocol as follows:
Incubation overnight in 100μl lysis solution (40mM Tris pH9.0, 50mM KCl, 0.5% Tween-20, with 0.4μg/ml Proteinase-K) at 50-55°C followed by 15 minutes at 95°C, centrifugation at 13,000 RPM for 12 minutes. The resulting supernatant was transferred to a new sterile tube and used for PCR genotyping. Tail DNA used for qPCR analysis was isolated using the Qiagen DNeasy Blood and Tissue kit (Qiagen, 69506).

2.2.1.2. General protocol

All PCRs were run using 15.0μM each primer, 0.5mM dNTPs (Promega), 0.25U Taq DNA Polymerase (Roche), 1x PCR Buffer (Roche) in a final reaction volume of 25μl. PCR products were visualized under UV light after separation by standard 1% agarose gel electrophoresis stained with Ethidium Bromide. Genotyping of mice used in experiments was repeated at time of sacrifice using a fresh tail clip.

Cycling conditions for routine genotyping protocols were as follows:
Human *HIP14* BAC (h*HIP14*): Initial denaturation 94°C for 2min, followed by 35 cycles of 94°C 30s, 60°C 45s, 72°C 1min, followed by a 10min extension at 72°C.

Endogenous murine *Hip14* and detection of null mice (*Hip14-/-*): Initial denaturation 94°C for 2min, followed by 35 cycles of 94°C 30s, 62°C 45s, 72°C 1min, followed by a 7min extension at 72°C.

HIP14 BAC transgenic mice (BAC) were genotyped using PCR protocol h*HIP14.* Offspring of BAC,*Hip14*+/- x *Hip14*+/- mating pairs were genotyped each with two PCR reactions: both h*HIP14 and* m*Hip14* as above.

2.2.1.3. Primers

Seven primer pairs spanning the human *HIP14* gene and surrounding sequence (Table 2.1, primers 1-4 and 11-13) were used in the initial selection of *HIP14* BAC founders, in order to identify founders carrying the entire construct (Table 3.1). Subsequently, additional primer pairs were generated to cover greater resolution in the 5' region of the gene, but these primers were not used for routine genotyping (Table 2.1, primers 5-10). Primer pairs 1-13 were all designed using Primer3 (http://frodo.wi.mit.edu/primer3/).

After identification of founders and establishment of lines, routine genotyping for h*HIP14* BAC mice was done using the primer pair for exon 7 (Table 2.1, primer pair 11). The initial seven primer pairs were designed and confirmed to detect as little as one copy of the human *HIP14* BAC but no detection of endogenous murine *Hip14.*

Inclusion of FVB WT genomic DNA spiked with a one-copy equivalent of *HIP14* BAC ensures that the genotyping protocol provides adequate sensitivity to detect one copy of the BAC (Figure 3.2b) (Protocol online at http://www.med.umich.edu/tamc/spike.html). Human genomic DNA serves as an additional control.

	Primer name	Description		Primer sequence
1	HIP14h_Pr1	Upstream/promoter area 1	F	cccagaggtccaaacaacat
			R	gcttttccaaccaggcttc
2	HIP14h_Pr2	Upstream/promoter area 2	F	tatttccctgcttccaatgc
			R	ttccccacttcctgtctctg
3	HIP14h_Ex1	Exon 1	F	cgggaggagggatttaacac
			R	gagtccggggaagaaagg
4	HIP14h_Int1	Intron 1 (5' region)	F	gaaccgtgctgagtggattc
			R	acacctccacctctgtcctc
5	HIP14h_Int1_5p	Intron 1(mid Intron 1)	F	ctttcctgtggtggttgtgg
			R	aaacttcccttgcctgtgtg
6	HIP14h_Int1_3p	Intron 1 (3' region)	F	ccacttcagatgccagtcac
			R	tggaaaccacactcccctac
7	HIP14h_Ex2	Exon 2	F	tctcaaacaacacaaaagcactac
			R	tgccaaagaaaacaactacaac
8	HIP14h_Ex3	Exon 3	F	attggtggaagcaggttatg
			R	gctgtgggtcactgggtag
9	HIP14h_Ex4	Exon 4	F	gcacaagaaataacaaggcatag
			R	attcaggtcccctccaag
10	HIP14h_Ex6	Exon 6	F	tgtggttgaaaggtcagaatagg
			R	cagtgagggagagacagcac
11	HIP14h_Ex7	Exon 7	F	cacagtcattagccttcttctgg
			R	gggtcctcctatcaacaccat
12	HIP14h_STOP	Stop codon (spans stop codon)	F	tttggggtgctgtttttagc
			R	attttcaggcaccactcagc
13	HIP14h_3'UTR	3' untranslated region	F	aatgggcgtaaaacagcatc
			R	ccacagaataacacggtaagtagc

Table 2.1 - - Summary of Human HIP14 primers designed for *HIP14* BAC founder identification and subsequent PCR genotyping. Primer pairs indicated in grey were generated for initial BAC characterization; primers indicated in white were developed subsequently for further assessment of founders carrying truncated BAC constructs.

2.2.2. Quantitative PCR (qPCR)

To assess relative transgene copy number in founder genomic DNA using qPCR, we designed a primer pair specific for human *HIP14* exon 1 using "Primer Express 3.0" (Table 2.2, primer pair 14). Relative transgene copy number was assessed on the ABI 7500 Fast system using Power SYBR Green PCR Mastermix (Applied Biosystems) and the relative quantitation settings, and signal was normalized to mouse actin (Table 2.2, primer pair 18).

2.2.3. qrtPCR assessment of gene expression

Tissue was collected as described in section 2.1.2 above. Prior to beginning the experiment, all surfaces and instruments were treated with RNaseZap (Ambion). Total RNA was isolated using the Qiagen RNeasy Plus Mini kit according to the kit instructions. RNA was quantified by spectophotometer (Nanodrop ND-1000) . Samples were subsequently treated with DNase I (Invitrogen) to ensure total removal of genomic DNA, and cDNA was generated using the SuperScript® III First-Strand Synthesis System (Invitrogen).

qrtPCR was performed using *Power* SYBR Green PCR master mix (Applied Biosystems, 4367659) on the ABI 7500 Fast Real Time PCR System (Applied Biosystems) using the $\Delta\Delta C_T$ method in standard mode. Relative gene expression was normalized to mouse actin (as above). Primers used in qrtPCR are listed in table 2.2 (primer pairs 15-18).

	Primer name	Description		Application	Primer sequence
14	hHIP14 F2/R2	Exon 1	F	qPCR (human)	CCCCGGGAGGGTGAAAC
			R		AGCCCGCTTCGGTATCGTA
15	hHIP14 F1/R1	Exon 1-2 (intron-spanning)	F	rt-qPCR (human)	TACCGAAGCGGGCTGTGT
			R		AGTTTTCCGTCCAAGAGGTTCAC
16	mHIP14_Janine_F1/R1	Exon 3-4 (intron-spanning)	F	rt-qPCR (mouse)	ACGGCAACCAGACAAAGAAA
			R		GATCCACAATAGCACCTTTCG
17	mHIP14_rt2f_F1/R1	Exon 14-15 (intron-spanning)	F	rt-qPCR (mouse)	TGGTTGTGTCTCTTACTGGGG
			R		CATCCACGGGGAGCATGTG
18	mbact F1/R1	mouse actin (endogenous control)	F	qPCR & rt-qPCR	ACGGCCAGGTCATCACTATTG
			R		CAAGAAGGAAGGCTGGAAAAGA

Table 2.2 – Summary of primer pairs used for qPCR and rt-qPCR

Primer pair 15 was designed using Primer Express Software, version 3.0 (Applied Biosystems #4363991); primer pairs 16 and 18 were designed using Primer 3; primer pair 17 was obtained from Primerbank (http://pga.mgh.harvard.edu/primerbank/index.html, PrimerBank ID 27369784a2). Relative quantitations were calculated using the AB 7500 Fast software.

2.2.4. Western blot assessment of protein expression

2.2.4.1. Preparation of tissue protein lysates

Immediately after sacrifice, the tissue(s) of interest were dissected from mice and snap-frozen in liquid nitrogen before storage at -80°C. In some cases, tissues were collected and immersed in RNAlater, stored at 4 degrees overnight, and subsequently transferred to -80°C.

Tissue was homogenized using a Dounce homogenizer on ice in 1 volume of TEEN (50mM Tris pH 7.5, 1mM EDTA, 1mM EGTA, 150mM NaCl) + 1% SDS buffer. Samples were allowed to incubate on ice for 5 minutes, after which 4 volumes of TEEN + 1% Triton X-100 was added. The sample was passed through a 25 gauge needle 5 times to shear DNA, and samples were sonicated for 5 seconds on 20% power to disrupt cell membranes. Samples were spun at 14,000RPM at 4°C for 15 minutes to pellet debris, the pellet discarded, and the supernatant transferred to a new tube. Protein concentration was determined using the Bradford Assay (Biorad) in order to aid equal loading on western blot. The above buffers were supplemented with the following reagents: 1x Complete Protease Inhibitors (Roche), 1 mM sodium orthovanadate (Sigma), 800mM PMSF (Sigma), 5mM zVAD (Calbiochem). Extra lysate was split into aliquots to minimize future freeze/thaw cycles and stored at -80°C for future use.

2.2.4.2. General protocol

Equal amounts of protein were loaded and run on 4-12% Bis-Tris SDS-PAGE gels using the NuPage system (Invitrogen). Gels were transferred to PVDF membrane and membranes were blocked with 5% milk in TBS. Subsequently,

membranes were rinsed 3x in PBS prior to immunoblotting.

2.2.4.3. Antibodies and reagents

Immunoblots were obtained using an in-house polyclonal rabbit HIP14 antibody (PEP1) raised against aa 49-60 described previously (Singaraja, 2002). Beta tubulin antibody T4026 was assessed as a loading control (Sigma) for figures 3.2 and 4.2.

As the proteins selected as loading controls may undergo developmental changes in expression, additional loading controls were used for experiments investigating developmental expression of HIP14 (Chapter 5). Prior to immunoblotting, membranes were briefly stained with Ponceau S Solution (Sigma P-7170) and rinsed quickly in ddH_20, then wrapped in clean transparency films and scanned in order to record total protein loading. In addition to B-tubulin, membranes were immunoblotted with mouse anti-actin (Millipore 1501R) and rabbit anti-Calnexin (Sigma C4731) on the same blots.

Bands were visualized and quantified using the LiCor gel imaging system (Odyssey). HIP14 was quantified as HIP14 signal divided by loading control.

2.2.5. Assessment of protein palmitoylation

2.2.5.1. Acyl-Biotin Exchange

Protein palmitoylation of SNAP-25 and PSD-95 was assessed using an Acyl-Biotin-Exchange with Immunoprecipitation (ABE/IP) method an *in vitro* chemistry that exchanges biotin moieties onto sites of protein palmitoylation (Drisdel and Green, 2004). ABE consists of three steps: (A) N-ethylmaleimide blockade of free protein thiols, (B) release of palmitoyl-modification through hydroxylamine-mediated cleavage of the thioester linkage, (C) biotinylation of newly exposed palmitoylation site thiols. For ABE/IP analysis, the protein of interest is first immunoprecipitated with the steps of ABE chemistry being applied as the purified protein remains attached to antibody beads (Kang Rujun, 2008).

Following biotinylation with the thiol-specific biotinylation reagent Biotin-BMCC (Pierce #21900), the protein is eluted from the antibody and subjected to Western analysis. An additional important control is the parallel processing of one-third of each sample through ABE chemistry omitting the hydroxylamine cleavage step. These hydroxylamine-minus samples control for the possibility spurious signal due to inappropriate biotinylation.

Palmitoylation (the Biotin-BMCC label) was detected using a Streptavidin Alexa Fluor 680 conjugate antibody (Molecular Probes #S-32358). For PSD-95, a rabbit polyclonal antibody used for IP was generously provided by the late Dr. Alaa El-Husseini. PSD-95 mouse monoclonal antibody MAI-25629 was used for Western blot (Affinity Bioreagents, Golden, CO). For SNAP-25, a mouse monoclonal antibody SMI-81 (Covance, Emeryville, CA) was used for IP and a rabbit polyclonal SNAP-25 antibody used for Western blot (Synaptic Systems #111 002). All palmitoylation assessments were done on whole brain homogenate of mice of combined gender aged 1-3 months. Each sample was split in two and processed as technical replicates, in order to reduce assay variability. Quantifications of Western blot signals were performed using LiCor Odyssey analysis. The signal for palmitoylation (Biotin) was divided by the signal for total protein.

2.3. Neuropathological assessments

2.3.1. Brain sample preparation

Mice received tail injections of heparin and were terminally anesthetized by intraperitoneal injection of avertin, followed by intracardiac perfusion with fresh cold 4% paraformaldehyde (for 1 and 3 months) or 3% paraformaldehyde plus 0.15% glutaraldehyde added immediately before use (for 12 months) in PBS, pH 7.0 for 10 minutes. The perfused brain was removed and post-fixed in 4% (1 or 3 months) or 3% (for 12 months) paraformaldehyde for 24 hours, and then removed and stored in PBS + 0.08% sodium azide at 4 degrees. Prior to

sectioning, brains were cryopreserved in 30% sucrose in PBS + 0.08% Azide at 4°C for a minimum of 48 hrs.

2.3.1.1. Brain weight

After cryopreservation in sucrose but prior to sectioning, brains were gently patted dry to remove excess liquid and weighed. The cerebellum was then removed and weight recorded separately. Forebrain weight is calculated as whole brain weight minus cerebellum weight.

2.3.1.2. Brain stereology

Immediately prior to sectioning, brains were embedded in OCT (Tissue-Tek) and frozen on dry ice. Brains were cut coronally into 25μm thick sections using a cryostat microtome (HM 500 M, Microm Int. GmbH, Walldorf, Germany). Every eighth section throughout the striatum from Bregma 1.34 mm to -0.94 mm was collected. Sections were incubated for 30 minutes in hydrogen peroxide in PBS, washed, and incubated in blocking (5% normal goat serum(NGS), 5% bovine serum albumin(BSA), PBS + Triton X-100) for 30 minutes. After washing, sections were incubated overnight in Neu-N antibody (1:1000, with 5% NGS in Triton X-100), a marker of neuronal nuclei (Mullen *et al.*, 1992). Subsequently, sections were washed, and incubated for 2 hours in Secondary antibody (1:1000 biotinylated goat anti-mouse IgG with 1% NGS in PBS). After an additional wash, samples were incubated 2 hours in A/B solution (1:1000 A and B in PBS), washed, and incubated in DAB (1:10 in buffer) for 3-4 minutes. Sections were mounted onto slides with coverslips.

Stereology was performed as previously described (193). Briefly, the striatum in each of the individual sections was traced using Stereoinvestigator 10.0 software (Microbrightfield, Williston, VT). For neuronal counts, the physical fractionator probe was used with a grid size of 500 x 500 and counting frame of 25 x 25, the nucleator probe for neuronal size and a minimum of 200-300 cells counted or

analyzed for size per animal. Counts and neuronal soma size were determined using the StereoInvestigator software. For striatal volume, the Cavalieri principle was employed where the total striatal area was multiplied by section thickness (25 μm) and sectional sampling interval (8) as previously described (Cavalieri, 1966). The cortex was delineated using the corpus callosum as the ventral boundary in the same sections used for striatal analyses. Cortical volume was determined according to the Cavalieri principle as previously described. All quantitative analyses were performed blind with respect to genotype.

2.4. Neurochemistry

Immunohistochemistry was performed on sections from 1 month old mice of mixed gender. Every eighth section spanning from the crossing of the corpus callosum to the start of the hippocampus was selected with a total of 11 sections on average per animal used in calculations for each of DARPP-32, enkephalin and substance P. The following primary antibodies were used for visualization of DARPP-32, enkephalin and substance P: a mouse monoclonal anti-DARPP-32, #C24-6a (obtained from Dr. Paul Greengard and Dr. Hugh Hemming; 1:20,000), a rabbit polyclonal anti-enkephalin, met (1:500; Chemicon, St. Louis, MO, USA) and a rat monoclonal anti-Substance P (1:500; Accurate Chemical, Westbury, NY, USA). Sections incubated without primary antibody served as controls. Following overnight incubation in primary antibody, sections were washed in PBS and then incubated with horseradish peroxidase (HRP) conjugated secondary antibodies (Jackson ImmunoResearch Laboratories) followed by DAB. All sections underwent the same duration of development in DAB. Sections were then mounted onto slides and counterstained with 0.5% cresyl violet and then coverslipped. Sections were photographed using a Zeiss Axioplan 2 microscope and Coolsnap HQ Digital CCD camera (Photometrics, Tucson, AZ, USA). The amount of DARPP-32, enkephalin and substance P was determined using MetaMorph software version 6.3 (Universal Imaging Corporation, Downingtown, PA). After delineating the striatum for each image, labeling of DARPP-32, enkephalin and substance P was identified using the threshold held at a constant level for all images within experiments and then analyzed using the “integrated

morphometry" feature. Relative levels of DARPP-32, enkephalin and substance P staining were calculated as the sum of the integrated optical density (IOD) for each image divided by the area of the region selected then multiplied by the sampling interval (8) and section thickness (25 μm).

2.5. Behavioural assessments

Mice were acclimatized to the behavioural testing holding room under reverse lighting (12-10pm dark cycle) at least one week prior to behaviour testing at 3 months. Group-housed mice of both genders were assessed. Single-housed mice were removed from the analysis. The experimenter was blind to genotype.

2.5.1. Rotarod

Motor coordination and learning were examined using an accelerating rotorod (Ugo-Basile, Norfolk, UK).

2.5.1.1. Rotarod test of motor learning

Naïve mice were trained for 3 days on a fixed-speed rotarod at 3 months of age. Mice were given three trials of 2 minutes each per day, for three days (9 trials total) on a rotarod at fixed speed (18RPM). The inter-trial interval was 2 hours. Mice falling from the rod were returned, up to a maximum of 10 falls/trial. The time to first fall and total number of falls per trial were recorded.

2.5.1.2. Accelerating rotarod test of motor coordination and balance

Performance on an accelerating rotarod was assessed on day 4, following 3 days of training described above. Testing at subsequent ages was done at 3-month intervals without further training. Mice were placed on a rod accelerating from 5 to 40 RPM over 300 seconds, and latency to fall was recorded. Three trials were measured in one day at each age (Van Raamsdonk, 2005b).

2.5.2. Spontaneous activity measures

Spontaneous activity was assessed using the Med Associates activity monitor system (Med Associates Inc., St Albans, VT, USA) as described (Singaraja R. *et al.,* manuscript in preparation). Mice were given transgel (Charles River) and acclimatized to the room for at least 1 hour prior to testing, and testing did not commence until 1 hour after the beginning of the dark lighting cycle. The chamber was cleaned with ethanol and allowed to dry between each animal. Each mouse was placed in the center of the testing chamber. A number of automated readouts were recorded for 60 minutes, binned at 5 minute intervals.

2.5.3. Swimming T-maze training and reversal phase

For the swimming T-maze and reversal task, mice were tested in a white acrylic maze with arm dimensions 38 x 14cm (Van Raamsdonk, 2005b). The maze was filled with water and a platform (10 x 14cm) submerged below the water surface in one arm of the t-maze. Mice were released at the base of the stem of the T and learned to swim to the submerged platform – the time to platform, total number of arm entries and arm re-entries were recorded. For training, mice received 4 trials per day for 3 days (12 total trials). On the 4^{th} day, the platform was switched to the opposite arm of the t-maze and mice were required to change strategies to find the platform in its new location. Mice received 4 trials; incorrect arm entries as well as attempts to locate the platform in its original location (an indication of impaired strategy shifting) were recorded.

2.5.4. Novel object recognition

Open field and novel object recognition testing was done using black plastic 50x50cm open boxes with 16cm sides. Testing was conducted in normal room lighting. Recordings were collected using automated behavioural analysis software Ethovision (Noldus, Leesburg, VA, USA)) via live video collected from a ceiling mounted video camera. Testing proceeded over 2 days. On day 1, open field activity is recorded for 10 minutes; center entries and time spent in the center are scored. Mice are then removed from the box for a 5 minute inter-trial-interval (ITI) and two different novel objects are placed in the upper two corners

of the box, far enough from edges to allow movement around the box perimeter. Mice are reintroduced to the box (trial 1) in the lower left corner and recorded for 5 minutes. The number of investigations of the novel objects is scored. Mice are then removed from the box for another 5 minute ITI, and the top-right corner object in each box is moved to the lower right corner. Mice are reintroduced to the box and behaviour is measured for 5 minutes, again recording number of investigations. On the second day, the 10 minute open field and trial 1 were identical to day 1. In trial 2, instead of moving the top right corner object, it is replaced with a different and unfamiliar object, and behaviour is recorded for 5 minutes. The percentage of investigations of the moved object (day 1) or the novel object (day 2) is calculated.

2.5.5. Elevated plus maze

A plus-maze, two opposite arms of which are enclosed by walls ("closed arms") and two walls of which are not enclosed ("open arms") is elevated one meter from floor level (arm length 35cm, arm width 8cm, wall height 15cm). Automated behavioural assessment is done using Ethovision software (Noldus, Leesburg, VA, USA) from live videorecording via a ceiling-mounted camera.

During testing, mice are placed in the base of one closed arm and recording begins. Mice are allowed to freely explore the maze for 5 minutes in the light. The distance traveled, velocity, and time spent in various areas of the maze is assessed.

2.6. Physiological assessments

2.6.1. Measurement of body weight

Body weight of mice was recorded by briefly removing the mouse from its home cage and recording body weight on a small digital scale. Wherever possible, body weight was recorded at the same time of day.

2.6.2. Measurement of testis weight

Testes were harvested from mice, gently punctured 4-5 times with a 25G needle, and transferred to an EM Fixative (1.5% paraformaldehyde/1.5%

glutaraldehyde/0.1M NaCac, pH7.3, prepared fresh) at room temperature. Approximately 2 hours afterward, testes were gently cut in half with a very sharp razor to ensure complete fixation of the tissue. Testes were weighed approximately 24 hours after collection. Any adherent tissue was gently removed, and the two testes halves were gently patted dry before weighing.

2.7. Assessment of fertility

2.7.1. Histological examination of testes

Male mice were sacrificed by CO_2. The right testis was removed and the epididymis and fat pad were dissected away, taking care not to apply pressure on the organ. The testis was carefully punctured approximately uniformly 5 times with a 25 gauge needle, and placed in a minimum of 4ml of EM Fixative (1.5% paraformaldehyde/1.5% glutaraldehyde/0.1M NaCac, pH7.3, prepared fresh).

2.7.2. Sperm count

Male mice were sacrificed by CO_2. The testes and epididymis were dissected intact and immediately transferred to a small dish containing 750ul of filter-sterilized PBS. The epididymis was carefully dissected away from the fat pad and testis, the latter saved for other applications. The entire epididymis was then cut approximately 5 times, the dish gently swirled, and the tissue left to incubate at 37°C for approximately 1.5 hours to allow sperm to swim out. Left and right epididymis were collected and counted separately. After incubation, the epididymis was removed. The remaining buffer was diluted 1:3 and 10ul was transferred to a hemocytometer for quantification. Each of the four 16-square grids was counted and combined to generate one reading. Three separate readings from new dilutions for each of left and right epididymis were counted.

2.8. Statistical analysis

Statistical analyses were performed using the Graphpad Prism software, version 5a. Pairwise comparisons at a single timepoint were calculated using Student's t-test. Parametric analysis of single timepoint data was performed using One-way ANOVA, with post-hoc Tukey analysis. Non-parametric analysis (for western blot,

and palmitoylation assays) was done using the one-way ANOVA Kruskal-Wallis test with post-hoc analysis using Dunn's Multiple comparison test. Longitudinal behavioural analysis was assessed with repeated-measures ANOVA and post-hoc Bonferroni analysis. Data are reported as mean ± standard error of the mean (SEM).

3. ESTABLISHMENT AND CHARACTERIZATION OF *HIP14* TRANSGENIC MICE

Overexpression of HIP14 *in vitro* appears to reduce the number of inclusions in mHTT-expressing neurons, whereas its downregulation leads to an increase in inclusion formation and cell death (Yanai, 2006). The HD-like phenotype of *Hip14* null mice emphasized the importance of HIP14 in neuronal health and disease processes. These *in vitro* and *in vivo* findings combined suggested that investigation of HIP14 overexpression and/or upregulation as a potential therapeutic avenue for HD was warranted. If loss of HIP14 results in a phenotype resembling HD, could overexpression of HIP14 delay the onset of HD-like phenotypes in a mouse model of HD? Could overexpression of HIP14 be detrimental? The goal of this study was to generate a transgenic mouse model of HIP14 overexpression, providing a powerful *in vivo* tool with which to further our understanding of HIP14 biology, both in the context of normal physiology and disease processes.

3.1. Generation of *HIP14* BAC transgenic mice

We selected a BAC transgenic approach as this paradigm utilizes a DNA insert large enough (150-300kb) to ensure that upstream endogenous regulatory sequence are included, allowing the gene to be expressed in an appropriate temporal and tissue-specific manner (Chandler Kelly J *et al.*, 2007). We initiated this project with the future intention of exploring *HIP14* transgenic overexpression by crossing the mouse to other mouse models of disease. Therefore, because the ultimate goal was to understand HIP14 biology in the context of human disease, we selected a *HIP14* construct from a human BAC library.

3.1.1. Selection of a *HIP14* BAC

A search of the UCSC Genome Browser (Mar. 2006 (NCBI36/hg18) Assembly) and the NCBI Clone Registry (http://www.ncbi.nlm.nih.gov/genome/clone/query.cgi) revealed 5 BAC end pairs at chromosome 12q21.2 spanning the entire human genomic sequence

containing *HIP14*.

To aid in selection of the best construct, we consulted with bioinformatics experts on genomic regulatory elements. Observations of *in silico* available data reveal key insights. Regarding predictions of the transcription initiation site, the UCSC genome browser entry for *HIP14* reveals that it has a very well-defined transcription start region (TSR). The available data regarding CpG islands and transcripts suggests that almost all transcription initiation takes place at this site; RIKEN CAGE data also points to a single initiation region. Interestingly, one transcript in humans initiates just downstream of the primary first exon. This is of particular interest, as the region immediately 3' to the dominant first exon is highly conserved. Regarding potential regulatory sequences surrounding *HIP14*, it was noted that potential regions of interest extend over ~200kb 5' of the *HIP14* gene. The large first intron of *HIP14* with numerous conserved segments may indicate that a significant proportion of regulation is intronic (Wyeth Wasserman, personal communication). No NRSF sites (a DNA sequence element involved in neuronal gene transcriptional regulation) were found in the sequences upstream of *HIP14*. Predicted NRSF sites with a very low score (~65%) were found just downstream of the 3' end of exon 1 (Elodie Portales-Casamar, personal communication).

Four of the *HIP14*-containing BACs were not selected based on the inadequate inclusion of upstream sequence to help ensure inclusion of regulatory DNA, and/or inclusion of a neighboring gene beginning ~5kb 3' of *HIP14*, *CSRP2*. Human BAC RP11-463M12 was selected for a number of reasons. This BAC had been previously used for the purposes of chromosomal mapping of *HIP14* (Singaraja, 2002). This BAC clone contains the entire human *HIP14* gene, ~84kb upstream (5') regulatory sequence and ~6kb downstream (3') sequence (Figure 3.1a). The total size of this BAC, including a vector sequence of 8.5kb, is 190,052bp. In addition, the BAC construct does not contain other intact genes. While this BAC construct does contain the final 2 exons (1,244bp) of another

gene, *CSRP2*, the lack of clearly defined promoter sequences in this area does not make this a concern. Therefore, we proceeded to generate a mouse model based on the human BAC RP11-463M12.

We noted that only one of the two BAC end sequences for RP11-463M12 is listed in the NCBI clone registry (Accession number AZ515899). We confirmed that this is a reflection of the high-throughput nature of generating a long-range structure of the human genome, with no specific interest in any particular BAC; returning to re-verify any BAC end sequences of low quality (regardless of the reason) was cost-prohibitive (Dr. Pieter de Jong, personal communication). However, this emphasized the importance that the BAC ends be verified upon receipt from their source. Because of the lack of other suitable BAC constructs, we ordered and sequenced both BAC ends of RP11-463M12, confirming the 3' SP6 BAC-end and revealing the 5' T7 BAC-end to reside ~84kb upstream of *HIP14*, confirming its suitability for our purposes.

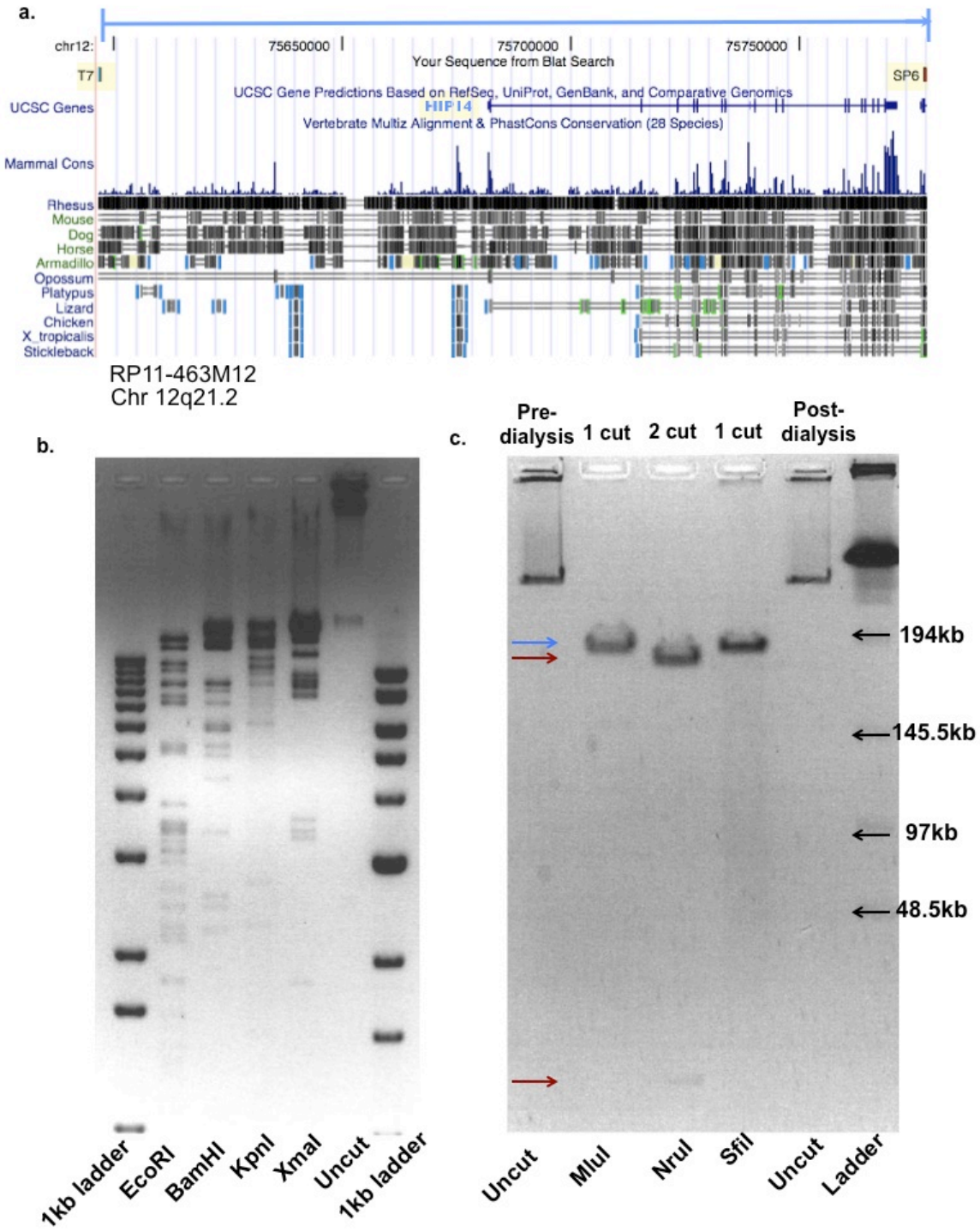

Figure 3.1 - Selection of a *HIP14* BAC construct. a. The genomic region contained in Human BAC RP11 463M12 is shown as the area spanned by the blue line. T7 and SP6 sites delineate the BAC ends (From UCSC Genome Browser, Mar 2006) **b.** Restriction Enzyme Fingerprint Mapping performed on purified BAC DNA, confirming the identity of the BAC insert via comparison to *in silico* prediction digests of BAC DNA. 500ng BAC DNA was cut with a variety of restriction enzymes and visualized on an agarose gel. 200ng of Uncut BAC DNA is loaded for comparison. **c.** Pulse-Field Gel Electrophoresis of *HIP14* BAC (RP11 463M12) demonstrating that BAC runs linearized at expected size (190,052bp). Restriction-digest treated samples showing 1 cut (Mlu1 and Sfi1) and 2 cuts (Nru1) are seen here.

3.1.2. Creation of a *HIP14* BAC transgenic mouse

Because the *HIP14* BAC RP11-463M12 selected does not contain any other intact genes, linearization by restriction enzyme digestion to remove unwanted sequences is not necessary, requiring fewer manipulations of the BAC and less opportunity for undesired deletions or rearrangements.

Once the identity and region spanned by the BAC had been confirmed, we proceeded to purify the BAC for microinjection following a standard protocol (http://www.gensat.org/GensatProtocols.pdf) and as described in Materials and Methods in section 2.1.1.2 above. A series of restriction enzyme digest analyses confirmed the expected BAC fingerprint (Figure 3.1b). Pulse-field gel electrophoresis analysis of uncut and linearized BAC DNA confirmed the correct size (190,052bp) and DNA purity (Figure 3.1c). The purified BAC DNA was provided to an in-house transgenic pronuclear microinjection service for generation of transgenic mice. The BAC DNA was microinjected into 494 FVB/N pronuclei, 378 of which survived and were implanted to pseudopregnant ICR females.

3.1.3. Identification and selection of *HIP14* BAC transgenic founder mice

A reliable and reproducible means to identify founder mice that have successfully integrated the transgene of interest is the necessary first step in establishing a transgenic mouse line. Forty-five live-born pups were produced, of which 11 were positive for the BAC by PCR genotyping. Nine of these 11 pups (Figure 3.2b) produced a strong positive band for all seven primer sets spanning the BAC construct, indicating integration of an intact BAC construct. Two of eleven lines appeared to have integrated a partial construct (Table 3.1). Ten dead pups were found, and the percentage positive for the *HIP14* transgene was no different (20%) from live-born pups, suggesting that incorporation of the construct is not lethal in early development.

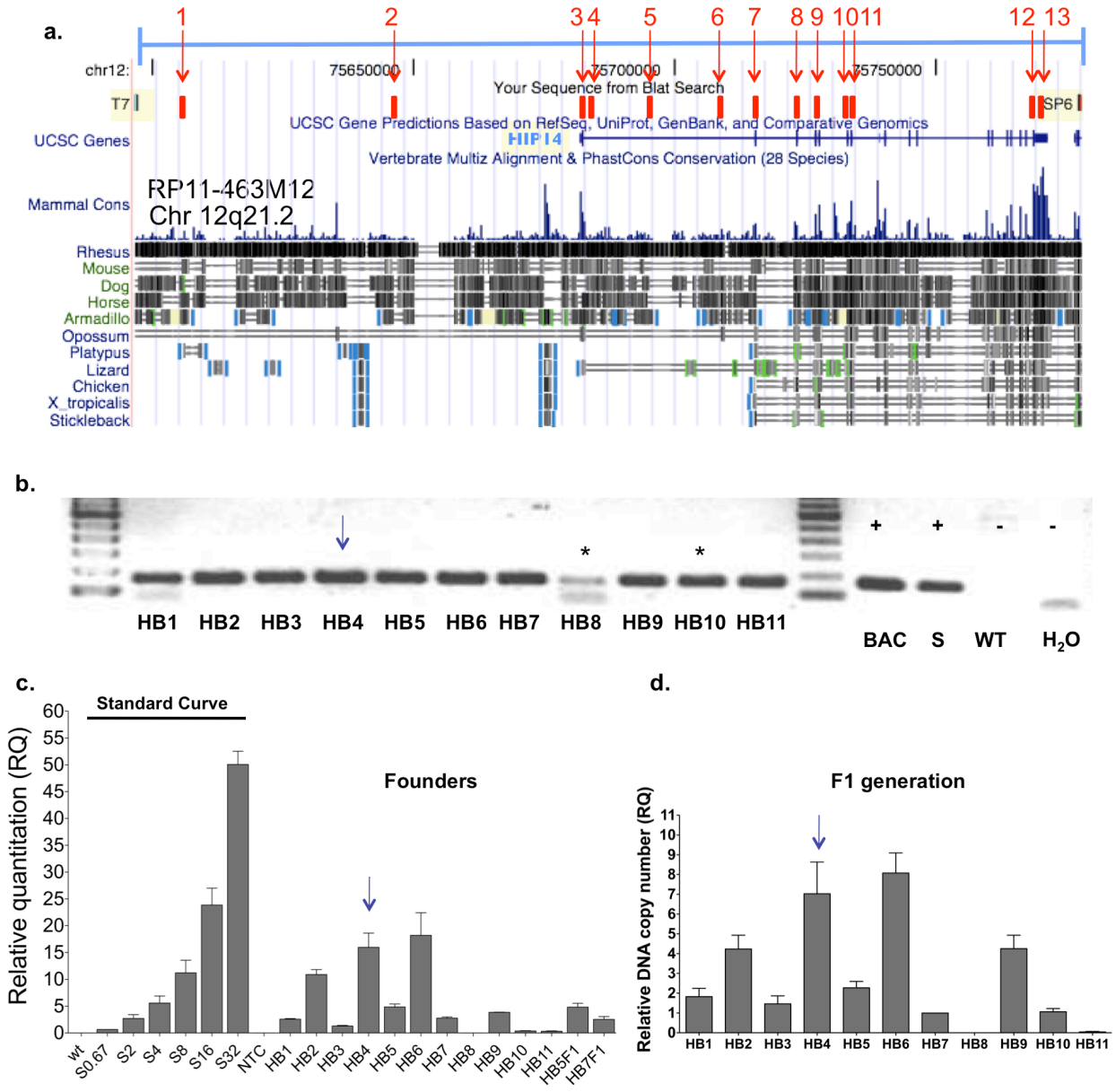

F**igure 3.2 - Identification and copy number assessment of HIP14 BAC transgenic founders. a.** The location of primer pairs used for PCR genotyping in characterization of HIP14 BAC transgenic mice (listed in Table 2.1) are indicated on a schematic generated using the UCSC Genome Browser. Numbered primer pairs correspond to Table 2.1. **b.** PCR genotyping confirmation of tail DNA from FVB mice generated from microinjections with a human *HIP14* BAC. Eleven mice tested positive for the transgene, of which 9 were positive for all 7 primer sets assessed. Figure shows results for "Promoter region 2" primers. BAC=*HIP14* BAC (5ng), S= FVB WT genomic DNA spiked with *HIP14* BAC at 1-copy number (200ng), WT= FVB WT genomic DNA, H20=ddH_2O, *=these mice not positive on all primer sets. **c**. qPCR assessment of relative transgene genomic copy number in Hip14 BAC founder mice. HIP14 BAC-spiked FVB genomic DNA was run in a standard curve for estimation of BAC copy number on the same plate as genomic tail DNA from each HIP14 BAC founder mouse. Relative quantitation was calculated relative to the standard curve one-copy equivalent. Each sample was loaded in triplicate, and the plate run in duplicate. Error bars indicate the variation between the two plates. The highest BAC copy number was detected in lines HB2, HB4, and HB6. HB5F1 and HB7F1 are tail DNA from F1 offspring of founders HB5 and HB7, respectively, run on the same plate. **d.** qPCR assessment transgene copy number in the HIP14 BAC F1 offspring reveals a pattern consistent with that observed in founders (n=6). Copy number estimates of F1 were calculated relative to HB7.

In order to assess the relative BAC transgene copy number at the level of the genome, purified tail DNA from each founder was assessed using qPCR and a primer pair specific to human exon 1 (Table 2.2, primer pair 14). A standard curve of FVB genomic DNA spiked with the *HIP14* BAC construct at a one-copy genome equivalent was run on the same plate for comparison. Relative quantitation was calculated using the standard curve one-copy equivalent. Each sample was loaded in triplicate and the plate run in duplicate. While true statistical assessment was not possible because each founder represented only 1n, error bars shown give an indication of the variation between the two independent assessments of each founder (Figure 3.2c). The highest copy number was detected in lines HB6 (18.22±4.23), HB4 (15.97±2.66), and HB2 (10.92±0.90). Moderate copy number estimates in lines HB1, 3, 5, 7, and 9 ranged from 1.3±0.13(HB3) to 4.9±0.54 (HB5).

A similar pattern and range of copy number estimates was observed in the F1 offspring (Figure 3.2d), relative to a standard curve one-copy equivalent. Very low copy number was estimated in line HB10, consistent with earlier results suggesting that this line carries a BAC construct truncated between exon 1 and the 5' region of intron 1 (Figure 3.2b and Table 3.1). HB8 DNA did not yield a product, consistent with a truncation 5' of exon 1 (Table 3.1). Founder HB11 failed to produce any BAC+ offspring.

Lines HB2, HB4, and HB6 were bred to FVB WT for preliminary expression analysis. Within this chapter, "WT" and "BAC" refer to the genotypes BAC-/-; *Hip14*+/+ and BAC+/-; *Hip14*+/+, respectively.

Primer	Primer 1	Primer 2	Primer 3	Primer 4	Primer 11	Primer 12	Primer 13
Region	Promoter region 1	Promoter region 2	Exon 1	Intron 1	Exon 7	STOP	3' UTR
Founder line							
HB1	+	+	+	+	+	+	+
HB2	+	+	+	+	+	+	+
HB3	+	+	+	+	+	+	+
HB4	+	+	+	+	+	+	+
HB5	+	+	+	+	+	+	+
HB6	+	+	+	+	+	+	+
HB7	+	+	+	+	+	+	+
HB8	+	+	-	-	-	-	-
HB9	+	+	+	+	+	+	+
HB10	+	+	+	-	-	-	-
HB11	+	+	+	+	+	+	+

Table 3.1 - Identification of HIP14 BAC transgenic founders. Nine of the eleven transgenic BAC lines integrated an intact BAC, as assessed by the seven primer pairs indicated. Pink panels indicate failure of the primer pair to yield a product.

3.2. HIP14 expression in the BAC transgenic mice

DNA copy-number has been shown to correlate relatively well with expression (Chandler Kelly J, 2007). Therefore, we anticipated that the lines with the highest copy number would be the best-suited for generation of a HIP14-overexpressing mouse model.

3.2.1. mRNA expression

Using primers spanning exon 1-2 of human *HIP14*, we confirmed expression of human *HIP14* in cDNA derived from cortex of BAC mice, line HB4 ($p<0.0001$, $n=5$, figure 3.3a). No signal was observed in WT mice, confirming that the primers are specific for human *HIP14*. BAC-derived human *HIP14* expression was not different between lines HB4 and HB6 ($p=0.27$, $n=3$, Figure 3.3b).

In order to assess whether murine *Hip14* is altered in the presence of the human *HIP14* BAC, we assessed expression of mouse *Hip14* using primers spanning exons 14-15. Cortical expression of murine *Hip14* did not differ between WT and BAC mice, line HB4 ($P=0.24$, $n=5$, figure 3.3c). To confirm that signal was not

genomic in origin, all qrtPCR primers were intron-spanning, and mRNA was treated with DNase I prior to cDNA generation.

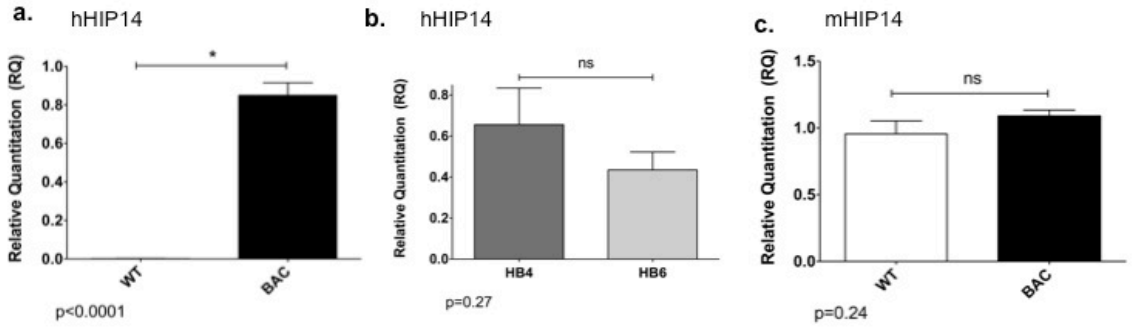

Figure 3.3 – mRNA Expression in *HIP14* BAC transgenic mice. a. Human *HIP14* mRNA is expressed in cortex of *HIP14* BAC transgenic line HB4 at 1 month. No signal is detected in WT littermates ($p<0.0001$, $n=5$). **b.** Human *HIP14* mRNA expression does not differ between lines HB4 and HB6 cortex ($p=0.27$, $n=3$). **c.** Expression of endogenous murine *Hip14* is not altered in the presence of the human *HIP14* BAC in line HB4 ($p=0.24$, $n=5$).

3.2.2. Protein expression

We next assessed protein expression in the brains of the three *HIP14* BAC lines with the highest BAC copy number. Protein expression was assessed using antibody that detects both human and mouse HIP14; thus, HIP14 detected in BAC mice represents both murine and human HIP14, relative to WT mice in which only murine HIP14 is present. HIP14 expression in cortex, striatum, hippocampus, and cerebellum of lines HB2, HB4, and HB6 revealed HB4 to be the highest-expressing BAC line (Figure 3.4a-h). A modest but significant level of HIP14 overexpression (≈23% greater than WT) was observed in cortex in mice aged 1mo (1.22±0.001 relative to WT,$p=0.0015$, $n=3$). Assessment of striatum revealed a non-significant trend to enhanced HIP14 expression (1.08±0.001 relative to WT, $p=0.2649$, $n=3$). A pairwise t-test comparing protein expression in each brain subregion failed to detect any significant difference between levels in the two highest expressing lines, HB4 and HB6 (Cortex $p=0.68$, Striatum $p=0.48$, Hippocampus $p=0.99$, Cerebellum $p=0.38$), although a mild trend to increased expression was observed in line HB4. Line HB4 was selected for subsequent analysis.

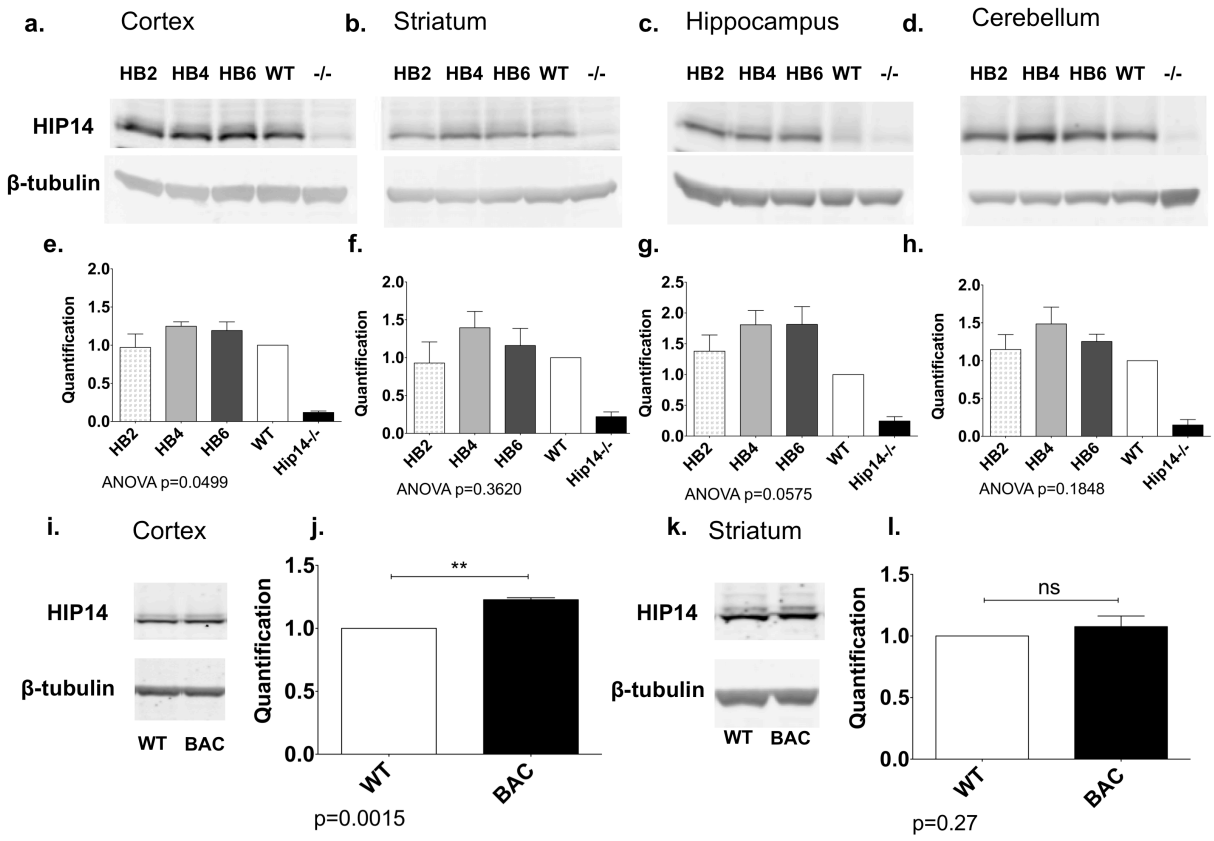

Figure 3.4 - HIP14 protein expression in *HIP14* BAC transgenic mice. a. HIP14 protein expression in the three *HIP14* BAC transgenic lines with highest BAC copy number. HIP14 expression was assessed in cortex **(a,e),** striatum **(b,f),** hippocampus **(c,g),** and cerebellum **(d,h)** of lines HB2, HB4, and HB6 using a rabbit polyclonal HIP14 antibody described previously (Singaraja R *et al.* 2002). HIP14 signal was normalized to B-tubulin loading control, assessed on the same blot. One-way ANOVA comparisons of the three lines with WT revealed a significant difference in cortex (ANOVA p=0.0499; HB2 n=4; HB4, HB6, WT n=5), but not in striatum, hippocampus, or cerebellum (ANOVA p=0.3620, p=0.0575, p=0.1848 respectively; HB2 n=3; HB4, HB6, WT n=4). All post-hoc analyses are non-significant. HB4 and HB6 appeared to have similar levels of HIP14 overexpression; subjective observation suggests slightly higher expression in HB4. **(i,j)** A modest (≈23% greater than WT) level of HIP14 overexpression is confirmed in 1mo cortex lysate of line HB4 compared to WT littermates (p=0.0015, n=3). **(k,l)** HIP14 is non-significantly overexpressed (≈8% greater than WT) in 1mo striatum of line HB4 compared to WT littermates (p=0.27, n=3).

3.3. Neuropathological assessment of *HIP14* BAC transgenic mice

Neuropathological deficits, particularly involving the striatum, are a prominent feature in *Hip14*-/- mice as well as in HD patients and mouse models of HD (Slow Elizabeth J, 2003, Vonsattel, 2008). As such, *HIP14* BAC mice were assessed

for a series of neuropathological endpoints used routinely in assessing mouse models of HD such as the YAC128 model (Slow Elizabeth J, 2003).

3.3.1. *HIP14* BAC transgenic mice demonstrate a mild decrease in brain weight that becomes apparent at advanced age.

In line HB4, *HIP14* BAC mice showed no difference in whole brain weight (Figure 3.5a, p=0.28), cerebellum weight (Figure 3.5b, p=0.08), or forebrain weight (Figure 3.5c, p=0.39) at 1 month (whole brain WT: 321.5±3.8, BAC*:* 315.2±4.1g; cerebellum weight WT: 51.41±0.82, BAC*:* 49.35±0.78g; forebrain weight WT: 270.1±3.2, BAC*:* 265.9±3.5g). Assessments at 3 months likewise revealed no difference in whole brain (WT: 336.9±1.5, BAC*:* 336.1±3.5g, p=0.82) or forebrain weight (WT: 281.0±1.3, BAC*:* 282.1±3.2g, p=0.71), but a mildly significant decrease in cerebellum weight in BAC transgenic mice relative to WT littermates was apparent (WT: 55.90±0.55, BAC*:* 53.98±0.68g, p=0.048). At 12 months of age, no statistical difference between the two genotypes was observed (whole brain WT: 367.9±2.7, BAC*:* 362.4±1.9g, p=0.10; cerebellum weight WT: 62.26±0.88, BAC*:* 61.14±0.52g, p=0.26; forebrain weight WT: 304.2±1.8, BAC*:* 301.2±1.6g, p=0.24).

However, brain weight was also assessed at 12 months in a second *HIP14* BAC line (HB6), in which HIP14 expression is similar (Figure 3.4). A significant reduction in whole brain and forebrain weight was observed, with a similar trend in cerebellum (whole brain WT: 358.2±2.8, BAC*:* 345.8±3.0g, p=0.01; cerebellum weight WT: 60.24±0.72, BAC*:* 57.94±0.76g, p=0.06; forebrain weight WT: 298.0±2.3, BAC*:* 287.9±2.5g, p=0.01). Combining the data for both lines (HB4 and HB6) also demonstrated reduced brain weight in the BACs (Figure 3.5, whole brain WT: 363.8±2.2, BAC*:* 353.6±2.4g, p=0.005; cerebellum weight WT: 61.41±0.63, BAC*:* 59.40±0.56g, p=0.02; forebrain weight WT: 302.4±1.8, BAC*:* 294.2±2.0g, p=0.005). Therefore, it appears that a trend to a modest reduction in

brain weight is present in line HB4. This reduction in brain weight is significant at 12 months in a second line, HB6. Combining data from both HB4 and HB6 at 12 months is also significant, but is largely an effect of reductions in HB6.

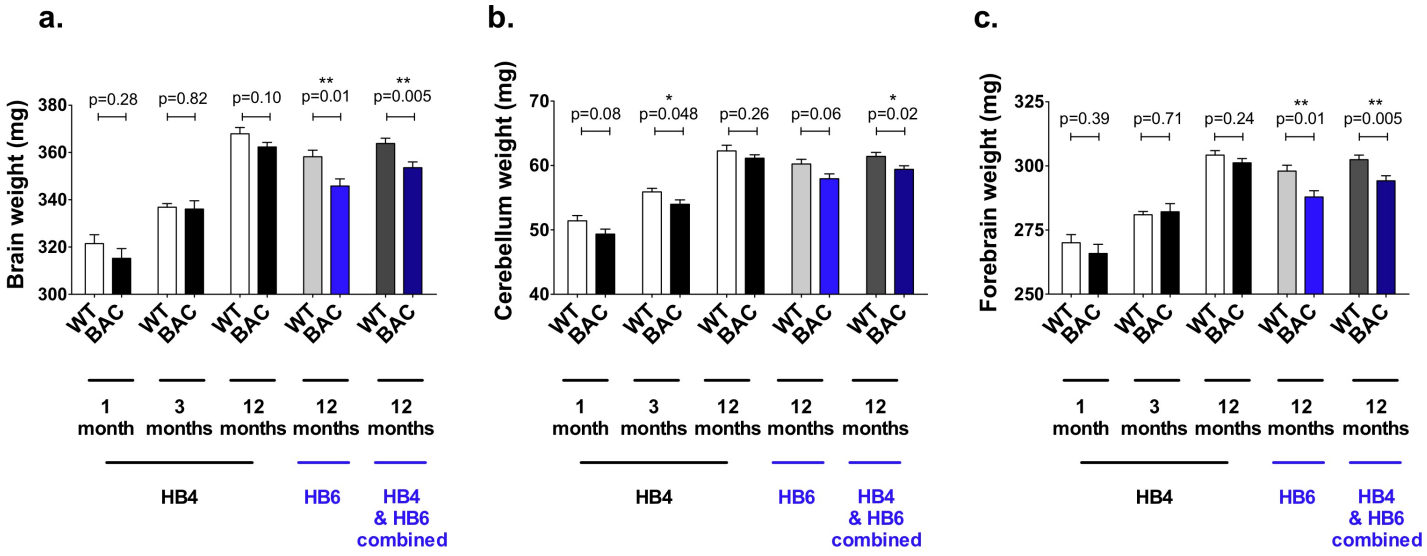

Figure 3.5 - A mild decrease in brain weight becomes apparent in *HIP14* BAC transgenic mice at advanced age. a. Line HB4 *HIP14* BAC transgenic mice show no difference in brain weight at 1 month (p=0.28), 3 months (p=0.82), or 12 months (p=0.10). However, examination of a second line (HB6) reveals significant decreases in brain weight at 12 months (p=0.01), and combining the 12 month data for both lines (HB4 and HB6) is also significant (p=0.005). **b.** Cerebellum weight in line HB4 is not significantly different at 1 months of age (p=0.08). However, by 3 months of age, cerebellum weight is modestly decreased in *HIP14* BAC transgenic mice (p=0.048) relative to WT littermates. By 12 months of age, cerebellum weight is not significantly different (p=0.26) in line HB4. However, a trend to decrease in cerebellar weight in a second line is apparent (HB6; p=0.06) and combining data for both HB4 and HB6 at 12 months reveals a significant decrease (p=0.02). **c.** Forebrain weight in *HIP14* BAC transgenic mice is no different from WT littermates at 1 month of age (p=0.39), nor at 3 months (p=0.71) or 12 months (p=0.24) in line HB4. In line HB6, however, forebrain weight is significantly decreased (p=0.01) and combining HB4 and HB6 12 month data reveals a significant decrease in forebrain weight (p=0.005). 1 month: WT and BAC both n=12; 3 months: WT n=10 and BAC n=6; 12 months: WT n=11 and BAC n=14. Line HB6 at 12 months WT n=8 and BAC n=13. Combined HB4 and HB6 at 12 months: WT n=19 and BAC n=28. *p<0.05, **p<0.01.

3.3.2. Absence of striatal or cortical neuropathology by stereology in *HIP14* BAC transgenic mice

Striatal pathology is a prominent feature in human HD (Sturrock and Leavitt, 2010, Vonsattel, 2008) and *Hip14-/-*mice (192). Therefore, we assessed *HIP14* BAC transgenic mice for similar striatal pathology using the same endpoints used in characterization of the *Hip14-/-* mice.

Striatal volume of *HIP14* BAC transgenic mice was no different from WT littermates at 1 month (WT:10.38±0.32, BAC: 10.07±0.40 mm^3, p=0.56), or 3

months of age (WT:12.56±0.33, BAC: 12.98±0.53 mm^3, p=0.48; Figure 3.6a). Similarly, no difference in striatal neuron count was observed (1 month: WT:2.01±0.10, BAC: 2.01±0.07 million cells, p=0.99; 3 months: WT:2.00±0.07, BAC: 2.00±0.09 million cells, p=0.99; Figure 3.6b), nor was any difference observed in striatal neuron soma size at 1 and 3 months (1 month: WT:66.73±2.07, BAC: 67.80±2.23 μm^2, p=0.73; 3 months: WT:57.47±1.82, BAC: 55.60±0.92 μm^2, p=0.45; Figure 3.6c). Finally, cortical volume was not different from WT at 1 month (WT:26.86±0.52, BAC: 26.83±0.56 mm^3, p=0.97) and at 3 months (WT:29.17±0.81, BAC: 31.11±1.75 mm^3, p=0.27) of age (Figure 3.6d). Therefore, striatal and cortical pathology are not apparent at early ages in human *HIP14* BAC transgenic mice.

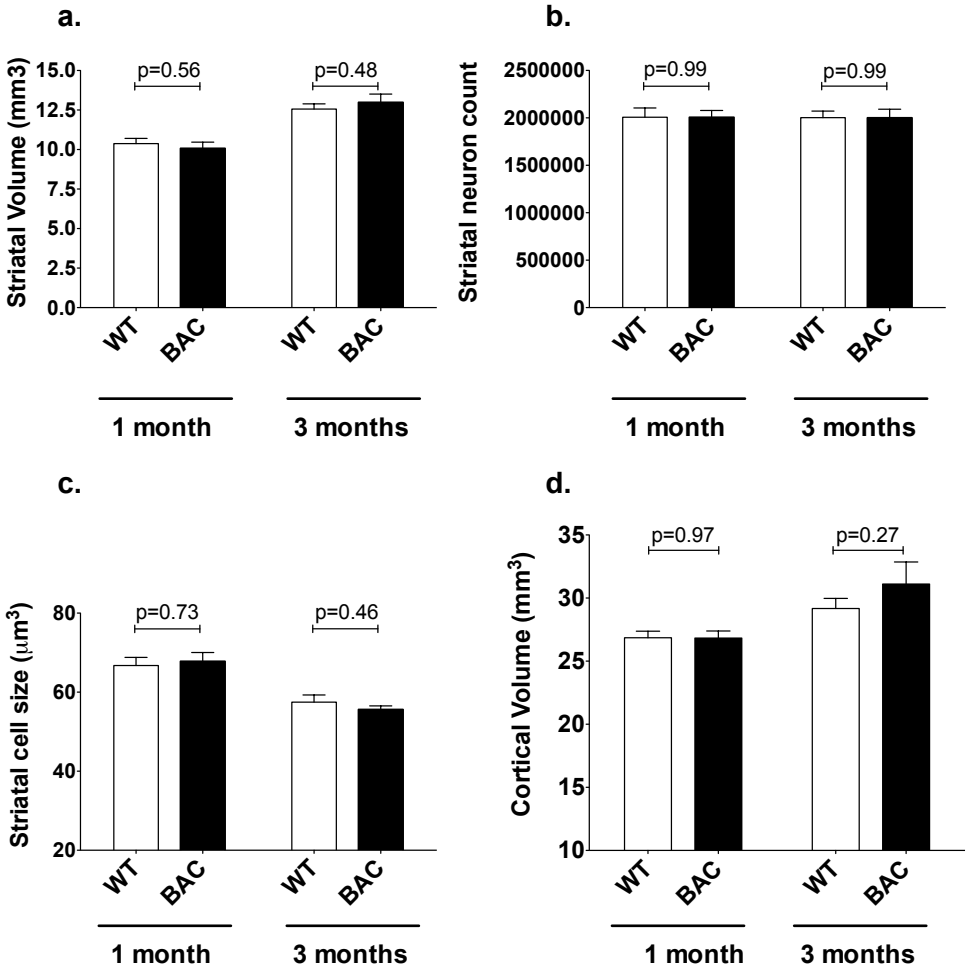

Figure 3.6 - Absence of neuropathological changes by stereology in *HIP14* BAC transgenic mice. a. Striatal volume is no different in *HIP14* BAC transgenic mice relative to WT littermates at 1 month (p=0.56) or 3 months (p=0.48), of age. **b.** Striatal neuron count was similarly unchanged at 1 and 3 months of age (both p=0.99). **c.** Striatal neuron size was likewise unchanged at 1 (p=0.73) and 3 months (p=0.46) of age. **d**. Cortical volume is unchanged in *HIP14* BAC mice at 1 month (p=0.97) and at 3 months (p=0.27). 1 month: n=12 and 12 for WT and BAC mice, respectively. 3 months: n=9 and 5 for WT and BAC mice, respectively. ns=not significant (p>0.05).

3.3.3. Mild decrease in DARPP-32 in *HIP14* BAC mice

Disruptions in neurochemical features of striatal neurons are a well-described feature in human HD. The striatal atrophy and cell loss observed in HD is largely due to loss of striatal GABAergic MSNs, cells that express high levels of DARPP-32 expression (Deng, 2004). These MSNs are subdivided into two types: those expressing enkephalin and dopamine D1 receptors, and those expressing substance-P and dopamine D2 receptors. Expression levels of enkephalin and DARPP-32 are affected early in HD, whereas substance P remains largely

unchanged until later in the disease (Deng, 2004). *Hip14-/-* mice demonstrate a similar pattern of reduced staining of DARPP-32 and enkephalin in the striatum, while levels of substance-P are unchanged (Singaraja, 2011). These neurochemical endpoints were assessed as part of our initial characterization of the *HIP14* BAC transgenic mouse. Interestingly, DARPP-32 expression levels were reduced by ~11% in *HIP14* BAC transgenic mice relative to WT littermates (Figure 3.7a; WT:47,380±792, n=11; BAC:42,180±729 relative levels, n=11; p=0.0001). In contrast, enkephalin levels were statistically unchanged (Figure 3.7b; WT: 32,640±5342, n=12; BAC:35,480±7886 relative levels, n=12; p=0.77), although the data was highly variable and a non-significant trend to increase in the *HIP14* BAC mice was observed. Finally, substance P values were unchanged (Figure 3.7c; WT: 483.2±71.7, n=12; BAC:458.8±76.2 relative levels, n=12; p=0.82). All neurochemical assessments were performed on brains from mice aged 1 month.

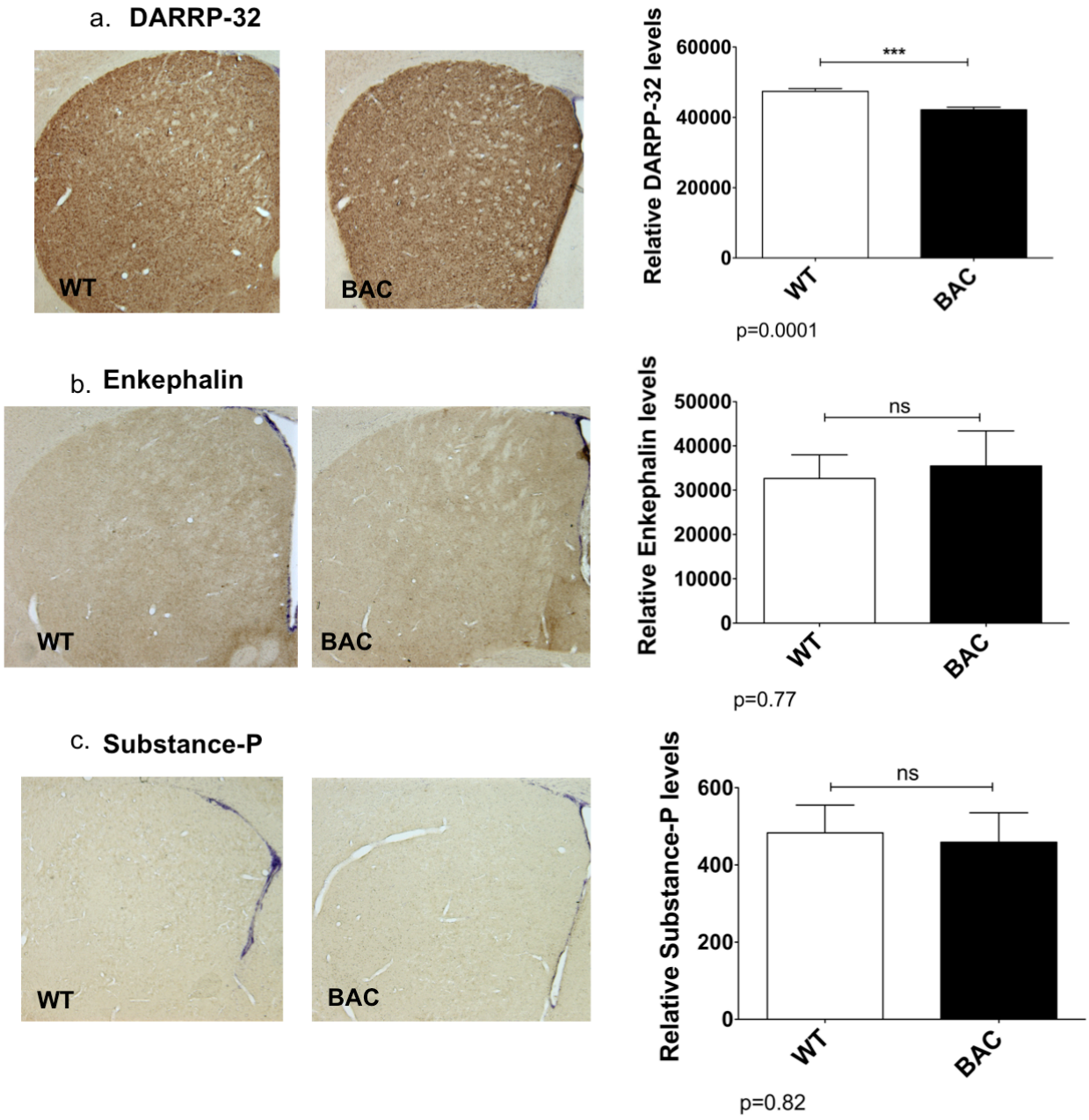

Figure 3.7 – Neurochemical analysis of *HIP14* BAC transgenic striatum. a.Striatal DARPP-32 is decreased in *HIP14* BAC transgenic mice relative to WT controls (p=0.0001). **b.** In contrast, Enkephalin levels are statistically unchanged (p=0.77), although the data for this endpoint is highly variable and suggestive of a nonsignificant trend to an increase in the *HIP14* BAC mice. **c.** Substance P is unchanged in *HIP14* BAC transgenic mice (p=0.82). ns= not significant, ***p<0.0001. n=11 for a, and n=12 for b-c.

3.4. Behavioural assessment of *HIP14* BAC transgenic mice

3.4.1. Tests of motor function

Based on the HD-like phenotype observed in the *Hip14*-/- mice (192) and *in vitro* data supporting an important role for HIP14 in HD (Yanai, 2006), we performed behavioural analyses similar to those used in assessment of YAC128 mice and *Hip14*-/- mice.

3.4.1.1. Absence of deficits in motor coordination in HIP14 BAC mice

Patients with HD develop obvious deficits in motor co-ordination (Hayden, 1981), and *Hip14-/-* mice displayed shorter latency to fall in accelerating rotarod testing (192). Therefore, we routinely assessed motor coordination in the *HIP14* BAC transgenic mice.

Repeated measures ANOVA failed to reveal significant differences in *HIP14* BAC mice performance on the rotarod relative to WT littermates at any of the ages assessed, up to 12 months (Effect of genotype: $F(1,69)=2.08$, $p=0.1630$, WT n=13 and BAC n=12; Figure 3.8). Post-Hoc analysis was likewise not significant. Separation of genders failed to reveal any significant deficits (Females WT n=4, BAC n=7, Males WT n=9 and BAC n=5; Figure 3.8b-c). Body weight of BAC mice was the same as WT littermates (see section 3.5 below).

Rotarod performance was also assessed with larger numbers of mice at 3 and 6 months. Once again, repeated measures ANOVA failed to reveal any significant difference between WT and *HIP14* BAC transgenic littermates (Data not shown; effect of genotype: $F(1,240)=0.08$, $p=0.7735$; WT n=25, BAC n=17), and examination of either gender alone once again failed to reveal any significant effects (Females WT n=10 and BAC n=12, Males WT n=15 and BAC n=10).

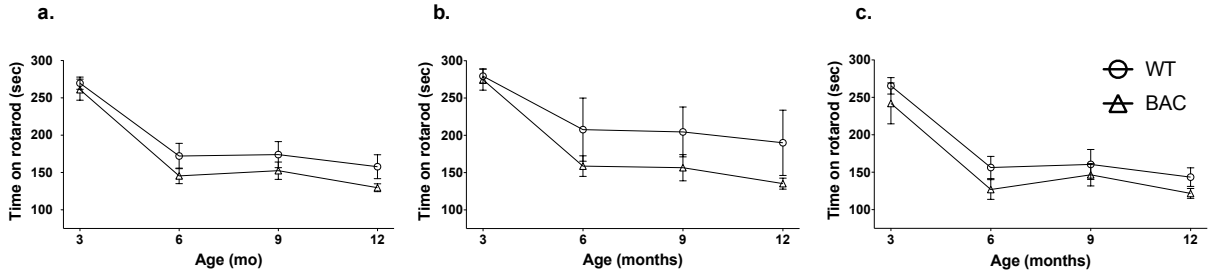

Figure 3.8 – *HIP14* BAC transgenic mice do not display any significant deficits in motor coordination. **a.** *HIP14* BAC transgenic mice of mixed gender do not demonstrate any motor coordination deficits at 3,6,9, or 12 months $F(1,69)=2.08$, $p=0.1630$, WT n=13 and BAC n=12. Examination of each gender alone likewise fails to reveal significant differences in females (**b**, $F(1,27)=2.20$, $p=0.1718$; WT n=4, BAC n=7) or males (**c**, $F(1,36)=1.94$, $p=0.1890$; WT n=9 and BAC n=5).

3.4.1.2. Assessment of spontaneous activity reveals hypoactivity in HIP14 BAC mice

Similar to the YAC128 mice in dark-phase open field testing, *Hip14-/-* mice display features of hyperactivity (192). As such, we assessed the same endpoints in our *HIP14* BAC transgenic mice as part of their characterization.

Initial assessment of 30 minute sessions of spontaneous activity in a smaller cohort of mice up to 12 months revealed a significant effect of genotype in only average velocity ($F(1,69)=6.10$, $p=0.0213$).Spontaneous activity was assessed with a larger number of animals for 60 minute intervals at 3 and 6 months, revealing a modest hypoactive phenotype (Figure 3.9, Table 3.2). A significant effect of genotype in mixed genders was apparent in all measures except, interestingly, for average velocity (Table 3.2), relative to WT littermates. Post-hoc Bonferroni testing revealed a significant difference at 3 months in vertical time ($p<0.01$, Figure 3.9g) and jump count ($p<0.05$, Figure 3.9h) and time ($p<0.05$, Figure 3.9k). Significant effects at six months of age were seen in ambulatory time ($p<0.05$, Figure 3.9a) and counts ($p<0.05$, Figure 3.9d), stereotypic time ($p<0.05$, Figure 3.9b) and counts ($p<0.05$, Figure 3.9e), time resting ($p<0.05$, Figure 3.9f), and vertical counts ($p<0.05$, Figure 3.9j).

Upon examination of either gender alone, only vertical counts remained significantly different in females. The effect appeared to be more robust in males, where significant differences remained in time resting, vertical counts, vertical time, jump counts, and jump time (Table 3.2). Therefore, it appears that *HIP14* BAC transgenic mice display a modest but significantly hypoactive phenotype.

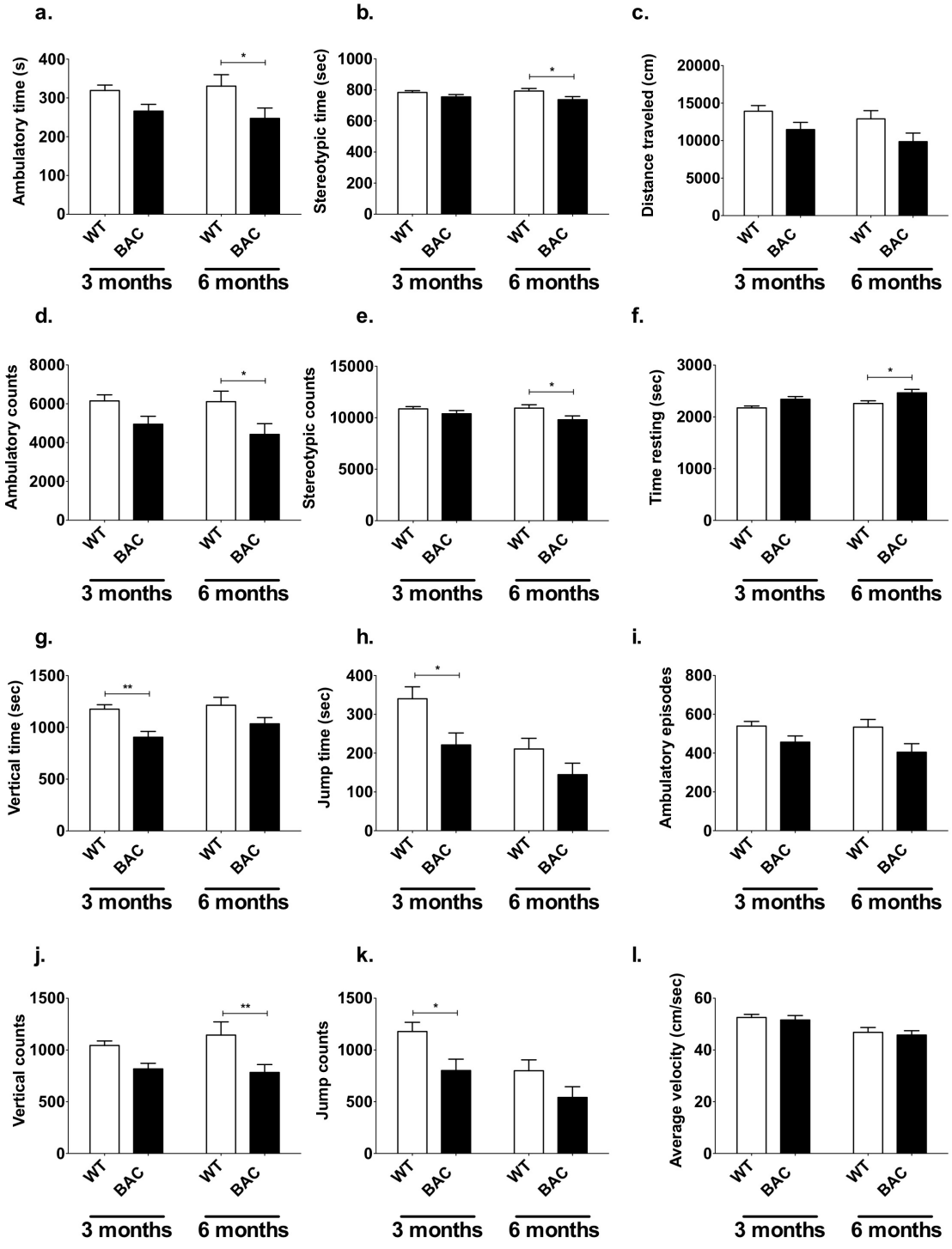

Figure 3.9– *HIP14* BAC transgenic mice appear to display features of hypoactivity. Spontaneous activity was assessed in Med Associates boxes at 3 and 6 months of age. Repeated measures ANOVA reveals a significant effect of genotype in all measures except for average velocity (l) in mixed genders. In females alone, significant effects were seen in vertical counts only (Table 3.2). In males alone, vertical counts and time, and jump counts and time (Table 3.2) were significantly reduced. Data for mixed genders is shown. *p<0.05, **p<0.01.

Endpoint	Gender	Repeated-measures ANOVA (Effect of genotype)	Significance
Ambulatory Time	Mixed	**F(1,40)=5.85, p=0.0202**	*
	Females	ns	ns
	Males	ns	ns
Ambulatory counts	Mixed	**F(1,40)=5.89, p=0.0199**	*
	Females	ns	ns
	Males	ns	ns
Stereological Time	Mixed	**F(1,40)=4.85, p=0.0334**	*
	Females	ns	ns
	Males	ns	ns
Stereological counts	Mixed	**F(1,40)=4.37, p=0.0429**	*
	Females	ns	ns
	Males	ns	ns
Distance Traveled	Mixed	**F(1,40)=4.43, p=0.0417**	*
	Females	ns	ns
	Males	ns	ns
Time Resting	Mixed	**F(1,40)=7.50, p=0.0092**	**
	Females	ns	ns
	Males	F(1,18)=5.19, p=0.0352	*
Vertical Counts	Mixed	**F(1,39)=11.80, p=0.0014**	**
	Females	F(1,19)=5.66, p=0.0280	*
	Males	F(1,18)=5.80, p=0.0270	*
Vertical Time	Mixed	**F(1,39)=10.74, p=0.0022**	**
	Females	ns	ns
	Males	F(1,18)=8.17, p=0.0104	*
Jump Counts	Mixed	**F(1,39)=6.16, p=0.0174**	*
	Females	ns	ns
	Males	F(1,18)=6.79, p=0.0179	*
Jump Time	Mixed	**F(1,39)=6.29, p=0.0164**	*
	Females	ns	ns
	Males	F(1,18)=11.72, p=0.0030	**
Average Velocity	Mixed	F(1,41)=0.28, p=0.5999	ns
	Females	ns	ns
	Males	ns	ns
Ambulatory episodes	Mixed	**F(1,40)=5.51, p=0.0239**	*
	Females	ns	ns
	Males	ns	ns

Table 3.2 - Statistical analysis of spontaneous activity in *HIP14* BAC transgenic mice. *p<0.05, **p<0.01.

3.4.2. Learning and cognitive tests

3.4.2.1. Intact motor learning in HIP14 BAC mice

Learning deficits during training on the rotarod task is a feature observed in the YAC128 mouse model of HD (Van Raamsdonk, 2005b). We trained mice at 3 months of age, with three trials per day over three days, on a 2-minute rotarod task prior to testing for motor coordination as described in section 3.4.1 above. The time to first fall (Figure 3.10a) and the number of falls per trial (Figure 3.10b) were assessed.

HIP14 BAC transgenic mice did not appear to display any deficits in this task. Repeated measures ANOVA revealed no effect of genotype on the latency to fall (Figure 3.10a, Effect of genotype: F(1,200)=0.39, p=0.5356) or on the number of falls (Figure 3.10b, Effect of genotype ANOVA F(1,200)=0.04, p=0.8406) in mice of mixed gender. Examination of day averages in either gender alone also failed to reveal any deficits in females (Latency to fall F(1,18)=0.93, p=0.3604, number of falls F(1,18)=0.40, p=0.5430) nor in males (Latency to fall F(1,24)=0.03, p=0.8764, number of falls F(1,24)=0.20, p=0.6629). Rotarod training was subsequently also examined in a larger cohort, which likewise failed to reveal significant effects (Latency to fall F(1,94)=0.05, p=0.8298, number of falls F(1,94)=0.02, p=0.8917, WT n=27, BAC n=22, data not shown).

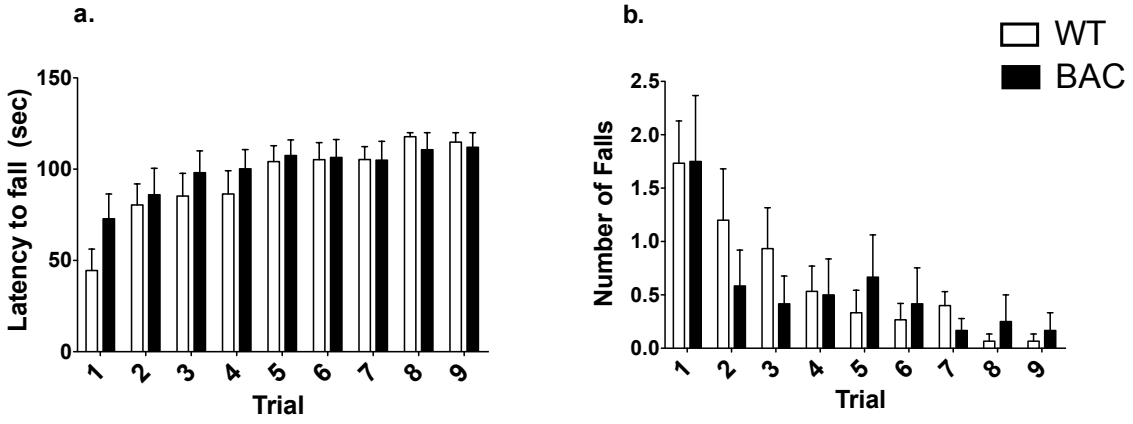

Figure 3.10 – *HIP14* BAC transgenic mice do not demonstrate deficits in the rotarod task of motor learning. *HIP14* BAC of mixed gender mice perform equivalent to WT littermates. Repeated measures ANOVA fails to reveal any effect of genotype on latency to fall (**a**, F(1,200)=0.39, p=0.5356) or number of falls (**b**, F(1,200)=0.04, p=0.8406). WT n=15, BAC n=12.

3.4.2.2. Normal performance on swimming t-maze in HIP14 *BAC mice*

The swimming t-maze has been used to characterize cognitive phenotypes and perseveration (cognitive inflexibility) in the YAC128 mouse model of HD (Van Raamsdonk, 2005b). We assessed whether the *HIP14* BAC transgenic mice display any baseline deficits in this test. Because it is not influenced by weight gain effects, the swimming t-maze and reversal test is a particularly useful behavioural test and has been widely used in our lab. Mice are trained to swim to a submerged and invisible platform in one arm of a T-maze filled with water (Figure 3.11a). On the fourth day, the platform is moved to the opposite arm of the T-maze.

HIP14 BAC mice did not display deficits in any aspect of the task. Both genotypes acquired the task over training days, with no difference in time to platform (Figure 3.11b, $F(1,264)=0.26$, $p=0.6146$) or number entries to the incorrect arm (Figure 3.11c, $F(1,264)=0.13$, $p=0.7201$). When the platform was moved on day 4, the time to reach the platform (Figure 3.11e, $F(1,72)=0.77$, $p=0.3890$) and number of arm entry errors (Figure 3.11f, $F(1,75)=0.12$, $p=0.7361$) were likewise similar. The number of entries to the original arm, a measure of perseveration, was not different (Figure 3.11g, $F(1,72)=0.00$, $p=0.9531$). Swim speed was also indistinguishable between genotypes (Figure 3.11d, $F(1,72)=0.66$, $p=0.4252$). Likewise, separation of genders failed to reveal any significant deficits.

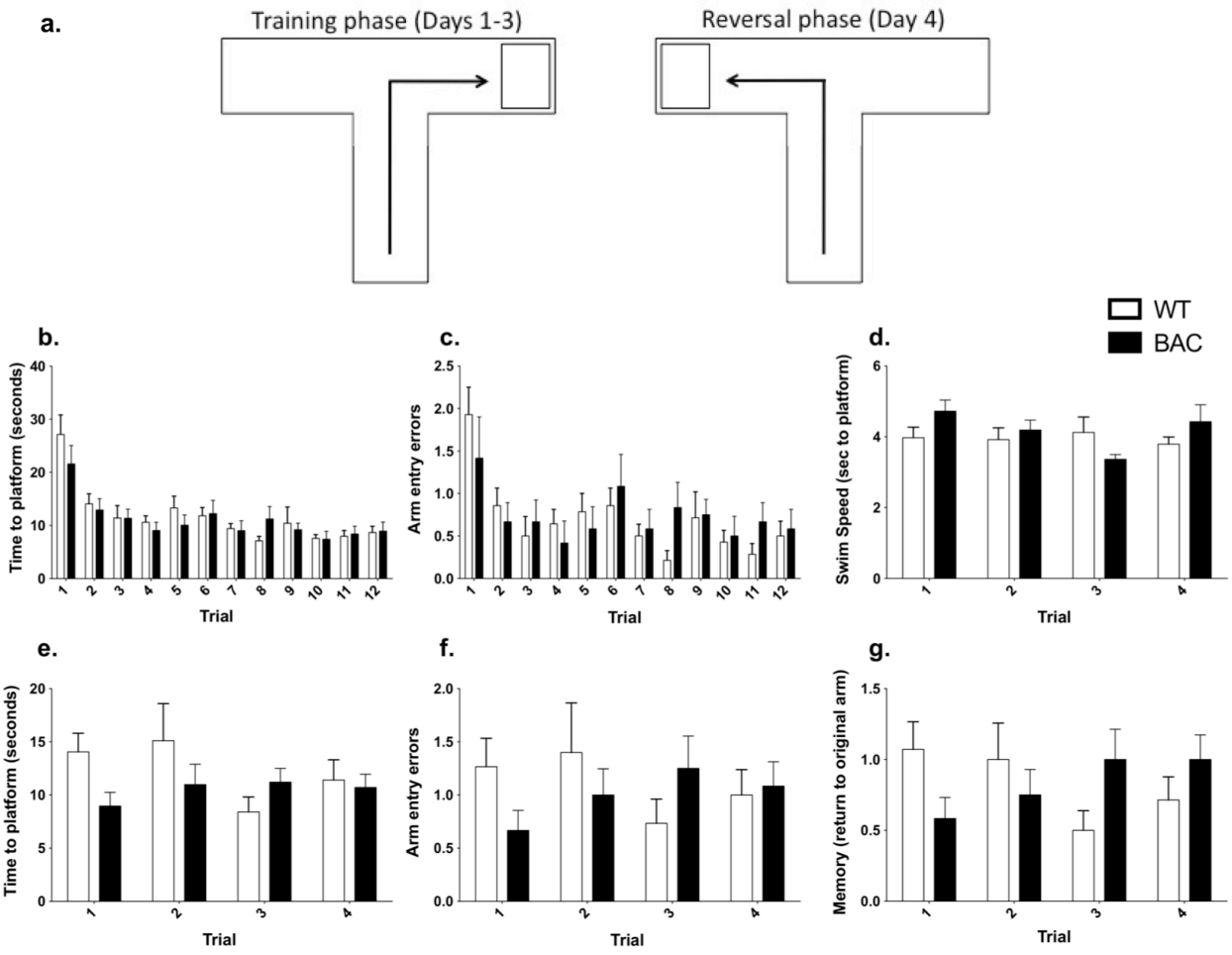

Figure 3.11 – BAC mice do not display deficits in Swimming T-maze learning or reversal. a. Schematic of apparatus used for swimming T-maze test. **b.** Mice were trained in a swimming T-maze to find a submerged platform in one arm of the maze. The time to reach platform does not differ between genotypes during the first 12 trials (two-way repeated measures ANOVA, effect of genotype: $F(1,264)=0.26$, $p=0.6146$). **c.** The number of incorrect arm entries prior to locating the platform is also not different (two-way repeated measures ANOVA, effect of genotype: $F(1,264)=0.13$, $p=0.7201$). **d**. Swim speed does not differ between genotypes (two-way repeated measures ANOVA, effect of genotype: $F(1,72)=0.66$, $p=0.4252$). **e**. On trial 1 of day 4 the platform was switched to the opposite arm of the T-maze. Time to the platform in its new location also did not differ in BAC mice relative to WT littermates (two-way repeated measures ANOVA, effect of genotype: $F(1,72)=0.77$, $p=0.3890$). **f**. Likewise, the number of erroneous arm entries was also not different (two-way repeated measures ANOVA, effect of genotype: $F(1,75)=0.12$, $p=0.7361$). **g.** Memory of the original platform arm (an indication of perseveration) was also not different (two-way repeated measures ANOVA, effect of genotype: $F(1,72)=0.00$, $p=0.9531$). Data represent mean± SEM. n = 14 WT mice, 12 BAC mice. Bonferroni post-hoc testing on all of the above data was not significant.

3.4.3. Tests of anxiety

3.4.3.1. Reduced anxiety-like in HIP14 *BAC mice*

The elevated plus-maze (EPM) is a behavioural test designed to assess anxiety-like behaviour in mice. This test exploits the mouse's innate aversion to bright open spaces, which conflicts with their innate novelty-seeking tendencies. (Holmes *et al.*, 2000). The test apparatus consists of a plus-shaped maze elevated one meter above the floor. Two opposite arms are enclosed by walls, and two arms are open. During testing, the mouse is placed at the end of one closed arm and allowed to explore the arms freely. Mice displaying increased anxiety-like behaviours will spend more time in closed arms as opposed to open arms and display an aversion to exploration of open arms, with an accompanying aversion to exploration of exposed open-arm ends or edges.

The distance traveled (Figure 3.12b, p=0.06) and average velocity (Figure 3.12c, p=0.08) was not different, although assessing males alone revealed a significant increase in *HIP14* BAC mice (both measures p=0.04). Many very similar endpoints are measured as part of EPM testing, so with this in mind, measures of time spent in open arm (as opposed to frequency of entry to open arm) were assessed, since frequency may be influenced by increased locomotion. *HIP14* BAC mice spent significantly more time in open arms (Figure 3.12d, p=0.01) and in the open arm ends (Figure 3.12e, p=0.01); in addition, a significant increase in exploration over the edge of open arms was observed (Figure 3.12f, p=0.005). Likewise, latency to enter the end-region of an open arm was reduced (Figure 3.12g). While increased distance traveled and average velocity appear more prominent in males, reduced anxiety-like phenotype was clearly present in mice of both genders.

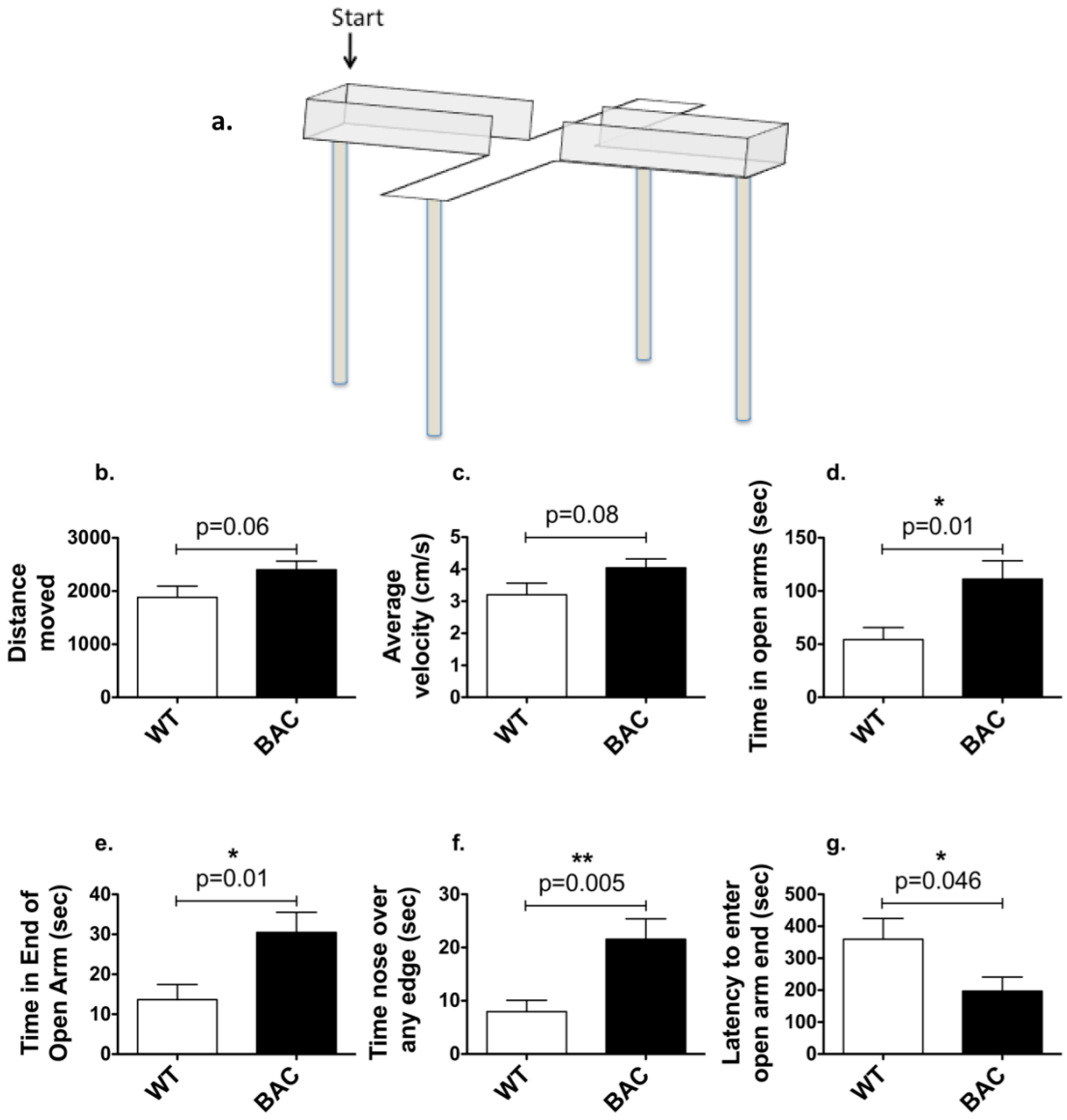

Figure 3.12 BAC transgenic mice display decreased anxiety relative to WT littermates. a. Schematic of Elevated Plus Maze setup. **b**. Distance traveled (p=0.06) and **c**. average velocity (p=0.08) were not significantly different in HIP14 BAC mice relative to WT controls, although assessment of males alone revealed a significant increase in both of these measures (not shown; both p=0.04) while females did not (not shown, distance traveled p=0.82, average velocity p=0.95). Both genders displayed a significant increase in time in open arms (**d**, p=0.01) and in open arm ends (**e**, p=0.01), as well as time of nose over the open arm edge (**f**, p=0.005). Latency to enter the end of open arms was significantly reduced (**g**, p=0.046). WT n=13, BAC n=14. *p<0.05, **p<0.01.

3.4.3.2. Defecation in open field

Defecation is recorded during measurement of spontaneous activity (section 3.4.1.2 above), and is thought to serve as a measure of anxiety (Blizard and Adams, 2002) although this can be highly variable (personal observation). *HIP14* BAC mice did not differ from WT littermates at 3 or 6 months of age (Effect of genotype $F(1,40)=0.49$, $p=0.4859$). Examination of either gender alone was likewise unremarkable (Females $F(1,20)=0.05$, $p=0.8286$, Males $F(1,18)=0.27$, $p=0.6084$).

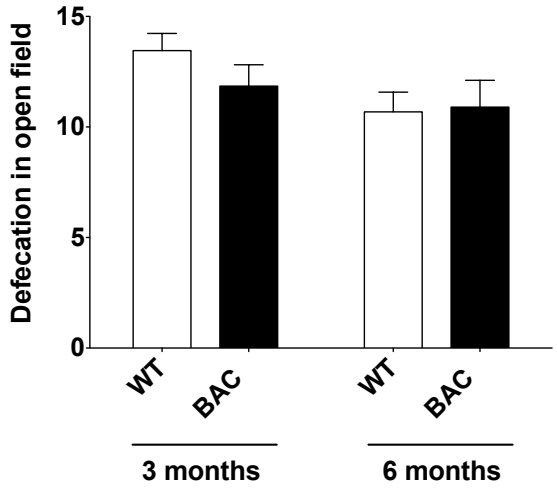

Figure 3.13 – Defecation in Open field does not differ between *HIP14* BAC mice and WT littermates. Two way repeated measures ANOVA effect of genotype $F(1,40)=0.49$, $p=0.4859$). WT n=22 and BAC n=20.

3.5. Other assessments

3.5.1. Body weight is unchanged in *HIP14* BAC mice

Body weight in mice is widely considered an important measure in assessing the general health (Crawley and Paylor, 1997). Body weight of BAC mice was not different from littermates throughout the lifespan (Figure 3.14). Additional measurements taken from other cohorts also revealed no difference (data not shown).

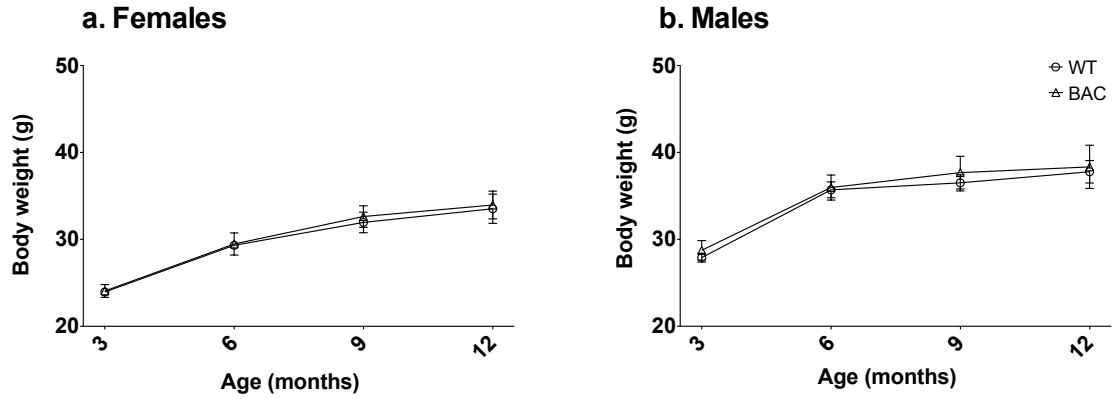

Figure 3.14 - Body weight is no different from WT littermates in *HIP14* BAC transgenic mice. a. Female *HIP14* BAC transgenic mice display no differences in body weight up to 12 months of age (Repeated measures ANOVA effect of genotype F(1,27)=0.04, p=0.8372). **b.** Similarly, no difference in body weight was apparent in *HIP14* BAC transgenic male mice (Repeated measures ANOVA effect of genotype F(1,36)=0.17, p=0.6839).

3.5.2. Testis weight is unchanged in *HIP14* BAC mice

Testes were routinely collected from mice undergoing perfusion for neuropathological assessment. Testicular pathology is a feature of HD in both mice and human HD patients (Van Raamsdonk *et al.*, 2007a). *HIP14* BAC mice showed no difference in testicular weight (Figure 3.15) at 9 months (WT: 0.09052±0.00118, BAC*:* 0.09354±0.003198g, p=0.30) nor at 12 months of age (WT: 0.08171±0.005467, BAC*:* 0.08666±0.002437g, p=0.37).

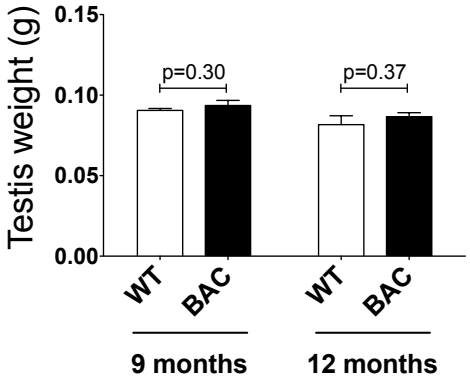

Figure 3.15 – *HIP14* BAC transgenic mice do not display testicular atrophy. No significant change in testicular weight is observed at 9 (p=0.30) or 12 (p=0.37) months of age. 9 months: WT n=9 and BAC n=5; 12 months: WT n=5 and BAC n=8.

3.6. Summary of findings in the human *HIP14* BAC transgenic mouse

In summary, we have generated a transgenic mouse expressing human *HIP14* via a BAC transgenic approach. The line with the highest level of *HIP14* expression, HB4, was selected for further characterization. BAC-derived human *HIP14* mRNA was expressed; however, levels of HIP14 protein overexpression were modest, at ~8-20% greater than WT endogenous HIP14 expression. Brain weight appeared unaffected in line HB4 but was reduced in a second line (HB6) at 12 months. While striatal and cortical stereological assessments in young mice were unremarkable, a small reduction in striatal DARPP-32 was apparent. Assessment of behaviour failed to reveal deficits in motor coordination up to 12 months, however a mild hypoactive phenotype was apparent in spontaneous activity measures in the dark phase of the light cycle. This contrasted with an apparent hyperactivity, more noted in males, in the light observed in Elevated Plus Maze testing. No cognitive deficits were apparent in rotarod learning or swimming t-maze task. No peripheral changes were immediately apparent, as body weight and testicular weight were unchanged. In summary, despite modest overexpression of HIP14, mild phenotypic changes were observed. The implications of these findings are discussed in chapter 6 below.

4. HUMAN *HIP14* COMPENSATES FOR LOSS OF MURINE *HIP14* IN *HIP14*-/- MICE

The similarities between mice lacking murine *Hip14* and HD suggested a critical role for HIP14 in the pathogenesis of HD. However, we wished to determine whether these phenotypes resulted from the loss of murine *Hip14*, and not, for example, a spontaneous mutation or a by-product of unintended mutagenesis events occurring in the generation of the *Hip14-/-* model (Osokine *et al.*, 2008). Crossing the *Hip14-/-* mouse to the *HIP14* BAC transgenic mice would allow us to address this question. Moreover, an important aspect in creation of a novel transgenic mouse model is confirmation of the correct regulation, expression, and function of the transgene (Chandler Kelly J, 2007). Despite the high similarity of human *HIP14* to its murine ortholog, an important aspect of characterization is to confirm appropriate temporal and spatial regulation in the context of the murine cellular machinery. In order to assess whether BAC-derived human *HIP14* can compensate for the loss of its murine ortholog, we generated humanized mice expressing human HIP14 in the absence of murine *Hip14*.

4.1. Breeding strategy to generate mice expressing Human, but not murine, HIP14

In order to generate humanized transgenic mice expressing human *HIP14* in the absence of murine *Hip14*, we crossed BAC mice (BAC, *Hip14*+/+) with mice heterozygous for endogenous *Hip14* (*Hip14*+/-). The 25% resulting BAC, *Hip14*+/- offspring were bred to *Hip14*+/- littermates, and offspring of these mating pairs included all genotypes in this study, in order to ensure that controls were littermates.

4.2. Assessment of HIP14 expression in human *HIP14* BAC transgenic mice crossed to mice lacking murine *Hip14*

4.2.1. mRNA expression

As mRNA expression had not been previously assessed in *Hip14-/-* mice, we first investigated transcript levels in these mice in the absence of the *HIP14* BAC. Two primers specific for murine *Hip14* were obtained; one 5' and one 3' of the gene trap construct located in *Hip14* intron 5 (primer pairs 16 and 17 respectively, Table 2.2).

Murine *Hip14* transcripts were detected at 49.5% (p=0.0092) and 14% (p=0.0003) of WT levels in *Hip14*-/- cortex, 5' and 3' of the gene trap insert, respectively (n=3, Figure 4.1a). Similar detection of mRNA transcripts in gene-trapped mouse models has been previously reported (Hoshii *et al.*, 2007, Lako and Hole, 2000, Roshon *et al.*, 2003, Trimborn *et al.*, 2010, Voss *et al.*, 1998). Using the 3' primer pair, we next confirmed that the murine *Hip14* transcript levels are significantly reduced in *Hip14*-/- compared to WT littermates ($p<0.0001$) and not significantly affected by the presence of the human *HIP14* BAC in BAC-/- mice (Figure 4.1b, ANOVA $p<0.0001$, n=6). In addition, primers specific for human *HIP14* (Table 2.2, primer pair 15) confirmed expression of human *HIP14* mRNA transcript, and no amplification was detected in WT or *Hip14-/-* littermates (Figure 4.1c, ANOVA $p<0.0001$, n=6). Mouse beta-actin primers (Table 2.2, primer pair 18) served as a loading control.

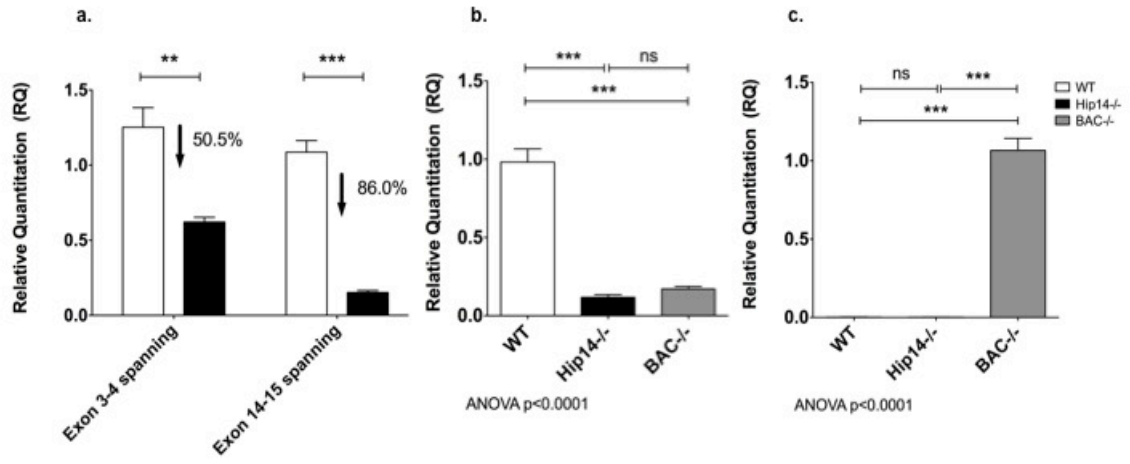

Figure 4.1 - *HIP14* mRNA expression in *Hip14-/-* and BAC-/- mice. mRNA expression was assessed in cortex from mice aged 1 month, using intron-spanning primers specific for murine **(a,b)** and human **(c)** transcript. Murine beta-actin was measured as an endogenous loading control. **a.** Murine *Hip14* transcript is detected in *Hip14*-/- mice both 5' (p=0.0092), and to a lesser extent 3' (p=0.0003) of the gene trap vector located in intron 5 (n=3). **b.** Murine *Hip14* mRNA transcript is significantly reduced in *Hip14-/-* mice (p<0.0001) and is not altered in the presence of human *HIP14* (ANOVA p<0.0001, n=6). **c.** Human *HIP14* is expressed in BAC-/- mice (p<0.0001) and no signal is detected in WT or *Hip14*-/- littermates (ANOVA p<0.0001, n=6).

4.2.2. Protein expression in BAC-/- mice

We confirmed expression of HIP14 from the transgene using a previously described HIP14 antibody (Singaraja, 2002), which detects both mouse and human HIP14; thus, the band detected represents total HIP14 protein. A faint band visible in *Hip14-/-* lanes was confirmed to be non-specific, as it is not eliminated upon peptide competition assay using a >500 molar excess of the peptide used to generate the antibody (Appendix Figure 2). The human *HIP14* transgene expresses at 35% in cortex (Figure 4.2a) to 36% in striatum (Figure 4.2b) of endogenous levels. Protein expression was normalized to a beta tubulin loading control, and values are shown relative to wildtype levels. HIP14 levels in BAC-/- mice were significantly different from *Hip14*-/- in both cortex (p=0.0016 normalized to WT, p=0.019 as raw values) and in striatum (p=0.0091 normalized to WT, p=0.0083 as raw values).

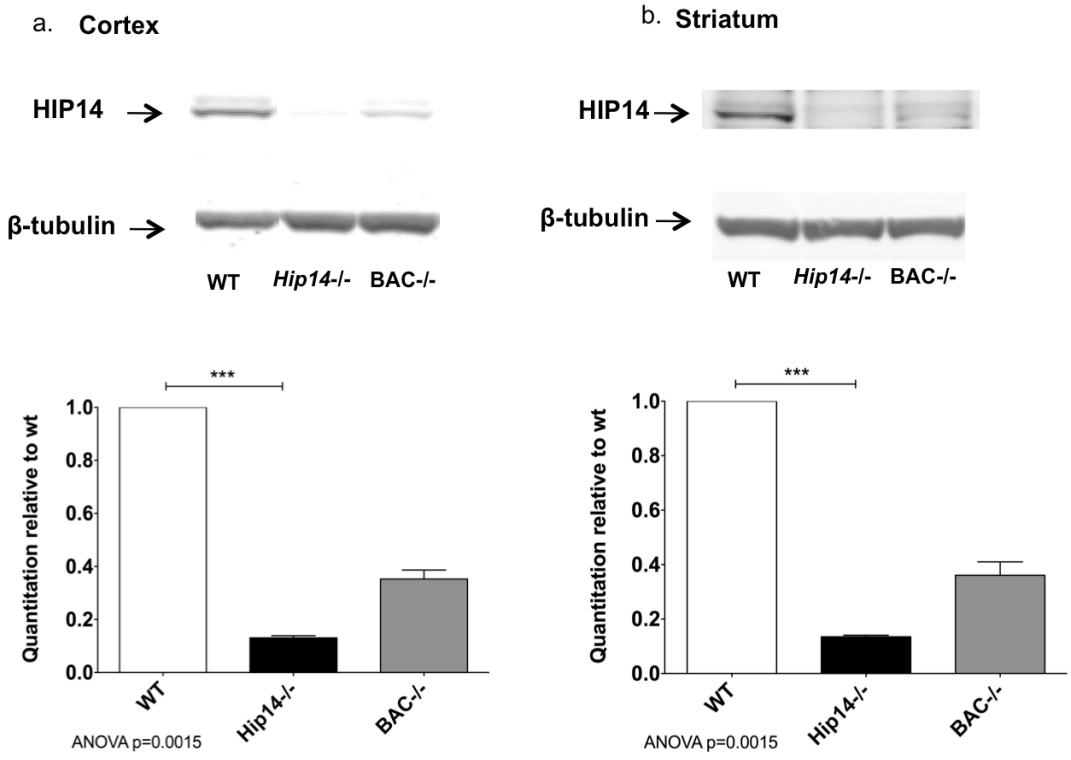

Figure 4.2 - HIP14 protein expression in BAC-/- mice. HIP14 protein expression in cortex **(a)** and striatum **(b)** was assessed by western blot using an in-house HIP14 polyclonal antibody. B-tubulin was used as a loading control. The Kruskal-Wallis non-parametric one-way ANOVA was significant (ANOVA p=0.0015) in both cortex and striatum, and a Dunn's Multiple Comparison post-hoc testing revealed wildtype to be significantly different ($p<0.05$) from *Hip14*-/- in both cases (n=5).

4.3. Human HIP14 compensation of neuropathological deficits in the murine *Hip14* knockout mouse

Mice lacking murine *Hip14* demonstrate neuropathological deficits, including a 17% loss in striatal volume by embryonic day E17.5, with an accompanying reduction in striatal neuron count (192). In order to assess whether BAC-derived HIP14 is functional, we measured a series of striatal and cortical neuropathological endpoints in *Hip14-/-* mice carrying the human *HIP14* BAC transgene, as compared to wildtype and *Hip14*-/- littermates.

4.3.1. Decrease in brain weight in *Hip14-/-* mice is rescued by human HIP14

Brain weight is significantly decreased in *Hip14*-/- mice throughout their lifespan (192). In the current study, whole brain weight (WT: 336.9±1.51, *Hip14-/-:* 310.7±2.60g, Figure 4.3a), cerebellum weight (WT: 55.90±0.55, *Hip14-/-:* 49.47±0.78g, Figure 4.3b), and forebrain weight (WT: 281.0±1.27, *Hip14-/-:* 261.2±2.27g, Figure 4.3c) were all significantly reduced by 3 months of age and were rescued to WT levels in BAC-/- mice (cortex: 331.5±4.37, cerebellum: 54.61±0.90, forebrain: 276.9±3.62g, all ANOVA p0.0001). While cerebellum was similarly rescued at 1 month of age (WT: 51.41±0.82, *Hip14-/-:* 46.45±0.83, BAC-/-: 50.34±1.38g, ANOVA p=0.0038, Figure 4.3b), a non-significant similar trend was observed in whole brain weight (WT: 321.5±3.78, *Hip14-/-:* 309.8±3.74, BAC-/-: 319.2±5.32g, ANOVA p=0.14, Figure 4.3a), and in forebrain weight (WT: 270.1±3.15, *Hip14-/-:* 263.4±3.06, BAC-/-: 268.9±4.27g, ANOVA p=0.36, Figure 4.3c). n=12, 12 and 11 at 1 month and n=10, 10, and 11 at 3 months for WT, *Hip14*-/-, and BAC-/- mice, respectively.

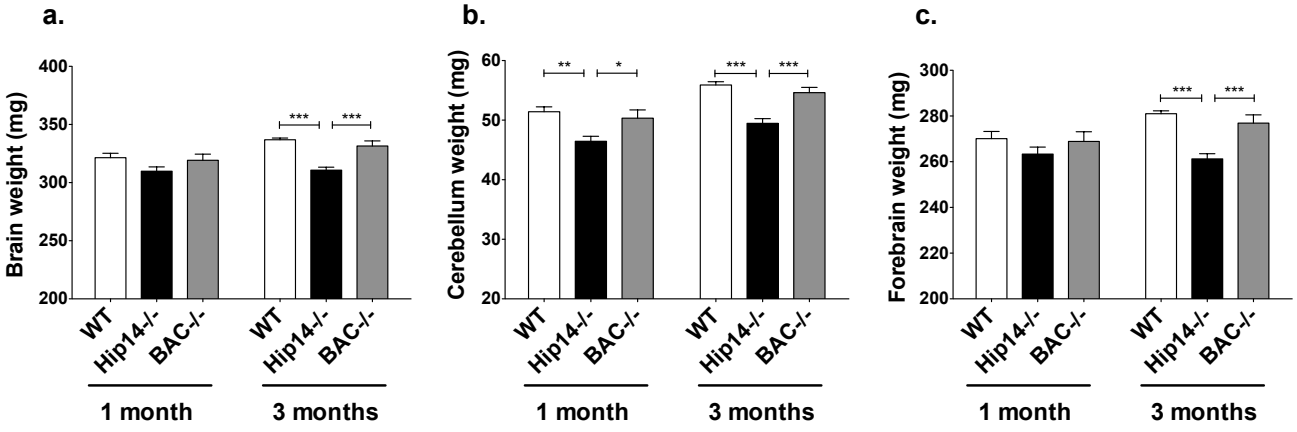

Figure 4.3 - BAC-derived Human HIP14 restores brain weight to WT levels. a. Total brain weight shows significant decrease in *Hip14*-/- mice at 3 months of age, which is rescued to WT levels in BAC-/- mice (ANOVA p<0.0001). A similar trend is present in mice aged 1 month, but is not significant (ANOVA p=0.14). **b.** Cerebellum weight is significantly decreased in *Hip14*-/- mice at both 1 and 3 months of age, and is rescued to WT levels at both ages in BAC-/- mice (1 month ANOVA p=0.0038, 3 months ANOVA p<0.0001). **c.** Forebrain weight is significantly reduced in *Hip14*-/- mice at 3 months of age, and rescued to WT levels in BAC-/- mice at 3 months (ANOVA p<0.0001). A similar trend is apparent but non-significant at 1 month (ANOVA p=0.36). 1 month n=12, 12, and 11 for WT, *Hip14*-/-, and BAC-/- respectively. 3 months: n=10, 10, and 11 for WT, *Hip14*-/-, and BAC-/- respectively. * p<0.05, **p<0.01, ***p<0.0001.

4.3.2. Neuropathology in *Hip14-/-* mice are rescued by human HIP14

Similar to previous findings (192), *Hip14-/-* mice demonstrated a 15.7% reduction in striatal volume at 1 month (wt:10.4±0.3, *Hip14*-/-: 8.8±0.4 mm^3). This was fully rescued to wildtype levels in *Hip14-/-* carrying the BAC transgene (Figure 4.4a; BAC-/-: 10.3±0.2 mm^3; ANOVA p=0.002). At 3 months of age, one-way ANOVA analysis neared significance (WT:12.56±0.33, *Hip14*-/-: 11.48±0.31, BAC-/-: 12.41±0.33 mm^3, ANOVA p=0.0514), although post-hoc Tukey tests were not. Pairwise t-tests revealed that *Hip14-/-* 3mo striatal volume was significantly reduced compared to WT littermates (p=0.03), and neared significance compared to BAC-/- (p=0.0527); WT did not differ from BAC-/- (p=0.75). Striatal neuron count was reduced by 14.3% at 1month in *Hip14-/-* mice (WT:2.0±0.1, *Hip14*-/-: 1.7±0.08 million cells), and this was rescued by the human *HIP14* transgene (Figure 4.4b; BAC-/-: 2.1±0.03 million cells; ANOVA p=0.004). The reduction observed in *Hip14-/-* mice was less robust by 3 months of age, and one-way ANOVA comparing the three genotypes was not significant (WT:2.0±0.06, *Hip14*-/-: 1.9±0.07, BAC-/-: 2.0±0.06 million cells, ANOVA p=0.5953); nor were any pairwise t-test comparisons between genotypes, although the observed trend resembles that at 1 month. Striatal neuronal soma size was unchanged in all three genotypes at 1 month (ANOVA p=0.62) or 3 months (ANOVA p=0.25; Figure 4.4c). In addition, an 11.9% reduction of cortical volume in the *Hip14-/-* at 1 month was rescued in the presence of human HIP14 (Figure 4.4d; WT:26.86±0.52, *Hip14*-/-: 23.66±0.75, BAC-/-: 26.22±0.60 mm^3; ANOVA p=0.003). Similar rescue was observed at 3 months of age, although one-way ANOVA analysis failed to reach significance (WT:29.17±0.81, *Hip14*-/-: 27.36±0.75, BAC-/-: 28.95±0.69 mm^3; ANOVA p=0.1936). Pairwise t-tests were also not significant at 3 months.

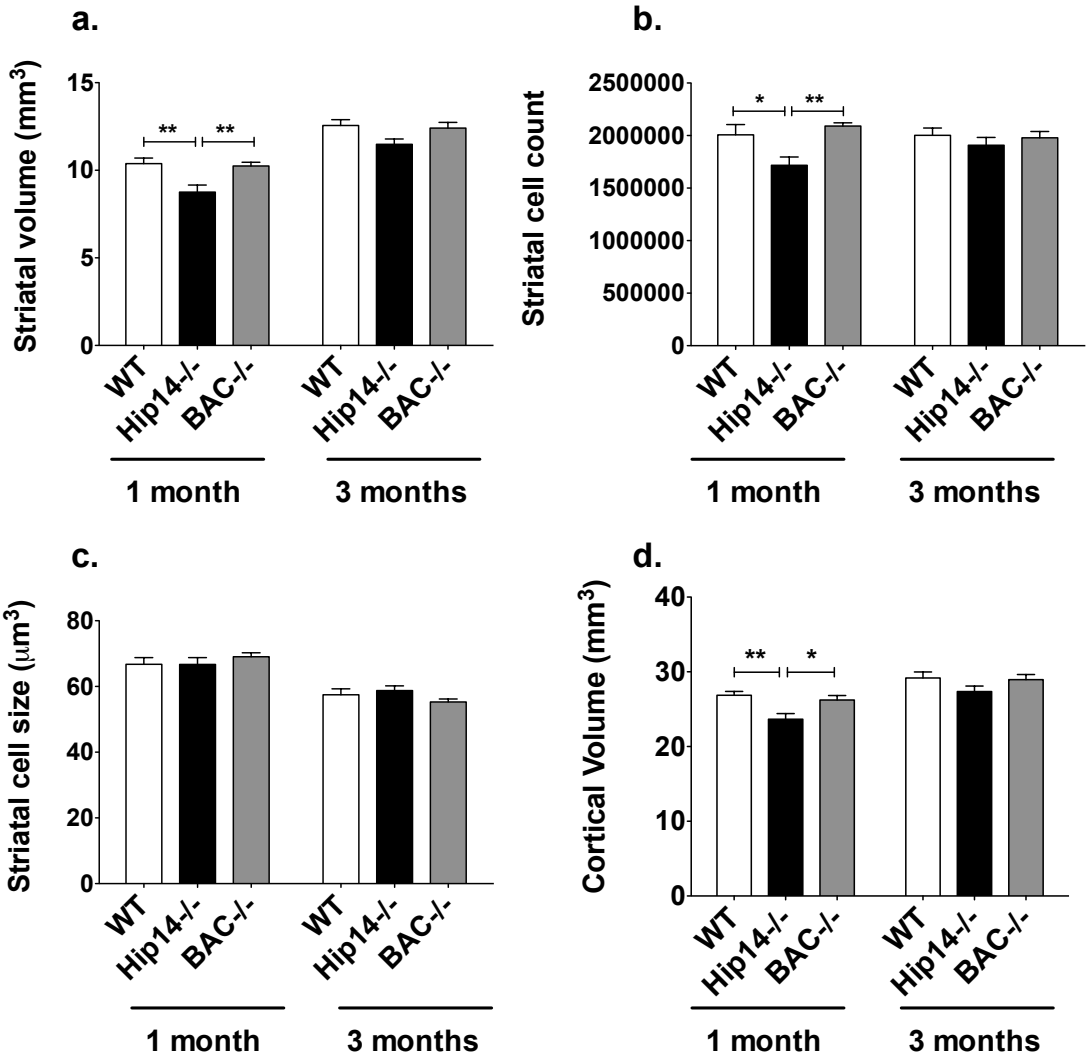

Figure 4.4 – Striatal and cortical pathology in BAC-/- mice. a. Striatal volume was significantly decreased in *Hip14*-/- mice and rescued to WT levels in BAC-/- mice at 1 month of age (ANOVA p=0.002). At 3 months of age, one-way ANOVA analysis nears significance (ANOVA p=0.05). Pairwise t-tests reveal a significant difference between *Hip14-/-* mice and WT (p=0.03) , and near-significance between and BAC-/- (p=0.05) **b.** Striatal neuron count was significantly reduced in *Hip14*-/- mice and rescued to WT levels at 1 month of age (ANOVA p=0.004). At 3 months, one-way ANOVA (p=0.60) and all pairwise t-tests failed to reach significance, though a similar trend is visible. **c.** No difference was observed in striatal neuron size was observed between the three genotypes at 1 month (ANOVA p=0.62) or 3 months (ANOVA p=0.25) of age. **d.** Cortical volume is significantly reduced in *Hip14*-/- mice at 1 month and is significantly rescued in BAC-/ - mice at 1 month of age (ANOVA p=0.003). At 3 months of age, a similar trend is observed but statistical analyses are not significant (ANOVA p=0.1936) 1 month n=12, 12, and 11 for WT, *Hip14*-/-, and BAC-/- respectively. 3 months: n=10, 10, and 11 for WT, *Hip14*-/-, and BAC-/- respectively. *p<0.05, **p<0.01.

4.4. Human HIP14 restores levels of DARPP-32 and enkephalin in *Hip14-/-* MSNs.

The striatal neuron populations affected in HD consist of GABAergic projection neurons and parvalbumin-immunoreactive interneurons, while other neuron populations in the striatum remain relatively spared. The majority (95%) of striatal neurons consist of projection neurons; therefore, the striatal atrophy and cell loss observed in HD is largely due to loss of striatal GABAergic MSNs, cells that express high levels of DARPP-32 (Deng, 2004). These MSNs are subdivided into two types: those expressing enkephalin and dopamine D2 receptors, and those expressing substance-P and dopamine D1 receptors. Levels of enkephalin and DARPP-32 are affected early in HD, whereas substance P remains largely unchanged until later in the disease (Deng, 2004). As in HD patients, *Hip14-/-* mice demonstrate reduced levels of DARPP-32 and enkephalin in the striatum, while levels of substance-P are unchanged. Similar to previous findings, striatal expression of DARPP-32 were reduced by ~39% in *Hip14-/-* mice as compared to wildtype (WT: 47380±792, *Hip14*-/-: 28829±2572), and this was restored to wildtype levels in *Hip14-/-* expressing the human *HIP14* BAC (Figure 4.5a; BAC-/-: 44553±1872; ANOVA $p<0.0001$). Enkephalin staining was reduced by ~84% compared to wildtype (WT: 28773±4040, *Hip14*-/-: 4702±755), while in the human *HIP14* BAC mice were similar to wildtype (Figure 4.5b; BAC-/-: 28637±4002; ANOVA $p<0.001$) Striatal levels of substance-P were similar for all genotypes (Figure 4.5c; WT: 483.2±71.7, *Hip14*-/-: 535.6±62.8, BAC-/-: 541.3±39.1; ANOVA $p=0.8$.). This data demonstrates that BAC-derived human *HIP14* compensates for the neurochemical deficits observed in the *Hip14-/-* mice.

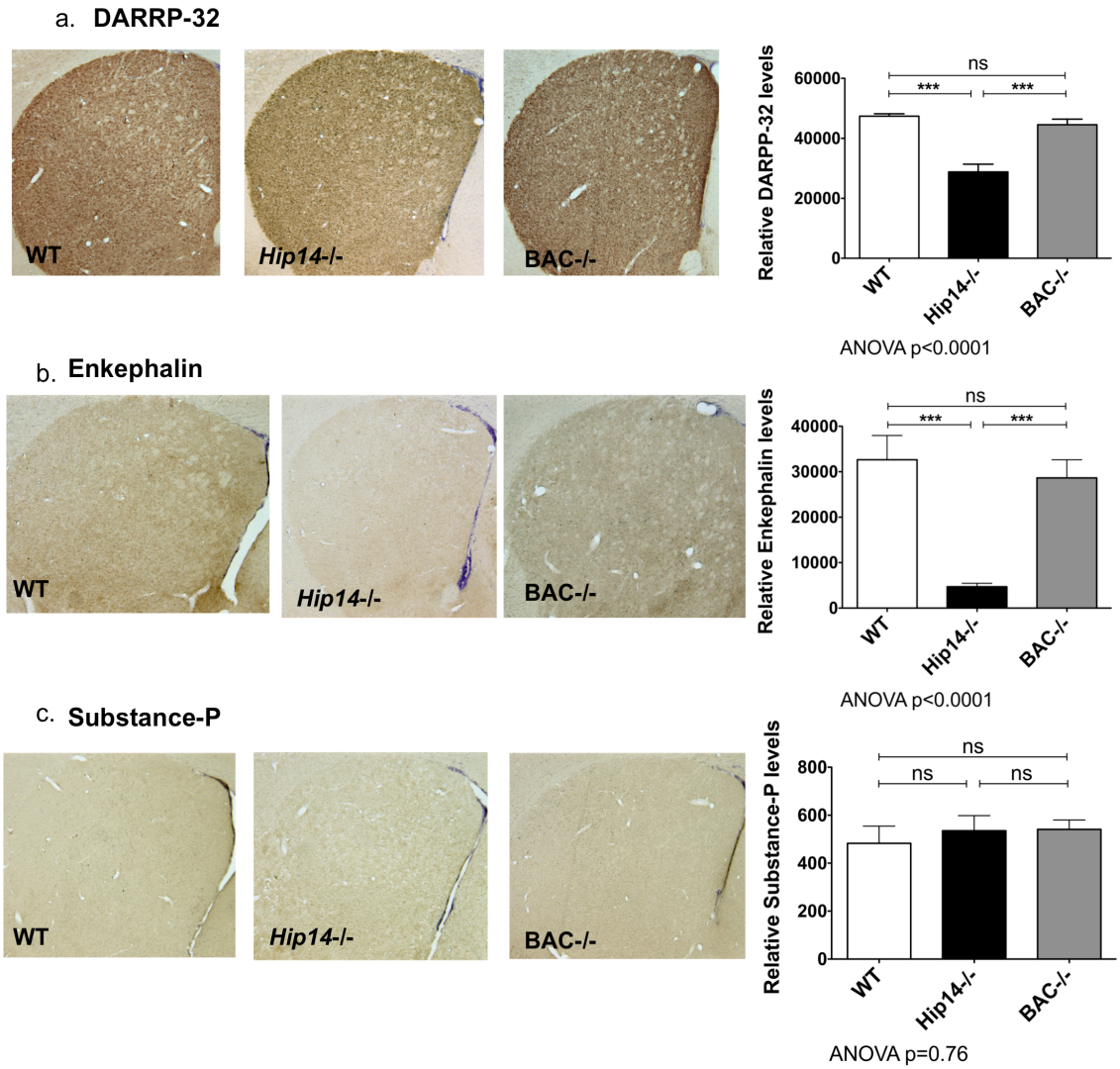

Figure 4.5 - Neurochemical deficits in *Hip14*-/- mice are rescued by human HIP14. Immunohistochemistry was assessed in mice aged 1month. Staining intensity was reduced in the *Hip14*-/- and restored to normal levels for DARRP-32 (a; ANOVA p<0.0001) and Enkephalin (b; ANOVA p<0.0001). Substance-P (c) was unchanged (ANOVA p=0.8). ***p<0.0001.

4.5. Human HIP14 rescues the behavioural deficits seen in murine *Hip14* knockout mice

Hip14-/- mice demonstrate behavioural changes as early as 3 months of age (192). Therefore, we assessed whether human HIP14 can correct the behavioural changes seen in *Hip14*-/- mice.

4.5.1. Tests of motor coordination and spontaneous activity

Motor dysfunction is one of the hallmarks of HD (Hayden, 1981). The *Hip14-/-* mouse demonstrates deficits in motor coordination as early as 3 months and throughout life, though these changes are not progressive in nature (192). As anticipated, a significant effect of age was observed in all of the following analyses ($p<0.0001$). Unless age x genotype interaction was found to be significant, discussion of age effects was omitted.

4.5.1.1. Accelerating rotarod test of motor coordination

Hip14-/- mice demonstrate deficits in motor coordination as early as 3 months of age (192). We therefore assessed mice for performance on an accelerating rotarod at 3 and 6 months of age. Repeated measures ANOVA revealed a significant effect of genotype $F(2,300)=600$, $p=0.0035$ (Figure 4.6a). Bonferroni post-hoc analysis revealed that BAC-/- mice performed consistently better than *Hip14-/-* littermates, remaining on the rotarod apparatus for a longer time before falling ($p<0.05$ at trials 1, 4 and $p<0.01$ at trials 5, 6). BAC-/- performance was also superior to WT littermates, and this was more apparent at later trials (trial 5 $p<0.05$). Surprisingly, WT mice failed to perform significantly better than *Hip14*-/- littermates at any of the six trials. To further explore the poor performance of WT mice, the analysis was repeated with genders separated. In females, a significant effect of genotype and significant interaction of age x genotype were observed (Figure 4.6b; ANOVA Genotype: $F(2,135)=6.53$, $p=0.0049$, Interaction $F(10,135)=2.32$, $p=0.0150$). Bonferroni post-hoc analysis revealed a significant difference between *Hip14*-/- and BAC-/- mice in later trials ($p<0.01$ in trials 4 and 6, $p<0.0001$ in trial 5). A non-significant trend of WT performing superior to *Hip14*-/- is apparent, as is consistently superior performance in BAC-/- relative to both. However, repeated-measures ANOVA failed to reveal significant differences in males alone (Figure 4.6c). A non-significant trend of similarly poor performance in WT and *Hip14*-/- was apparent, as was a consistently superior performance in BAC-/- mice relative to both other genotypes. Therefore, the poor performance in WT mice appeared to be an effect seen largely in males.

However, it is clear in the female group that human *HIP14* BAC can compensate for loss of murine *Hip14.* As previous assessments indicated that the *Hip14*-/- phenotype was not progressive in nature (Singaraja, 2011) and rescue in BAC-/- mice was apparent, we did not assess later ages.

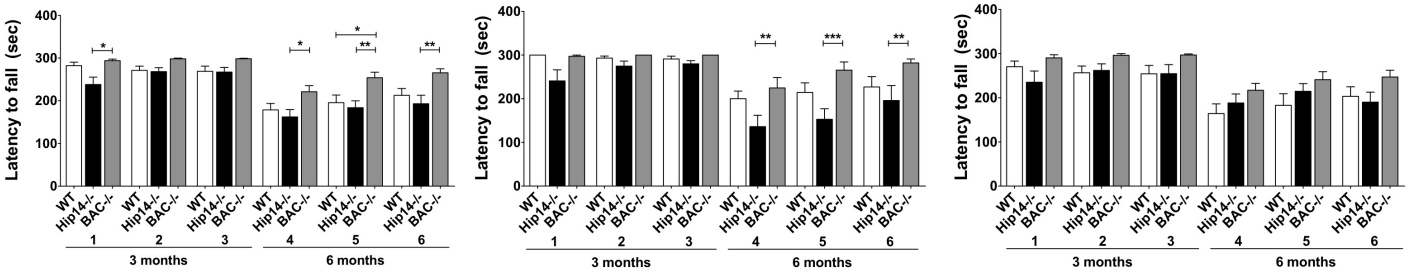

Figure 4.6 - Human HIP14 rescues motor coordination deficits seen in *Hip14*-/- mice. a. Repeated measures ANOVA in combined genders reveals a significant effect of genotype F(2,300)=600, p=0.0035. Bonferroni post-hoc analysis reveals that BAC-/- mice perform consistently better than *Hip14*-/- mice ($p<0.05$ in trials 1,4; $p<0.01$ in trials 5,6) and superior to WT mice in later trials ($p<0.05$ trial 5). All other post-hoc comparisons are non-significant ($p>0.05$). n=25, 20, and 17 for WT, *Hip14*-/-, and BAC-/- respectively. **b.** Repeated measures ANOVA analysis of females alone reveals a significant effect of genotype (F(2,135)=6.53, p=0.0049) and genotype x age interaction (F(10,135)=2.32, p=0.0150). Bonferroni post-tests reveal a consistently superior performance in BAC-/- mice relative to WT littermates ($p<0.01$ trials 4 and 6, $p<0.0001$ trial 5). n=10, 10, 9 for WT, *Hip14*-/-, and BAC-/- respectively. **c.** Repeated measures ANOVA on males alone failed to reveal significant effects of genotype, although a non-significant trend of superior performance was observed in BAC-/- mice relative to both WT and *Hip14*-/- littermates. n=15, 10, 8 for WT, *Hip14*-/-, and BAC-/- respectively. *p<0.05, **p<0.01, ***p<0.0001.

4.5.1.2. Normalization of spontaneous activity in *Hip14-/-* mice by human HIP14

Hip14-/- mice are hyperactive in various measures of dark-phase assessment of spontaneous activity, similar to observations of hyperactivity in young YAC128 mice (Slow Elizabeth J, 2003, Van Raamsdonk, 2005b). A series of measures of spontaneous activity were assessed at 3 and 6 months of age (Figure 4.7, Table 4.1). The most robust changes were observed in stereotypic time and count endpoints, where repeated measures ANOVA revealed a significant effect of genotype in mixed gender, as well as each gender alone. Post-hoc Bonferroni testing revealed an increase in both measures in *Hip14*-/- vs. WT, and a robust rescue in BAC-/- mice (Figure 4.7b, e). Many endpoints demonstrated a significant effect of genotype in mixed gender and also in males alone: Ambulatory time (Figure 4.7a), ambulatory counts (Figure 4.7d), jump time

(Figure 4.7h), jump counts (Figure 4.7k), time resting (Figure 4.7f), and ambulatory episodes (Figure 4.7i), suggesting that changes in males may be largely responsible for changes observed. In contrast, vertical counts (Figure 4.7j) was the only endpoint with significant effect of genotype in both mixed genders and females alone. Interestingly, by 6 months of age, the three phenotypes were indistinguishable by this measure. Finally, distance traveled (Figure 4.7c), vertical time (Figure 4.7g), and average velocity (Figure 4.7l) all showed a significant effect of genotype in mixed gender but not in either gender alone (Table 4.1).

Of the 12 measures assessed, ambulatory time and counts, stereotypic time and counts, distance traveled, time resting, and ambulatory episodes all demonstrated hyperactivity in *Hip14*-/- mice and a robust normalization to wildtype values in BAC-/-. However, observations in vertical time and jump counts and time showed a decrease in BAC-/- relative to both genotypes that was significant upon post-hoc Bonferroni testing at 3 months in all three measures (Figure 4.7g, h, k). This suggested that a modest hypoactivity may be present in BAC-/- mice relative to WT littermates.

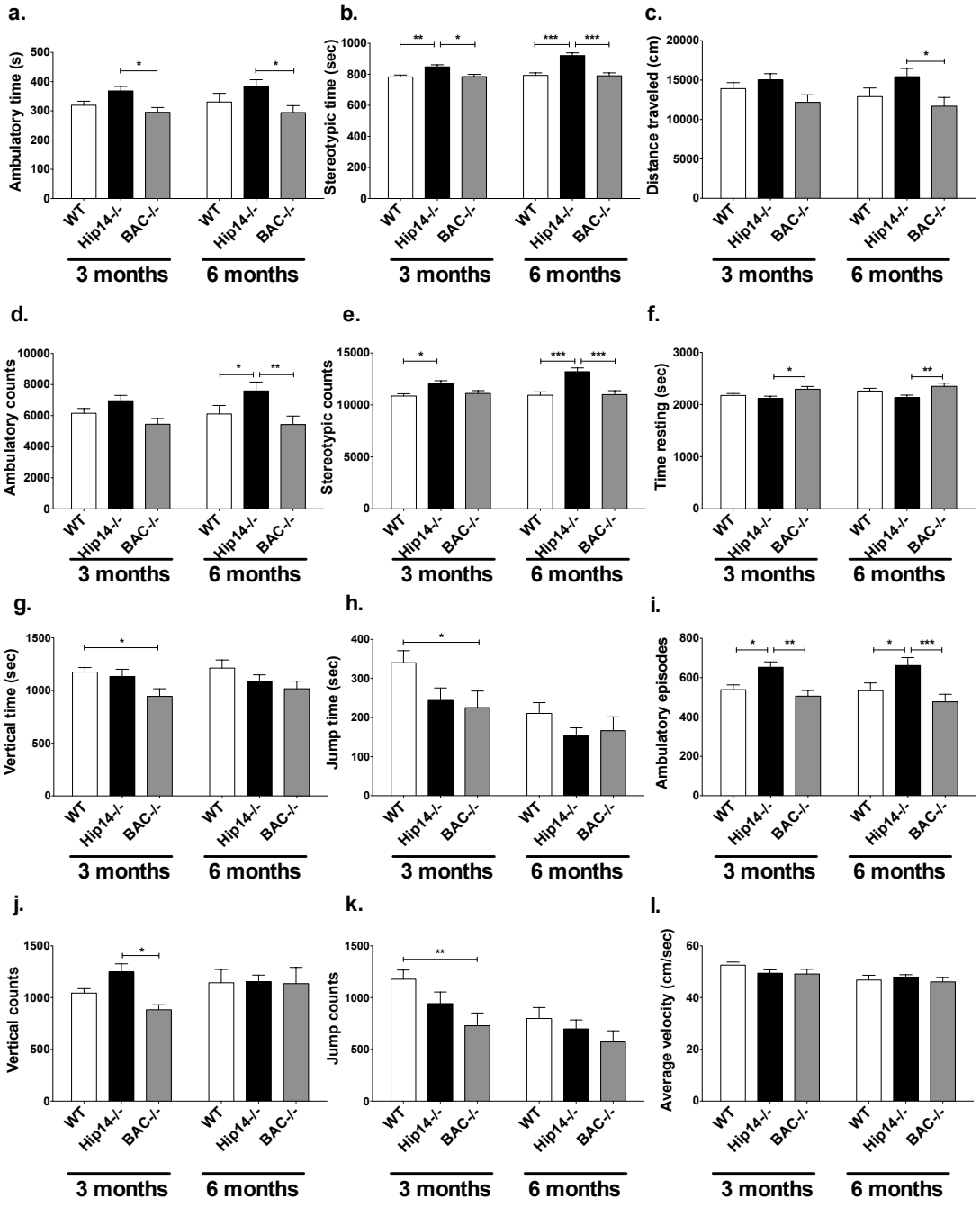

Figure 4.7 - Human HIP14 normalizes the hyperactivity observed in *Hip14*-/- mice to WT levels. Spontaneous activity was assessed in Med Associates boxes at 3 and 6 months of age. Repeated measures ANOVA reveals a significant effect of genotype in all measures except for vertical counts (j), jump time (h), and average velocity (l) in mixed genders. The most robust effects were observed for stereotypic time (b) and counts (e) in mixed genders as well as in either gender alone. In females alone, significant effects were seen in vertical counts only (Table 4.1). Several endpoints were significant in males alone (Ambulatory time (a) and counts (d), jump time (h) and counts (k), time resting (f), and ambulatory episodes (i)), suggesting that the phenotype observed is largely due to changes in males. Finally, post-hoc analysis revealed a significant difference of BAC-/- relative to WT in vertical time ($p<0.05$), jump counts ($p<0.05$) and jump time ($p<0.01$) at 3 months of age, suggestive of a modest potential hypoactive phenotype in these mice. *$p<0.05$, **$p<0.01$, ***$p<0.0001$.

Endpoint	Gender	Repeated-measures ANOVA (Effect of genotype)	Significance
Ambulatory Time	Mixed	**F(2,53)=5.05, p=0.0099**	**
	Females	ns	ns
	Males	F(2,25)=3.45, p=0.048	*
Ambulatory counts	Mixed	**F(2,53)=5.36, p=0.0076**	**
	Females	ns	ns
	Males	F(2,25)=3.71, p=0.039	*
Stereological Time	Mixed	**F(2,53)=19.70, p<0.0001**	***
	Females	F(2,25)=10.03, p=0.0006	**
	Males	F(2,25)=12.93, p=0.0001	**
Stereological counts	Mixed	**F(2,53)=15.13, p<0.0001**	***
	Females	F(2,25)=4.80, p=0.017	*
	Males	F(2,25)=11.35, p=0.0003	**
Distance Traveled	Mixed	**F(2,53)=3.60, p=0.034**	*
	Females	ns	ns
	Males	ns	ns
Time Resting	Mixed	**F(2,53)=4.99, p=0.010**	**
	Females	ns	ns
	Males	F(2,25)=4.38, p=0.023	*
Vertical Counts	Mixed	F(2,51)=1.89, p=0.1611	ns
	Females	F(2,23)=3.67, p=0.042	*
	Males	ns	ns
Vertical Time	Mixed	**F(2,51)=3.28, p=0.046**	*
	Females	ns	ns
	Males	ns	ns
Jump Counts	Mixed	**F(2,51)=3.25, p=0.047**	*
	Females	ns	ns
	Males	F(2,25)=3.49, p=0.046	*
Jump Time	Mixed	F(2,51)=2.77, p=0.072	ns
	Females	ns	ns
	Males	F(2,25)=6.26, p=0.0063	**
Average Velocity	Mixed	F(2,54)=0.68, p=0.51	ns
	Females	ns	ns
	Males	ns	ns
Ambulatory episodes	Mixed	**F(2,53)=8.68, p=0.0005**	**
	Females	ns	ns
	Males	F(2,25)=5.89, p=0.0080	**

Table 4.1 - Statistical analysis of spontaneous activity in BAC-/- mice. *p<0.05, **p<0.01, ***p<0.0001.

4.6. Human HIP14 rescues palmitoylation deficits in *Hip14* -/- mice

HIP14 functions as a PAT for a number of critical neuronal proteins, including PSD-95, SNAP-25, GluR1, GluR2, and NR2B among others (Huang, 2004). Palmitoylation of these neuronal proteins is decreased in both the YAC128 and in

the *Hip14-/-* mouse models, and the defect in palmitoylation is thought to underlie defects in trafficking observed in HD (Singaraja, 2011). We sought to confirm that BAC-derived human HIP14 is a functional enzyme, and to assess whether the human protein product could compensate for the loss of murine *Hip14*. Similar to previous findings, we observed reduced palmitoylation of PSD-95 in the *Hip14-/-* mice (Figure 4.8a, ANOVA p=0.007,n=5). Palmitoylation of SNAP-25 was similarly reduced in the *Hip14-/-* mice, and returned to wildtype levels in the BAC-/- mouse (Figure 4.8b, ANOVA p=0.007 n=5). In both comparisons, post-hoc analysis revealed a significant difference between WT vs *Hip14*-/- and between *Hip14*-/- and BAC-/- ($p<0.05$).

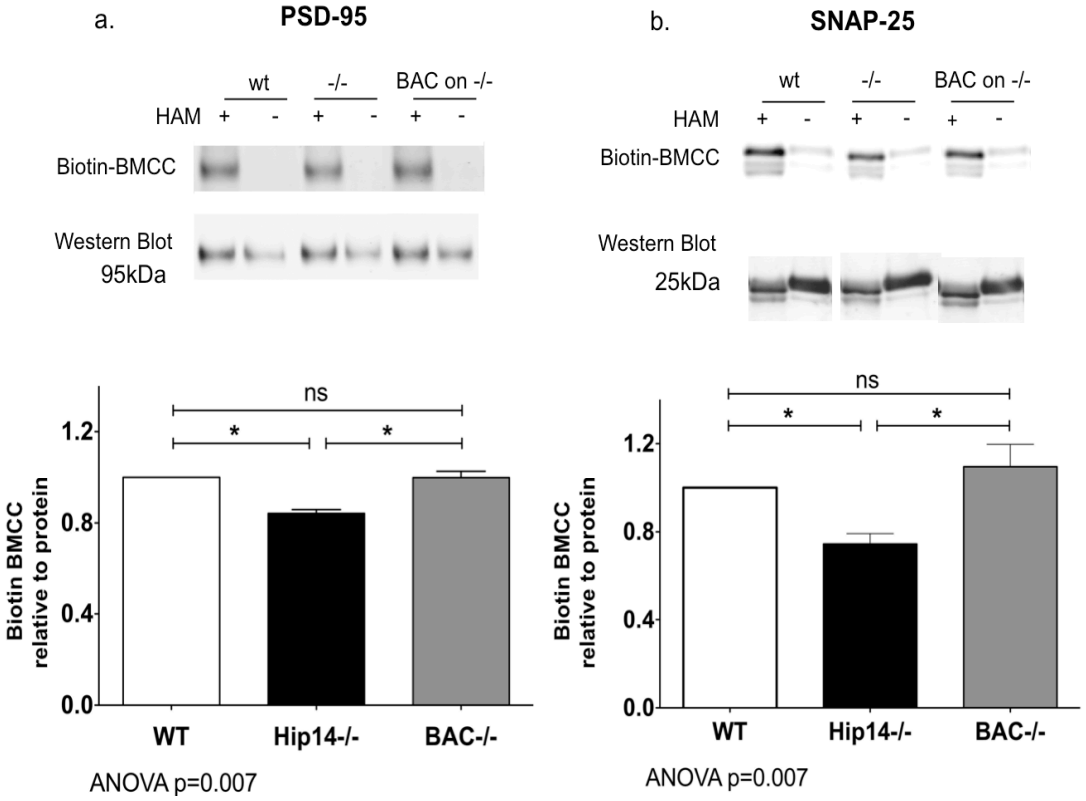

Figure 4.8 - Rescue of palmitoylation deficits of key HIP14 substrates in the *Hip14*-/- mouse. Biotin BMCC assay on HIP14 substrates PSD-95 (a) and SNAP-25 (b). ANOVA p=-0.007, n=5 each. *p<0.05.

4.7. The reduction in body weight seen in *Hip14-/-* mice is only partially rescued by human HIP14

One of the features of HD in human patients is a progressive loss of weight (Walker, 2007, Zuccato *et al.*, 2010), and *Hip14-/-* mice fail to gain weight (Singaraja, 2011) and demonstrate reduced body weight as early as 2 weeks

(data not shown). We therefore assessed whether BAC-derived human HIP14 can compensate for this deficit. *Hip14*-/- mice aged 3 months demonstrate reduced body weight relative to WT, and this is partially rescued by human HIP14 in BAC-/- mice in both genders (Figure 4.9). This pattern is more apparent by 6 months of age in both females (*Hip14-/-* 82.5% and BAC-/- 87.6% of WT) and males (*Hip14-/-* 83.5% and BAC-/- 90.8% of WT). Weekly measurements in a small subset of mice studied revealed that a similar pattern of partial rescue in body weight is present at early as 2 weeks of age (data not shown).

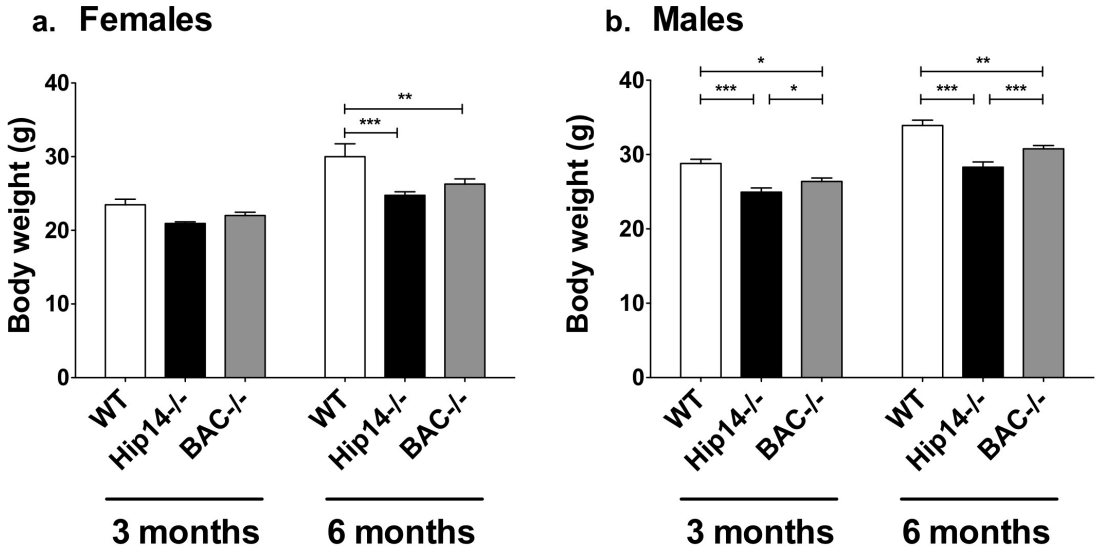

Figure 4.9 - Partial rescue of body weight by human HIP14. *Hip14-/-* mice demonstrate reduced body weight as early as 2 weeks of age (data not shown). **a.** Body weight is decreased in *Hip14-/-* females (89.2% of WT) at 3 months of age, and this is partially rescued (93.8% of WT) in BAC-/- mice (WT 23.47±0.76, *Hip14*-/- 20.94±0.23g, BAC-/- 22.02±0.44g). At 6 months, a similar partial rescue is observed (WT 30.00±1.74, *Hip14*-/- 24.75±0.49g and 82.5% of WT, BAC-/- 26.29±0.69g and 87.6% of WT). Repeated measures ANOVA reveals a significant effect of genotype in females alone ($F(2,27)=7.53$, $p=0.0025$). Bonferroni post-tests reveal that WT differs significantly from both *Hip14*-/- ($p<0.0001$) and BAC-/- ($p<0.01$). n=10, 10, and 9 for WT, *Hip14*-/-, and BAC-/- respectively. **b.** In males, *Hip14-/-* body weight is similarly decreased at 3 months (86.7% of WT) with partial rescue (91.7% of WT) in BAC-/- (WT 28.79±0.56, *Hip14*-/- 24.95±0.57g, BAC-/- 26.39±0.47g). By 6 months, partial rescue is further apparent (WT 33.91±0.71, *Hip14*-/- 28.30±0.70g and 83.45% of WT, BAC-/- 30.78±0.44g and 90.75% of WT). A highly significant effect of genotype is present in males ($F(2,37)=26.81$, $p<0.0001$). Bonferroni post-tests reveal a highly significant difference between WT and *Hip14*-/- at 3 and 6 months of age ($p<0.0001$), and a significant, but less robust, difference between WT and BAC-/- mice at both ages (3 months $p<0.05$, 6 months $p<0.01$). However, BAC-/- mice are also significantly different from *Hip14-/-* at both 3 ($p<0.05$) and 6 months ($p<0.0001$). n=15, 10, and 8 for WT, *Hip14*-/-, and BAC-/- respectively.

4.8. Summary of findings in rescue of *Hip14*-/- phenotype by human HIP14

We generated humanized *HIP14* BAC transgenic mice in order to assess whether BAC-derived human HIP14 can compensate for the loss of its murine ortholog. Assessment of mRNA confirmed expression of human *HIP14* mRNA in these mice and its absence in *Hip14-/-*. Surprisingly, assessment of murine *Hip14* mRNA levels revealed that these are present at ~49.5% and ~14% in *Hip14-/-* mice using primers that are 5' and 3' of the gene trap, respectively. Protein expression in BAC-/- mice was ~35% of endogenous levels in cortex and striatum. Despite this modest level of BAC-derived HIP14 expression, rescue of deficits in brain weight, striatal and cortical stereological measures, and neurochemical endpoints was observed. Assessment of motor coordination and spontaneous activity also showed rescue, with performance often exceeding that of WT littermates, though a potential mild hypoactive phenotype was observed. Deficits in palmitoylation of HIP14 substrates SNAP-25 and PSD-95 are observed. Interestingly, the decreased body weight in *Hip14-/-* mice was partially but not completely rescued. The implications of these findings are discussed in chapter 6 below.

5. FURTHER CHARACTERIZATION OF THE BIOLOGY OF HIP14

Characterization of the *Hip14-/-* mouse lent many critical insights into HIP14 biology and, in particular, the consequences of loss of *Hip14*. However, our understanding of the normal biology of HIP14 remained limited. For example, HIP14 appears to be most highly expressed in the brain (Singaraja, 2011), but the temporal and spatial changes in HIP14 expression were not known, and this information would potentially lead to a better understanding of the disease process. One question that remained was whether loss of *Hip14* in other non-neuronal tissues leads to pathology. Similarly, we asked whether loss of murine *Hip14* recapitulates peripheral phenotypes seen in HD, such as testicular pathology. Likewise, were there other HD-related phenotypes in the brain that we had not yet uncovered? In this chapter, we sought to explore a more general understanding of HIP14 biology.

5.1. *In silico* characterization of HIP14 expression

There now exist several online resources to assess HIP14 expression (Saunders, 2010). A number of these and other databases were reviewed for *in silico* information on HIP14 expression (Table 5.1). However, *in silico* data was limited. The Genomics Institute of the Novartis Research Foundation has generated a gene atlas of protein-encoding transcripts using mouse and human tissue (Su *et al.*, 2004). This information is accessible via the BioGPS gene annotation portal (http://biogps.gnf.org). A collection of tissue samples constitute a dataset, which is assessed with one or more probes, each probe with unique properties and annealing to a particular region in the gene of interest. In humans, one dataset (GeneAtlas U133A) with two probes revealed supramedian expression levels in a number of neuronal tissues, including retina, pineal gland, prefrontal cortex, parietal lobe, cingulate/occipital/temporal lobe, subthalamic nucleus, and cerebellar peduncles (GeneAtlas dataset U133A, probes 217486_s_at and 212982_at). In mice, two datasets (GNF1M and MOE430) cover a range of

tissues with a total of six probes. The majority of probes anneal to the 3' UTR region of *Hip14*. Four out of six probes reveal *Hip14* expression above median levels in neuronal tissues, particularly in the cerebellum. Elevated levels of expression are also observed in some tissues of the eye (retina, preoptic tissue, and eyecup) (Dataset GNF1M, probes gnf1m08189 and gnf13162 ; Dataset MOE430, probes 1434397_at , 1447656 , 1455986 , and 1458363).

Expression database	**HIP14 entry?**	**Website**
Genomics Institute of the Novartis Research Foundation	Yes	http://biogps.gnf.org/
Allen Mouse Brain Atlas	Yes	http://mouse.brain-map.org/welcome.do
MGI Gene Expression Database (GXD)	Yes	http://www.informatics.jax.org/expression.shtml
Edinburgh Mouse Atlas of Gene Expression (EMAGE)	No	http://www.emouseatlas.org/emage/home.php
Genepaint Digital Atlas of Gene Expression	No	http://www.genepaint.org/
EURExpress Transcriptome Atlas	Yes-no expression information	http://www.eurexpress.org/ee/
Allen Developing Mouse Brain atlas	No	http://developingmouse.brain-map.org/
Brain Gene Expression Map (BGEM)	No	http://www.stjudebgem.org/web/mainPage/mainPage.php
Expression Nervous System Atlas (GENSAT)	No	http://www.gensat.org/searchgenes.jsp
Gene Expression in 4D	No	http://4dx.embl.de/4DXpress/welcome.do

Table 5.1 – Online Databases of information on gene expression

The Allen Brain atlas lists RNA *in situ* hybridization (ISH) expression data for a number of genes throughout the brain; both expression level (approximate total transcript count) and expression density (fraction of expressing cells) is shown.

Highest expression level and density was observed in cerebral cortex. Olfactory bulb and retrohippocampal region showed similarly elevated values for both endpoints as well. An intermediate level of expression and density was apparent in striatum. A moderate level of expression but relatively low expression density is reported in cerebellum. An important caveat: the data derives from saggital sections of a single C57BL/6J male mouse aged 55 days and therefore represents an n of one (Lein *et al.*, 2007).

Finally, the MGI Gene Expression Database (GXD) reveals Taqman rtPCR gene expression data for *Hip14* expression in the developing embryo, in both the embryonic and extraembryonic components. The data reveals that *Hip14* is expressed in the oocyte and in embryos aged E1.5-E4.5 but not E2, as assessed in 150 pooled embryos at each age. Therefore, it appears that *Hip14* is expressed very early in development (Guo Guoji *et al.*, 2010).

In summary, the limited *in silico* gene expression data for HIP14 available reveals that HIP14 is highly expressed in neuronal tissues, including tissues of the eye, and is expressed at very early stages of development.

5.2. The expression of HIP14 in the brain throughout development

HIP14 clearly plays a critical role in brain development. The *Hip14-/-* HD-like phenotype appears to emerge between embryonic days E14.5 and E17.5, when striatal pathology is first apparent (192). We set out to elucidate the expression patterns of HIP14 within the brain and brain subregions in early development. In addition to deepening our understanding of HIP14 biology, this knowledge will be critical in the design of future experiments, for example, in designing experiments in which HIP14 is selectively ablated from particular subregions of the brain in future mouse models.

5.2.1. Western blot analysis of HIP14 protein expression in the brain

Because consequences of loss of *Hip14* appear early in development (192), it is likely that the developing brain is particularly sensitive to changes in levels of expression of HIP14 at this time, in late embryogenesis. We anticipate that highest levels of HIP14 coincide with onset of the neuropathological phenotype in *Hip14-/-* mice in the tissues affected. In order to confirm this experimentally, we next assessed the temporal and spatial pattern of HIP14 protein expression over development.

5.2.1.1. Selection of appropriate loading controls

Assessments of HIP14 expression in earlier chapters of this thesis have been normalized to β-tubulin. However, previous assessments have investigated HIP14 expression within a given tissue at one age. Because the expression of a protein typically used as a loading control may itself change over development, we first assessed a select number of proteins typically used as loading controls in western blot analysis of protein expression in the brain regions of interest. All quantifications are arbitrarily assessed relative to the value at 2 months.

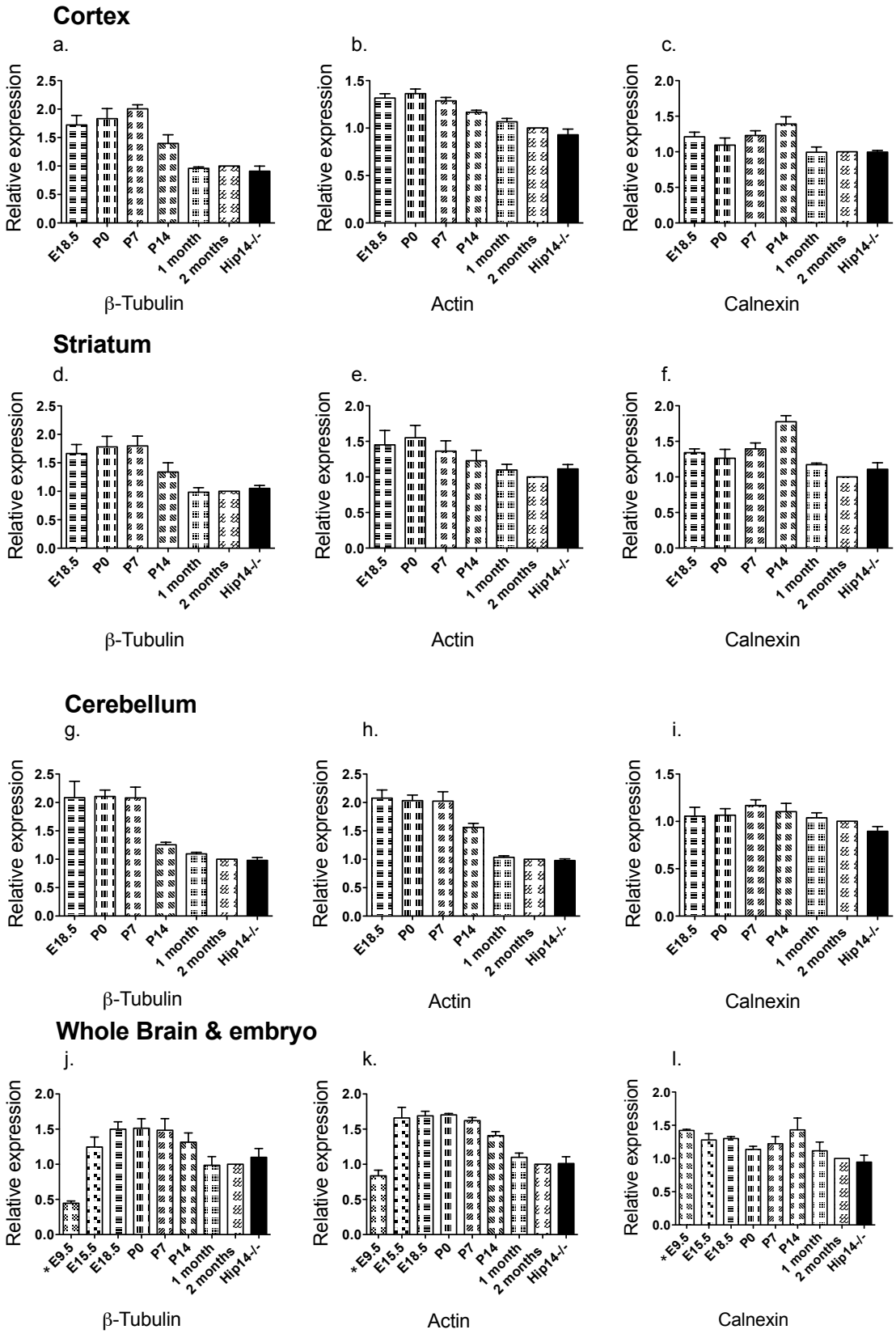
Cortex
a.
b.
c.
Striatum
d.
e.
f.
Cerebellum
g.
h.
i.
Whole Brain & embryo
j.
k.
l.
Relative expression
E18.5
P0
P7
P14
1 month
2 months
Hip14-/-
* E9.5
E15.5
β-Tubulin
Actin
Calnexin

Figure 5.1 - Evaluation of loading controls for assessing protein expression over development. Beta-tubulin (a,d,g,j), actin (b,e,h,k), and calnexin (c,f,I,l) protein expression was assessed in mouse whole brain (j-l) and brain subregions (a-i) over development in order to identify the optimal candidate for loading control in the assessment of HIP14 protein expression over development. An ideal loading control is relatively stable in expression across ages assessed. Beta tubulin appeared to be most highly expressed in early development between E18.5 to P7, dropping by ~33-50% by 1 month of age in all brain regions assessed (a,d,g,j). A similar pattern in actin was observed (b,e,h,k). Notably, pooled whole embryos at E9.5 were much lower, despite equal protein loading as assessed by Bradford assay and ponceau stain (data not shown). Calnexin clearly displayed the most stable pattern of expression (c,f,I,l); however, a peak in calnexin expression at P14 was apparent in forebrain structures (c.f) as well as whole brain (l), but not cerebellum (l). Pooled whole E9.5 embryo lanes showed similar levels of calnexin to whole brain (l). Based on these findings, we selected calnexin as an appropriate loading control for assessment of developmental expression of HIP14 in the brain. (n=3 for each age and each brain region or subregion).

Glyceraldehyde 3-phosphate dehydrogenase (GAPDH) was included in preliminary assessments, but showed the greatest differences in expression over different ages, with expression at 2 months elevated 2.5 times that of E18.5, and so was not included in further assessments (data not shown). β tubulin displayed a relatively uniform pattern in all brain regions examined (cortex, striatum, cerebellum, and whole brain; Figure 5.1a,d,g, and j respectively). Expression peaks at P7 before decreasing by approximately 50% (cortex,striatum, cerebellum) to 33% (whole brain) by one month of age. Actin is similarly elevated at earlier developmental ages before decreasing to one third to one half of peak levels by one month (Figure 5.1 b,e,h,k). Actin appears to peak at highest levels at E18.5 to P0. Calnexin expression is the most stable of the four loading controls assessed (Figure 5.1 c,f,i,l). In cortex and striatum, calnexin expression is relatively uniform apart from an apparent peak at P14. A similar pattern is seen in whole brain. Cerebellar calnexin expression is relatively uniform. Prior to blotting, membranes were stained with Ponceau-S red, which revealed uniform loading (data not shown). Given these findings, we selected calnexin as a loading control, bearing in mind the apparent peak in expression at P14 in results interpretation.

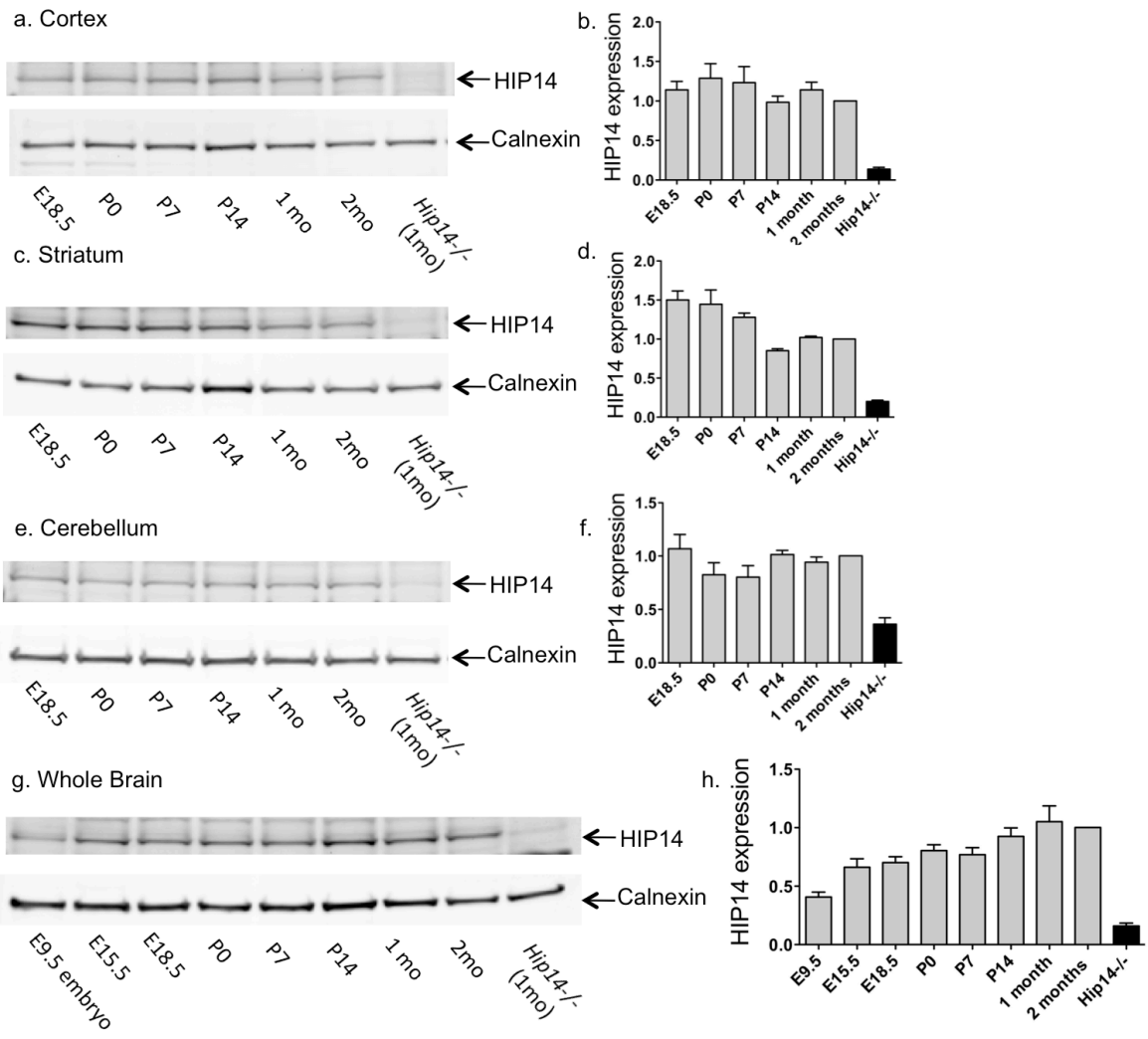

Figure 5.1 - Developmental expression of HIP14 in the brain. a. Representative blot of HIP14 expression in cortex. Calnexin is quantified as a loading control. HIP14 expression is highest at P0 in cortex. c. HIP14 expression on striatum is highest at E18.5 and undergoes the largest decrease by 50% at 2 months. e. Cerebellar HIP14 expression is relatively stable, but highest at E18.5. g. In contrast to brain subregions, HIP14 expression in whole brain progressively increases over time, doubling and reaching highest levels by 1 month of age. b,d,f,h Quantification of HIP14 expression. n=3 for each tissue at each age.

5.2.1.2. Developmental expression of HIP14 in the brain

HIP14 expression was assessed in cortex, striatum, and cerebellum at E18.5, P0, P7, P14, 1 month, and 2 months of age. HIP14 expression was also assessed in whole brain at the same ages, as well as at E15.5. Expression at E9.5 from 3 whole embryos pooled was also included. *Hip14-/-* brain aged 1 month was assessed as a negative control.

HIP14 expression in cortex (Figure 5.2a,b) and striatum (Figure 5.2c,d) appeared to follow a similar pattern. Highest expression was observed at earlier developmental ages, with highest expression at P0 in cortex and E18.5 to P0 in striatum. The observed decrease in expression at P14 in both tissues was an artifact of the peak in calnexin expression at P14 (Figure 5.1). Expression in the cerebellum (Figure 5.2 e, f) decreased approximately 25% at P0 and P7 before returning to E18.5 levels and remaining relatively stable from P14-2 months. Assessment of HIP14 expression in whole brain (Figure 5.2 g,h) revealed a progressive twofold increase in expression from E15.5 to 2 months despite the opposite pattern of HIP14 expression observed in cortex and striatum. The difference in findings may arise due to the inclusion of other brain structures in whole brain lysate, such as brainstem and white matter. Levels of expression at E9.5 in pooled whole embryos are shown here for comparison.

We next assessed HIP14 expression across brain regions at the same ages (Figure 5.3). At both E18.5 (Figure 5.3a) and P0 (Figure 5.3b), highest HIP14 expression was observed in cortex, while levels in striatum, cerebellum, and whole brain were comparable. A similar pattern was observed by 1 week (P7, Figure 5.3c), although a mild elevation in striatum and cerebellum was apparent relative to whole brain. By 2 weeks of age (P14, Figure 5.3d), a different pattern was observed. Levels of HIP14 expression in cortex and striatum were half of that in whole brain, while a mildly elevated expression was observed in cerebellum. A similar pattern persisted at 1 month (Figure 5.3e) and 2 months (Figure 5.3f). An apparent spike in HIP14 expression at 1 month is likely due to a bubble in the loading control of one replicate; the true level of expression in cortex at 1 month is likely similar to that observed at 2 months of age (Figure 5.3f).

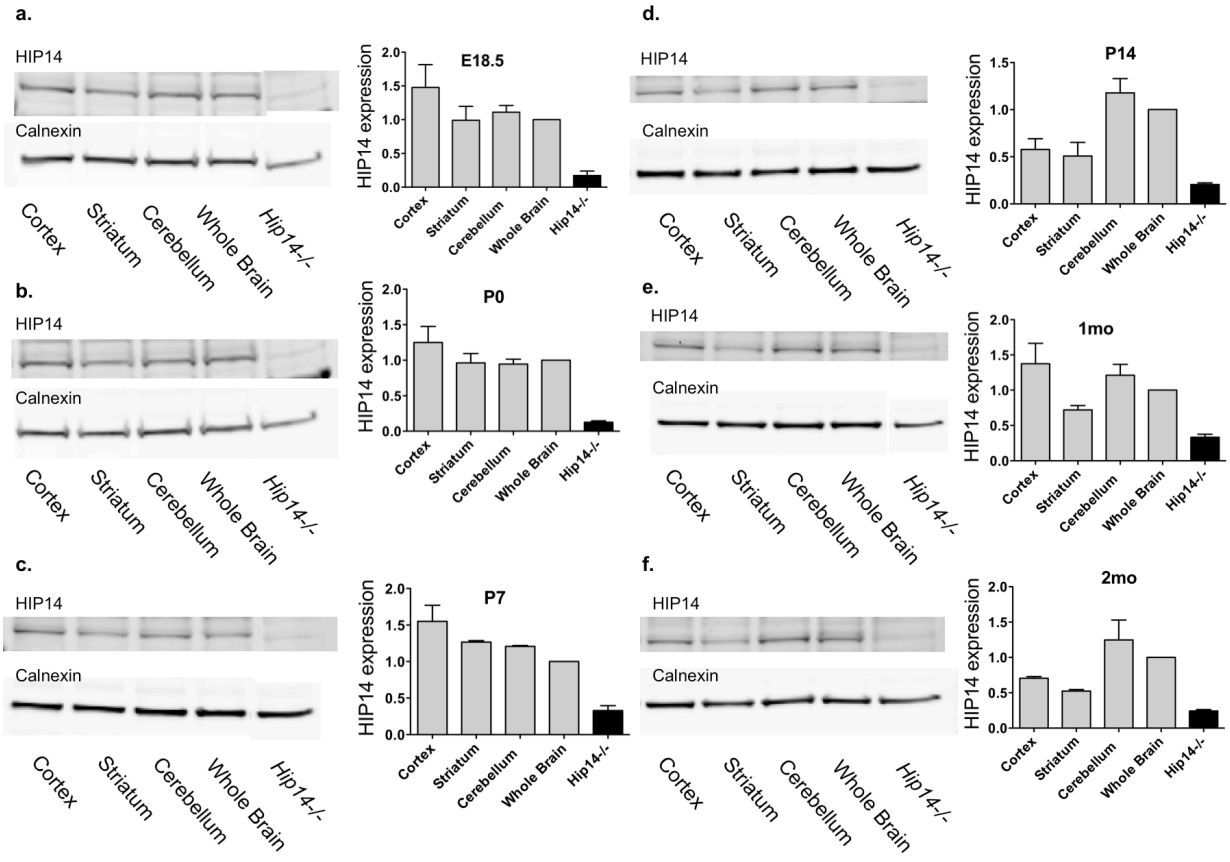

Figure 5.3- HIP14 expression over brain regions in early development. Brain expression of HIP14 in cortex, striatum, cerebellum, and whole brain of FVB wildtype mice was assessed in tissue at six different ages over early development. Values are normalized to calnexin as a loading control, and values shown are relative to whole brain levels. **a.** At E18.5, HIP14 expression is highest expression in cortex, while levels in striatum and cerebellum are similar to whole brain. **b.** A similar pattern is observed at P0. **c.** By P7 (1 week), a similar pattern is observed. Levels in cortex are ~1.5x that of whole brain levels, and levels in striatum and cerebellum are also mildly elevated at ~1.25x whole brain levels. **d.** At P14 (2 weeks), a different pattern emerges. HIP14 expression in cortex and striatum is ~0.5x whole brain levels, while levels are mildly higher than whole brain in cerebellum. A similar pattern persists at 1 month (**e.**) and 2 months (**f.**) of age. The apparent elevated levels of HIP14 expression in cortex at 1 month may be an artifact, due to the presence of a bubble in the loading control in one of the three replicates. The true value in cortex at 1 month is likely similar to that observed at 2 months (**f.**) n=3 for each brain region at each age.

In summary, the highest level HIP14 expression in the brain is observed in cortex in early life. Similarly, the largest change in HIP14 expression over time appears to occur in cortex, with levels decreasing from ~1.5x to ~0.5x that of whole brain between E18.5 and 2 months of age. A similarly remarkable decrease occurs in striatum over these ages.

5.3. The biology of HIP14 in the testes

Hip14-/- x *Hip14-/-* matings were set up as part of a modified breeding strategy to obtain greater numbers of *Hip14-/-* offspring for experiments. However, initial anecdotal observations suggested impaired fertility in these mating pairs.

Testicular pathology has been reported in human HD (Van Raamsdonk, 2007a), as well as in the YAC128 (Van Raamsdonk, 2007a) and R6/2 (Sathasivam *et al.*, 1999) mouse models of HD. Normal endogenous huntingtin (*Hdh*) appears to play a critical role in testicular biology, as *Hdh* inactivation results in reduced sperm production and male infertility (Dragatsis Ioannis *et al.*, 2000). In addition, testicular atrophy and degeneration caused by mutant HTT in YAC128 mice is worsened in the absence of endogenous murine *Hdh,* implicating both a gain of function (toxic mutant HTT) and a loss of function (normal *Hdh*) (Van Raamsdonk *et al.*, 2005a).

Accumulating reports have highlighted a role for huntingtin interacting proteins in testicular biology. For example, Huntingtin Interacting Protein 1, a clathrin coat adaptor protein, plays an important role in male fertility and testicular biology. Mice lacking Hip1 (*Hip1*-/-) display pathological changes in sperm maturation, resulting in reduced fertility of *Hip1*-/- male mice (Khatchadourian *et al.*, 2007, Rao *et al.*, 2001). Huntingtin Associated Protein 1 (Hap1), a protein critical for intracellular trafficking, is expressed in the testis (Dragatsis Ioannis, 2000). Notably, it has been previously reported that gene expression patterns of the testis are similar to those observed in the brain (Guo J. *et al.*, 2003), supportive of the hypothesis that HIP14 may play a critical role in the testes as well as brain. The prominent HD-like phenotype described thus far in the *Hip14-/-* mice, together with the large body of evidence of testicular pathology in HD and HD-related models and anecdotal evidence of a potential fertility deficit in *Hip14-/-* mice led us to assess the testicular phenotype in this model.

5.3.1. Absence of *Hip14* results in reduced fertility

Because of the association of testicular pathology with HD described above, we hypothesized that the anecdotal reports of impaired breeding in *Hip14-/-* mice originated in males. In order to assess the fertility of *Hip14*-/- males, we crossed *Hip14-/-* males or WT males of equivalent age to WT females. Females were of identical age and were crowded prior to mating in order to synchronize estrous cycles. After 6 months, 90.91 % (10 of 11 mating pairs) of WT males successfully bred. In contrast, only 61.54% (8 of 13 mating pairs) of *Hip14-/-* males bred successfully. At 6 months, matings with *Hip14-/-* males produced significantly fewer litters per month (p=0.03), suggesting impaired fertility in *Hip14-/-* males. Similarly, the total number of litters (p=0.046) and total number of pups (p=0.054) were also reduced (data not shown). Qualitatively, it was observed that the ability of *Hip14-/-* males to breed is variable; many failed to produce any litters over this

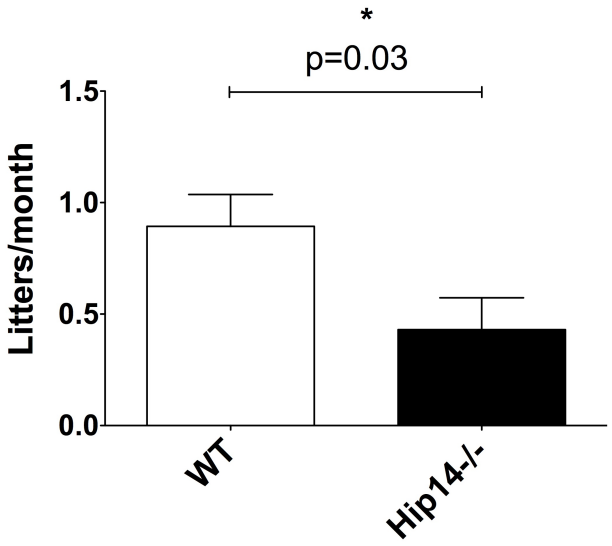

Figure 5.4 - Reduced fertility in *Hip14-/-* mice. *Hip14-/-* males crossed to WT females produce significantly fewer litters/month over a 6 month period compared to WT males crossed to WT females. WT n=11, *Hip14-/-* n=12.

time period (38.46%), however those that did breed did not appear to differ significantly from WT males. The significant differences observed, therefore, arise largely from the failure to breed in a proportion of *Hip14-/-* mice.

5.3.2. Functional consequences of loss of *Hip14* in testes

5.3.2.1. Testis weight

Testicular degeneration is observed in human HD patients (Van Raamsdonk, 2007a), and reduced testicular weight is observed in both YAC128 mice and in *Hip1-/-* mice (Khatchadourian, 2007, Van Raamsdonk, 2007a). We assessed whether testicular weight may also be decreased in *Hip14-/-* mice.

Surprisingly, testicular weight was increased by 29-35% in *Hip14-/-*mice (Figure 5.5) as early as 3 months of age (p=0.003) up to 14 months (p=-0.007).

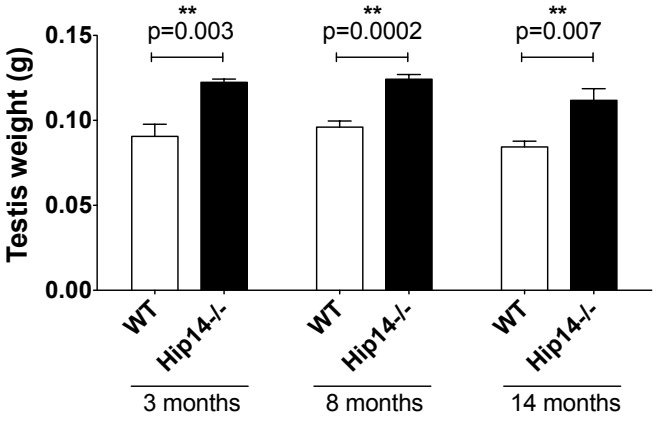

Figure 5.5 - Testicular weight is significantly increased throughout adult life in *Hip14-/-* mice. Testis weight is significantly increased in *Hip14-/-* mice at 3 months of age relative to WT littermates (p=0.003). A similar increase is observed at 8 months (p=0.0002) and 14 months (p=0.007) of age. n=5 for each genotype at all ages reported. *p<0.05, **p<0.01.

5.3.2.2. Sperm count

The testicular pathology in HD patients included a clear deficit in spermatogenesis (Van Raamsdonk, 2007a), and a reduction in sperm count is observed in a knockout model for another HTT interacting protein, the *Hip1-/-* mouse (Khatchadourian, 2007). Therefore, we assessed whether altered sperm count may be present in *Hip14-/-* mice.

Hip14-/- mice were clearly not aspermic, as seen in histological sections (section 5.3.4.1 below). Sperm count in aged *Hip14-/-* males (14 months) was not different from WT (Figure 5.6a, p=0.31). Notably, sperm count was fairly variable, though similarly variable in both genotypes. However, a trend to increased sperm motility was observed in *Hip14-/-* mice, though this finding fell short of significance (p=0.0541); Figure 5.6b).

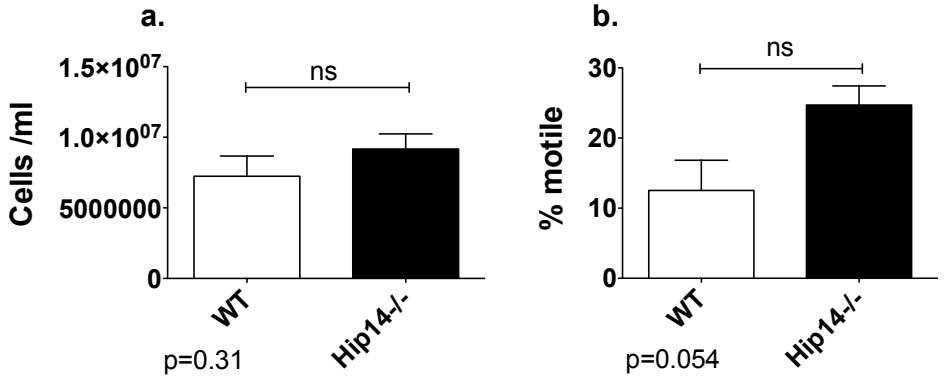

Figure 5.6 - Sperm count and mobility is not altered in *Hip14-/-* mice. **a.** Sperm count is not significantly different in *Hip14-/-* mice compared to WT littermates (p=0.31). n=5 both genotypes. **b.** Sperm motility is not significantly different in *Hip14-/-* mice, although a trend to increased motility is apparent p=0.054). n=4 both genotypes.

5.3.3. Light microscopic (LM) assessment of testes in *Hip14-/-* mice

5.3.3.1. Quantitative assessment of seminiferous tubule area

Previous pathological assessments of testes from human HD patients revealed a significant decrease in seminiferous tubule cross-sectional area and an increase in seminiferous tubule wall thickness (Van Raamsdonk, 2007a). As a preliminary quantitative assessment, seminiferous tubule area was measured in slides generated from 8 month old *Hip14-/-* and WT littermates (Figure 5.7). No significant difference between WT and *Hip14-/-* was observed.

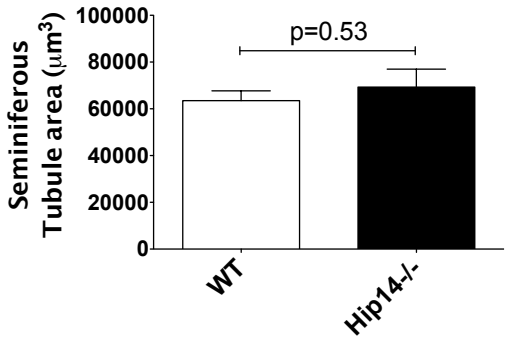

Figure 5.7 - Quantitative assessment of seminiferous tubule area in WT and *Hip14-/-* mouse. No difference is observed between *Hip14-/-* and WT littermates.

5.4. Novel cognitive behavioural findings in *Hip14-/-* mice

Cognitive decline is a common feature in HD (Sturrock and Leavitt, 2010) and cognitive dysfunction has been described as an early phenotype in the YAC128 mouse model of HD (Van Raamsdonk, 2005b). A recent study reported deficits in object recognition and spatial context learning in the YAC128 model as early as 7 months of age (Southwell *et al.*, 2009). Subsequent testing at earlier ages reveals that impaired learning in both paradigms is present in the YAC128 as early as 4 months of age, and is significantly different from WT littermates by 5 months (Amber Southwell, unpublished data).

The Novel Object recognition test offers many benefits over previously used behavioural testing paradigms. Notably, this test does not require training, nor does it depend on swim speed or running, minimizing the effect of motor ability and motivation. Mice are introduced to two novel objects and their ability to discern an object's novel location (day 1, Figure 5.8a) or the replacement of one object with another novel object (day 2, Figure 5.8d) is assessed by the preferential investigation of the moved or novel object. Mice with intact spatial context memory, which is thought to represent "hippocampal" learning, will be expected to display increased investigation of a moved object. Mice with intact object identity, which is thought to represent "cortical" learning, will be expected to display increased investigation of the novel identity of an object.

Because *Hip14-/-* mice display an HD-like phenotype, we assessed whether similar learning deficits might be present. First, we assessed whether *Hip14-/-* mice display deficits in spatial learning. As anticipated, WT mice displayed significantly increased investigation of the moved target object in trial 2 (Figure 5.8b, $p<0.05$). In contrast, *Hip14*-/- mice failed to investigate the object when moved to a novel location (Figure 5.8b, ns), suggesting that spatial ("hippocampal") memory was impaired. A similar pattern was observed in YAC128 mice (Figure 5.8c, $p<0.05$); WT mice successfully investigated the moved object, whereas YAC128 littermates did not.

We next assessed object recognition, which is thought to rely on cortical memory. Interestingly, both WT and *Hip14-/-* mice displayed increased investigation of the novel object in trial 2 (Figure 5.8e, $p<0.05$). Unlike WT littermates ($p<0.05$), YAC128 mice were impaired on this task (Figure 5.8f, ns).

Therefore, *Hip14-/-* mice appear to display selective learning deficits in spatial learning and intact object recognition; YAC128 mice are impaired on both cognitive tasks.

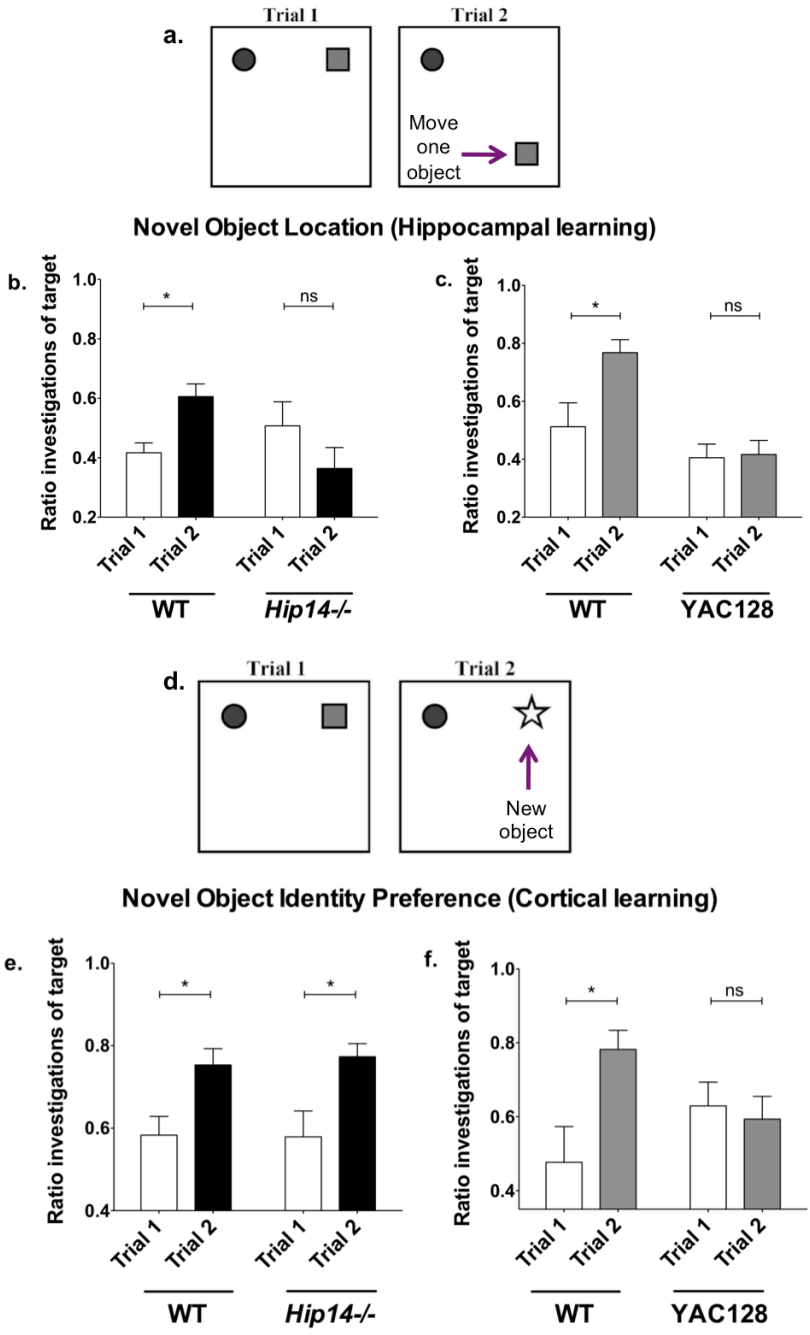

Figure 5.8 - *Hip14-/-* mice display spatial learning deficits. a. Schematic of novel object location testing. **b.** WT mice display significantly increased ($p<0.05$) investigation of the target object in trial 2, while *Hip14-/-* mice do not. **c.** Similarly, YAC128 mice fail to investigate the target (moved) object in trial 2. **d.** Schematic of novel object identity testing paradigm. **e.** Both WT and *Hip14-/-* mice investigate the novel object significantly more in trial 2 ($p<0.05$). **f.** In contrast, YAC128 mice fail to preferentially investigate the novel object in trial 2. WT n=13, *Hip14-/-* n=11. *$p<0.05$, **$p<0.01$. Figure schematics adapted from Southwell *et al* 2009. YAC128 data courtesy of Amber Southwell.

5.5. Summary of findings

In this chapter, we have described a series of findings that further our understanding of HIP14 and HIP14 biology. *In silico* databases provide expression data on HIP14 that collectively confirm predominant CNS expression of HIP14, and that HIP14 is expressed very early in development. LacZ staining in embryos confirms strong expression in the CNS. Assessment of HIP14 expression in western blots reveals highest expression of HIP14 *in utero* in forebrain but an opposite trend in whole brain, suggesting that HIP14 expression in non-forebrain tissues differs significantly. Although we were unable to assess HIP14 expression in testis, it is clear that a testicular phenotype and impaired fertility are present, and further studies may reveal the etiology of the pathology observed. Cognitive testing in *Hip14*-/- mice reveals a spatial context ("hippocampal") learning deficit, which agrees with electrophysiological findings and indicates that further assessment of the hippocampus in *Hip14-/-* mice is warranted.

6. DISCUSSION AND FUTURE DIRECTIONS

The goal of this thesis was to gain insight into HIP14 biology through creation of a novel transgenic mouse model overexpressing HIP14 and to further characterize the *Hip14-/-* mouse. Ultimately, the *HIP14* BAC transgenic mouse may be used as a tool for assessing the therapeutic potential of HIP14 overexpression *in vivo* in HD, by crossing this line with the YAC128 mouse model of HD. Despite the modest levels of HIP14 overexpression obtained, the *HIP14* BAC transgenic mouse did prove to be useful for furthering our understanding of HIP14 biology, and some mild phenotypes did emerge.

Cross of the *HIP14* BAC transgenic mouse to the *Hip14-/-* line confirmed that human *HIP14* can compensate for loss of its murine ortholog for most phenotypes and revealed surprising new insights into the levels of expression required for physiological homeostasis of HIP14-dependent phenotypes. Despite a level of expression of only ~1/3 endogenous murine levels, human HIP14 was able to rescue the majority of deficits observed in *Hip14-/-* mice. Whether the partial rescue of body weight in BAC-/- mice arises due to species differences or due to the greater sensitivity of this phenotype to levels of HIP14 expression remains to be determined.

A survey of *in silico* databases revealed a number of resources on gene expression but relatively few with information for HIP14. Assessment of HIP14 expression in whole brain and brain subregions in development reveals highest expression levels in the forebrain, specifically cortex, at late embryonic to juvenile ages. The role of HIP14 in peripheral tissues is highlighted by a novel testicular phenotype, suggesting that further peripheral roles for HIP14 remain unexplored.

The present study highlights a number of future directions. The potential therapeutic role for HIP14 overexpression or upregulation in HD remains to be determined. New approaches for understanding HIP14 biology both *in vitro* and

in vivo, remain to be studied. *In vitro* approaches serve as a relatively inexpensive means of assessing HIP14 overexpression prior to the commitment of resources required in creation of a novel mouse model. Assessment of HIP14 overexpression *in vivo* remains a priority and as such, the findings of this study highlight important considerations in creation of future mouse models of HIP14 overexpression. Finally, the findings from this study point to novel *Hip14-/-* phenotypes that remain unexplored.

6.1. The *HIP14* BAC transgenic mouse

The goal of this thesis was to generate a transgenic mouse overexpressing HIP14. Subsequently, this model could be crossed to existing mouse models as a means of achieving HIP14 overexpression *in vivo*, particularly in mouse models of HD. A number of approaches exist to create transgenic mouse models, each with specific advantages and disadvantages.

We selected a bacterial artificial chromosome transgenic approach (Shizuya *et al.*, 1992). The genomic size of *HIP14* (~90kb) renders it amenable to a BAC transgenic approach while allowing for inclusion of sufficient surrounding regulatory sequence (the average BAC insert size is ~200kb) (Asami *et al.*, 2010, Giraldo and Montoliu, 2001, Yang Xiangdong W *et al.*, 1997). The benefits of such an approach are numerous. Inclusion of surrounding regulatory genomic sequence helps to ensure that BAC-derived gene expression most closely resembles endogenous temporal and spatial patterns (Heaney and Bronson, 2006, Van Keuren *et al.*, 2009). In addition, the inclusion of such surrounding sequence helps to serve as a means of better isolating the transgene from influence by elements in the genomic region of integration (Giraldo and Montoliu, 2001, Heaney and Bronson, 2006). We decided against use of a cDNA construct with an exogenous promoter, as this often results in an ectopic pattern of expression that may be dissimilar from that observed in normal physiology. In addition, this approach excludes introns, where genomic regulatory motifs often reside (Chandler Kelly J, 2007, Giraldo and Montoliu, 2001, Van Keuren, 2009).

The *HIP14* BAC chosen for our study was selected with careful consideration. A search of the UCSC genome browser (Mar. 2006 (NCBI36/hg18) Assembly) revealed five BAC end pairs containing *HIP14*. The *HIP14* BAC used in this study (RP11-463M12) was selected in consultation with bioinformatic experts; of the *HIP14*-containing BACs available, this construct is the sole candidate to exclude another intact gene (CSRP2) and which includes as much upstream sequence as possible (80kb *c.f.* 20kb in the best alternative construct). Despite these careful considerations, regulation of *HIP14* may be influenced by sequences as distant as 200kb 5' of the gene (Wyeth Wasserman, personal communication). Inclusion of such a large segment of upstream sequence, however, is not feasible due to the lack of availability of a DNA construct meeting this criterion. If such a construct were available, this would carry the potential risk of including upstream regulatory sequence for a neighboring gene, *OSBPL8* as well as a number of pseudogenes that lie in the intervening sequence.

We selected a human transgene, as our research is aimed primarily at furthering our understanding of human health and disease. Attempts at generating knockin models of disease for HD and another triplet repeat disorder, Friedrich Ataxia (an approach in which a disease-causing triplet repeat expansion is inserted into the murine ortholog) have previously failed to reproduce the features of these diseases seen in humans (Miranda *et al.*, 2002) or resulted in a milder phenotype (Menalled, 2005). The advantages of using the human gene when generating transgenic mice to study human disease have been demonstrated in mouse models of both HD and Friedrich Ataxia. Models generated using the human gene with artificial chromosome systems of transgenesis (Sarsero *et al.*, 2004, Slow Elizabeth J, 2003) have been highly successful in generating mice that accurately reproduce the key aspects of disease. These models likely recapitulate the correct underlying molecular cause of disease as seen in patients, rendering these models highly suitable for future use in preclinical

studies. As our intent was to use this model in crosses to other mouse models of human disease, we selected a human transgene.

6.1.1. *HIP14* BAC mice display modest levels of HIP14 overexpression

Once *HIP14* BAC founders were generated and identified, genomic copy number of the BAC was assessed via qPCR, a rapid and accurate method for assessing relative transgene copy number (Chandler Kelly J, 2007). Lines HB2, HB4, and HB6 were identified to carry the highest BAC copy number, ranging from ~11 copies in line HB2 to ~18 copies in HB6, although the level of mRNA expression in HB4 and HB6 was not later found to be significantly different.

Although transgene copy number is typically fixed in founder progeny, this is not always the case, and striking discrepancies between founder transgene copy number and estimates in offspring can occur (Chandler Kelly J, 2007). Therefore, copy number was assessed in a number of founder offspring. As expected, a similar pattern of copy number was observed, with the highest values again in lines HB2, HB4, and HB6. Interestingly, copy number in offspring of founder HB9 were higher than observed in founders, and similar to those in HB2.

As higher transgene copy number is usually observed to correlate with increased expression (Chandler Kelly J, 2007), we anticipated that those lines with highest transgene copies would also demonstrate highest levels of expression. Indeed, preliminary assessments of HIP14 protein expression in nine lines confirmed that HB2, 4, and 6 were those with highest levels of protein expression. Further analysis was largely focused on the line with highest copy number and expression level, HB4.

Unfortunately, the resulting *HIP14* BAC transgenic lines failed to generate a robust level of HIP14 overexpression despite the inclusion of multiple copies of *HIP14*. Several features intrinsic to a BAC transgenic approach may explain why.

The BAC transgene site of integration is random; it is possible that the BAC may integrate into a silent locus, rendering transcriptional activity unpredictable (Heaney and Bronson, 2006, Ristevski, 2005). The inclusion of sufficient surrounding sequence in artificial chromosome approaches (as compared to cDNA approaches) often minimizes this problem, but in many cases the transgene may remain subject to position effects that influence transgene function (Heaney and Bronson, 2006). Insertional mutagenesis of a gene at the site of integration is another potential concern, and can result in a phenotype that is mistakenly attributed to transgene overexpression (Ristevski, 2005). In addition, transgene copy number is difficult to control. Typically, the BAC transgene construct integrates as a tandem-copy transgene concatemer at a single site (Ristevski, 2005). Copy number is important, but a high copy number is not always desirable. For example, high tandem copy number may result in gene silencing, possibly through silencing by methylation (Dobie *et al.*, 1997). These are important considerations for future attempts at generating similar models exploring gene overexpression *in vivo.*

Despite the apparent protective effect of HIP14 overexpression in the context of HD *in vitro* (e.g. reduction of mHTT-induced inclusion formation), it is possible that similar overexpression is toxic *in vivo*. Reports that HIP14 has oncogenic properties (Ducker, 2004) and may serve as a Mg2+ transporter (Goytain, 2008) appear to support this hypothesis, as do findings in *D. melanogaster*, in which overexpression of dHIP14 results in abnormal wing phenotypes (Andrews, 2006, Kang Kyung-Hwa and Bier, 2010). One may postulate that the BAC transgenic approach, which serves to better ensure endogenous patterns of expression may also facilitate endogenous regulation, which may serve to inhibit significant overexpression. The finding that expression of the human *HIP14* transcript did not appear to influence expression of endogenous murine *Hip14* (Figure 3.3c) appears to suggest that this is not the case. Thus, the modest phenotype described in this study likely does not arise due to endogenous regulation of HIP14 expression, but may be influenced by other factors described above.

Finally, the presence of different miRNA binding sites in human and mouse *HIP14* may be another potential contributor to the modest levels of overexpression observed. miRNAs are small endogenous RNAs that are involved in post-transcriptional repression, binding to the 3' UTR of mammalian genes. Subsequent to the generation of the *HIP14* BAC model, data on miRNA binding sites has become available (Friedman *et al.*, 2009). A survey of TargetScan (www.targetscan.org) data reveals seven conserved miRNA binding sites in the 3' UTR of human *HIP14*. Three of these are conserved in murine *Hip14*. Potentially, endogenous miRNAs may undergo differential interaction with sequences present in human *HIP14.*

6.1.2. Subtle neuropathological changes in a *HIP14* BAC transgenic mouse

Because the *HIP14* BAC transgenic mouse was being considered for potential crosses to mouse models of HD, and due to the severe neuropathological deficits that occur in mice lacking *Hip14*, we assessed for baseline neuropathological changes in the *HIP14* BAC mice. The cumulative observations suggest a mild neuropathological phenotype. A mild trend to decreased brain weight at 12 months is observed in HB4, this is significant in the line HB6. However, because the level of HIP14 expression is similar in these two lines, this suggests that the decrease in brain weight observed in the HB6 line may not arise secondary to HIP14 expression levels. For example, random integration of the *HIP14* transgene in HB6 may have resulted in insertional mutagenesis.

Reduced DARPP-32 expression levels is a feature of HD (Deng, 2004) and is likewise seen in mice lacking murine *Hip14* (192). However, the observed reduction in DARPP-32 staining in HB4 BAC striatum without concomitant reduction in striatal neuron counts suggests that a decrease in DARPP-32 expression levels occurs without, or at least prior to, cell loss. Further assessments in additional cohorts will lend insights into whether this change is true or an effect of cohort.

6.1.3. Mild behavioural changes in a *HIP14* BAC transgenic mouse

Despite mild neuropathological changes, no deficits in motor coordination or cognition were apparent in *HIP14* BAC mice; body weight was likewise unchanged. Results pointing to a mildly hypoactive phenotype in spontaneous activity contrasted with apparent hyperactivity in locomotor measures of the Elevated Plus Maze. These apparent conflicting findings may be due to different testing conditions: while spontaneous activity is assessed in the dark, elevated plus maze is assessed in the light. Thus, it appears that *HIP14* BAC transgenic mice are mildly hypoactive in the dark and hyperactive in light testing conditions, with both findings being more prominent in male mice.

The finding that *HIP14* BAC mice appeared less anxious relative to WT littermates, exploring open arms sooner and spending more time in open arm and open arm ends in the EPM testing paradigm, was prominent in both genders. An apparent hyperactive phenotype in the light was significant in males only. Therefore, this data suggests that *HIP14* BAC mice display reduced anxiety and an increased tendency to novelty seeking. While this was not reflected in the measures of defecation in open field (Blizard and Adams, 2002), this may be explained by the observed variability in this latter test (personal observation).

6.1.4. Conclusions from the *HIP14* BAC transgenic mouse

Although the findings outlined in chapter 3 do not definitively answer our experimental questions regarding the effect of HIP14 overexpression *in vivo*, some general conclusions can be made. The modest levels of overexpression obtained despite multiple transgene copies may arise due to a problem intrinsic to the transgene construct (e.g. undetected mutation), its integration (e.g. position effect variegation), or due to regulatory mechanisms in place that prevent HIP14 overexpression. The possibility that HIP14 overexpression may be harmful is supported by findings in *D. melanogaster*. Overexpression of dHIP14 by a number of wing-drivers all resulted in abnormal wing morphology, and in one case also resulted in impaired survival (Andrews, 2006). In an independent study,

overexpression of HIP14 in the wing resulted in similar findings (Kang Kyung-Hwa and Bier, 2010).

Previous *in vitro* studies found that HIP14 overexpression reduced the number of inclusions in cells co-expressing mHTT (Yanai, 2006). While controversial, it is believed by some that inclusions may serve as a sink for sequestering toxic soluble mHTT. As such, their appearance may be an indication of protective mechanisms in place that allow the cell to evade cell death (Slow Elizabeth J. *et al.*, 2006), and they may not be toxic in and of themselves. The possibility exists, therefore, that the disappearance of inclusions upon overexpression of HIP14 may signify enhanced, not decreased, toxicity. Further studies will be necessary to explore this hypothesis.

It is clear from the phenotype observed in *Hip14-/-* mice that loss of *Hip14* is harmful. The current studies suggest that the same may be true of HIP14 overexpression. However, further studies of HIP14 overexpression *in vivo* and assessment of its feasibility as a therapeutic approach are warranted, and possible approaches are discussed in section 6.4.2 below.

6.2. Rescue of HD-like phenotype in mice lacking murine *Hip14*

Once the *HIP14* BAC mice were successfully established, we sought to assess this mouse model's suitability for future experiments. In the generation of a transgenic mouse, a number of complications may preclude normal protein expression and function, and this is particularly true when the transgene originates from a species different from that of the host. Insertional mutagenesis, transgene silencing due to position variegation effects, and undetected mutations in the transgene construct may occur. In addition, the transgene product may be processed differently in the context of the host organism (Van de Sluis and Voncken, 2010, Voncken, 2003). Although BAC-derived transcription of human *HIP14* mRNA was detected in *HIP14* BAC mice, whether this expression resulted

in a functional HIP14 enzyme remained to be determined. Despite the detection of mRNA transcripts, the transcripts or translated products may be unstable; indeed, this phenomenon is exploited in the generation of hypomorphic mice (Baker Darren J, 2011). If the protein is translated, it may not retain enzymatic activity and therefore this should be assessed functionally.

The HD-like phenotype of *Hip14-/-* mice highlighted an important role for HIP14 in the pathogenesis of HD, but it remained to be conclusively demonstrated that these phenotypes are the result of loss of *Hip14*, and not, for example, a by-product of unintended mutagenesis events inherent to the ES-cell construct used or other events occurring during generation of the *Hip14-/-* mouse model.

Because of the very high level of sequence conservation between human and mouse HIP14 protein (98% identical), we predicted that human *HIP14* would be compatible with the murine cellular and transcriptional machinery. Previous studies investigating the ability of a human protein to rescue loss of its murine ortholog in humanized mice report full (Coutinho *et al.*, 2005, Hodgson *et al.*, 1996) or partial (Abrahams *et al.*, 2005, Bradley *et al.*, 2007, Chen Jean Y *et al.*, 2002, Cheung *et al.*, 2004) rescue of the murine null phenotype, the latter yielding insights into differences in species specificity.

The objectives addressed in this chapter were fourfold: First, to confirm that defects seen in *Hip14-/-* mice are indeed the result of the absence of *Hip14*. Second, to determine the levels of HIP14 sufficient to rescue the phenotype in *Hip14-/-* mice. Third, because the *HIP14* BAC transgenic mouse appeared to display only modest levels of HIP14 overexpression over endogenous, we asked whether certain phenotypes are more sensitive to loss of *Hip14*. Finally, we asked whether human HIP14 can compensate for loss of the murine protein, and in the murine physiological context. In addition, through these studies we sought to confirm that the BAC transgene produces a functional protein.

6.2.1. Assessment of HIP14 expression in *Hip14-/-* mice and mice expressing only human HIP14

The detection of mRNA transcript in a murine knockout model generated using a gene trap vector is not without precedent. Alternative splicing may allow excision of the gene trap vector, resulting in a low level of expression of the WT transcript. In a previous study of gene trap mouse lines, >96% of gene trapping in non-embryonic lethal mouse lines resulted in a complete absence of the WT transcript; in the remainder of cases, the average reduction in mRNA levels was 91.6% (Zambrowicz *et al.*, 2003). Descriptions of this are found in the literature (Hoshii, 2007, Lako and Hole, 2000, Roshon, 2003, Trimborn, 2010, Voss, 1998). Interestingly, a recent paper describes a DHHC5 mutant mouse generated using a similar gene trap vector to that used for generation of *Hip14-/-* mice, resulting in a *Zdhhc5* hypomorphic allele. Assessment of mRNA revealed transcript levels of ~16% (Li Y, 2010).

A faint band in the *Hip14-/-* lane of western blots appears to be non-specific, as it remains after peptide competition assay (Appendix Figure 2), suggesting that any *Hip14* mRNA generated does not generate HIP14 protein. However, it is possible but unlikely that a very low level of HIP14 protein is generated. This cannot be ruled out via western blot, as this method may not be sensitive enough to detect very small levels of protein in the context of several non-specific bands (Appendix Figure 2). If protein is generated, it is possible that the gene-trapped *Hip14* is a hypomorphic allele. If so, it raises the possibility that complete absence of *Hip14 in vivo* may be embryonic lethal. Indeed, double *Hip14-/-, Hip14L-/-* mutants are not born and succumb *in utero* (Shaun Sanders and Liza Sutton, unpublished data). More sensitive methods would be necessary to further explore this possibility. Finally, Western Blot analysis in cortex and striatum confirmed that the BAC-/- mice demonstrated a modest level of expression of ~35% of wildtype levels; as described below, this level of expression was found to be sufficient to rescue most of the phenotypes observed in *Hip14-/-* mice.

6.2.2. Rescue of *Hip14-/-* HD-like neuropathology by human HIP14

BAC-derived human HIP14 is observed to compensate for all measures of neuropathology in *Hip14-/-* mice at 1 and 3 months, including decreased brain brain, cerebellar, and forebrain weight, as well as decreases in striatal volume, neuron count, and cortical volume. Similarly, decreases in striatal DARPP-32 and Enkephalin expression in *Hip14-/-* mice are compensated for by human HIP14, while Substance-P levels are unchanged.

As part of these analyses, it is interesting to note the reduction in cerebellar weight in *Hip14-/-* mice; this finding differs from observations in HD, as the cerebellum is largely spared in HD patients until late-stage disease (Sturrock and Leavitt, 2010). Similarly, cerebellar weight is unchanged at 12 months in the YAC128 mouse model of HD (Slow Elizabeth J, 2003). This finding points to potential cerebellar neuropathology in the *Hip14-/-* mice that may be worthwhile exploring in more detail (e.g. cerebellar volume & cell counts) in future studies.

6.2.3. HD-like motor deficits resulting from loss of murine *Hip14-/-* are rescued by human HIP14

Hip14-/- mice display a trend toward motor coordination deficits as early as three months, becoming significant by six months and non-progressive thereafter (192). In the rotarod test of motor coordination, BAC-/- mouse performance is superior to both WT and *Hip14-/-* littermates at all ages assessed and in both genders. An unexpectedly poor performance in WT may arise due to better than anticipated performance in *Hip14-/-* mice. Regardless, human HIP14 did appear to compensate for the loss of murine *Hip14*.

Hip14-/- mice are hyperactive in spontaneous activity testing (192). We observed similar significant hyperactivity at both 3 and 6 months as assessed by a variety of automated measures, which was more apparent in males. This hyperactiviy was normalized to WT values in a number of measures, but the rescue was most robustly seen in measures of stereotypy. Interestingly, despite this hyperactivity, a number of vertical measures (vertical time, and jump counts and time) revealed

a trend to reduced vertical time and jumps in *Hip14-/-*, a trend that was more pronounced in BAC-/- mice. In light of the findings described in chapter 3, where a mild hypoactive phenotype in *HIP14* BAC mice (in the presence of endogenous murine *Hip14)* was apparent, this observation may be due to a property of human HIP14 or another property of the BAC transgene unrelated to HIP14 expression. In summary, relatively low levels of human HIP14 appear to compensate for the behavioural deficits resulting from loss of the murine protein.

6.2.4. BAC-derived human HIP14 is a functional PAT

As described above, one of the primary goals of this chapter was to confirm that HIP14 expressed from the BAC transgene retains functional enzyme activity as a PAT. Two substrates of HIP14, PSD-95 and SNAP-25, display reduced palmitoylation in brains of *Hip14-/-* mice (192). We confirmed that these two substrates display reduced palmitoylated in *Hip14-/-* brains, and that palmitoylation of these substrates is normalized in BAC-/- brains, suggesting that BAC-derived human HIP14 can compensate for the lost HIP14 PAT activity. Thus, BAC-derived human HIP14 results in a functional PAT enzyme.

6.2.5. Partial body weight restoration suggests a unique sensitivity to HIP14 expression levels in the periphery

Careful assessment of body weight as early as 2 weeks of age revealed that human HIP14 only partially compensates for the reduction in body weight in *Hip14-/-* mice; BAC-/- body weight is intermediate between WT and *Hip14-/-* littermates in both genders. The interpretations of this finding are discussed below.

6.2.6. Summary of findings

In this study we have demonstrated that human HIP14 can compensate for the *Hip14-/-* phenotype in functional measures of neuropathology, behaviour, and PAT enzyme function. While the HD-like phenotype observed in *Hip14-/-* mice is presumed to have resulted from the loss of murine *Hip14*, the possibility remained that the ES cell line used to generate this mouse line may carry

additional genetic alterations that influence the observed phenotype. The rescue we observed in this study demonstrates that the prominent phenotypes observed in *Hip14-/-* mice are the result of the absence of HIP14 itself.

As human and mouse HIP14 protein are highly similar (98% of amino acids identical), we anticipated that the human transgene would compensate for the loss of its murine ortholog. Rescue of a murine knockout phenotype by the human ortholog in which lower amino acid identity was present (90%) has been previously observed (Hodgson, 1996). In addition, previous findings showed that human HIP14 is able to compensate for the endocytosis defect and temperature sensitive lethality resulting from loss of Akr1p, a *S. cerevisiae* ortholog of *HIP14* (Singaraja, 2002).

As anticipated, BAC-derived human HIP14 was capable of restoring a normal phenotype in neuropathological, behavioural, and functional enzymatic measures in mice lacking murine *Hip14*. Thus, our findings suggest that human HIP14 undergoes the necessary post-translational modifications and protein interactions necessary to perform these functions in the mouse cellular context, and thus can compensate for the loss of its murine ortholog in most measures assessed. Because neuropathological deficits in the *Hip14-/-* mouse appear during prenatal development by embryonic day E17.5, these findings furthermore suggest that the human *HIP14* BAC transgene is appropriately expressed in prenatal development.

As part of our study, we sought to assess what levels of HIP14 expression are sufficient to rescue the *Hip14-/-* phenotype. Surprisingly, the human *HIP14* transgene is expressed at only ~35% of endogenous levels in cortex and striatum of mice lacking murine *Hip14*. Despite this relatively low level of expression, the neuropathological, behavioural, and biochemical measures of HIP14 assessed in this study are all fully rescued. It is interesting to note previous investigations of another DHHC PAT null mouse model, *Zdhhc8*-/-, which revealed similar deficits

in both heterozygotes (*Zdhhc8*+/-) and homozygotes (*Zdhhc8*-/-) relative to WT littermates (Mukai, 2008). For example, the density of glutamatergic synaptic contacts was decreased to a similar extent in both *Zdhhc8*+/- and *Zdhhc8*-/- mice. In addition, the number of mushroom spines, number of dendritic branch points, and number of primary dendrites were also affected in both genotypes (Mukai, 2008). In contrast, neuropathological assessments of *Hip14+/-* mice at 12 months revealed no loss in striatal volume, an endpoint showing the greatest changes in *Hip14*-/- mice as early as E17.5 (Singaraja, 2011). As *Hip14*+/- mice express only 50% of endogenous HIP14, this data is in agreement with the findings of the current study; namely, that only a fraction of endogenous HIP14 expression levels are sufficient to prevent the neuropathological changes observed in *Hip14-/-* mice.

The literature contains many previous examples of a human transgene's ability to rescue the phenotype in the murine ortholog null mice. While many of the earlier studies reported full rescue of the murine phenotype (Coutinho, 2005, Hodgson, 1996), many others report a partial rescue (Abrahams, 2005, Bradley, 2007, Chen Jean Y, 2002, Cheung, 2004). In reports of full rescue, often the endpoints assessed were fairly limited; for example, rescue of embryonic lethality (Chandler Jennifer *et al.*, 2001, Hodgson, 1996). The possibility remains that more detailed study of these humanized mice may reveal subtle incompletely rescued phenotypes. Indeed, many authors commented on subtly different patterns of expression of the human gene in transgenic mice (Manson *et al.*, 1997, Pook *et al.*, 2001, Sarsero, 2004).

Many similar studies report partial rescue of murine knockout phenotypes by the human transgene. For example, human *NR2E1* rescues a murine *Nr2e1* knockout phenotype in all aspects except for retinal vessel number, which appeared to be partially rescued but still significantly different from wildtype mice, potentially resulting from the particular sensitivity of the mouse eye to gene dosage (Abrahams, 2005). A similar partial rescue was observed in a study of

Hip1 and *Hip1r*. Mice lacking *Hip1*, another huntingtin interacting protein, display testicular degeneration and reduced fertility (Khatchadourian, 2007, Rao, 2001). In a study generating human *HIP1* transgenic mice crossed to mice lacking both murine *Hip1* and *Hip1r*, mild cataracts and male infertility were reported, despite these phenotypes being absent in knockout mice of either murine gene alone. The authors observed lack of expression of human HIP1 in cells normally expressing its murine ortholog, and suggested that human HIP1 may fail to serve all functions normally carried out by murine *Hip1* (Bradley, 2007). Another study demonstrated the ability of a human *CFTR* YAC transgene to rescue the murine knockout phenotype, but observed differences in human transgene expression relative to that normally observed *in vivo*. One YAC line appeared to fully rescue, while a second with fewer copies appeared to partially compensate for loss of murine *Cftr*. While the human transgene appeared to follow a pattern of expression similar to that of the mouse gene, its expression was different from both human and mouse *Cftr* in the Brunner Glands of the intestine, where expression is normally present in both species. The authors speculate that this may result from either an element required for tissue-specific expression that is absent in the YAC, or from an impaired interaction between the mouse transcriptional machinery and human transgene DNA due to evolutionary divergence. Thus, subtle differential expression of mouse vs. human genes has been previously observed.

While most major endpoints in the *Hip14-/-* mice were restored to wildtype levels in the presence of the human *HIP14* transgene, the reduced body weight observed in the *Hip14*-/- mice was only partially restored to wildtype levels. This partial rescue was consistent, beginning as early as 2 weeks of age up to 6 months. In light of the partial rescue observed for some phenotypes in previous studies, this was not an unexpected finding.

The incomplete rescue of body weight in the humanized mice may occur for a number of reasons. Firstly, as observed for retinal vessel number in a similar

study on *Nr2e1* mice (Abrahams, 2005), maintenance of some physiological features may be more sensitive to gene dosage than the other endpoints assessed in this study. A higher level of expression (>35% of endogenous) may be required to restore body weight to wildtype levels. A second alternative is that the role of HIP14 in the periphery may require a regulatory cis-element that is absent in the human BAC transgene used in this study. The BAC selected was chosen in consultation with experienced bioinformaticians, with the goal to include as much regulatory genomic sequence surrounding *HIP14* to the exclusion of another gene; nonetheless, this possibility remains. Finally, functions of HIP14 in the periphery may require an interaction between transcriptional machinery and DNA regulatory elements that is incompatible between the former in mice and the latter in humans. Further studies will be necessary to elucidate the levels of expression and species differences in HIP14 in the periphery and potentially in other metabolic measures.

In summary, we have generated the first transgenic mouse model for *HIP14*, and are the first to demonstrate intact palmitoyl-transferease activity in a transgenic DHHC PAT model. Humanized mice for HIP14 were able to rescue defects in neuropathology, behaviour, and HIP14 PAT activity, and partially restored body weight to wildtype levels. We report that human HIP14 compensates for the key features resulting from loss of the murine ortholog at an expression level equivalent to only ~1/3 that of endogenous murine HIP14, which is sufficient for full rescue of most phenotypes. The humanized mouse described in this study may be useful in future studies seeking to further explore HIP14 function *in vivo.* With evidence that human *HIP14* can compensate for loss of its murine ortholog, human *HIP14* BAC constructs bearing any number of modifications may be used to generate transgenic mice which, when crossed to the murine knockout, will yield further key insights into the biology of HIP14. Such modifications may include a tag or introduction of a mutation to the DHHC domain required for PAT activity, in order to parse out the potential for a role for HIP14 outside of its role as a PAT.

6.3. Further characterization of HIP14 biology

While our studies of HIP14 to date have revealed a great deal about the consequences of loss of HIP14 (192), much investigation into the normal biology of HIP14 remains unexplored. What information on HIP14 expression is available from existing *in silico* databases? The *Hip14-/-* phenotype arises *in utero* (192). Does the temporal and spatial pattern of expression of HIP14 in the brain reveal insights into why this occurs? What pathology may result from the loss of *Hip14* in the periphery? Does the *Hip14-/-* mouse display other phenotypic abnormalities that remain unexplored?

6.3.1. *In silico* data on HIP14 expression

A search of databases for *in silico* data on gene expression revealed very little information on HIP14 (Table 5.1). This finding was particularly surprising in light of the relatively large volume of existing data pointing to a role for HIP14 in health and disease.

Gene Expression data available from the Genomics Institute of the Novartis Research Foundation (GNF) revealed information on HIP14 expression profiles in humans and mice. The two probes in humans revealed a high level of expression in BDCA4+ Dendritic Cells, and expression in a number of neuronal tissues was above median levels. In mice, expression data from two datasets using a number of different probes also confirmed elevated expression in neural tissues and retina or eyecup in most cases.

Information from the Allen Brain Atlas (ABA) was limited; assessment of HIP14 expression was derived from only one adult mouse. The findings are in conflict with previous findings (Singaraja, 2002); while the ABA reports highest expression level (and density) in the cerebral cortex, previous published assessment of *HIP14* RNA levels by Northern Blot reveal highest expression clearly in the cerebellum (Singaraja, 2002). The ABA reports moderate to low expression of the latter. Notably, the published findings were generated with

human tissue (Singaraja, 2002), therefore it is possible that the observed differences in expression arise from species differences, differences in tissue handing, or other factors.

Data found on the MGI Gene Expression Database (GXD) reveals that *Hip14* is expressed very early in development and in the embryo. Further quantitative data on these findings was limited. Because the *in silico* expression data on HIP14 was limited, we proceeded to experimentally assess HIP14 expression in early development.

6.3.2. The developmental expression of HIP14 in the brain

The striatal volume loss observed in *Hip14-/-* mice appears *in utero*, between E14.5 and E17.5 (192). The appearance of the phenotype at this age led us to ask whether this phenotype coincides with a particularly high level of HIP14 expression. Microdissection of the mouse brain at early embryonic ages is challenging as the structures of interest are not yet formed. We collected microdissected brain tissue as early as was technically feasible (E18.5) up to 2 months of age in order to assess HIP14 expression patterns from early life to adulthood. Whole brain was successfully collected as early as E15.5; assessments at E9.5 were done using whole embryos.

Gene expression over development involves large changes in gene expression, and this may potentially include proteins that are routinely selected as loading controls for assessing adult tissue. As such we first set out to identify a loading control that displays stable expression levels over the ages of interest. Assessments of various loading controls revealed that GAPDH, β-tubulin, and actin levels change over the range of developmental ages assessed, while calnexin levels were relatively stable apart from an apparent peak at P14. As such, we selected calnexin as the ideal loading control.

Assessment of HIP14 expression levels revealed the highest expression from late embryogenesis to one week (E18.5-P7) in both cortex and striatum.

Expression within the cerebellum over time was relatively stable. Interestingly, striatum displayed the greatest intra-tissue fold-change, with a 50% decrease in expression levels between E18.5 and 2 months. This was particularly interesting in light of the appearance of striatal volume loss between E14.5-E17.5 (192), suggesting that forebrain structures are particularly sensitive to levels of HIP14 at this early stage of development. The apparent opposite trend of an increase in HIP14 expression from E18.5 to 1 month in whole brain may arise due to inclusion of brainstem and white matter in the whole brain samples, suggesting that peak HIP14 expression occurs at later ages outside of forebrain structures.

We next compared HIP14 expression across different brain regions at each age. Interestingly, expression was highest in cortex from E18.5 to P7, with relatively similar levels in striatum, cerebellum, and whole brain. From the age of 2 weeks onward, however, a different pattern was apparent, with HIP14 expression levels in cortex and striatum half of that in whole brain. By this comparison, both the highest levels of HIP14 expression (in late embryogenesis) and the largest fold-change in HIP14 expression over time in comparison to other brain regions (from ~1.5x to ~0.5x whole brain levels) occur in the cortex, and to a lesser extent in the striatum.

HIP14 has been previously shown to play a critical role at the pre-synapse (Ohyama, 2007, Stowers and Isacoff, 2007). Given that the striatum receives input from the cortex (Graybiel, 2000), this it is tempting to speculate that striatal volume loss appearing in *Hip14-/-* during embryogenesis may arise due to loss of HIP14 required for presynaptic input to the striatum. Further studies will be necessary to further explore this hypothesis.

6.3.3. The biology of HIP14 in the testes

The mounting similarities between the *Hip14-/-* mouse phenotype, human HD, and HD mouse models prompted us to investigate whether additional features of HD were also present in the *Hip14-/-* mouse. Testicular atrophy and degeneration has been reported in human HD (Van Raamsdonk, 2007a) and mouse models of

HD (Sathasivam, 1999). Loss of endogenous huntingtin (*Hdh*) in the mouse results in testicular pathology (Dragatsis Ioannis, 2000). In addition, a knockout mouse model of another huntingtin interacting protein, *Hip1*, displays testicular abnormalities (Khatchadourian, 2007, Rao, 2001). The existing data pointing to testicular pathology in HD made assessment of the testes in *Hip14-/-* mice a clear first step in studying the role of HIP14 in the periphery. In addition, anecdotal reports from early attempts to set up *Hip14-/- x Hip14-/-* matings suggested impaired fertility.

In a direct assessment of fertility in *Hip14-/-* males, five of 13 *Hip14-/-* males (~38.5%) failed to produce offspring, in comparison to one in eleven (~9%) of WT males. The observation of reduced number of litters per month impaired breeding in *Hip14-/-* males. However, this effect appears to be secondary to a failure of a subset of the *Hip14-/-* males to breed; those males successful in producing offspring appeared to breed relatively well. This variable phenotype is reminiscent of findings in *Hip1-/-* mice; histological assessment revealed an apparent normal appearance of seminiferous tubules in some areas despite obvious pathology in others (Khatchadourian, 2007). Other knockout mouse models with testicular abnormalities have been found to have similarly heterogeneous phenotypes (Eddy, 1999, Grover *et al.*, 2004, Lufkin *et al.*, 1993, Zhao *et al.*, 1998).

Reduced testis weight was a prominent phenotype in aged (12mo) YAC128 mice (Van Raamsdonk, 2007a). Surprisingly, testicular weight was significantly increased by ~35% as early as 3 months of age and consistent throughout life. This finding contrasted with all studies in HD (Van Raamsdonk, 2007a), HD mouse models (Sathasivam, 1999, Van Raamsdonk, 2007a) and other HIP mouse models (Khatchadourian, 2007, Rao, 2001) to date. In these HD and HD-related cases, testicular atrophy, reduced sperm count and/or abnormal sperm is observed; this is not surprising in light of the fact that spermatogenesis is attributed to 80-90% of testis volume, and testicular volume is thought to serve as

a crude measure of spermatogenesis in humans in most clinical scenarios (Allan and Hendelsman, 2005). Small testes secondary to intrinsic testicular pathology (and not secondary to pituitary pathology, such as in hypogonadotropic hypogonadism) is observed in many clinical scenarios, and appears to be the cause of this finding in HD and HD-related mouse models cited above (Khatchadourian, 2007, Rao, 2001, Sathasivam, 1999, Van Raamsdonk, 2007a). In contrast, testicular enlargement (clinically known as “macroorchidism”) is a distinctive and highly unusual finding (Allan and Hendelsman, 2005) reported in human cases of juvenile fragile X syndrome, hypothyroidism, McCune Albright Syndrome, congenital adrenal hyperplasia, and bilateral testicular tumours, among others (Allan and Hendelsman, 2005). The reasons for enlarged testes in *Hip14-/-* mice may arise due to an increase in the number of a particular type of cell, edema, or other causes. Assessments to further explore this are ongoing.

Reduced sperm count has been observed in HD (Van Raamsdonk, 2007a) and in mice lacking *Hdh* (Dragatsis Ioannis, 2000). In addition, *Hip1*-/- mice also display reduced sperm count and sperm abnormalities. The finding that both sperm count and sperm motility in *Hip14-/-*
males did not differ significantly from WT littermates confirmed that altered sperm count is not the cause of impaired fertility and testicular pathology. A trend to increased sperm motility in *Hip14-/-* is likely due to high variability in this measure. A remaining possibility is altered sperm function in *Hip14-/-* mice, and further assessments would be necessary to assess this.

In order to investigate the etiology of testicular pathology, we prepared toluidine blue stained testis slides from *Hip14-/-* mice. While *Hip14-/-* mice are clearly spermatogenic, occasional residual cytoplasmic bodies are observed, which are normally phagocytosed by Sertoli cells. A potential dissociation between stages is observed; cells in an early developmental state are observed in close proximity to late-stage cells (Wayne Vogl, personal communication). Finally, qualitative assessment suggests that greater numbers of Leydig cells may be present.

Overall, phenotypic changes are present but very subtle. In an attempt to assess for quantitative changes in *Hip14-/-* testes, we measured the average seminiferous epithelium area in WT and *Hip14-/-* mice and found no significant differences. Further assessments are ongoing.

In summary, mildly impaired fertility and testicular pathology is present in *Hip14-/-* males. Although sperm count is unaltered and histological sections of the testis appear grossly unremarkable to a large extent, the consistent increase in testicular size suggests that some testicular pathology is present. In addition, a remaining possibility is that mating behaviour in *Hip14-/-* males is altered. Further assessment will be required to determine the etiology of these changes.

6.3.4. Cognitive deficits in *Hip14-/-* mice

We assessed *Hip14-/-* mice for cognitive changes using the novel object location and identity preference test. Assessments in YAC128 mice as early as 5 months of age reveals deficits in both spatial context ("hippocampal") learning as well as object identity ("cortical") learning (Amber Southwell, unpublished data; Figure 5.9). At 4 months of age, deficits in spatial context learning are apparent in *Hip14-/-* mice; mice fail to recognize the novel location of an object, indicating a deficit in spatial learning, which is thought to be mediated by the hippocampus (Mumby *et al.*, 2002). However, *Hip14-/-* mice performed as well as WT on the novel object identity preference task, suggesting that cortical learning is intact. Interestingly, collaboration with a laboratory specializing in electrophysiological measures in *Hip14-/-* mice revealed that hippocampal long term potentiation (LTP) is absent (Austen Milnerwood, personal communication). These behavioural findings become particularly interesting in light of this finding and point to a unique and unexplored role for HIP14 in learning and memory. Further exploration of the role of HIP14 in hippocampal LTP is certainly warranted.

6.4. Future directions

The findings described in this thesis highlight a number of avenues that warrant further assessment, both expanding on the existing analyses and for novel studies on HIP14.

6.4.1. Future directions from the current study

The human *HIP14* BAC mouse is a tool that may be further used to explore human HIP14 expression *in vivo.* The findings described in chapter 4 suggest that while low levels of human HIP14 compensate for the majority of the *Hip14-/-* phenotype, some aspects of the phenotype appear resistant to rescue. In particular, body weight is only partially compensated by BAC-derived human HIP14. Are peripheral phenotypes particularly vulnerable to changes in expression levels of HIP14? Alternatively, is partial rescue in the periphery due to species differences between murine and human HIP14?

Whichever of these two scenarios proves to be true, the findings point to a particularly sensitive requirement for HIP14 in the periphery, in light of apparent full rescue in neurologically-driven endpoints (behaviour and neuropathology). Supportive of this is the finding that testis weight, like body weight, is only partially restored to WT values in BAC-/- mice (data not shown). It may be of interest to use the *Hip14-/-* and *HIP14* BAC models to explore potential roles for HIP14 in the testis and other peripheral organs. For example, a preliminary necropsy of a *Hip14-/-* mouse (n=1) suggested pathological changes in the heart, liver, and spleen (UBC Animal Care Centre, personal communication). This study suggests that many non-CNS phenotypes of the *Hip14-/-* mouse remain unexplored.

The role of HIP14 expression levels and unique properties of HIP14 in different species (human versus mouse) remains unresolved. Although it is clear that a surprisingly low (~1/3) level of expression is sufficient to compensate for most deficits in *Hip14-/-* mice, whether this is a particular property of human HIP14 is

unknown. *Hip14+/-* mice do not display striatal volume loss at 12 months (192), suggesting that 50% of murine *Hip14* is sufficient to prevent striatal neuropathology. Are ~1/3 levels of endogenous murine *Hip14* equally sufficient?

In addition, more careful assessment of *Hip14* mRNA in the brain and periphery may be warranted. For example, careful assessment of the subcellular localization of human HIP14 in the BAC-/- mice may reveal important insights. Similarly, while we have assessed expression levels of murine and human *HIP14* using species-selective *HIP14* primers, nonspecific primers evaluating total HIP14 mRNA would allow assessment of total mRNA and comparison to western blot findings. In other words, are mRNA levels similar to observations of HIP14 protein in BAC-/- mice?

While we have assessed brain pathology using stereological analyses of the striatum and cortex, the reduced cerebellar weight in *Hip14-/-* mice (rescued in BAC-/-) suggests that cerebellar pathology may be present. Greater insight into the phenotype may be obtained by a more detailed analysis of cerebellum and other structures, such as hippocampus and hypothalamus.

We have described the temporal and spatial expression of HIP14 in early development (section 5.2). Our findings reveal highest expression of HIP14 in late embryogenesis and up to 1 week of age in forebrain structures, particularly in the cortex. Both the highest levels of expression and the greatest fold-change in HIP14 expression between late embryogenesis and early adulthood are seen in the cortex. This finding suggests that cortex would be particularly sensitive to loss of HIP14 in early life, when striatal pathology is first apparent. As cortex provides presynaptic input to the striatum, this data suggests that the *Hip14-/-* mouse phenotype may arise largely due to presynaptic loss of HIP14 in cortical neurons; if so, one would expect that selective ablation of HIP14 in cortex will replicate the *Hip14-/-* phenotype. A number of existing studies point to a critical role for HIP14 at the presynapse (Ohyama, 2007, Stowers and Isacoff, 2007). Future

experiments may explore this hypothesis, whether by creation of a mouse with temporally or spatially selective ablation of *Hip14*, or by ASO-mediated knockdown of *Hip14* in either cortical (presynaptic) or striatal (postsynaptic) neurons of corticostriatal co-culture. In addition, assessment of *Hip14* mRNA expression over a similar range of ages to that described in this study may yield additional insights. Finally, as technology advances at increasing pace, a more detailed exploration of the *in silico* resources available may reveal further insights into both *Hip14* and related genes of interest.

The etiology of impaired fertility and testicular pathology in *Hip14-/-* mice remains unresolved. Because 80-90% of testicular volume is attributed to spermatogenesis (Allan and Hendelsman, 2005), and we found sperm count to be unchanged, one potential cause may be altered sperm function. Alternatively, a number of pathological processes in the testes may contribute to increased testicular size, such as edema. In addition, the increased testes weight may arise due to increased proliferation of a cell population other than sperm (e.g. Sertoli cells, Leydig cells), though this was not obvious from qualitative observations (Wayne Vogl, personal communication). Further histological quantification of tissue sections and assessment of serum markers of pituitary and testicular function (e.g. FSH, LH) may reveal insights into the origin of the pathology observed. Similarly, assessment of HIP14 expression in testis may enable insights into potential changes in HIP14 expression that may occur over life in this tissue; unfortunately, this has proven difficult to assess via western blot; mRNA assessment may be more successful. Finally, the impaired fertility of *Hip14*-/- mice may arise due to altered mating behaviours in *Hip14-/-* males, and this remains to be assessed.

6.4.2. Novel approaches to study HIP14 overexpression and HIP14 biology

While the current study has contributed to the further understanding of HIP14 biology, many questions that we hoped to address remain unresolved. What are

the effects of HIP14 overexpression? Is HIP14 overexpression *in vivo* harmful? The mild neuropathological changes in *HIP14* BAC mice described in chapter 3 suggest that the latter may be possible, but these changes may also arise due to other factors, such as insertional mutagenesis. Most importantly, for the purpose of interventions in human disease, we ask whether overexpression of HIP14 delay or ameliorate features features of HD in mice and potentially in humans? The modest level of HIP14 overexpression achieved in the *HIP14* BAC mouse model made it difficult to conclusively answer these questions. In the sections below, we outline possible strategies to address these questions in future studies.

6.4.2.1. In vitro approaches

A significant drawback to studying disease *in vivo* is the cost involved. Creation, characterization, and maintenance of a novel mouse model of disease is a significant and expensive undertaking. In addition, initial attempts are not always successful and/or the model generated may not satisfy all desired criteria, as we have encountered in this study. One way to manage these risks is to conduct preliminary studies *in vitro*. ES cells used to generate mouse models can undergo preliminary characterization *in vitro*. A construct of interest (considerations on this are discussed further in section 6.4.2.2 below) can be electroporated into ES cells, and preliminary investigation can be done *in vitro*. By identifying ES cells expressing a range of HIP14 overexpression (e.g. 2-, 4-, and 10-fold of endogenous) via qrtPCR, the effects of this overexpression on viability and presence of abnormal phenotypes can be assessed *in vitro*. In addition, selected ES cells can be induced to differentiate to a cell type of interest (e.g. neurons) in order to further assess *in vitro* phenotypes in a particular cell type. ES cells exhibiting the properties of interest can be selected for blastocyst injections in order to generate a transgenic mouse. These preliminary studies would afford the researcher much greater control over the level of overexpression of HIP14, and permit the most informed decision when selecting ES cells for further study *In vivo*.

6.4.2.2. In vivo approaches

One of the most appealing features of artificial chromosome approaches to transgenesis is the inclusion of intronic and regulatory DNA, ensuring a pattern of expression similar to endogenous. However, this may not always be desirable in the context of therapeutic trials, as therapeutic interventions typically will not accurately recapitulate endogenous gene expression events *in vivo.* For this reason, many investigators choose to modify the construct carrying the gene of interest in generating transgenic models. The gene of interest may originate from genomic DNA or cDNA according to the investigator's preferences; the latter, while less representative of endogenous expression, is often better suited to addressing a scientific question, namely, exploring HIP14 overexpression at non-physiological levels. Selection of a particular promoter can drive expression that is ubiquitous, or spatially or temporally controlled. Use of Cre/Lox systems can facilitate this (Sauer, 1998). A *HIP14* construct can be designed and used to electroporate ES cells in the strategy described above in section 6.4.2.1. For ubiquitous expression, the CAGGS promoter is a common choice (Okabe *et al.*, 1997). The promoter options available for a particular temporal (e.g. pre- or post-developmental) or tissue-specific (e.g. ubiquitous, whole brain, brain subregion) expression pattern are vast and important considerations in this selection are discussed elsewhere (Ristevski, 2005, Van de Sluis and Voncken, 2010).

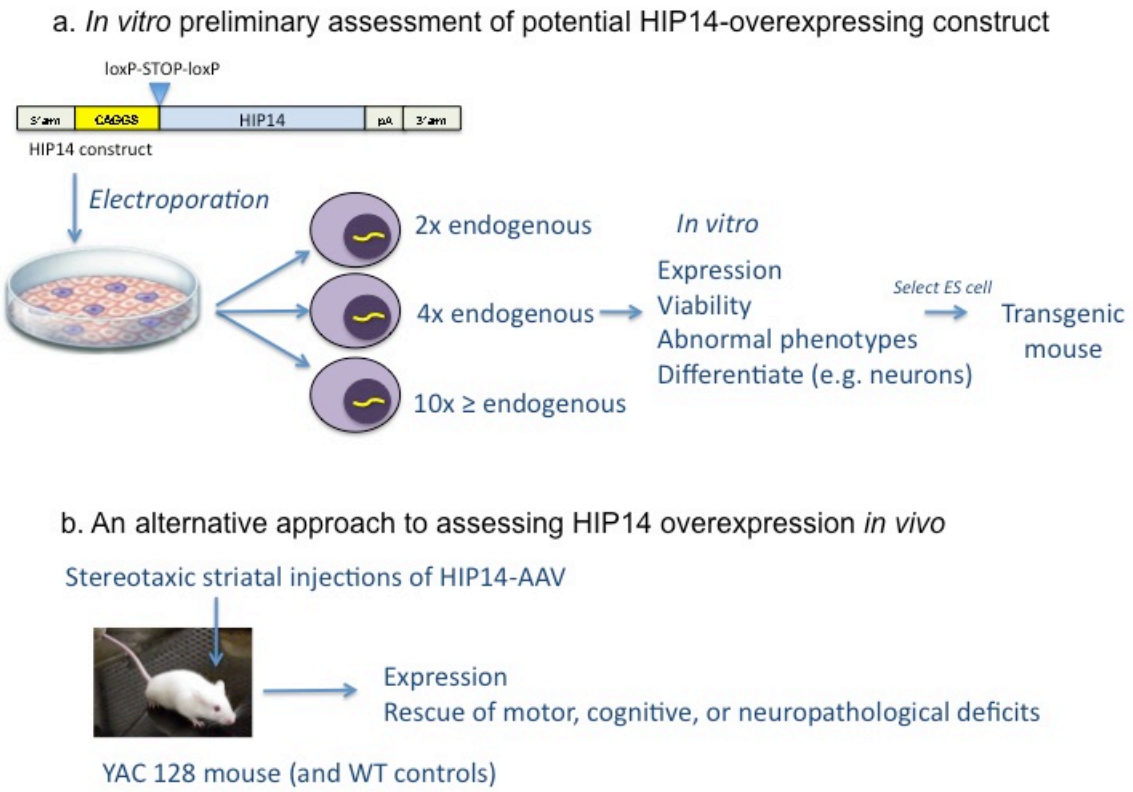

Figure 6.1 - Novel approaches to studying HIP14 overexpression *in vitro* and *in vivo.* **a.** Electroporation of ES cells with a construct of interest allows characterization of a transgene overexpression prior to investing the resources necessary in generation of a mouse model. **b**. In addition to generating a mouse model via the ES cell strategy outlined in (a), stereotaxic injections of *HIP14*-carrying virus is an alternative means of delivering HIP14 for overexpression *In vivo.*

Creation of a novel mouse model of HIP14 overexpression would afford insights into HIP14 overexpression *in vivo* and this mouse may be later crossed to other mouse models of disease, including YAC128. However, a gene therapy approach is an alternative means to explore the potential therapeutic value of HIP14 overexpression in existing mouse models. This approach sidesteps the costly and labour intensive need to create a novel mouse model, despite the insights that the latter would afford in its own right into the biology of HIP14. Stereotaxic injections of YAC128 mice and WT controls with *HIP14*-containing AAV is an alternate means to deliver increased HIP14 expression directly to the brain. Indeed, this scenario more likely represents the type of future intervention in human patients by the current paradigms and limitations of clinical medicine. In

summary, the rapidly advancing transgenic technologies provide the researcher with a number of options for further study of HIP14 *in vivo.*

BIBLIOGRAPHY

1. Abad-Rodriguez, J., Ledesma, M. D., Craessaerts, K., Perga, S., Medina, M., Delacourte, A., Dingwall, C., De Strooper, B., Dotti, C. G., 2004. Neuronal membrane cholesterol loss enhances amyloid peptide generation. J. Cell. Biol. 167(5):953-60.

2. Abrahams, B. S., Kwok, M. C. H., Trinh, E., Budaghzadeh, S., Hossain, S. M., Simpson, E. M., 2005. Pathological aggression in "fierce" mice corrected by human nuclear receptor 2E1. J. Neurosci. 25(27):6263-70.

3. Allan, C. M., Hendelsman, D. J. *In vivo* FSH Actions. In: Skinner MK, Griswold MD, editors. Sertoli Cell Biology. San Diego: Elsevier Academic Press; 2005. p. pp. 187.

4. Andrews, B. Pinguid, the Drosophila homolog of huntingtin interacting protein 14, encodes an essential protein involved in TGF-beta signalling. Vancouver: Simon Fraser University; 2006.

5. Arstikaitis, P., Gauthier-Campbell, C., Herrera, R. C. G., Huang, K., Levinson, J. N., Murphy, T. H., Kilimann, M. W., Sala, C., Colicos, M. A., El-Husseini, A., 2008. Paralemmin-1, a modulator of filopodia induction Is required for spine maturation. Mol. Biol. Cell. 19:2026-38.

6. Asami, J., Inoue, Y. U., Terakawa, Y. W., Egusa, S. F., Inoue, T., 2010. Bacterial artificial chromosomes as analytical basis for gene transcriptional machineries. Transgenic Res. 20(4):913-24.

7. Baekkeskov, S., Kanaani, J., 2009. Palmitoylation cycles and regulation of protein function (Review). Mol. Membrane Biol. 26(1-2):42-54.

8. Baker, D. J., 2011. Hypomorphic Mice. Methods Mol. Biol. 693:233-44.

9. Baker, T. L., Booden, M. A., Bussi, J. E., 2000. S-Nitrosocysteine increases palmitate turnover on Ha-Ras in NIH 3T3 cells. J. Biol. Chem. 275(29):22037-47.

10. Baker, T. L., Zheng, H., Walker, J., Coloff, J. L., Buss, J. E., 2003. Distinct rates of palmitate turnover on membrane-bound cellular and oncogenic H-Ras. J. Biol. Chem. 278(21):19292-300.

11. Bellizzi III, J. J., Widom, J., Kemp, C., Lu, J.-Y., Das, A. K., Hofmann, S. L., Clardy, J., 2000. The crystal structure of palmitoyl protein thioesterase 1 and the molecular basis of infantile neuronal ceroid lipofuscinosis. Proc. Natl. Acad. Sci. U.S.A. 97(9):4573–8.

12. Bijlmakers, M.-j., Marsh, M., 2002. The on-off story of protein palmitoylation. Trends Cell Biol. . 13(1):32-42.

13. Bizzozero, O., 1997. The mechanism amd functional roles of protein palmitoylation in the nervous system. Neuropediatrics. 28:23-6.

14. Blizard, D. A., Adams, N., 2002. The Maudsley Reactive and Nonreactive strains: a new perspective. Behav. Genet. 32(5):277-99.

15. Botto, L. D., May, K., Fernhoff, P. M., Correa, A., Coleman, K., Rasmussen, S. A., Merritt, R. K., O'Leary, L. A., Wong, L.-Y., Elixson, E. M., Mahle, W. T., Campbell, R. M., 2003. A population-based study of the 22q11.2 deletion: phenotype, incidence, and contribution to major birth defects in the population. Pediatrics. 112:101-7.

16. Bradley, S. V., Hyun, T. S., Oravecz-Wilson, K. I., Li, L., Waldorff, E. I., Ermilov, A. N., Goldstein, S. A., Zhang, C. X., Drubin, D. G., Varela, K., Parlow, A., Dlugosz, A. A., Ross, T. S., 2007. Degenerative phenotypes caused by the combined deficiency of murine HIP1 and HIP1r are rescued by human HIP1. Hum. Mol. Genet. 16(11):1279-92.

17. Brown, D. A., 2006. Lipid rafts, detergent-resistant membranes, and raft targeting signals. Physiology (Bethesda). 21(6):430-9.

18. Calero, G., 2003. The crystal structure of palmitoyl protein thioesterase-2 (PPT2) reveals the basis for divergent substrate specificities of the two lysosomal thioesterases, PPT1 and PPT2. J. Biol. Chem. 278(39):37957-64.

19. Camp, L. A., Hofmann, S. L., 1993. Purification and properties of a palmitoyl-protein thioesterase that cleaves palmitate from H-Ras. J. Biol. Chem. 268(30):22566-74.

20. Cattaneo, E., Zuccato, C., Tartari, M., 2005. Normal huntingtin function: an alternative approach to Huntington's disease. Nat. Rev. Neurosci. 6(12):919-30.

21. Cavalieri, B. Geometria Degli Indivisibili. Turin: Unione Tipographico-Editrice; 1966.

22. Caviston, J. P., Holzbaur, E. L. F., 2009. Huntingtin as an essential integrator of intracellular vesicular trafficking. Trends Cell Biol. 19(4):147-55.

23. Chandler, J., Hohenstein, P., Swing, D. A., Tessarollo, L., Sharan, S. K., 2001. Human BRCA1 gene rescues the embryonic lethality of Brca1 mutant mice. Genesis. 29(2):72-7.

24. Chandler, K. J., Chandler, R. L., Broeckelmann, E. M., Hou, Y., Southard-Smith, E. M., Mortlock, D. P., 2007. Relevance of BAC transgene copy number in mice: transgene copy number variation across multiple transgenic lines and correlations with transgene integrity and expression. Mamm. Genome. 18(10):693-708.

25. Chang, S.-C., Magee, A. I., 2009. Acyltransferases for secreted signalling proteins (Review). Mol. Membrane Biol. 26(1-2):104-13.

26. Charollais, J., Van Der Goot, F. G., 2009. Palmitoylation of membrane proteins (Review). Mol. Membrane Biol. 26(1-2):55-66.

27. Chen, J. Y., Levy-Wilson, B., Goodart, S., Cooper, A. D., 2002. Mice expressing the human CYP7A1 gene in the mouse CYP7A1 knock-out background lack induction of CYP7A1 expression by cholesterol feeding and

have increased hypercholesterolemia when fed a high fat diet. J. Biol. Chem. 277(45):42588–95.

28. Chen, W.-Y., Shi, Y.-Y., Zheng, Y.-L., Zhao, X.-Z., Zhang, G.-J., Chen, S.-Q., Yang, P.-D., He, L., 2004. Case-control study and transmission disequilibrium test provide consistent evidence for association between schizophrenia and genetic variation in the 22q11 gene ZDHHC8. Hum. Mol. Genet. 13(23):2991-5.

29. Cheng, H., Vetrivel, K. S., Drisdel, R. C., Meckler, X., Gong, P., Leem, J. Y., Li, T., Carter, M., Chen, Y., Nguyen, P., Iwatsubo, T., Tomita, T., Wong, P. C., Green, W. N., Kounnas, M. Z., Thinakaran, G., 2009. S-palmitoylation of gamma-secretase subunits nicastrin and APH-1. J. Biol. Chem. 284(3):1373-84.

30. Cheung, C., Akiyama, T. E., Ward, J. M., Nicol, C. J., Feigenbaum, L., Vinson, C., Gonzalez, F. J., 2004. Diminished hepatocellular proliferation in mice humanized for the nuclear receptor peroxisome proliferator-activated receptor alpha. Cancer Res. 64(11):3849-54.

31. Cho, S., Dawson, G., 2000. Palmitoyl protein thioesterase 1 protects against apoptosis mediated by Ras–Akt–caspase pathway in neuroblastoma cells. J. Neurochem. 74 1478–88.

32. Cho, S., Dawson, P. E., Dawson, G., 2000. Antisense palmitoyl protein thioesterase 1 (PPT1) treatment inhibits PPT1 activity and increases cell death in LA-N-5 neuroblastoma cells. Journal of Neuroscience Research. 62:234-40.

33. Citri, A., Malenka, R. C., 2008. Synaptic plasticity: multiple forms, functions, and mechanisms. Neuropsychopharmacology. 33(1):18-41.

34. Conibear, E., Davis, N. G., 2010. Palmitoylation and depalmitoylation dynamics at a glance. J. Cell Sci. 123(23):4007-10.

35. Coutinho, J. M., Singaraja, R. R., Kang, M., Arenillas, D. J., Bertram, L. N., Bissada, N., Staels, B., Fruchart, J.-C., Fievet, C., Joseph-George, A. M., Wasserman, W. W., Hayden, M. R., 2005. Complete functional rescue of the ABCA1-/- mouse by human BAC transgenesis. J. Lipid Res. 46(6):1113-23.

36. Craven, S. E., El-Husseini, A. E., Bredt, D. S., 1999. Synaptic targeting of the postsynaptic density protein PSD-95 mediated by lipid and protein motifs. Neuron 22(3):497-509.

37. Crawley, J. N., Paylor, R., 1997. A proposed test battery and constellations of specific behavioral paradigms to investigate the behavioral phenotypes of transgenic and knockout mice. Horm. Behav. 31(3):197-211.

38. Dekker, F. J., Rocks, O., Vartak, N., Menninger, S., Hedberg, C., Balamurugan, R., Wetzel, S., Renner, S., Gerauer, M., Schölermann, B., Rusch, M., Kramer, J. W., Rauh, D., Coates, G. W., Brunsveld, L., Bastiaens, P. I. H., Waldmann, H., 2010. Small-molecule inhibition of APT1 affects Ras localization and signaling. Nat. Chem. Biol. 6(6):449-56.

39. Demily, C., Legallic, S., Bou, J., Houy-Durand, E., Van Amelsvoort, T., Zinkstokd, J., Manouvrier-Hanue, S., Vogels, A., Drouin-Garraud, V., Philip, N.,

Philippe, A., Heron, D., Sarda, P., Petit, M., Thibaut, F., Frebourg, T., Campion, D., 2007. ZDHHC8 single nucleotide polymorphism rs175174 is not associated with psychiatric features of the 22q11 deletion syndrome or schizophrenia. Psychiatr. Genet. 17:311-2.

40. Deng, Y. P., Albin, R. L., Penney, J. B., Young, A. B., Anderson, K. D., Reiner, A., 2004. Differential loss of striatal projection systems in Huntington's disease: a quantitative immunohistochemical study. J. Chem. Neuroanat. 27:143–64.

41. Devedjiev, Y., Dauter, Z., Kuznetsov, S. R., Jones, T. L. Z., Derewenda, Z. S., 2000. Crystal structure of the human acyl protein thioesterase I from a single X-ray data set to 1.5 A. . Structure. 8:1137-46.

42. Dietrich, L. E. P., Ungermann, C., 2004. On the mechanism of protein palmitoylation. E.M.B.O. Rep. 5(11):1053-7.

43. Dobie, K., Mehtali, M., McLenaghan, M., Lathe, R., 1997. Variegated gene expression in mice. Trends Genet. 13(4):127-30.

44. Doetschman, T., 2009. Influence of genetic background on genetically engineered mouse phenotypes. Methods Mol. Biol. 530:423-33.

45. Dorfleutner, A., Ruf, W., 2003. Regulation of tissue factor cytoplasmic domain phosphorylation by palmitoylation. Blood. 102(12):3998-4005.

46. Dragatsis, I., Efstratiadis, A., Zeitlin, S., 1998. Mouse mutant embryos lacking huntingtin are rescued from lethality by wild-type extraembryonic tissues. Development. 125(8):1529-39.

47. Dragatsis, I., Levine, M. S., Zeitlin, S., 2000. Inactivation of Hdh in the brain and testis results in progressive neurodegeneration and sterility in mice. Nat. Genet. 26(3):300-6.

48. Drew, L. J., Crabtree, G. W., Markx, S., Stark, K. L., Chaverneff, F., Xu, B., Mukai, J., Fenelon, K., Hsu, P.-K., Gogos, J. A., Karayiorgou, M., 2010. The 22q11.2 microdeletion: fifteen years of insights into the genetic and neural complexity of psychiatric disorders. Int. J. Dev. Neurosci. 29(3):259-81.

49. Drisdel, R. C., Green, W., 2004. Labeling and quantifying sites of protein palmitoylation. Biotechniques. 36(2):276-85.

50. Ducker, C. E., Stettler, E. M., French, K. J., Upson, J. J., Smith, C. D., 2004. Huntingtin interacting protein 14 is an oncogenic human protein: palmitoyl acyltransferase. Oncogene. 23(57):9230-7.

51. Duncan, J. A., Gilman, A. G., 2002. Characterization of Saccharomyces cerevisiae Acyl-protein Thioesterase 1, the Enzyme Responsible for G protein alpha subunit deacylation in vivo. J. Biol. Chem. 277(35):31740-52.

52. Dunphy, J. T., Linder, M. E., 1998. Signalling Functions of protein palmitolylation. Biochim. Biophys. Acta. 1436(1-2):245-61.

53. Duyao, M. P., Auerbach, A. B., Ryan, A., Persichetti, F., Barnes, G. T., McNeil, S. M., Ge, P., Vonsattel, J.-P., Gusella, J. F., Joyner, A. L., Macdonald, M. E., 1995. Inactivation of the mouse Huntington's disease gene homolog Hdh. Science. 269(5222):407-10.

54. Eddy, E. M. The effects of gene knockouts on spermatogenesis. In: Gagnon C, editor. The Male gamete: applications. Vienna: Cache River Press; 1999. p. 23–6.

55. Ehrlich, I., 2004. Postsynaptic density 95 controls AMPA receptor incorporation during long-term potentiation and experience-driven synaptic plasticity. J. Neurosci. 24(4):916-27.

56. El-Husseini, A. E., Craven, S. E., Chetkovich, D. M., Firestein, B. L., Schnell, E., Aoki, C., Bredt, D. S., 2000a. Dual palmitoylation of PSD-95 mediates Its vesiculotubular sorting, postsynaptic targeting, and ion channel clustering. J. Cell Biol. 148(1):159-71.

57. El-Husseini, A. E.-D., Schnell, E., Chetkovich, D. M., Nicoll, R. A., Bredt, D. S., 2000b. PSD-95 involvement in maturation of excitatory synapses. Science. 290(5495):1364-8.

58. El-Husseini, A. E.-D., Bredt, D. S., 2002. Protein palmitoylation: a regulator of neuronal development and function. Nat. Rev. Neurosci. 3(10):791-802.

59. El-Husseini, A. E.-D., Schnell, E., Dakoji, S., Sweeney, N., Zhou, Q., Prange, O., Gauthier-Campbell, C., Aguilera-Moreno, A., Nicoll, R. A., Bredt, D. S., 2002. Synaptic strength regulated by palmitate cycling on PSD-95. Cell. 108(6):849-63.

60. Faber, P. W., Barnes, G. T., Srinidhi, J., Chen, J., Gusella, J. F., Macdonald, M. E., 1998. Huntingtin interacts with a family of WW domain proteins. Hum. Mol. Genet. 7(9):1463-74.

61. Fan, M. M. Y., Raymond, L. A., 2007. N-methyl-D-aspartate (NMDA) receptor function and excitotoxicity in Huntington’s disease. Prog. Neurobiol. 81(5-6):272-93.

62. Fang, C., Deng, L., Keller, C. A., Fukata, M., Fukata, Y., Chen, G., Luscher, B., 2006. GODZ-mediated palmitoylation of GABA(A) receptors Is required for normal assembly and function of GABAergic inhibitory synapses. J. Neurosci. 26(49):12758-68.

63. Friedman, R. C., Farh, K. K.-H., Burge, C. B., Bartel, D. P., 2009. Most mammalian mRNAs are conserved targets of microRNAs. Genome Res. 19:92–105.

64. Fukata, M., Fukata, Y., Adesnik, H., Nicoll, R., Bredt, D., 2004. Identification of PSD-95 palmitoylating enzymes. Neuron. 44(6):987-96.

65. Fukata, Y., Fukata, M., 2010. Protein palmitoylation in neuronal development and synaptic plasticity. Nat. Rev. Neurosci. 11(3):161-75.

66. Gafni, J., Hermel, E., Young, J. E., Wellington, C. L., Hayden, M. R., Ellerby, L. M., 2004. Inhibition of calpain cleavage of huntingtin reduces toxicity: accumulation of calpain/caspase fragments in the nucleus. J. Biol. Chem. 279(19):20211-20.

67. Gao, T., Collins, R. E., Horton, J. R., Zhang, X., Zhang, R., Dhayalan, A., Tamas, R., Jeltsch, A., Cheng, X., 2009. The ankyrin repeat domain of Huntingtin interacting protein 14 contains a surface aromatic cage, a potential site for methyl-lysine binding. Proteins. 76(3):772-7.

68. Gauthier-Campbell, C., Bredt, D. S., Murphy, T. H., El-Husseini, A. E.-D., 2004. Regulation of dendritic branching and filopodia formation in hippocampal neurons by specific acylated protein motifs. Mol. Cell Biol. 15(5):2205-17.

69. Giot, L., Bader, J. S., Brouwer, C., Chaudhuri, A., Kuang, B., Li, Y., Hao, Y. L., Ooi, C. E., Godwin, B., Vitols, E., Vijayadamodar, G., Pochart, P., Machineni, H., Welsh, M., Kong, Y., Zerhusen, B., Malcolm, R., Varrone, Z., Collis, A., Minto, M., Burgess, S., McDaniel, L., Stimpson, E., Spriggs, F., Williams, J., Neurath, K., Ioime, N., Agee, M., Voss, E., Furtak, K., Renzulli, R., Aanensen, N., Carrolla, S., Bickelhaupt, E., Lazovatsky, Y., DaSilva, A., Zhong, J., Stanyon, C. A., Finley Jr., R. L., White, K. P., Braverman, M., Jarvie, T., Gold, S., Leach, M., Knight, J., Shimkets, R. A., McKenna, M. P., Chant, J., Rothberg, J. M., 2003. A protein interaction map of Drosophila melanogaster. Science. 302(5651):1727-36.

70. Giraldo, P., Montoliu, L., 2001. Size matters: use of YACs, BACs and PACs in transgenic animals. Transgenic Res. 10(2):83-103.

71. Glaser, B., Schumacher, J., Williams, H., Jamra, R., Ianakiev, N., Milev, R., Ohlraun, S., Schulze, T., Czerski, P., Hauser, J., 2005. No association between the putative functional ZDHHC8 single nucleotide polymorphism rs175174 and schizophrenia in large European samples. Biol. Psychiatry. 58(1):78-80.

72. Glaser, B., Moskvina, V., Kirov, G., Murphy, K., Williams, H., Williams, N., Owen, M., Odonovan, M., 2006. Analysis of ProDH, COMT and ZDHHC8 risk variants does not support individual or interactive effects on schizophrenia susceptibility. Schizophr. Res. 87(1-3):21-7.

73. Goytain, A., Hines, R. M., Quamme, G. A., 2008. Huntingtin-interacting proteins, HIP14 and HIP14L, mediate dual functions, palmitoyl acyltransferase and Mg2+ transport. J. Biol. Chem. 283(48):33365-74.

74. Graham, R. K., Deng, Y., Slow, E. J., Haigh, B., Bissada, N., Lu, G., Pearson, J., Shehadeh, J., Bertram, L., Murphy, Z., Warby, S. C., Doty, C. N., Roy, S., Wellington, C. L., Leavitt, B. R., Raymond, L. A., Nicholson, D. W., Hayden, M. R., 2006. Cleavage at the caspase-6 site is required for neuronal dysfunction and degeneration due to mutant huntingtin. Cell. 125(6):1179–91.

75. Graybiel, A. M., 2000. The basal ganglia. Curr. Biol. 10(14):R509-R11.

76. Greaves, J., Salaun, C., Fukata, Y., Fukata, M., Chamberlain, L. H., 2008. Palmitoylation and membrane interactions of the neuroprotective chaperone cysteine-string protein. J. Biol. Chem. 283(36):25014–26.

77. Greaves, J., Prescott, G. R., Gorleku, O. A., Chamberlain, L. H., 2009. The fat controller: roles of palmitoylation in intracellular protein trafficking and targeting to membrane microdomains (Review). Mol. Membrane Biol. 26(1-2):67-79.

78. Greaves, J., Chamberlain, L. H., 2011. DHHC palmitoyl transferases: substrate interactions and (patho)physiology. Trends Biochem. Sci. 36(5):245-53.

79. Gregory, S. G., Barlow, K. F., Mclay, K. E., Kaul, R., Swarbreck, D., Dunham, A., Scott, C. E., Howe, K. L., Woodfine, K., Spencer, C. C. A., Jones, M. C., Gillson, C., Searle, S., Zhou, Y., Kokocinski, F., Mcdonald, L., Evans, R., Phillips, K., Atkinson, A., Cooper, R., Jones, C., Hall, R. E., Andrews, T. D., Lloyd, C., Ainscough, R., Almeida, J. P., Ambrose, K. D., Anderson, F., Andrew, R. W., Ashwell, R. I. S., Aubin, K., Babbage, A. K., Bagguley, C. L., Bailey, J., Beasley, H., Bethel, G., Bird, C. P., Bray-Allen, S., Brown, J. Y., Brown, A. J., Buckley, D., Burton, J., Bye, J., Carder, C., Chapman, J. C., Clark, S. Y., Clarke, G., Clee, C., Cobley, V., Collier, R. E., Corby, N., Coville, G. J., Davies, J., Deadman, R., Dunn, M., Earthrowl, M., Ellington, A. G., Errington, H., Frankish, A., Frankland, J., French, L., Garner, P., Garnett, J., Gay, L., Ghori, M. R. J., Gibson, R., Gilby, L. M., Gillett, W., Glithero, R. J., Grafham, D. V., Griffiths, C., Griffiths-Jones, S., Grocock, R., Hammond, S., Harrison, E. S. I., Hart, E., Haugen, E., Heath, P. D., Holmes, S., Holt, K., Howden, P. J., Hunt, A. R., Hunt, S. E., Hunter, G., Isherwood, J., James, R., Johnson, C., Johnson, D., Joy, A., Kay, M., Kershaw, J. K., Kibukawa, M., Kimberley, A. M., King, A., Knights, A. J., Lad, H., Laird, G., Lawlor, S., Leongamornlert, D. A., Lloyd, D. M., Loveland, J., Lovell, J., Lush, M. J., Lyne, R., Martin, S., Mashreghi-Mohammadi, M., Matthews, L., Matthews, N. S. W., Mclaren, S., Milne, S., Mistry, S., M Oore, M. J. F., Nickerson, T., O'dell, C. N., Oliver, K., Palmeiri, A., Palmer, S. A., Parker, A., Patel, D., Pearce, A. V., Peck, A. I., Pelan, S., Phelps, K., Phillimore, B. J., Plumb, R., Rajan, J., Raymond, C., Rouse, G., Saenphimmachak, C., Sehra, H. K., Sheridan, E., Shownkeen, R., Sims, S., Skuce, C. D., Smith, M., Steward, C., Subramanian, S., Sycamore, N., Tracey, A., Tromans, A., Van Helmond, Z., Wall, M., Wallis, J. M., White, S., Whitehead, S. L., Wilkinson, J. E., Willey, D. L., Williams, H., Wilming, L., Wray, P. W., Wu, Z., Coulson, A., Vaudin, M., Sulston, J. E., Durbin, R., Hubbard, T., Wooster, R., Dunham, I., Carter, N. P., Mcvean, G., Ross, M. T., Harrow, J., Olson, M. V., Beck, S., Rogers, J., Bentley, D. R., 2006. The DNA sequence and biological annotation of human chromosome 1. Nature. 441(7091):315-21.

80. Grover, A., Sairam, M. R., Smith, C. E., Hermo, L., 2004. Structural and functional modifications of sertoli cells in the testis of adult follicle-stimulating hormone receptor knockout mice. Biol. Reprod. 71(1):117-29.

81. Guo, G., Huss, M., Tong, G. Q., Wang, C., Sun, L. L., Clarke, N. D., Robson, P., 2010. Resolution of cell fate decisions revealed by single-cell gene expression analysis from zygote to blastocyst. Dev. Cell. 18(4):675-85.

82. Guo, J., Zhu, P., Wu, C., Yu, L., Zhao, S., Gu, X., 2003. *In silico* analysis indicates a similar gene expression pattern between human brain and testis. Cytogenet. Genome Res. 103(1-2):58-62.

83. Gupta, P., Soyombo, A. A., Atashband, A., Wisniewski, K. E., Shelton, J. M., Richardson, J. A., Hammer, R. E., Hofmann, S. L., 2001. Disruption of PPT1 or PPT2 causes neuronal ceroid lipofuscinosis in knockout mice. Proc. Natl. Acad. Sci. U.S.A. 98(24):13566–71.

84. Hancock, J. F., Magee, A. I., Childs, J. E., Marshall, C. J., 1989. All ras proteins are polyisoprenylated but only some are palmitoylated. Cell. 57(7):1167-77.

85. Harjes, P., Wanker, E. E., 2003. The hunt for huntingtin function: interaction partners tell many different stories. Trends Biochem. Sci. 28(8):425-33.

86. Hawtin, S. R., Tobin, A. B., Patel, S., Wheatley, M., 2001. Palmitoylation of the vasopressin V1a receptor reveals different conformational requirements for signaling, agonist-induced receptor phosphorylation, and sequestration. J. Biol. Chem. 276(41):38139-46.

87. Hayashi, T., Rumbaugh, G., Huganir, R., 2005. Differential regulation of AMPA receptor subunit trafficking by palmitoylation of two distinct sites. Neuron. 47(5):709-23.

88. Hayashi, T., Thomas, G. M., Huganir, R. L., 2009. Dual palmitoylation of NR2 subunits regulates NMDA receptor trafficking. Neuron. 64(2):213-26.

89. Hayden, M. R. Chapter 5: Clinical features. Huntington's Chorea. New York: Springer-Verlag; 1981. p. pp59-92.

90. Heaney, J. D., Bronson, S. K., 2006. Artificial chromosome-based transgenes in the study of genome function. Mamm. Genome. 17(8):791-807.

91. Heinonen, O., Kyttala, A., Lehmus, E., Paunio, T., Peltonen, L., Jalanko, A., 2000. Expression of palmitoyl protein thioesterase in neurons. Mol. Genet. Metab. 69(2):123-9.

92. Hess, D. T., Patterson, S. I., Smith, D. S., Skene, J. H. P., 2002. Neuronal growth cone collapse and inhibition of protein fatty acylation by nitric oxide. Nature. 366(6455):562-5.

93. Hines, R. M., Kang, R., Goytain, A., Quamme, G. A., 2010. Golgi-specific DHHC zinc finger protein GODZ mediates membrane Ca2+ transport. J. Biol. Chem. 285(7):4621-8.

94. Hirano, T., Kishi, M., Sugimoto, H., Taguchi, R., Obinata, H., Ohshima, N., Tatei, K., Izumi, T., 2009. Thioesterase activity and subcellular localization of

acylprotein thioesterase 1/lysophospholipase 1. Biochim. Biophys. Acta. 1791(8):797-805.

95. Hodgson, J. G., Smith, D. J., McCutcheon, K., Koide, H. B., Nishiyama, K., Dinulos, M. B., Stevens, M. E., Bissada, N., Nasir, J., Kanazawa, I., Disteche, C. M., Rubin, E. M., Hayden, M. R., 1996. Human huntingtin derived from YAC transgenes compensates for loss of murine huntingtin by rescue of the embryonic lethal phenotype. Hum. Mol. Genet. 5(12):1875-85.

96. Holmes, A., Parmigiani, S., Ferrari, P., Palanza, P., Rodgers, R., 2000. Behavioral profile of wild mice in the elevated plus-maze test for anxiety. Physiol. Behav. 71(5):509-16.

97. Hoshii, T., Takeo, T., Nakagata, N., Takeya, M., Araki, K., Yamamura, K.-I., 2007. LGR4 regulates the postnatal development and integrity of male reproductive tracts in mice. Biol. Reprod. 76(2):303-13.

98. Huang, K., Yanai, A., Kang, R., Arstikaitis, P., Singaraja, R., Metzler, M., Mullard, A., Haigh, B., Gauthiercampbell, C., Gutekunst, C., 2004. Huntingtin-Interacting Protein HIP14 Is a palmitoyl transferase involved in palmitoylation and trafficking of multiple neuronal proteins. Neuron. 44(6):977-86.

99. Huang, K., El-Husseini, A., 2005. Modulation of neuronal protein trafficking and function by palmitoylation. Curr. Opin. Neurobiol. 15:527-35.

100. Huang, K., Sanders, S., Singaraja, R., Orban, P., Cijsouw, T., Arstikaitis, P., Yanai, A., Hayden, M. R., El-Husseini, A., 2009. Neuronal palmitoyl acyl transferases exhibit distinct substrate specificity. F.A.S.E.B. J. 23(8):2605-15.

101. Huang, K., Sanders, S. S., Kang, R., Sutton, L., Wan, J., Singaraja, R., Young, F., Liu, L., El-Husseini, A., Davis, N. G., Hayden, M., 2011. Wildtype HTT modulates the enzymatic activity of the neuronal palmitoyl transferase HIP14. Hum. Mol. Genet. Jun 2. [Epub ahead of print].

102. Humeau, Y., Gambino, F., Chelly, J., Vitale, N., 2009. X-linked mental retardation: focus on synaptic function and plasticity. J. Neurochem. 109(1):1-14.

103. Huntington Disease Collaborative Research Group, 1993. A novel gene containing a trinucleotide repeat that is expanded and unstable on Huntington's disease chromosomes. The Huntington's Disease Collaborative Research Group. Cell. 72(6):971-83.

104. Jeong, H., Then, F., Jr, T. J. M., Mazzulli, J. R., Cui, L., Savas, J. N., Voisine, C., Paganetti, P., Tanese, N., HART, A. C., Yamamoto, A., Krainc, D., 2009. Acetylation targets mutant huntingtin to autophagosomes for degradation. Cell. 137(1):60-72.

105. Johnson, D. R., Bhatnagar, R. S., Knoll, L. J., Gordon, J. I., 1994. Genetic and biochemical studies of protein N-myristoylation. Annu. Rev. Biochem. 63:869-914.

106. Kalchman, M. A., Graham, R. K., Xia, G., Koide, H. B., Hodgson, J. G., Graham, K. C., Goldberg, Y. P., Gietz, R. D., Pickart, C. M., Hayden, M. R.,

1996. Huntingtin is ubiquitinated and interacts with a specific ubiquitin-conjugating enzyme. J. Biol. Chem. 271(32):19385–94.

107. Kanaani, J., El-Din El-Husseini, A., Aguilera-Moreno, A., Diacovo, J. M., Bredt, D. S., Baekkeskov, S., 2002. A combination of three distinct trafficking signals mediates axonal targeting and presynaptic clustering of GAD65. J. Cell Biol. 158(7):1229-38.

108. Kanaani, J., Diacovo, M. J., El-Din El-Husseini, A., Bredt, D. S., Baekkeskov, S., 2004. Palmitoylation controls trafficking of GAD65 from Golgi membranes to axon-specific endosomes and a Rab5a-dependent pathway to presynaptic clusters. J. Cell Sci. 117(10):2001-13.

109. Kang, K.-H., Bier, E., 2010. dHIP14-dependent palmitoylation promotes secretion of the BMP antagonist Sog. Dev. Biol. 346(1):1-10.

110. Kang, R., Swayze, R., Lise, M. F., Gerrow, K., Mullard, A., Honer, W. G., El-Husseini, a. A., 2004. Presynaptic trafficking of synaptotagmin I is regulated by protein palmitoylation. J. Biol. Chem. 279(48):50524-36.

111. Kang, R., Wan, J., Arstikaitis, P., Takahashi, H., Huang, K., Bailey, A. O., Thompson, J. X., Roth, A. F., Drisdel, R. C., Mastro, R., Green, W. N., Iii, J. R. Y., Davis, N. G., El-Husseini, A., 2008. Neural palmitoyl-proteomics reveals dynamic synaptic palmitoylation. Nature. 456(7224):904-9.

112. Kao, L.-R., Peterson, J., Ji, R., Bender, L., Bender, A., 1996. Interactions between the ankyrin repeat-containing protein Akr1p and the pheromone response pathway in Saccharomyces cerevisiae. Mol. Cell Biol. . 16(1):168-78.

113. Karayiorgou, M., Gogos, J., 2004. The molecular genetics of the 22q11-associated schizophrenia. Brain Res Mol Brain Res. 132(2):95-104.

114. Kato, H., Allen, N. D., Emson, P. C., Kiyama, H., 2000. GAP-43 N-terminal translocation signal targets b-galactosidase to developing axons in a pan-neuronal transgenic mouse line. Brain Res Dev Brain Res. 121(1):109-12.

115. Kelsoe, J. R., Spence, M. A., Loetscher, E., Foguet, M., Sadovnick, A. D., Remick, R. A., Flodman, P., Khristich, J., Mroczkowski-Parker, Z., Brown, J. L., Masser, D., Ungerleider, S., Rapaport, M. H., Wishart, W. L., Luebbert, H., 2001. A genome survey indicates a possible susceptibility locus for bipolar disorder on chromosome 22. Proc. Natl. Acad. Sci. U.S.A. 98(2):585-90.

116. Khatchadourian, K., Smith, C. E., Metzler, M., Gregory, M., Hayden, M. R., Cyr, D. G., Hermo, L., 2007. Structural abnormalities in spermatids together with reduced sperm counts and motility underlie the reproductive defect in HIP1-/- mice. Mol. Reprod. Dev. 74(3):341-59.

117. Kim, E., Sheng, M., 2004. PDZ domain proteins of synapses. Nat. Rev. Neurosci. 5(10):771-81.

118. Kraut, R., Menon, K., Zinn, K., 2001. A gain-of-function screen for genes controlling motor axon guidance and synaptogenesis in Drosophila. Curr. Biol. 11(6):417-30.

119. Kreitzer, A. C., Malenka, R. C., 2008. Striatal plasticity and basal ganglia circuit function. Neuron. 60(4):543-54.

120. Kutzleb, C., Sanders, G., Yamamoto, R., Wang, X., Lichte, B., Petrasch-Parwez, E., Kilimann, M. W., 1998. Paralemmin, a prenyl-palmitoyl-anchored phosphoprotein abundant in neurons and implicated in plasma membrane dynamics and cell process formation. J. Cell Biol. 143(3):795-813.

121. Lako, M., Hole, N., 2000. Searching the unknown with gene trapping. Expert Rev. Mol. Med. 2(5):1-11.

122. Laux, T., Fukami, K., Thelen, M., Golub, T., Frey, D., Caroni, P., 2000. GAP43, MARCKS, and CAP23 modulate PI(4,5)P(2) at plasmalemmal rafts, and regulate cell cortex actin dynamics through a common mechanism. J. Cell Biol. 149(7):1455-71.

123. Lee, Y.-S., Silva, A. J., 2009. The molecular and cellular biology of enhanced cognition. Nat. Rev. Neurosci. 10(2):126-40.

124. Lehtovirta, M., Kyttala, A., Eskelinen, E., Hess, M., Heinonen, O., Jalanko, A., 2001. Palmitoyl protein thioesterase (PPT) localizes into synaptosomes and synaptic vesicles in neurons: implications for infantile neuronal cereoid lipofuscinosis (INCL). Hum. Mol. Genet. 10(1):69-75.

125. Lein, E. S., Hawrylycz, M. J., Ao, N., Ayres, M., Bensinger, A., Bernard, A., Boe, A. F., Boguski, M. S., Brockway, K. S., Byrnes, E. J., Chen, L., Chen, L., Chen, T.-M., Chi Chin, M., Chong, J., Crook, B. E., Czaplinska, A., Dang, C. N., Datta, S., Dee, N. R., Desaki, A. L., Desta, T., Diep, E., Dolbeare, T. A., Donelan, M. J., Dong, H.-W., Dougherty, J. G., Duncan, B. J., Ebbert, A. J., Eichele, G., Estin, L. K., Faber, C., Facer, B. A., Fields, R., Fischer, S. R., Fliss, T. P., Frensley, C., Gates, S. N., Glattfelder, K. J., Halverson, K. R., Hart, M. R., Hohmann, J. G., Howell, M. P., Jeung, D. P., Johnson, R. A., Karr, P. T., Kawal, R., Kidney, J. M., Knapik, R. H., Kuan, C. L., Lake, J. H., Laramee, A. R., Larsen, K. D., Lau, C., Lemon, T. A., Liang, A. J., Liu, Y., Luong, L. T., Michaels, J., Morgan, J. J., Morgan, R. J., Mortrud, M. T., Mosqueda, N. F., Ng, L. L., Ng, R., Orta, G. J., Overly, C. C., Pak, T. H., Parry, S. E., Pathak, S. D., Pearson, O. C., Puchalski, R. B., Riley, Z. L., Rockett, H. R., Rowland, S. A., Royall, J. J., Ruiz, M. J., Sarno, N. R., Schaffnit, K., Shapovalova, N. V., Sivisay, T., Slaughterbeck, C. R., Smith, S. C., Smith, K. A., Smith, B. I., Sodt, A. J., Stewart, N. N., Stumpf, K.-R., Sunkin, S. M., Sutram, M., Tam, A., Teemer, C. D., Thaller, C., Thompson, C. L., Varnam, L. R., Visel, A., Whitlock, R. M., Wohnoutka, P. E., Wolkey, C. K., Wong, V. Y., Wood, M., Yaylaoglu, M. B., Young, R. C., Youngstrom, B. L., Feng Yuan, X., Zhang, B., Zwingman, T. A., Jones, A. R., 2007. Genome-wide atlas of gene expression in the adult mouse brain. Nature. 445(7124):168-76.

126. Li, J., Mahajan, A., Tsai, M.-D., 2006. Ankyrin repeat: a unique motif mediating protein-protein interactions. Biochemistry. 45:15168-78.

127. Li, Y., Hu, J., Hofer, K., Wong, A. M. S., Cooper, J. D., Birnbaum, S. G., Hammer, R. E., Hofmann, S. L., 2010. DHHC5 interacts with PDZ domain 3 of

post-synaptic density-95 (PSD-95) protein and plays a role in learning and memory. J. Biol. Chem. 285(17):13022-31.

128. Linder, M. E., Deschenes, R. J., 2007. Palmitoylation: policing protein stability and traffic. Nat. Rev. Mol. Cell Biol. 8(1):74-84.

129. Liu, H., Heath, S. C., Sobin, C., Roos, J. L., Galke, B. L., Blundell, M. L., Lenane, M., Robertson, B., Wijsman, E. M., Rapoport, J. L., Gogos, J. A., Karayiorgou, M., 2002. Genetic variation at the 22q11 PRODH2/DGCR6 locus presents an unusual pattern and increases susceptibility to schizophrenia. Proc. Natl. Acad. Sci. U.S.A. 99(6):3717–22.

130. Lobo, S., Greentree, W. K., Linder, M. E., Deschenes, R. J., 2002. Identification of a Ras palmitoyltransferase in Saccharomyces cerevisiae. J. Biol. Chem. 277(43):41268-73.

131. Lufkin, T., Lohnes, D., Mark, M., Dierich, A., Gorry, P., Gaub, M.-P., Lemeur, M., Chambon, P., 1993. High postnatal lethality and testis degeneration in retinoic acid receptor a mutant mice. Proc. Natl. Acad. Sci. U.S.A. 90(15):7225-9.

132. Lunkes, A., Lindenberg, K. S., ıem, L. a. B.-H., Weber, C., Devys, D., Landwehrmeyer, G. B., Mandel, J.-L., Trottier, Y., 2002. Proteases acting on mutant huntingtin generate cleaved products that differentially build up cytoplasmic and nuclear inclusions. Mol. Cell. 10(2):259-69.

133. Mansilla, F., Birkenkamp-Demtroder, K., Kruhøffer, M., Sørensen, F. B., Andersen, C. L., Laiho, P., Aaltonen, L. A., Verspaget, H. W., Ørntoft, T. F., 2007. Differential expression of DHHC9 in microsatellite stable and instable human colorectal cancer subgroups. Br. J. Cancer. 96(12):1896-903.

134. Manson, A. L., Trezise, A. E. O., MacVinish, L. J., Kasschau, K. D., Birchall, N., Episkopou, V., Vassaux, G., Evans, M. J., Colledge, W. H., Cuthbert, A. W., Huxley, C., 1997. Complementation of null CF mice with a human CFTR YAC transgene. E.M.B.O. J. 16(14):4238–49.

135. Mansouri, M. R., Marklund, L., Gustavsson, P., Davey, E., Carlsson, B., Larsson, C., White, I., Gustavson, K.-H., Dahl, N., 2005. Loss of ZDHHC15 expression in a woman with a balanced translocation t(X;15)(q13.3;cen) and severe mental retardation. Eur. J. Hum. Genet. 13(8):970-7.

136. Marshall, V. M., Allison, J., Templeton, T., Foote, S. J., 2004. Generation of BAC transgenic mice. Methods Mol. Biol. . 256:159-82.

137. Meckler, X., Roseman, J., Das, P., Cheng, H., Pei, S., Keat, M., Kassarjian, B., Golde, T. E., Parent, A. T., Thinakaran, G., 2010. Reduced Alzheimer's disease ß-amyloid deposition in transgenic mice expressing S-palmitoylation-deficient APH1aL and nicastrin. J. Neurosci. 30(48):16160-9.

138. Menalled, L. B., 2005. Knock-in mouse models of Huntington's disease. NeuroRx. 2(3):465–70.

139. Mill, P., Lee, A. W. S., Fukata, Y., Tsutsumi, R., Fukata, M., Keighren, M., Porter, R. M., Mckie, L., Smyth, I., Jackson, I. J., 2009. Palmitoylation regulates epidermal homeostasis and hair follicle differentiation. P.L.o.S. Genet. 5(11):e1000748.

140. Miranda, C. J., Santos, M. M., Ohshima, K., Smith, J., Li, L., Bunting, M., Cossee, M., Koenig, M., Sequeiros, J., Kaplan, J., Pandolfo, M., 2002. Frataxin knockin mouse. F.E.B.S. Lett. 512(1-3):291-7.

141. Mitchell, D. A., Vasudevan, A., Linder, M. E., Deschenes, Robert J., 2006. Protein palmitoylation by a family of DHHC protein S-acyltransferases. J. Lipid Res. 47(6):1118-27.

142. Mitchison, H., Mole, S. E., 2001. Neurodegenerative disease: the neuronal ceroid lipofuscinoses (Batten disease). Curr. Opin. Neurol. 14(6):795-803.

143. Mitchison, H. M., Hofmann, S. L., Becerra, C. H. R., Munroe, P. B., Lake, B. D., Crow, Y. J., Stephenson, J. B. P., Williams, R. E., Hofman, I. L., Taschner, P. E. M., Martin, J.-J., Philippart, M., Andermann, E., Andermann, F., Mole, S. E., Gardiner, R. M., ORawe, A. M., 1998. Mutations in the palmitoyl-protein thioesterase gene (PPT; CLN1) causing juvenile neuronal ceroid lipofuscinosis with granular osmiophilic deposits. Hum. Mol. Genet. 7(2):291-7.

144. Mizumaru, C., Saito, Y., Ishikawa, T., Yoshida, T., Yamamoto, T., Nakaya, T., Suzuki, T., 2009. Suppression of APP-containing vesicle trafficking and production of β-amyloid by AID/DHHC-12 protein. J. Neurochem. 111(5):1213-24.

145. Mukai, J., Liu, H., Burt, R. A., Swor, D. E., Lai, W.-S., Karayiorgou, M., Gogos, J. A., 2004. Evidence that the gene encoding ZDHHC8 contributes to the risk of schizophrenia. Nat. Genet. 36(7):725-31.

146. Mukai, J., Dhilla, A., Drew, L. J., Stark, K. L., Cao, L., Macdermott, A. B., Karayiorgou, M., Gogos, J. A., 2008. Palmitoylation-dependent neurodevelopmental deficits in a mouse model of 22q11 microdeletion. Nat. Neurosci. 11(11):1302-10.

147. Mullen, R. J., Buck, C. R., Smith, A. M., 1992. NeuN, a neuronal specific nuclear protein in vertebrates. Development. 116(1):201-11.

148. Mumby, D. G., Gaskin, S., Glenn, M. J., Schramek, T. E., Lehmann, H., 2002. Hippocampal damage and exploratory preferences in rats: memory for objects, places, and contexts. Learn. Mem. 9(2):49-57.

149. Nadolski, M. J., Linder, M. E., 2007. Protein lipidation. F.E.B.S. J. 274(20):5202-10.

150. Nasir, J., Floresco, S. B., OKusky, J. R., Diewert, V. M., Richman, J. M., Zeisler, J., Borowski, A., Marth, J. D., Phillips, A. G., Hayden, M. R., 1995. Targeted disruption of the Huntington's disease gene results in embryonic lethality and behavioral and morphological changes in heterozygotes. Cell. 81(5):811-23.

151. Noritake, J., Fukata, Y., Iwanaga, T., Hosomi, N., Tsutsumi, R., Matsuda, N., Tani, H., Iwanari, H., Mochizuki, Y., Kodama, T., Matsuura, Y., Bredt, D. S., Hamakubo, T., Fukata, M., 2009. Mobile DHHC palmitoylating enzyme mediates activity-sensitive synaptic targeting of PSD-95. J. Cell Biol. 186(1):147-60.

152. Ohno, Y., Kihara, A., Sano, T., Igarashi, Y., 2006. Intracellular localization and tissue-specific distribution of human and yeast DHHC cysteine-rich domain-containing proteins. Biochim. Biophys. Acta. 1761(4):474-83.

153. Ohyama, T., Verstreken, P., Ly, C. V., Rosenmund, T., Rajan, A., Tien, A.-C., Haueter, C., Schulze, K. L., Bellen, H. J., 2007. Huntingtin-interacting protein 14, a palmitoyl transferase required for exocytosis and targeting of CSP to synaptic vesicles. J. Cell Biol. 179(7):1481-96.

154. Okabe, M., Ikawa, M., Kominami, K., Nakanishi, T., Nishimune, Y., 1997. 'Green mice' as a source of ubiquitous green cells. F.E.B.S. Lett. 407(3):313-9

155. Osoegawa, K., Mammoser, A. G., Wu, C., Frengen, E., Zeng, C., Catanese, J. J., de Jong, P. J., 2001. A bacterial artificial chromosome library for sequencing the complete human genome. Genome Res. 11(3):483-96.

156. Osokine, I., Hsu, R., Loeb, G. B., McManus, M. T., 2008. Unintentional miRNA ablation is a risk factor in gene knockout studies: a short report. P.L.o.S. Genet. 4(2):e34.

157. Osten P, Khatri L, Perez JL, Georg Ko hr, Guenter Giese, Christopher Daly, Torsten W Schulz, Allen Wensky, Laveria M Lee, Ziff, E. B., 2000. Mutagenesis reveals a role for ABP/GRIP binding to GluR2 in synaptic surface accumulation of the AMPA receptor. Neuron. 27(2):313-25.

158. Otani, K., Ujike, H., Tanaka, Y., Morita, Y., Kishimoto, M., Morio, A., Uchida, N., Nomura, A., Kuroda, S., 2005. The ZDHHC8 gene did not associate with bipolar disorder or schizophrenia. Neurosci. Lett. 390(3):166-70.

159. Oyama, T., Miyoshi, Y., Koyama, K., Nakagawa, H., Yamori, T., Ito, T., Matsuda, H., Arakawa, H., Nakamura, Y., 2000. Isolation of a novel gene on 8p21.3-22 whose expression is reduced significantly in human colorectal cancers with liver metastasis. Genes Chromosomes Cancer. 29(1):9-15.

160. Planey, S., Zacharias, D., 2009. Palmitoyl acyltransferases, their substrates, and novel assays to connect them (Review). Mol. Membrane Biol. 26(1):14-31.

161. Ponimaskin, E., Dumuis, A., Gaven, F., Barthet, G. l., Heine, M., Glebov, K., Richter, D. W., Oppermann, M., 2005. Palmitoylation of the 5-hydroxytryptamine4a receptor regulates receptor phosphorylation, desensitization, and beta-arrestin-mediated endocytosis. Mol. Pharmacol. 67(5):1434-43.

162. Pook, M. A., Al-Mahdawi, S., Carroll, C. J., Cossee, M., Puccio, H., Lawrence, L., Clark, P., Lowrie, M. B., Bradley, J. L., Cooper, J. M., Kœnig, M., Chamberlain, S., 2001. Rescue of the Friedreich's ataxia knockout mouse by human YAC transgenesis. Neurogenetics. 3(4):185-93.

163. Prescott, G. R., Gorleku, O. A., Greaves, J., Chamberlain, L. H., 2009. Palmitoylation of the synaptic vesicle fusion machinery. J. Neurochem. 110(4):1135-49.

164. Putilina, T., Wong, P., Gentleman, S., 1999. The DHHC domain: A new highly conserved cysteine-rich motif. Mol. Cell Biochem. 195(1-2):219-26.

165. Qanbar, R., Bouvier, M., 2003. Role of palmitoylation/depalmitoylation reactions in G-protein-coupled receptor function. Pharmacol. Ther. 97(1):1-33.

166. Rao, D. S., Chang, J. C., Kumar, P. D., Mizukami, I., Smithson, G. M., Bradley, S. V., Parlow, A. F., Ross, T. S., 2001. Huntingtin interacting protein 1 Is a clathrin coat binding protein required for differentiation of late spermatogenic progenitors. Mol. Cell Biol. 21(22):7796-806.

167. Raymond, F. L., Tarpey, P. S., Edkins, S., Tofts, C., OMeara, S., Teague, J., Butler, A., Stevens, C., Barthorpe, S., Buck, G., Cole, J., Dicks, E., Gray, K., Halliday, K., Hills, K., Hinton, J., Jones, D., Menzies, A., Perry, J., Raine, K., Shepherd, R., Small, A., Varian, J., Widaa, S., Mallya, U., Moon, J., Luo, Y., Shaw, M., Boyle, J., Kerr, B., Turner, G., Quarrell, O., Cole, T., Easton, D. F., Wooster, R., Bobrow, M., Schwartz, C. E., Gecz, J., Stratton, M. R., Futreal, P. A., 2007. Mutations in ZDHHC9, which encodes a palmitoyltransferase of NRAS and HRAS, cause X-linked mental retardation associated with a Marfanoid habitus. Am. J. Hum. Genet. 80(5):982-7.

168. Ren, J., Wen, L., Gao, X., Jin, C., Xue, Y., Yao, X., 2008. CSS-Palm 2.0: an updated software for palmitoylation sites prediction. Protein Eng. Des. Sel. 21(11):639-44.

169. Ristevski, S., 2005. Making better transgenic models: conditional, temporal, and spatial approaches. Mol. Biotechnol. . 29(2):153-63.

170. Rocks, O., Peyker, A., Kahms, M., Verveer, P. J., Koerner, C., Lumbierres, M., Kuhlmann, J., Herbert, W., Wittinghofer, A., Bastiaens, P. I. H., 2005. An acylation cycle regulates localization and activity of palmitoylated Ras isoforms. Science. 307(5716):1746-52.

171. Rocks, O., Peyker, A., Bastiaens, P. I. H., 2006. Spatio-temporal segregation of Ras signals: one ship, three anchors, many harbors. Curr. Opin. Cell Biol. 18(4):351–7.

172. Rocks, O., Gerauer, M., Vartak, N., Koch, S., Huang, Z.-P., Pechlivanis, M., Kuhlmann, J., Brunsveld, L., Chandra, A., Ellinger, B., Waldmann, H., Bastiaens, P. I. H., 2010. The palmitoylation machinery is a spatially organizing system for peripheral membrane proteins. Cell. 141(3):458-71.

173. Roos, R. A., 2010. Huntington's disease: a clinical review. Orphanet J. Rare Dis. 5(1):40.

174. Roshon, M., DeGregori, J. V., Ruley, H. E., 2003. Gene trap mutagenesis of hnRNP A2/B1: a cryptic 3' splice site in the neomycin resistance gene allows continued expression of the disrupted cellular gene. B.M.C. Genomics. 4(1):1-11.

175. Roth, A., Wan, J., Bailey, A. O., Sun, B., Kuchar, J. A., Green, W. N., Phinney, B. S., Yates, J. R. r., Davis, N. G., 2006. Global analysis of protein palmitoylation in yeast. Cell. 125(5):1003-13.

176. Roth, A. F., Feng, Y., Chen, L., Davis, N. G., 2002. The yeast DHHC cysteine-rich domain protein Akr1p is a palmitoyl transferase. J. Cell Biol. 159(1):23-8.

177. Saito, S., Ikeda, M., Iwata, N., Suzuki, T., Kitajima, T., Yamanouchi, Y., Kinoshita, Y., Takahashi, N., Inada, T., Ozaki, N., 2005. No association was found between a functional SNP in ZDHHC8 and schizophrenia in a Japanese case-control population. Neurosci. Lett. 374(1):21-4.

178. Salaun, C., Greaves, J., Chamberlain, L. H., 2010. The intracellular dynamic of protein palmitoylation. J. Cell Biol. 191(7):1229-38.

179. Saleem, A. N., Chen, Y.-H., Baek, H. J., Hsiao, Y.-W., Huang, H.-W., Kao, H.-J., Liu, K.-M., Shen, L.-F., Song, I.-w., Tu, C.-P. D., Wu, J.-Y., Kikuchi, T., Justice, M. J., Yen, J. J. Y., Chen, Y.-T., 2010. Mice with alopecia, osteoporosis, and systemic amyloidosis due to mutation in Zdhhc13, a gene coding for palmitoyl acyltransferase. P.L.o.S. Genet. 6(6):e1000985.

180. Sarsero, J. P., Li, L., Holloway, T. P., Voullaire, L., Gazeas, S., Fowler, K. J., Kirby, D. M., Thorburn, D. R., Galle, A., Cheema, S., Koenig, M., Williamson, R., Ioannou, P. A., 2004. Human BAC-mediated rescue of the Friedreich ataxia knockout mutation in transgenic mice. Mamm. Genome. 15(5):370–82.

181. Sathasivam, K., Hobbs, C., Turmaine, M., Mangiarini, L., Mahal, A., Bertaux, F., Wanker, E. E., Doherty, P., Davies, S. W., Bates, G. P., 1999. Formation of polyglutamine inclusions in non-CNS tissue. Hum. Mol. Genet. 8(5):813-22.

182. Sauer, B., 1998. Inducible gene targeting in mice using the Cre/lox system. Methods. 14(4):381-92.

183. Saunders, T. L., 2010. A survey of internet resources for mouse development. Methods Enzymol. 476:3-21.

184. Schmidt, M. F. G., Bracha, M., Schlesinger, M. J., 1979. Evidence for covalent attachment of fatty acids to Sindbis virus glycoproteins. Proc. Natl. Acad. Sci. U.S.A. 76(4):1687-91.

185. Schnell, E., Sizemore, M., Karimzadegan, S., Chen, L., Bredtt, D. S., Nicoll, R. A., 2002. Direct interactions between PSD-95 and stargazin control synaptic AMPA receptor number. Proc. Natl. Acad. Sci. U.S.A. 99(21):13902-7.

186. Shahinian, S., Silvius, J. R., 2003. Doubly-lipid-modified protein sequence motifs exhibit long-lived anchorage to lipid bilayer membranes. Biochemistry. 34(11): 3813-22.

187. Shin, H. D., Park, B. L., Bae, J. S., Park, T. J., Chun, J. Y., Park, C. S., Sohn, J.-W., Kim, B.-J., Kang, Y.-H., Kim, J. W., Kim, K.-H., Shin, T.-M., Woo, S.-I., 2010. Association of ZDHHC8 polymorphisms with smooth pursuit eye

movement abnormality. Am. J. Med. Genet. B. Neuropsychiatr. Genet. 153B(6):1167-71.

188. Shizuya, H., Birren, B., Kim, U.-J., Mancino, V., Slepak, T., Tachiri, Y., SImon, M., 1992. Cloning and stable maintenance of 300-kilobase-pair fragments of human DNA in Escherichia coli using an F-factor-based vector. Proc. Natl. Acad. Sci. U.S.A. 89(18):8794-7.

189. Sidera, C., Parsons, R., Austen, B., 2005. Post-translational processing of beta-secretase in Alzheimer's disease. Proteomics. 5(6):1533-43.

190. Siegel, G., Obernosterer, G., Fiore, R., Oehmen, M., Bicker, S., Christensen, M., Khudayberdiev, S., Leuschner, P. F., Busch, C. J. L., Kane, C., Hübel, K., Dekker, F., Hedberg, C., Rengarajan, B., Drepper, C., Waldmann, H., Kauppinen, S., Greenberg, M. E., Draguhn, A., Rehmsmeier, M., Martinez, J., Schratt, G. M., 2009. A functional screen implicates microRNA-138-dependent regulation of the depalmitoylation enzyme APT1 in dendritic spine morphogenesis. Nat. Cell Biol. 11(6):705-16.

191. Singaraja, R. R., Hadano, S., Metzler, M., Givan, S., Wellington, C. L., Warby, S., Yanai, A., Gutekunst, C.-A., Leavitt, B. R., Yi, H., Fichter, K., Gan, L., McCutcheon, K., Chopra, V., Michel, J., Hersch, S. M., Ikeda, J.-E., Hayden, M. R., 2002. HIP14, a novel ankyrin domain-containing protein, links huntingtin to intracellular trafficking and endocytosis Hum. Mol. Genet. 11(23):2815-28.

192. Singaraja, R. R., Huang, K., Sanders, S. S., Milnerwood, A., Hines, R., Lerch, J., Franciosi, S., Drisdel, R. C., Vaid, K., Young, F. B., Doty, C. N., Wan, J., Bissada, N., Henkelman, R. M., Green, W. N., Davis, N. G., Raymond, L. A., Hayden, M. R., 2011. Altered palmitoylation and neuropathological deficits in mice lacking HIP14. Hum. Mol. Genet. Jul 20. [Epub ahead of print].

193. Slow, E. J., Van Raamsdonk, J. M., Rogers, D., Coleman, S. H., Graham, R. K., Deng, Y., Oh, R., Bissada, N., Hossain, S. M., Yang, Y.-Z., Li, X.-J., Simpson, E. M., Gutekunst, C.-A., Leavitt, B. R., Hayden, M. R., 2003. Selective striatal neuronal loss in a YAC128 mouse model of Huntington disease. Hum. Mol. Genet. 12(13):1555-67.

194. Slow, E. J., Graham, R. K., Hayden, M. R., 2006. To be or not to be toxic: aggregations in Huntington and Alzheimer disease. Trends Genet. 22(8):408-11.

195. Smotrys, J. E., Linder, M. E., 2004. Palmitoylation of intracellular signaling proteins: regulation and function. Annu. Rev. Biochem. 73(1):559-87.

196. Soskic, V., Nyakatura, E., Roos, M., ller-Esterl, W. M., Godovac-Zimmermann, J., 1999. Correlations in palmitoylation and multiple phosphorylation of rat bradykinin B2 receptor in Chinese hamster ovary cells. J. Biol. Chem. 274(13):8539-45.

197. Southwell, A. L., Ko, J., Patterson, P. H., 2009. Intrabody gene therapy ameliorates motor, cognitive, and neuropathological symptoms in multiple mouse models of Huntington's disease. J. Neurosci. 29(43):13589-602.

198. Soyombo, A. A., Hofmann, S. L., 1997. Molecular cloning and expression of palmitoyl-protein thioesterase 2 (PPT2), a homolog of lysosomal palmitoyl-protein thioesterase with a distinct substrate specificity. J. Biol. Chem. 272(43):27456–63.

199. Stamler, J. S., Simon, D. I., Osborne, J. A., Mullins, M. E., Jaraki, O., Michel, T., Singel, D. J., Loscalzo, J., 1992. S-nitrosylation of proteins with nitric oxide: synthesis and characterization of biologically active compounds. Proc. Natl. Acad. Sci. U.S.A. 89(1):444-8.

200. Stein, V., House, D. R. C., Bredt, D. S., Nicoll, R. A., 2003. Postsynaptic density-95 mimics and occludes hippocampal long-term potentiation and enhances long-term depression. J. Neurosci. 23(13):5503-6.

201. Stowers, R. S., Isacoff, E. Y., 2007. Drosophila huntingtin-interacting protein 14 is a presynaptic protein required for photoreceptor synaptic transmission and expression of the palmitoylated proteins synaptosome-associated protein 25 and cysteine string protein. J. Neurosci. 27(47):12874-83.

202. Strittmatter, S. M., Fankhauser, I. C., Huang, P. L., Mashimo, H., Fishman, M. C., 1995. Neuronal pathfinding is abnormal in mice lacking the neuronal growth cone protein GAP-43. Cell. 80(3):445-52.

203. Sturrock, A., Leavitt, B. R., 2010. The clinical and genetic features of Huntington disease. J. Geriatr. Psychiatry Neurol. 23(4):243-59.

204. Su, A. I., Wiltshire, T., Batalov, S., Lapp, H., Ching, K. A., Block, D., Zhang, J., Soden, R., Hayakawa, M., Kreiman, G., Cooke, M. P., Walker, J. R., Hogenesch, J. B., 2004. A gene atlas of the mouse and human protein-encoding transcriptomes. Proc. Natl. Acad. Sci. U.S.A. 101(16):6062–7.

205. Sugars, K. L., Rubinsztein, D. C., 2003. Transcriptional abnormalities in Huntington disease. Trends Genet. 19(5):233-7.

206. Swerdlow, N. R., Paulsen, J., Braff, D. L., Butters, N., Geyer, M. A., Swenson, M. R., 1995. Impaired prepulse inhibition of acoustic and tactile startle response in patients with Huntington's disease. J. Neurol. Neurosurg. Psychiatry 58(2):192-200.

207. Ten Brinke, A., Vaandrager, A. B., Haagsman, H. P., Ridder, A. N. J. A., Van Golde, L. M. G., Batenberg, J. J., 2002. Structural requirements for palmitoylation of surfactant protein C precursor. Biochem J. 361(Pt 3):663-71.

208. Tian, L., Jeffries, O., Mcclafferty, H., Molyvdas, A., Rowe, I., Saleem, F., Chen, L., Greaves, J., Chamberlain, L., Knaus, H., Ruth, P., Shipston, M. J., 2008. Palmitoylation gates phosphorylation-dependent regulation of BK potassium channels. Proc. Natl. Acad. Sci. U.S.A. 105(52):21006-11.

209. Tian, L., Mcclafferty, H., Jeffries, O., Shipston, M. J., 2010. Multiple palmitoyltransferases are required for palmitoylation-dependent regulation of large conductance calcium- and voltage-activated potassium channels. J. Biol. Chem. 285(31):23954-62.

210. Topinka, J. R., Bredt, D. S., 1998. N-terminal palmitoylation of PSD-95 regulates association with cell membranes and interaction with K+ channel Kv1.4. Neuron. 20(1):125-34.

211. Toyoda, T., Sugimoto, H., Yamashita, S., 1999. Sequence, expression in Escherichia coli, and characterization of lysophospholipase II. Biochim. Biophys. Acta. 1437(2):182-93.

212. Trimborn, M., Ghani, M., Walther, D. J., Dopatka, M., Dutrannoy, V., Busche, A., Meyer, F., Nowak, S., Nowak, J., Zabel, C., Klose, J., Esquitino, V., Garshasbi, M., Kuss, A. W., Ropers, H.-H., Mueller, S., Poehlmann, C., Gavvovidis, I., Schindler, D., Sperling, K., Neitzel, H., 2010. Establishment of a mouse model with misregulated chromosome condensation due to defective Mcph1 function. P.L.o.S. One. 5(2):e9242.

213. Ueno, K., 2000. Involvement of fatty acid synthase in axonal development in mouse embryos. Genes Cells. 5(10):859-69.

214. Van de Sluis, B., Voncken, J. W., 2010. Transgene design. Methods Mol. Biol. 693:89-101.

215. Van Keuren, M. L., Gavrilina, G. B., Filipiak, W. E., Zeidler, M. G., Saunders, T. L., 2009. Generating transgenic mice from bacterial artificial chromosomes: transgenesis efficiency, integration and expression outcomes. Transgenic Res. 18(5):769-85.

216. Van Raamsdonk, J. M., Pearson, J., Rogers, D. A., Bissada, N., Vogl, W., Hayden, M. R., Leavitt, B. R., 2005a. Loss of wild-type huntingtin influences motor dysfunction and survival in the YAC128 mouse model of Huntington disease. Hum. Mol. Genet. 14(10):1379-92.

217. Van Raamsdonk, J. M., Pearson, J., Slow, E. J., Hossain, S. M., Leavitt, B. R., Hayden, M. R., 2005b. Cognitive dysfunction precedes neuropathology and motor abnormalities in the YAC128 mouse model of Huntington's disease. J. Neurosci. 25(16):4169-80.

218. Van Raamsdonk, J. M., Murphy, Z., Selva, D. M., Hamidizadeh, R. H., Pearson, J., Petersén, A. s., Björkqvist, M., Muir, C., Mackenzie, I. R., Hammond, G. L., Vogl, W., Hayden, M. R., Leavitt, B. R., 2007a. Testicular degeneration in Huntington disease. Neurobiol. Dis. 26(3):512-20.

219. Van Raamsdonk, J. M., Warby, S. C., Hayden, M. R., 2007b. Selective degeneration in YAC mouse models of Huntington disease. Brain Res. Bull. 72(2-3):124-31.

220. Veit, M., Sdlner, T. H., Rothman, J. E., 1996. Multiple palmitoylation of synaptotagmin and the t-SNARE SNAP-25. F.E.B.S. Lett. 385(1-2):119-23.

221. Veit, M., 2000. Palmitoylation of the 25-kDa synaptosomal protein (SNAP-25) in vitro occurs in the absence of an enzyme, but is stimulated by binding to syntaxin. Biochem. J. 345 Pt 1:145-51.

222. Verkruyse, L., Hofmann, S., 1996. Lysosomal targeting of palmitoyl-protein thioesterase. J. Biol. Chem. 271(26):15831-6.

223. Vesa, J., Hellsten, E., Verkruyse, L. A., Camp, L. A., Rapola, J., Santavuori, P., Hofmann, S. L., Peltonen, L., 1995. Mutations in the palmitoyl protein thioesterase gene causing infantile neuronal ceroid lipofuscinosis. Nature. 376(6541):584-7.

224. Vetrivel, K. S., Meckler, X., Chen, Y., Nguyen, P. D., Seidah, N. G., Vassar, R., Wong, P. C., Fukata, M., Kounnas, M. Z., Thinakaran, G., 2009. Alzheimer disease Abeta production in the absence of S-palmitoylation-dependent targeting of BACE1 to lipid rafts. J. Biol. Chem. 284(6):3793–803.

225. Voncken, J. W., 2003. Transgene Design. Methods Mol. Biol. 209:51-67.

226. Vonsattel, J. P. G., Difiglia, M., 1998. Huntington Disease. J. Neuropathol. Exp. Neurol. 57(5):369-84.

227. Vonsattel, J. P. G., 2008. Huntington disease models and human neuropathology: similarities and differences. Acta Neuropathol. . 115(1):55-69.

228. Voss, A. K., Thomas, T., Gruss, P., 1998. Efficiency assessment of the gene trap approach. Dev. Dyn. 212(2):171-80.

229. Walker, F. O., 2007. Huntington's disease. Lancet. 369(9557):218-28.

230. Warby, S. C., Chan, E. Y., Metzler, M., Gan, L., Singaraja, R. R., Crocker, S. F., Robertson, H. A., Hayden, M. R., 2005. Huntingtin phosphorylation on serine 421 is significantly reduced in the striatum and by polyglutamine expansion in vivo. Hum. Mol. Genet. 14(11):1569-77.

231. Wellington, C. L., Ellerby, L. M., Hackam, A. S., Margolis, R. L., Trifiro, M. A., Singaraja, R., McCutcheon, K., Salvesen, G. S., Propp, S. S., Bromm, M., Rowland, K. J., Zhang, T., Rasper, D., Roy, S., Thornberry, N., Pinsky, L., Kakizuka, A., Ross, C. A., Nicholson, D. W., Bredesen, D. E., Hayden, M. R., 1998. Caspase cleavage of gene products associated with triplet expansion disorders generates truncated fragments containing the polyglutamine tract. J. Biol. Chem. 273(15):9158-67.

232. Xu, M., St Clair, D., He, L., 2010. Testing for genetic association between the ZDHHC8 gene locus and susceptibility to schizophrenia: An integrated analysis of multiple datasets. Am. J. Med. Genet. 153B(7):1266-75.

233. Yamamoto, Y., Chochi, Y., Matsuyama, H., Eguchi, S., Kawauchi, S., Furuya, T., Oga, A., Kang, J. J., Naito, K., Sasaki, K., 2007. Gain of 5p15.33 is associated with progression of bladder cancer. Oncology. 72(1-2):132-8.

234. Yanai, A., Huang, K., Kang, R., Singaraja, R. R., Arstikaitis, P., Gan, L., Orban, P. C., Mullard, A., Cowan, C. M., Raymond, L. A., Drisdel, R. C., Green, W. N., Ravikumar, B., Rubinsztein, D. C., El-Husseini, A., Hayden, M. R., 2006. Palmitoylation of huntingtin by HIP14 is essential for its trafficking and function. Nat. Neurosci. 9(6):824-31.

235. Yang, W., Di Vizio, D., Kirchner, M., Steen, H., Freeman, M. R., 2010. Proteome scale characterization of human S-acylated proteins in lipid raft-enriched and non-raft membranes. Mol. Cell Proteomics. 9(1):54-70.

236. Yang, X. W., Model, P., Heintz, N., 1997. Homologous recombination based modification in Escherichia coli and germline transmission in transgenic mice of a bacterial artificial chromosome. Nat. Biotechnol. 15(9):859-65.

237. Yeh, D. C., Duncan, J. A., Yamashita, S., Michel, T., 1999. Depalmitoylation of endothelial nitric-oxide synthase by acyl-protein thioesterase 1 is potentiated by Ca(2+)-calmodulin. J. Biol. Chem. 274(46):33148–54.

238. Zambrowicz, B. P., Abuin, A., Ramirez-Solis, R., Richter, L. J., Piggott, J., BeltrandelRio, H., Buxton, E. C., Edwards, J., Finch, R. A., Friddle, C. J., Gupta, A., Hansen, G., Hu, Y., Huang, W., Jaing, C., Key, J., Billie Wayne , Kipp, P., Kohlhauff, B., Ma, Z.-Q., Markesich, D., Payne, R., Potter, D. G., Qian, N., Shaw, J., Schrick, J., Shi, Z.-Z., Sparks, M. J., Sligtenhorst, I. V., Vogel, P., Walke, W., Xu, N., Zhu, Q., Person, C., Sands, A. T., 2003. Wnk1 kinase deficiency lowers blood pressure in mice: a gene-trap screen to identify potential targets for therapeutic intervention. Proc. Natl. Acad. Sci. U.S.A. 100(24):14109-14.

239. Zeidman, R., Jackson, C., Magee, A., 2009. Protein acyl thioesterases (Review). Mol. Membr. Biol. 26(1):32-41.

240. Zeitlin, S., Liu, J.-P., Chapman, D. L., Papaioannou, V. E., Efstratiadis, A., 1995. Increased apoptosis and early embryonic lethality in mice nullizygous for the Huntington's disease gene homologue. Nat. Genet. 11(2):155-63.

241. Zhang, F. L., Casey, P. J., 1996. Protein prenylation: molecular mechanisms and functional consequences. Annu. Rev. Biochem. 65:241-69.

242. Zhang, J., Planey, S. L., Ceballos, C., Stevens, S. M., Keay, S. K., Zacharias, D. A., 2008. Identification of CKAP4/p63 as a major substrate of the palmitoyl acyltransferase DHHC2, a putative tumor suppressor, using a novel proteomics method. Mol. Cell Proteomics. 7(7):1378-88.

243. Zhang, Z., Lee, Y.-C., Kim, S.-J., Choi, M. S., Tsai, P.-C., Xu, Y., Xiao, Y.-J., Zhang, P., Heffer, A., Mukherjee, A. B., 2005. Palmitoyl-protein thioesterase-1 deficiency mediates the activation of the unfolded protein response and neuronal apoptosis in INCL. Hum. Mol. Genet. 15(2):337-46.

244. Zhao, G.-Q., Liaw, L., Hogan, B. L. M., 1998. Bone morphogenetic protein 8A plays a role in the maintenance of spermatogenesis and the integrity of the epididymis. Development. 125(6):1103-12.

245. Zuccato, C., Valenza, M., Cattaneo, E., 2010. Molecular mechanisms and potential therapeutical targets in Huntington's disease. Physiol. Rev. 90(3):905-81.

APPENDIX: ADDITIONAL DATA

BAC End	BAC End Sequence
T7	GGCCGCGGATTCCCATTTATGGGTATGGATGGGACAAAGATCCTTCTACTTTGTAGATGTTGAAAGTGCTTAA TACTTATTTTCTTGGGTACTTTATTTTCCTTGCAATGAGGACAGATCCATGTAACCTTGGGCTTCATCATTCAGC TGTAATAAAACCAAATTATGATGCAGGAACTAATGGCATAGGAGGGAAGGATCTGGGAGCACTCTCTAAAGGC AGCAGGGGTGGTTGCAGCAGTGGCGACCAGTTGCGTTCTTGGTACAGAAGTAACATCAGTGTGGGCAGCAT TAACTGCATTAAAACTGGTTCTTGGTGCAGAAGTGGCATCAGTGCAAGGTGTACCATCTAGTGCTTGGTGAC AGTGATGGTAGTTTCCTCATTGGCCCAGTTCTGTGGCATTACTCCTGGAAATTCAGCCAAAAGCCTGTTTCTC CAGGCTGCCCAAGCAAGTCTACGAGCATTGATTAAGCTCTTCTACAGTGTAGTCAGCTGGAGTTAGCTTCGG TTGCTGGAACCAAGAACTCTGGTTGATTTGGATTTTACACCTGTGCTCCCAGCACAGTGACTAACAGAGAAT
SP6	CCGCGGATTCAGTGTGTGGATTTGGAAAGTTACCAGCTAACCTCTTTGAGCTGCGCTGTTCTTGGCCAGAAA AAAGATGGTCTCTTTAAAGGAGCAGACTGGGCTTGTGGTTAGGACTGAGGCTGCTCTTAGGGAAACAGCCT TTCTGTGGGTGATCAAGAGTGCAGATACTGAGGACTGGTTTCAGCCTTCTCATTGGAGCTGAACCACAGAAG TCAGGAGCTTGCTTTGAGATGATCATCCTGAGCCACTTCTTGCCATACATCNAAATTGAACTGTAGGAAACAG GCCTCTCAAACATGCTGACACATTCATCTCTTCCAGCCCTGGCACAAAAACTGTTTCCGATGTGCAAAGTGT GGGAAGAGTCTTGAATCAACAACTCTGACTGAAAAAGAAGGTGAAATCTATTGTAAAGGTAAAATTCATTTCA GTTACTGCTGTCCATATGAATATTCCACACTGGTTCTTGTTTAATGAAATGTCACTGGCATTAAAAAAAAAAAAA GAAAAGTATGCCACTATTTTCTGAAATAAATATCCCA

Appendix Table 1 – Sequence of BAC End Pairs for Human BAC RP11-463M12

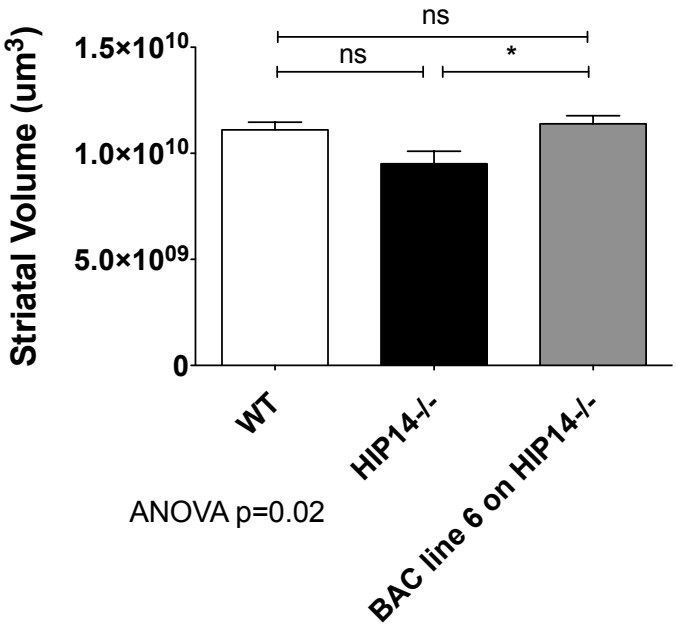

Appendix Figure 1– Striatal volume is rescued to WT values in a second *HIP14* BAC transgenic line crossed to *Hip14-/-*. We assessed a second *HIP14* BAC line (HB6) for ability of the BAC to compensate for loss of murine *Hip14* at 1 month of age. As in line 4, striatal volume was significantly rescued to WT values. *p<0.05.

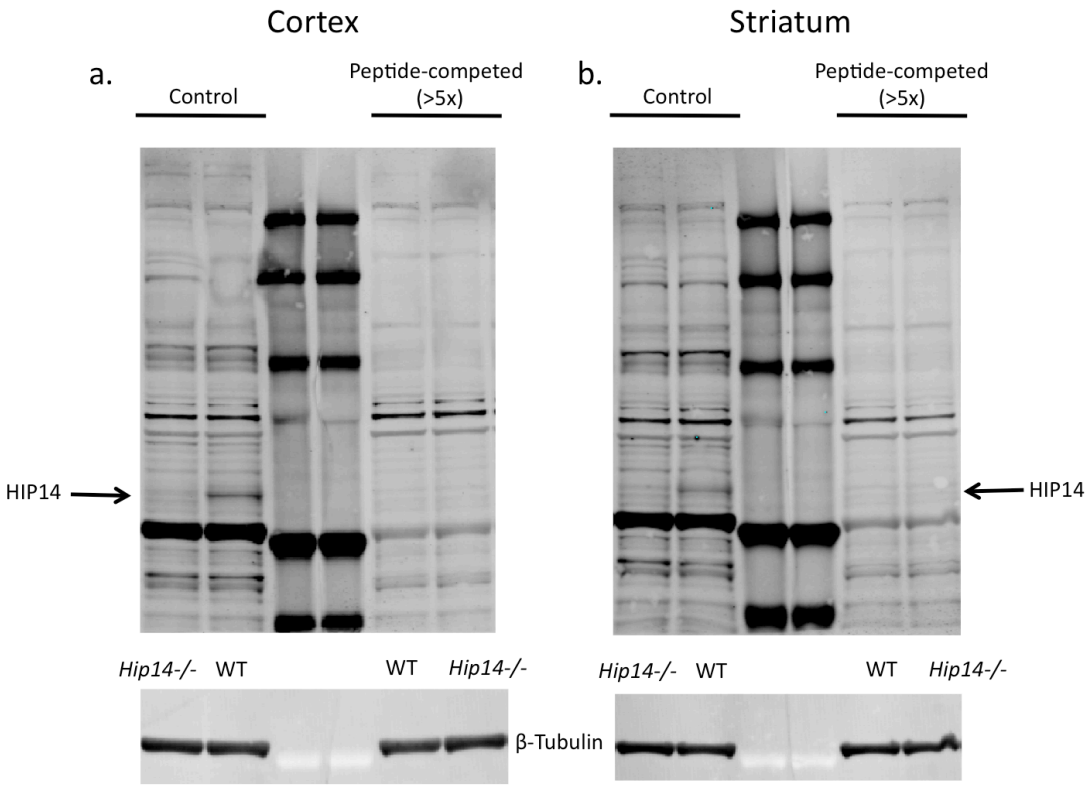

Appendix Figure 2- Peptide Competition Assay on PEP1 HD82 antibody for HIP14. Identical WT and *Hip14-/-* samples of **a.** Cortex and **b.** Striatum lysate were run in duplicate on the same gel on SDS-PAGE gels and transferred to PVDF membrane. After blocking, membranes were cut in half and subsequently processed in parallel. One half of each membrane was incubated in PEP1 primary antibody according to the standard protocol (control). The remaining half of the membrane was inciubated with PEP1 primary antibody solution that had been pre-incubated with a 5x molar excess of the peptide used to generate the antibody. Subsequently, both membranes were washed and incubated with secondary antibody according to the standard protocol described in Materials and Methods. Beta tubulin was probes as a loading control. Incubation with peptide-competed primary antibody enables identification of non-specific bands. The bands that disappear upon peptide-competition are specifically recognized by the antibody; those that remain are non-specific. Notably, the faint band apparent in *Hip14-/-* samples remains in the peptide-competed membrane, indicating that this is a non-specific band.